IGM83-000-387
CNRC 26498

POLYMER COMPOSITES

VOLUME 5/NO. 4/OCTOBER 1984

Composites '83
National Research Council of Canada
Industrial Materials Research Institute

CONTENTS

241 Introductory Remarks/L.A. UTRACKI, Guest Editor

242 S. SAVARD, L.-P. BLANCHARD, J. LEONARD, and R.E. PRUD'HOMME/Hydrolysis and Condensation of Silanes in Aqueous Solutions

250 I. CHUN and R.T. WOODHAMS/Use of Processing Aids and Coupling Agents in Mica-Reinforced Polypropylene

258 A. GARTON/A Novel Technique for the Study of Coupling Agent Phenomena

264 B. FISA, B. SANSCHAGRIN, and B. FAVIS/Mechanical Degradation of Mica During Processing with Polypropylene

277 L.A. UTRACKI, B.D. FAVIS, and B. FISA/Dynamic and Steady State Flow of Polypropylene/Mica Systems

289 M.R. KAMAL, A.T. MUTEL, and L.A. UTRACKI/Elongational Behavior of Short Glass Fiber Reinforced Polypropylene Melts

299 B.D. FAVIS, B. FISA, and B. SANSCHAGRIN/Factors Affecting the Surface Texture in Extruded Mica-Polypropylene Composites

307 M.A. KENNEDY, G.R. BROWN, and L.E. ST-PIERRE/The Effect of Silica on the Crystallization of Isotactic Poly(Propylene Oxide)

312 J.W.E. GEARING and M.R. STONE/The Dynamic Mechanical Method for the Characterization of Solid Composite Polymers

319 C.L. BEATTY/Evidence of Interaction of Fillers with Matrix Polymers via Transition Maps

327 G.P. TANDON and G.J. WENG/The Effect of Aspect Ratio of Inclusions on the Elastic Properties of Unidirectionally Aligned Composites

334 S.V. HOA and P. OUELLETTE/Damping of Composite Materials

339 F.K. LAUTENSCHLAEGER/The Optimum Property Concept—Part II. The Relative Order in Failure Property Maxima With Increasing Filler Levels

Continued on Back Cover

PUBLISHED BY THE SOCIETY OF PLASTICS ENGINEERS, INC.

POLYMER COMPOSITES

Published by the Society of Plastics Engineers

EDITOR

ROGER S. PORTER

% Polymer Science and Engineering
University of Massachusetts
Amherst, Mass. 01003

GUEST EDITOR

L. A. UTRACKI

c/o Industrial Materials Research Institute
National Research Council of Canada
75, Boul. de Mortagne
Boucherville, Quebec
Canada J4B 6Y4

ASSOCIATE EDITOR

RICHARD E. BALL

% Western New England College
Springfield, Mass. 01119

ADVISORY BOARD

LAWRENCE J. BROUTMAN
Illinois Institute of Technology

LAWRENCE CESSNA
Hercules Inc.

ANTHONY T. DI BENEDETTO
University of Connecticut

NIKOLAY ENIKOLOPYAN
USSR Academy of Sciences

JOSEPH N. EPEL
Budd Company

DAVID H. KAELBLE
Arroyo Computer Center

JOHN L. KARDOS
Washington University

FREDERICK J. MCGARRY
Massachusetts Institute of Technology

L. NICOLAIS
University of Naples

R. BYRON PIPES
University of Delaware

N. S. SCHNEIDER
Army Materials and Mechanics Research Center

PUBLICATIONS COMMITTEE

D. W. RILEY, Chairman
Extrusion Engineers

R. P. BRADDICKS, JR.
Plastics Consultant

R. D. FORGER
Society of Plastics Engineers

J. C. HAARSMA
S/C Electric Co.

J. L. HULL
Hull Corporation

D. JESIOLOWSKI
Wheaton Industries

V. E. MALPASS
Ferro Corporation

M. A. MENDELSOHN
Westinghouse Electric Corp.

R. S. PORTER
University of Massachusetts

A. A. SCHOENGOOD
Society of Plastics Engineers

G. R. THOM
Regal Plastics Company

A. M. VARNER
Moldflow USA, Inc.

A. E. WHITNEY, JR.
Plastics Consultant

Copyright by the Society of Plastics Engineers, Inc., 1984. Reproduction in whole or in part without written permission is strictly prohibited.

Polymer Composites (ISSN 0272-8397) is published at Waverly Press, Easton, MD 21601. Address changes, undeliverable copies and orders for subscriptions should be sent to Circulation Manager, Society of Plastics Engineers, 14 Fairfield Dr., Brookfield Center, CT 06805. Published quarterly. Second class postage paid at Brookfield Center, Conn. and additional entry offices. Accepted at special postal rate provided in P.M. Sec. 132.122.

Neither the Society of Plastics Engineers, Inc., nor **Polymer Composites** is responsible for the views expressed by individual contributors either in articles published in **Polymer Composites** or in technical papers presented at meetings of the Society.

Subscription rates for 1984: SPE members, 1 year—$24. Nonmembers, 1 year—$50. Delivery outside North America, add $8 per year.

SOCIETY OF PLASTICS ENGINEERS, INC.

Business and Executive Offices, 14 Fairfield Dr., Brookfield Center, Conn. 06805

ROBERT D. FORGER
Publisher

MICHAEL R. CAPPELLETTI
Circulation Manager

JANICE A. SCHOTT
Production Manager

JEANNETTE M. PIASTUCH
Copy Editor

OFFICERS OF THE SOCIETY

WILLIAM C. KUHLKE
President

RICHARD G. JOHNSON
President-elect

GREG R. THOM
First Vice President

JOHN R. KRETZSCHMAR
Second Vice President

JACQUES DE CRAENE
Vice President for International Affairs

BRUCE A. PETERSEN
Secretary

VIVIAN E. MALPASS
Treasurer

ROBERT D. FORGER
Executive Director

***POLYMER COMPOSITES* is indexed by:—Chemical Abstracts—Engineering Index, Inc.**

Introductory Remarks

The symposium "Composites-'83" of November 29, 1983, is the third one in a series on "Polymer Composites" and the ninth organized and sponsored by the National Research Council of Canada, Industrial Materials Research Institute (NRCC/IMRI). The remaining six symposia are part of the two other series on "Mathematical Modeling of Plastics Processing and Properties," and on "Polymer Blends".

Judging by the increasing number and pertinence of papers as well as by the growing attendance at each symposium, they appear to satisfy a need of the Canadian technical community. These meetings provide a source of neoteric information and an open forum for discussion and consultation. "Modeling", "Polyblends", and "Composites" are the three most important new trends in the plastics industry. The meetings provide contacts between the academic and commercial competence, and improve understanding, mutual respect, and cooperation between the participants.

Proceedings of these symposia, published in the technical journals of the Society of Plastics Engineers: *Polymer Engineering and Science* or *Polymer Composites*, are gaining an international recognition. This allows us to attract experts from major international centers of excellence as evidenced by the list of speakers to these symposia.

As in the past, the main theme of this symposium on composites is the preparation, processing and properties of thermoplastics reinforced with anisometric particle fillers. The first paper (by Savard, *et al.*) deals with preparation of micas for compounding with polymers. The paper is a follow-up on the previous report (by B. D. Favis, *et al.*) presented during symposium "Composites-'82" (*Polymer Comp.*, **5** (1), (1984)). The two following papers (by Chun and Woodhams, and by Garton) deal with polymer-filler interface; a new coupling agent (maleated polypropylene) and a new technique of the interface studies (by reflexion FTIR) are reported. Fisa, *et al.* discusses the effects of processing conditions on the mica flake size and size distribution. The subsequent three communications (by Utracki, *et al.*, Kamal, *et al.*, and Favis, *et al.*) are concerned with the melt flow behavior of polypropylene filled with either mica flakes or short glass fibers. Correlations between the rheological responses under various modes of deformation are discussed in terms of yield stress and particle orientation. The matrix modification on addition of filler particles is reported on by Kennedy, *et al.*; the authors observed that in spite of large increases in the number of nuclei, the rate of radial crystal growth, as well as the rate of bulk crystallization, decreased as a result of an increase of viscosity due to particle presence. The papers by Gearing and Beatty discuss the use of the dynamic testing methods in characterization of the filled polymers; the methods allow study of the polymer-filler interaction.

A new exact theory of the mechanical behavior of composites containing anisometric particles is proposed by Tandon and Weng. On the other hand, the use of a simplified theory in development of composites with specific dumping characteristics is discussed by Hoa and Ouellette. A generalized approach to evaluation of the failure properties of composites is reviewed by Lautenschlaeger; the method provides a simple, useful tool for optimization and balancing of material properties. Finally, the paper by Menges and Minte provides an overview of the present status, and maps the future, of the filament winding technology in automobile and aerospace industries.

As organizer of the symposium and guest editor of this issue, I would like to express my thanks to all speakers and participants for their contributions. The transcripts of the discussions provide evidence of the stimulating exchange of ideas and the informal, friendly atmosphere of the meeting, for which I am grateful. As for our readers, may I ask for your help towards further improvement of these annual symposia. I shall be grateful for any comments or suggestions regarding format and content.

L. A. Utracki
Guest Editor

Hydrolysis and Condensation of Silanes in Aqueous Solutions

S. SAVARD, L.-P. BLANCHARD, J. LÉONARD *and* R. E. PRUD'HOMME

Groupe de recherche sur les macromolécules
Départements de chimie et de génie chimique
Université Laval, Québec (Québec) Canada G1K 7P4

Aminosilanes hydrolyze rapidly in aqueous acidic solutions and exhibit good stability; however ^{1}H NMR measurements indicate that γ-MPS (γ-methacryloxypropyltrimethoxy silane) hydrolyzes slowly and condenses rapidly under similar conditions. The rate constant of these two reactions depends upon the pH of the solution, and the rate constant of the condensation reaction also depends upon the initial γ-MPS concentration. The hydrolysis is faster and the condensation slower at low pH's. These factors explain why an induction period is observed before the adsorption of γ-MPS onto mica takes place and why it does not occur if the induction period is too long. Using the Lentz technique, it is also shown that the main species resulting from the condensation of a concentrated γ-MPS solution is a cyclic trimer or tetramer, in agreement with literature results.

INTRODUCTION

Mica-reinforced composites when pretreated with silanes as coupling agents are known to have mechanical properties which are comparable to those of glass-fiber composites (1). In earlier work from this laboratory (2, 3), various aspects of the adsorption of silanes on mica surfaces were reported. The results obtained showed that the adsorption of this type of molecule, in the form of monolayers, is influenced at low silane concentrations by the pH of the solutions and by the concentration of silane.

The adsorption of monolayers of aminosilanes onto mica surfaces is efficient over a wide range of pH values because of the rapid hydrolysis of the silanes (2, 3). Plueddemann (4) obtained similar results with the deposition of CVBS, a cationic vinylbenzyl silane, onto glass fibers.

The adsorption of γ-MPS (γ-methacryloxypropyltrimethoxysilane), however, depends enormously on the time allowed for hydrolysis which in turn depends on the pH of the hydrolyzing solution (3) (*Fig. 1*): a short hydrolysis time, preceding the addition of mica, leads to a long induction period before the formation of monolayers of silane on the mica (*Fig. 1a*), whereas a too lengthy time for hydrolysis inhibits completely the adsorption of silane (*Fig. 1c*). The hydrolysis of γ-MPS in aqueous solutions is therefore a determining factor that governs the deposition of this silane onto mica surfaces.

Shih and Koenig (5) studied, by Raman spectroscopy, the symmetric vibration modes of the Si-O linkage in γ-MPS. They observed that the concentration of hydrolyzed silane in a neutral solution reached a maximum value after some 30 minutes of hydrolysis before decreasing continually thereafter. Daley and Rodriguez (6) observed a hydrolysis time of about 1 hour for γ-MPS in an acidic medium. They likewise noted a reduction in the rate of hydrolysis in the presence of glass fibers. Furthermore, Johannson, *et al.* (7) reported, from a ^{1}H NMR study, that complete hydrolysis takes place in an acidic medium in only 3 to 4 minutes after the silane solution becomes clear. In the above three cases and for experiments carried out under different conditions, different rates of hydrolysis were observed. It would then seem that the behavior of γ-MPS in aqueous media is related to the control of the following two parameters: pH of the solution and initial silane concentration.

More recently, Pohl (8) showed that the hydrolysis of different alkyltrialkoxysilanes in dilute acidic or basic solutions obeys pseudo-first order kinetics. The first step in the hydrolysis, corresponding to the transformation of the initial trialkoxysilane into a dialkoxysilanol, was studied by infrared spectroscopy. Subsequent steps are usually much more rapid (9). In another study (10), Pohl and Osterholtz measured, by ^{13}C NMR spectroscopy, the rate of condensation of alkylsilanetriols and found second order kinetics for this reaction catalyzed in acidic or basic media.

The above results allow the expression of an hypothesis to explain the phenomena observed in *Fig. 1*. The length of the induction period preceding the formation of the first silane monolayer depends on the rate of hydrolysis of the silane (*Figs. 1a* and

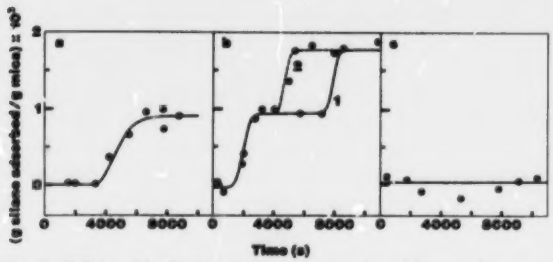

Fig. 1. Effect of hydrolysis time, prior to the addition of mica, on the kinetics of adsorption of γ-MPS at a pH of 5.5 (a – 300 s, b – 1500 s, and c – 5400 s of hydrolysis). The initial silane concentration of the aqueous solution was 0.025 g of silane/100 mL of H_2O; the silane to mica weight ratio was 0.5 g of silane to 100 g of mica.

1b). Moreover, a long hydrolysis time allows polycondensation of the silanetriol and inhibits completely the formation of monolayers on the mica (*Fig. 1c*), the oligomers thus formed being totally inefficient as coupling agents.

To verify this hypothesis, ^{1}H NMR spectroscopy measurements of the rates of hydrolysis and condensation of γ-MPS were made at different pH values and silane solution concentrations. These measurements lead to the evaluation of optimal conditions for the stability of γ-MPS and a control of its deposition on mica. Measurements were also made, in particular with the Lentz technique, to determine the nature of the species resulting from the condensation of γ-MPS.

EXPERIMENTAL

Coupling Agent

γ-MPS (γ-methacryloxypropyltrimethoxysilane) was obtained from Union Carbide (A-174) and used as received without further purification. Its chemical formula is as follows:

$$CH_2{=}C(CH_3)\overset{\overset{O}{\|}}{C}{-}O{-}(CH_2)_3Si(OCH_3)_3$$

Preparation of Solutions

To prepare acidic solutions of pH ≤ 3.0, the volumes of acetic acid and silane required to obtain the desired pH and initial silane concentration were added to 2 ml of D_2O. Zero time was taken at the moment silane was added to the acidic solution.

To prepare acidic solutions of pH 3.0 to 7.0, sodium acetate and acetic acid were added to 2 ml volumetric flasks which were then topped up with D_2O to the 2 ml mark. The silane was only added to this solution immediately prior to making NMR measurements. The error introduced thus on the concentrations which varied from 0.042 to 0.420 M was less than 1 percent. For solutions of pH = 7.0, the required amount of silane was simply added to 2 ml of D_2O.

Kinetic Measurements

The hydrolysis and condensation reactions of γ-MPS were followed by NMR spectroscopy. After introducing about 0.5 ml of the aqueous silane solution into a ^{1}H NMR tube, a series of spectra were recorded with a Bruker HX-90 or a Varian M-360 A instrument. The chemical shifts were measured with the use of TMS (tetramethylsilane) as an internal standard.

The rate of disappearance of alkyltrialkoxysilane was measured by integrating the deuterated methanol peak (*Fig. 2a*) located at 3.37 ppm (*Fig. 3*). It was assumed that hydrolysis was completed when integration of the methanol peak reached a constant value. The time *t* corresponding to a given concentration of trialkoxysilane was taken at the median of the time required to record the NMR spectrum. The data thus obtained were used to evaluate the rate of hydrolysis of the alkyltrialkoxysilane into alkylsilanetriol (*Fig. 2a*).

The condensation reaction was followed by measuring the disappearance of alkylsilanetriol with time (*Fig. 2b*). Concentrations of hydrolyzed silane were evaluated from relative peak integration measurements of the vinyl protons in the silanetriol (at 6.13 and 5.70 ppm's) and of the same protons in the oligomers (at 5.99 and 5.48 ppm's) (*Fig. 3*). The time *t* corresponding to a given concentration of silanetriol was taken at the median of the time required to record the NMR spectrum. It was thus possible to measure the rate of the condensation of silanetriol to oligomers.

Measurement of Insoluble Species

During the silanetriol condensation reaction (*Fig. 2b*), some of the products formed were found to be insoluble. To determine the quantity of insoluble species, ^{1}H NMR spectroscopy was applied to the solutions used earlier for the kinetic measurements. The total integration values of the vinyl proton (monomer and oligomers) peaks were measured relative to the integrated value of the deuterated methanol peak when hydrolysis is completed. This method yields a value only for those species which stay in solution. The other precipitated species which are undetectable are estimated by difference.

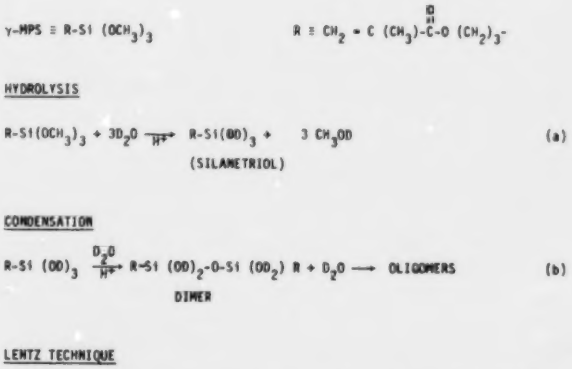
γ-MPS ≡ R-Si (OCH3)3
R ≡ CH2 = C (CH3)-C-O (CH2)3-
HYDROLYSIS
R-Si(OCH3)3 + 3D2O → R-Si(OD)3 + 3 CH3OD (a)
(SILANETRIOL)
CONDENSATION
R-Si (OD)3 → R-Si (OD)2-O-Si (OD2) R + D2O → OLIGOMERS (b)
DIMER
LENTZ TECHNIQUE
R'3-Si-OH + (CH3)3 Si-O-Si-(CH3)3 → R3'-Si-O-Si (CH3)3 + (CH3)3SiOH (c)
SILANOL HEXAMETHYLDISILOXANE TRIMETHYLSILYL ETHER

Fig. 2. Hydrolysis and condensation of silane.

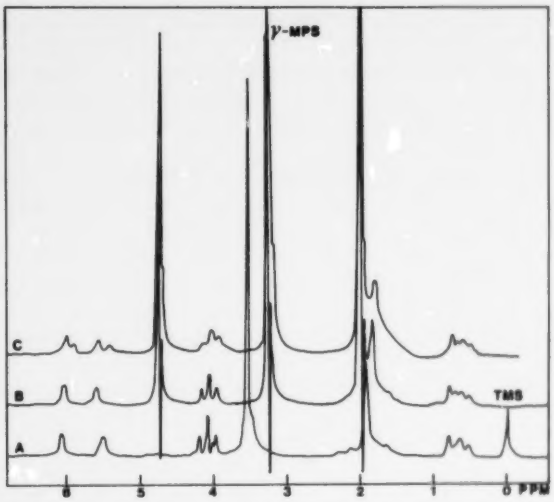

Fig. 3. ^1H NMR spectra of γ-MPS; a) unhydrolyzed γ-MPS ($CDCl_3$/TMS); b) hydrolyzed γ-MPS (silanetriol) (D_2O/AcOH). The initial silane concentration was 0.42 M and the pH of the solution was 2.4. Hydrolysis time was 30 min. c) Hydrolyzed and partially condensed γ-MPS (D_2O/AcOH). The initial silane concentration was 0.42 M and the pH of the solution was 2.4. Hydrolysis time was 270 min.

The Lentz Technique (11, 12)

The Lentz technique consists in trapping the silanol groups in γ-MPS oligomers in the form of trimethylsilylether (*Fig. 2c*). These condensed species are thus stabilized enabling their structure to be analyzed by mass spectrometry and NMR. Following Lentz's method, the following ingredients were mixed together with vigorous agitation. 20 ml of isopropyl alcohol, 10 ml of concentrated hydrochloric acid, 14 ml of hexamethyldisiloxane, and 20 g of ice. This solution was added slowly over a period of about 15 min to 20 ml of a γ-MPS solution hydrolyzed during 280 min (pH = 2.5, 0.42 M). The mixture was agitated at room temperature for 1 h, then heated to 50°C for 15 min before separating the two phases, the hexamethyldisiloxane and the condensation products being in the upper layer. A small volume of diethyl ether was added to the organic phase which was then washed with water and dried over $MgSO_4$. After evaporating the solvent under reduced pressure, 1.68 g of a colorless oil was recovered. This oil was analyzed by mass spectrometry and by NMR spectroscopy.

RESULTS

Kinetics of the Hydrolysis and Condensation of γ-MPS

Figure 4 shows a plot, with time, of ln [R—$Si(OCH_3)_3$], the concentration of alkyltrialkoxysilane. The linearity of the plot obtained (with a correlation coefficient greater than 0.99) shows that the reaction obeys first order kinetics with respect to trialkoxysilane. This behavior is similar to that observed by Pohl (6) who studied other silanes. The rate constant, k_1, for the hydrolysis reaction was evaluated from *Eq 1*

$$-\ln[R—Si(OCH_3)_3] = k_1 t + \ln[R—Si(OCH_3)_3]_0 \quad (1)$$

where $[R—Si(OCH_3)_3]_0$ is the initial concentration. The values of k_1 obtained at different pH values and at different initial concentrations are given in *Table 1*. One notes the strong dependence of k_1 on pH in the 3.5 to 7.0 range. The half life, $t_{1/2}$, of the unhydrolyzed species goes from 140 *s* at a pH of 3.5 to 46×10^3 *s* at a pH of 7. At pH below 3.0, the rate of reaction is too high to be followed by ^1H NMR spectroscopy. *Table 1* also shows that at a pH of 7.0, the initial silane concentration does not have very much influence on the rate of hydrolysis of γ-MPS.

Figure 5 shows that the silanetriol condensation reaction obeys second order kinetics with respect to silanetriol since a straight line is obtained when the reciprocal of the hydrolyzed silane is plotted as a function of time (correlation coefficient greater than 0.99). By ^{13}C NMR spectroscopy, Pohl (8) also recorded second order kinetics for the condensation of different silanes including γ-MPS.

The rate constant, k_2, for the condensation reaction was evaluated from *Eq 2*

$$1/[R—Si(OH)_3] = k_2 t + 1/[R—Si(OH)_3]_0 \quad (2)$$

where $[R—Si(OH)_3]$ and $[R—Si(OH)_3]_0$ are the instantaneous and initial silanetriol concentrations, respectively. Values of k_2 for reactions carried out

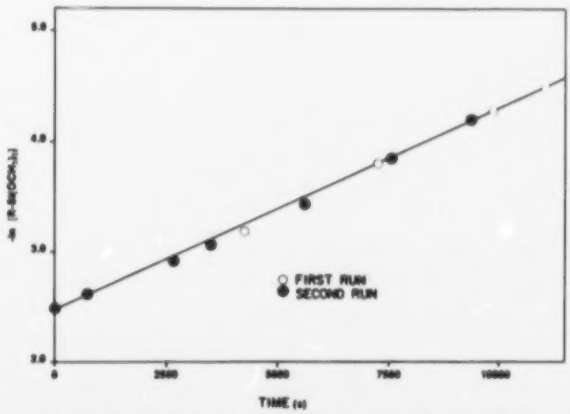

Fig. 4. Kinetics of the hydrolysis of silane. The initial silane concentration was 0.084 M and the pH of the solution was 5.5. Both experiments were carried out under identical conditions.

Table 1. Hydrolysis of γ-MPS

$$R—Si(OCH_3)_3 \xrightarrow[k_1]{D_2O} R—Si(OH)_3$$

pH	Initial concentration (M)	k_1 (s^{-1}) × 10^5	$t_{1/2}$ (s) × 10^{-4}
7.0	0.042	0.86	8.1
7.0	0.084	1.5	4.6
7.0	0.126	2.2	3.2
7.0	0.168	0.42	16.
5.5	0.084	18.	0.39
3.5	0.084	51.	0.014

at pH values between 2.5 and 5.5 are summarized in *Table 2*. Values of k_2 are seen to increase with pH. At pH values greater than 7.0, silanetriol condensation rate measurements are no longer possible by the NMR method since the rate of condensation becomes as rapid as the rate of hydrolysis of alkyltrialkoxysilane. *Table 2* also shows that k_2 increases with the initial concentration of hydrolyzed silane in acidic media: $t_{1/2}$ passes from 3.8×10^5 *s* at a concentration of 0.042 M to 2.0×10^4 *s* at a concentration of 0.42 M.

Measurement of Insoluble Species

It is interesting to note that a portion of the oligomers formed during the silanetriol condensation reaction become insoluble in aqueous solution. At a concentration of 0.126 M and a pH of 7.0, 25 percent of the initial amount of silane precipitates in the form of insoluble oligomers while at a pH of 2.7, no insoluble products can be detected after 1800 min of reaction. Increasing the initial concentration of γ-MPS to 0.295 M leads to a precipitation of 5 percent of the products after 1800 min of reaction at a pH of 2.7.

The Lentz Technique

After the hydrolysis of γ-MPS, silanetriol is the only species present in the solution. It condenses slowly to form dimers, trimers, tetramers, and so forth. These polysilanols are unstable and impossible to isolate. However, the Lentz technique enables one to stabilize free silanol groups by converting them to stable trimethylsilylethers. The separation of condensed species from γ-MPS thus becomes possible as is their study by spectroscopy. From the data in *Table 3*, one notes that the theoretical ratio of the vinyl proton peak areas (5.58 and 6.14 ppm) to the trimethylsilylether proton peak area (0.12 ppm) is different for each of the low molecular weight condensed species of γ-MPS. Only the cyclic trimer and tetramer (*Fig. 6*) show identical ratios. The use of the Lentz technique with concentrated γ-MPS solutions (0.42 M and pH of 2.5) allows the recovery, with a yield of 65 percent, of a product the ratio of which, determined by ^{1}H NMR, is 0.215. By comparison with the theoretical ratios of *Table 3*, this result suggests a cyclic trimer or tetramer structure for this γ-MPS based oligomer.

Mass spectrometric separation of the products recovered lends weight to the above conclusion. Indeed, the *m/e* fragments at 207 and 366 correspond to a median scission of the trimer and tetramer species.

This result does not completely exclude, however, the presence during condensation of trimethylsilylethers from monomer and dimer but these species cannot be detected in the products obtained by the Lentz reaction because of their high volatility which leads to their loss during the process of separation.

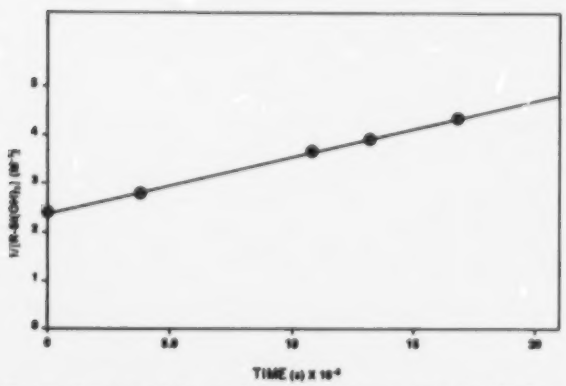

Fig. 5. Kinetics of the condensation of silane. The initial silane concentration was 0.42 M and the pH of the solution was 2.4.

Table 2. Condensation of γ-MPS

$$R\text{—}Si(OH)_3 \xrightarrow[k_2]{D_2O} \text{oligomers}$$

pH	Inidal concentration (M)	k_2 (M^{-1} s^{-1}) × 10^5	$t_{1/2}$ (s) × 10^{-4}
2.8	0.042	1.3	3.8
2.7	0.126	2.8	2.8
2.5	0.295	3.3	1.0
2.4	0.421	12.0	0.20
3.5	0.084	5.5	2.2
5.5	0.084	10.5	1.1

Table 3. Relative theoretical ratios (as calculated from ^{1}H NMR integrations) of different low molecular weight trimethylsilyl species derived from γ-MPS

Species considered	Theoretical ratio
Monomer	0.074
Dimer	0.111
Trimer	0.133
Tetramer	0.148
Pentamer	0.159
Cyclic trimer	0.222
Cyclic tetramer	0.222

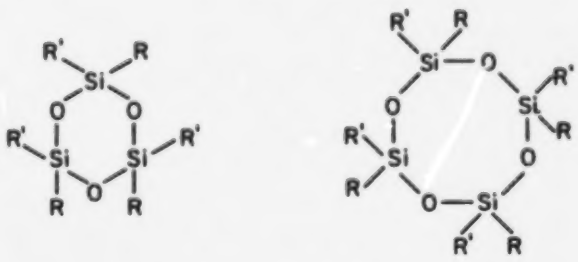

Fig. 6. Trimethylsilylether structures of cyclic trimer and tetramer produced by the condensation of hydrolyzed γ-MPS.

the time allowed for the hydrolysis of the alkoxyl group. *Figures 1a*, *1b*, and *1c* correspond, respectively, to the adsorption of silane after a hydrolysis time of 300, 1500, and 5400 *s*. The presence of an induction period prior to the formation of the first monolayer is to be noted. If one adds the hydrolysis time preceding the addition of mica to the induction period, identical values of 3000 s are obtained for experiments 1a and b.

The reasons for such behavior can be explained by a study of the kinetics of the hydrolysis of γ-MPS in aqueous solutions. From *Table 1* one notes that at a pH of 5.5 and a concentration of 0.084 M in γ-MPS, the half life of the unhydrolyzed species is 3900 *s*. There is a great similitude between this value and the one measured during the adsorption of γ-MPS on mica, namely, about 3000 *s*.

Thus, at a pH of 5.5, hydrolysis of silane is relatively rapid ($t_{1/2}$ = 3900 *s*) and the deposition on the mica surface of hydrolyzed silane follows immediately at 3000 to 4000 *s*. Furthermore, not only is the condensation of silanetriol, which depends on the concentration of this species in solution, slow under these conditions ($t_{1/2} = 1.1 \times 10^5$ *s*) but it becomes slower and slower as the silane is adsorbed on the mica (*Table 2*). The induction period preceding the appearance of the first monolayer is therefore related to the silane hydrolysis time and only hydrolyzed silane can react in an efficient manner with mica.

The results depicted in *Fig. 1c* cannot, however, be explained entirely by the kinetics of γ-MPS condensation (*Table 2*). At a concentration of 0.084 M and a pH of 5.5, the half life of silanetriol is 1.1×10^5 *s* while inhibition of adsorption of γ-MPS is observed after an hydrolysis time of 5400 *s*. However, the condensation process plays a certain role. The fact of leaving a longer period for the hydrolysis of silane in the experiment described in *Fig. 1c* allows the complete hydrolysis of γ-MPS. Thus the concentration of silanetriol is higher after 5400 *s* than it was for the experiments described in *Figs. 1a* and *b* because hydrolyzed silane cannot be withdrawn from the solution by adsorption before the addition of mica. In this case, the condensation of γ-MPS can become more rapid and thus inhibit the deposition of silane on the mica.

The data in *Tables 1* and *2* indicate that the maximum stability of hydrolyzed γ-MPS in an aqueous medium is reached at concentrations lower than 0.042 M in silane and for pH values between 2.4 and 4.0. An increase in silane concentration favors the polycondensation of γ-MPS while an increase in pH favors both silane condensation and a reduction of the rate of hydrolysis. Plueddemann (11) obtained identical results during a visual study of the stability of aqueous solutions of silanes bearing neutral organofunctional groups, γ-MPS being one of these.

The results of the present work confirm that stability of a hydrolyzed silane in an aqueous medium is required to obtain good efficiency as a coupling agent on an inorganic surface. Neutral unhydrolyzed silanes cannot be linked to the surface and one observes a loss of efficiency as a coupling agent when they are applied in the form of polysiloxanes (13, 14). The silanetriol and the linear oligomers of low molecular weight represent the only species which show good efficiency as coupling agents. γ-MPS is only slightly soluble in water when in the trialkoxyl form but it becomes soluble once hydrolyzed and it slowly condenses to give insoluble polysiloxanes. It has been noted that at a concentration of 0.126 M in γ-MPS and a pH of 7.0, there is precipitation of some 25 percent of the initial quantity of silane after 1800 min of reaction while at a pH of 2.7 it is impossible to detect the presence of insolubles under the same conditions. Two explanations can be put forth: 1) the polysiloxanes formed at a pH of 7.0 are of a higher molecular weight than those formed at a pH of 2.7 and thus less soluble; 2) the polysiloxanes formed at these two pH values can have similar molecular weights but their solubility can change with the pH. Ishida, *et al.* (15) showed, however, from GPC studies of polysiloxanes formed by γ-MPS at pH values of 2.6 and 7.1 that the species formed at a pH of 2.6 are of a much lower molecular weight than those formed at a pH of 7.1. It seems therefore that the molecular weight of the polysiloxanes formed during the condensation of γ-MPS varies with the pH and explanation 1) above would seem to be the more plausible one to retain though explanation 2) cannot be entirely ruled out.

During the experiments with the Lentz reaction, an experimental integration ratio of 0.215 was obtained for the recovered species condensed from γ-MPS. This ratio corresponds to cyclic trimer and/or tetramer of γ-MPS (*Table 3*). It is quite probable, however, that the volatility of the monomer and dimer is such that they are both lost during the evaporation process at reduced pressure of the organic phase required by the Lentz technique if in fact these species are present to any great extent. It must be noted here that at a concentration of 0.42 M, 65 percent of the initial silanetriol was recovered in the form of cyclic trimer or tetramer and that these species are the principal products formed under the conditions studied.

The suggestion that cyclic trimer or tetramer is present during the condensation of γ-MPS is supported by the results of other studies reported in the literature. Ishida, *et al.* (15) observed by GPC a low molecular weight oligomer during the condensation of γ-MPS in an acidic medium. They suggested a tetramer as a possible structure. During the study of the polycondensation of cyclohexanetriol (16) and of phenylsilanetriol (17) in an aqueous medium, Brown identified a cyclic tetrol tetramer with a structure very much like that proposed in the present work as one of the major products of the condensation reaction. Furthermore, Plueddemann (11), after having trapped the silanols by the Lentz technique, analyzed by chromatography the products of condensation of vinyltrimethoxysilane in a solution with a pH of 2.0. He obtained 30 percent of trimer and 13 percent of tetramer but made no comments regarding the structure of these

products. These results strongly suggest the existence of cyclic trimer and/or tetramer forms of γ-MPS. The product isolated in the present work has the structure of one of the two structures described in *Fig. 6*.

The formation of cyclic species can also explain the increase in the rate constant k_2 with the initial concentration $[R—Si(OH)_3]_0$ at a pH of 2.5 (*Table 2*). The formation of cyclic species in a polycondensation reaction can in fact occur in two different ways. First, cyclic molecules can be formed through the following sequence of reactions:

$$\text{monomer} \rightarrow \text{oligomer} \rightarrow \text{cycle.}$$

In the present case, the condensation of silanetriol leading to the formation of a cyclic trimer would be:

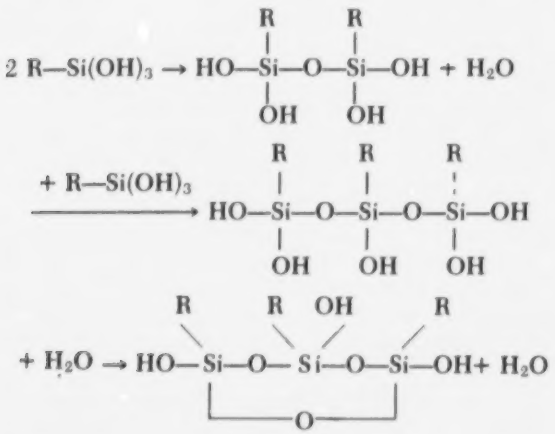

From the results obtained with the Lentz technique, it is found that the remaining hydroxyl groups do not react in the course of the polycondensation. Therefore, a silanetriol can be considered as a molecule of the HO—B—OH type with the assumption that all hydroxyl groups have the same reactivity whatever the size of the molecule.

If $[A]$ represents the overall concentration of molecules which can react, the overall rate of disappearance of the A molecules resulting from the formation of oligomers and cycles is given by:

$$-\frac{d[A]}{dt} = \frac{d[\text{oligomers}]}{dt} + \frac{d[\text{cycles}]}{dt}$$

The formation of linear oligomers is a second order reaction with respect to A molecules with a rate constant k_2'. The cyclization reaction is assumed to occur with a rate constant k_3 and is first order with respect to the A molecules; however, only a fraction of these molecules can undergo cyclization. Since the results presented in this paper show that the cyclic species are mainly trimers or tetramers, the cyclization would be first order with respect to trimers or tetramers. Limiting the discussion to the case of trimers, the rate of disappearance of the A molecules is then written as:

$$-\frac{d[A]}{dt} = k_2'[A]^2 + k_3[T] \qquad (3)$$

where $[T]$ is the concentration of trimers. The ratio $[T]/[A]_0$, where $[A]_0$ is the initial monomer concentration is given by (18):

$$\frac{[T]}{[A]_0} = (1-p)^2p^2 = \frac{[A]^2([A]_0 - [A])^2}{[A]_0^4} \qquad (4)$$

where p is the extent of the reaction and is equal to $([A]_0 - [A])/[A]_0)$. Substituting *Eq 4* in *Eq 3*, one obtains:

$$-\frac{d[A]}{[A]^2} = [k_2' + k_3([A]_0 - [A])^2 /[A]_0^3]dt = k_2 dt \qquad (5)$$

Integrating this equation would lead to *Eq 2*. In order to integrate the term in brackets, it is assumed that most of the A molecules react through a second order reaction. From analogy with *Eq 2*, one can therefore write:

$$[A] = [A]_0/(1 + k_2'[A]_0 t) \qquad (6)$$

Substituting *Eq 6* into *Eq 5* and integrating over t, one finally obtains:

$$\frac{1}{[A]} - \frac{1}{[A]_0} = \left(k_2' + \frac{k_3}{[A]_0}\right) t = k_2 t \qquad (7)$$

If we use the approach of Stoll, *et al.* (19) for the cyclization occurring in polycondensation, an equation of the same type is obtained. *Equation 7* indicates that k_2 is a function of $[A]_0$ and its value decreases with increasing $[A]_0$. This is in disagreement with the experimental results of *Table 2* where k_2 is shown to increase with increasing $[A]_0$.

The second way to explain the formation of cyclic species is through cyclomerization. If M, D, and T denote the monomer, dimer, and trimer, respectively, cyclotrimerizations and cyclotetramerizations can be described by the following reactions:

$$2D \rightarrow \text{C} - \text{tetramer}$$
$$D + M \rightarrow \text{C} - \text{trimer}$$
$$T + M \rightarrow \text{C} - \text{tetramer}$$
$$D + 2M \rightarrow \text{C} - \text{tetramer}$$
$$3M \rightarrow \text{C} - \text{trimer}$$

The first three reactions are second order reactions and the last two are third order. The overall rate of reaction is:

$$-\frac{d[A]}{dt} = k_2'[A]^2 + k_3'[A]^3 \qquad (8)$$

where k_2' is the rate constant for all the second order reactions and k_3' is the rate constant for all the third order reactions. Dividing *Eq 8* by $[A]^2$, introducing *Eq 6* and integrating, one obtains:

$$\frac{1}{[A]} - \frac{1}{[A]_0} = k_2' t + \frac{k_3'}{k_2'} \ln(1 + [A]_0 k_2' t) \qquad (9)$$

Expanding the logarithmic term in a series and

dropping higher terms, the final results is:

$$\frac{1}{[A]} - \frac{1}{[A]_0} = (k_2' + k_3'[A]_0)t = k_2 t. \qquad (10)$$

Equation 10 predicts an increase of k_2 with increasing $[A]_0$ and is therefore in agreement with the experimental results of *Table 2*. This behavior requires the occurrence of third order reactions. Although this type of reaction is less common than reactions of the first and second orders, cyclotrimerizations of a few monomers have been reported (20). In the case of the cyclotrimerization of isocyanate, a kinetic study shows results similar to those presented in this paper; moreover depending upon the catalyst used, the overall order of the reaction can be three or four (21).

CONCLUSIONS

Contrary to aminosilanes, γ-MPS shows limited stability in aqueous solutions. Its rates of hydrolysis and condensation are strongly dependent on the pH of the solution. Furthermore, the condensation process depends upon the initial silane concentration. A low rate of hydrolysis at a pH of 5.5 leads to high induction times preceding the deposition of this silane on mica. The major product from condensation in concentrated γ-MPS solutions has a cyclic trimer or tetramer structure.

ACKNOWLEDGMENTS

The authors gratefully acknowledge financial assistance received from the Industrial Materials Research Institute of the National Research Council of Canada to carry out this study.

REFERENCES

1. H. S. Katz and J. V. Milewski, "Handbook of Fillers and Reinforcements for Plastics," Ch. 20 Reinhold, Toronto, (1978).
2. B. D. Favis, L.-P. Blanchard, J. Léonard, and R. E. Prud'homme, *J. Appl. Polym. Sci.*, **28**, 1235 (1983).
3. B. D. Favis, L.-P. Blanchard, J. Léonard, and R. E. Prud'homme, *Polym. Compos.*, in press.
4. E. P. Plueddemann and G. L. Stark, *Mod. Plast.*, **54**, 102 (1977).
5. P. T. K. Shih and J. L. Koenig, *Mater. Sci. Eng.*, **20**, 137 (1975).
6. L. R. Daley and F. Rodriguez, *Polym. Eng Sci.*, **9**, 428 (1969).
7. O. Johannson, F. Stark, R. Baney, *et al.*, AFML TR 65 303-pt 1, (Sept., 1965).
8. E. R. Pohl, Proc. 38th Ann. Tech. Conf., Reinforced Plastics/Composites Inst., SPI, Section 4-B (1983).
9. K. J. McNeil, J. A. Di Caprio, D. A. Walsh, and R. F. Pratt, *J. Am. Chem. Soc.*, **102**, 1859 (1980).
10. E. R. Pohl and F. D. Osterholtz, *Am. Chem. Soc., Div. Polym. Chem. Polym. Prepr.*, **24**, 200 (1983).
11. E. P. Plueddemann, Proc. 24th Ann. Tech. Conf., Reinforced Plastics/Composites Inst., SPI, Section 19-A (1969).
12. C. W. Lentz, *Inorg. Chem.*, **3**, 574 (1964).
13. E. P. Plueddemann, "Composite Materials: Interfaces in Polymer Matrix Composites," Vol. 6, p. 173 (1974).
14. H. A. Clark and E. P. Plueddemann, *Mod. Plast.*, **40**, 133 (1963).
15. H. Ishida, J. D. Miller, and K. Hoh, *Polym. Compos.*, in press.
16. J. F. Brown, Jr., and L. H. Vogt, Jr., *J. Am. Chem. Soc.*, **87**, 4313 (1965).
17. J. F. Brown, Jr., *J. Am. Chem. Soc.*, **87**, 4317 (1965).
18. P. J. Flory, "Principles of Polymer Chemistry," Cornell Univ. Press, Ch. 8, Ithaca, N.Y., (1953).
19. M. Stoll, A. Romé, and G. Stoll-Comte, *Helv. Chim. Acta*, **17**, 1289 (1934).
20. G. Odian, "Principles of Polymerization," Ch. 5. Wiley, N.Y., (1981).
21. J. E. Kresta and H. K. Hsieh, *Makromol. Chem.*, **180**, 793 (1979).

DISCUSSION

R. T. Woodhams: I heard recently from Rena Latinenem from Finland, that he found evidence that the silanes seem to react preferentially at the edges of mica flakes. Is there any evidence from your kinetic studies that would indicate a difference in reactivity of one area of mica flakes vs. another?

J. W. Léonard: No. I do not think that you can find it from reaction kinetics. Reaction involves silane molecules and all the sides of the mica at the same time; it averages over the whole surface.

F. K. Lautenschlaeger: Maybe varying of the aspect ratio could provide some differentiation. But my question involves NMR. I think that this is an extremely useful technique which should be extended to other fillers, in particular, in cases where the formulations are very complex, where there are many chemical ingredients in the system, and where one does not really know whether coupling occurs or not. By NMR, it should be relatively easy to identify the ingredient(s) which interfere in the silane-mineral particle interaction.

L. A. Utracki: I am a little concerned about the results you presented today. Here, the kinetics of hydrolysis and coupling or oligomerization have been studied in the absence of filler particles. However, the importance of this work is in application to the "sizing" operation—i.e., one must extrapolate these data to the situation where filler particles are present. Mica, in particular, is a very complex system—there are numerous impurities left on the surface from the flotation and other supplier's treatment.

J. W. Léonard: We found in the literature that if the silane is not hydrolyzed then it acts very poorly as a coupling agent—does not seem to hold to the mica at all. For CVBS, we observed that it will preferentially react with the mica before condensation. In most cases, we feel that hydrolized silane will prefer to react with the mica than with itself. This may not be the case with γ-MPS and some other varieties of silanes. Then if you wait too long before adding mica, it will have time to condense and will not react at all.

B. D. Favis: Generally, the hydrolysis is carried out before mica is introduced. So the kinetic studies on hydrolysis and condensation in the absence of filler particles can be justified on this basis. If these reactions are not completed at the time of filler addition and the silane-mica reaction is relatively slow, then one cannot extrapolate the results to the actual coating operation.

I always had the impression that one of the major

limitations of the use of NMR is the sensitivity. One is limited to a higher range of the concentrations of silane molecules below which it is impossible to obtain a reasonable spectrum. Could you comment on the limitations of the technique.

J. W. Léonard: I agree that this is a serious limitation of the method. The other one is the rate of the reaction. However, we succeeded in getting the results I presented and, as you saw, the reproducibility was quite good. In our case, the concentration was about 0.1 mole/l. Maybe this is a little bit higher than the concentrations we used during the adsorption studies of silanes on mica. There we had to use very diluted solutions in order to see all these plateaus; as you know these monolayer plateaus are not visible if the silane concentrations are too high.

A. L. Gent: We found that mono-functional silanes, that is silanes with a molecule which has only one hydrolyzable group, do not react with hydrolyzed alumina, whereas the conventional, tri-functional silane reacts readily. Have you tried mono-functional silanes with mica?

These are simpler systems since the dimerization possibility is eliminated. It would be interesting to study the kinetics of these silanes.

J. W. Léonard: No, we never tried mono-functional silanes. Here, from the Lentz technique, we see that almost 100 percent of —OH groups react very rapidly. When we compare the various kinetic schemes the highest ratio is found for cyclic species. In that case, almost all hydroxyl groups have reacted.

Use of Processing Aids and Coupling Agents in Mica-Reinforced Polypropylene

I. CHUN *and* R. T. WOODHAMS

Department of Chemical Engineering and Applied Chemistry
University of Toronto, Toronto, Canada, M5S 1A4

Low molecular weight waxes prepared by the maleation of thermally degraded polypropylene are effective substitutes for silane coupling agents in filled polypropylene resins. The addition of 1 to 5 percent maleated polypropylene wax increased the tensile and flexural strength of mica-filled polypropylenes without significant changes in the modulus or fracture toughness. The waxes also aided dispersion, reduced melt viscosity, and permitted direct injection molding of powder blends without precompounding. The influence of maleated polypropylene wax coupling agents on the mechanical properties is similar to the published behavior of chlorinated paraffin waxes, but without the undesirable corrosiveness. The efficient utilization of untreated micas as reinforcing fillers for general purpose polypropylene homopolymers can have important cost savings in the fabrication of mica-reinforced automotive components.

INTRODUCTION

Although the use of silane coupling agents are commonly accepted as necessary economic penalties in order to achieve improved performance in various filled thermoplastics, the high cost of such filler treatment has encouraged numerous attempts to find less expensive alternatives. In 1980, Newman and Meyer (1) disclosed a unique treatment in which a chlorinated paraffin wax was employed to achieve favorable interfacial adhesion in mica-filled polypropylenes, thereby imparting a marked increase in the flexural strength of the composite without adversely affecting the notched Izod fracture toughness, flexural modulus or heat deflection temperatures. Later, Plueddemann and Stark (2) and Erickson, *et al* (4) investigated the coupling mechanism of this chlorinated paraffin wax system and proposed possible mechanisms of interaction. Despite the favorable increase in the performance of the resulting mica-filled polypropylenes, the chlorinated waxes tended to decompose at processing temperatures and evolve hydrogen chloride gas, a corrosive gas that sometimes caused damage to the metal surfaces of molds and processing machinery despite the recommended use of neutralizing agents such as magnesium oxide or amines. The effectiveness of the chlorinated wax was also dependent upon the residence time and temperature during processing, an additional factor which tended to deter the widespread acceptance of this method as an alternative to the use of silane coupling agents. However, the pronounced effect of a relatively small proportion (1 percent) of chlorinated paraffin wax on the mechanical properties of mica-filled polypropylene suggested that similar improvements could be achieved with other organic waxes which might be less sensitive to thermal decomposition and would not depend upon prereaction for their effectiveness.

The ideal coupling agent should possess sufficient adhesion to the filler surface so that separation will not occur during composite fracture. Secondly, the coupling agent should possess adequate cohesive or chemical attachment to the matrix to ensure a strong interfacial bond for maximum tensile and flexural strength of the composite. Although coupling agents frequently cause a decrease in the fracture toughness, in special cases surface modification of a filler can actually increase the impact strength (4, 5). In general, it is difficult to simultaneously increase the strength, modulus, and fracture toughness of a thermoplastic by the addition of fillers, since attempts to increase one property usually causes a decrease in one or more of the others. The coupling of a nonpolar hydrocarbon polymer such as polypropylene to an inorganic filler particle poses a particularly difficult chemical problem, and the published literature contains numerous procedures for the chemical modification of hydrocarbon polymers either by copolymerization or by post treatment to provide coupling ability. One chemical modification of polypropylene has been accomplished by radical initiated grafting of acrylic monomers. For example Sasaki and Ide (6) disclosed the grafting of acrylic acid or maleic anhydride onto polypropylene for improved coupling to aminosilane-treated glass fibers. Gaylord and

Mishra (7) have studied the complex interaction between maleic anhydride and polypropylene in the presence of peroxides. Mitsubishi Petrochemical (8) claimed a 125 percent increase in the flexural strength of a mica-filled polypropylene using a combination of maleated polypropylene and special petroleum resins. Shedd (9) describes the use of acrylic acid modified polyolefin resins as dispersing aids and coupling agents for mica-filled thermoplastics. Such carboxyl containing polyolefins are also attractive for metal coatings and hot melt adhesives (10).

It is clear from the extensive literature that carboxylic groups have been particularly favored for promoting increased wetting and adhesion of polyolefins to inorganic fillers.

In the following study, low molecular weight maleated polypropylene (isotactic) waxes were evaluated as coupling agents for mica-polypropylene composites. These maleated polypropylenes have been previously described by Guillet and Coover (11) and are commercially available under the Epolene E-43 tradename from the Eastman Chemical Products Co. (12). This wax is prepared by the thermal degradation of high molecular weight isotactic polypropylene, a process which induces random scission by a free radical process (13, 14).

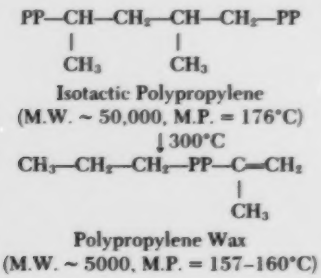

(1)

The thermal cracking reaction proceeds rapidly at temperature near 320°C and reaches a molecular weight of approximately 5000 g/mol after 30 minutes of heating.

Sawaguchi, *et al* (15) investigated the chemical structures of the thermally decomposed polypropylene and confirmed that the resulting unsaturated oligomers consisted mainly of vinylidene-type double bonds which retained the parent isotactic structure. Joyner and McConnell (16) reacted the unsaturated polypropylene oligomers with maleic anhydride using di-tert-butyl peroxide as initiator to form substituted succinic anhydride derivatives.

At the melt temperature the "ene" reaction described by Benn, Dwyer, and Chappell (17) can spontaneously occur even without the aid of peroxide.

This concerted reaction may only account for part of the product according to the mechanisms described by Gaylord and Mishra (7) when the reaction is conducted in the presence of a peroxide initiator such as di-t-butylperoxide or dicumylperoxide. Hydrogen abstraction is quickly followed by maleic anhydride addition according to the following scheme.

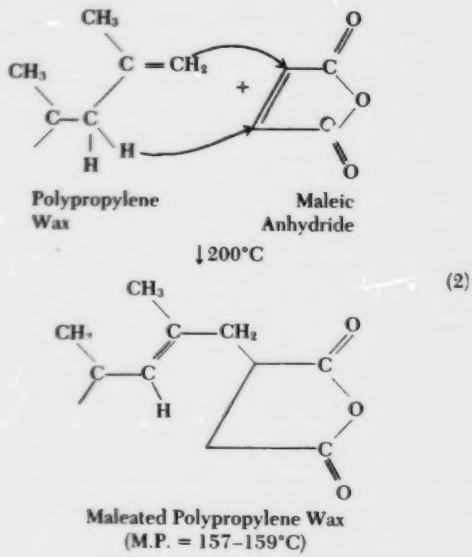

(2)

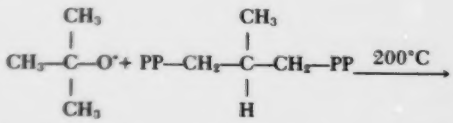

(3)

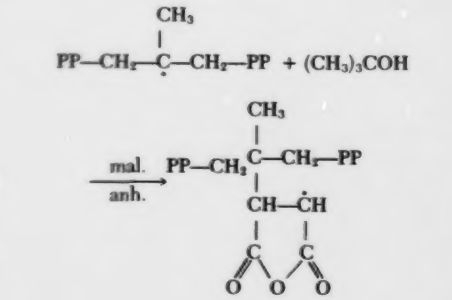

(4)

At 200°C the hydrogen atom selectivity may be nearly random so that substitution need not be solely restricted to the tertiary positions. The resulting maleate radical in *Eq 4* may undergo further polymerization with maleic anhydride, or terminate by hydrogen abstraction, recombination or disproportionation. Unreacted maleic anhydride can be conveniently removed by aqueous extraction of the powdered wax product.

The recovered maleated polypropylene may be used in granular form, ground to a fine powder or emulsified in aqueous ammonia solution. The use of the powdered or emulsified form is recommended for best results because the initial intimate particulate dispersion aids completion of the interfacial reaction with the filler surface during subsequent melt processing. The experimental technique is outlined in the following section.

EXPERIMENTAL

Isotactic polypropylene (250g Hercules Profax 6523PM resin) was heated for 30 min. at 320°C in a 500 mL glass reaction kettle equipped with a stirrer and heating mantle. After 30 min. the molten polypropylene had degraded to a melt viscosity of 500 cP (190°C, Brookfield Synchro-Lectric Viscometer) with a melting transition of 157 to 160°C.

The polypropylene oligomer (200 g) from the above reaction was mixed with maleic anhydride (10 g) in the same 500 mL reaction kettle equipped with a hot water condenser and dropping funnel. The mixture was heated to 200°C and a solution of di-t-butyl peroxide (0.51 g in 15 mL heptane) added dropwise over a period of 30 min. with constant stirring. After complete addition of the peroxide, the mixture was heated at 200°C for a further 30 min. when the reaction appeared to have reached completion. The recovered maleated wax had a melting point of 157 to 159°C and a melt viscosity of 700 cP at 190°C. The product was ground in a high speed pulverizer and sieved through a 48 mesh Tyler screen to remove the coarser particles.

Sample mixtures for injection molding were prepared by initially powder blending the components (mica, polypropylene, and maleated wax) in a plastic jar and then melt compounding the mixture in a Brabender twin screw counter-rotating extruder followed by granulation of the cooled strand. The data reported in this series were partially obtained using a plunger-type injection molding machine (Hilliard Model PM 225), which yielded standard ASTM tensile and Izod impact specimens. Additional samples were molded using a typical reciprocating screw injection molding machine (Engel Model ES80). Usually more than 10 specimens were tested to provide statistical reliability.

Phlogopite micas (Suzorite 60S and 200HK supplied by Marietta International) were selected for the majority of experiments. Silane pretreatments with γ-aminopropyl triethoxysilane (Union Carbide A-1100) and N-(3-trimethoxysilylpropyl)-N′-(p-vinylbenzyl) ethylenediamine monohydrochloride (Dow Corning Z-6032) were applied from methanol solution by the suppliers recommended techniques (18).

The contact angles of the cooled specimens were measured with a telescopic goniometer (Spindler and Hoyer) in which small particles of the polymeric materials (1 mm diameter) were placed on a sheet of mica and placed in an oven at 200°C for 10 minutes or until equilibrium was obtained.

RESULTS

The flexural properties parallel the tensile measurements for all the examples so that only the tensile data are reported here. The incorporation of a weighed proportion of the MPP wax into the mica-polypropylene molded composite produced in an increase in the tensile strength, reaching a limiting value near 5 percent by weight (relative to the mica mass). In *Fig. 1*, the tensile strength is seen

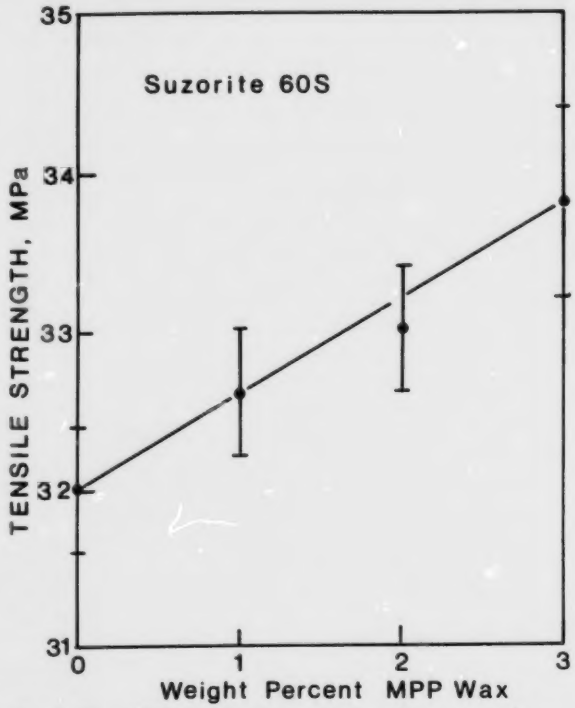

Fig. 1. The addition of maleated polypropylene wax produces a proportional increase in the tensile strength of the polypropylene (30 percent 60S mica) which reaches a maximum at approximately 5 percent MPP wax (relative to the mica).

to increase in proportion to the added wax for Suzorite 60S up to the largest wax concentration (3 percent of the mica weight). In this series the MPP wax was applied to the mica as a colloidal dispersion in dilute ammonia (pH 8) prior to mixing with polypropylene (Hercules Profax 6401). The method of preparing such dispersions has been described by von Bramer and McGillen (24), Johnson and Draper (25), and in Eastman Chemical Products brochures (26). *Figure 2* illustrates the influence of maleated polypropylene wax (MPP) on the tensile strength compared to untreated mica and mica treated with γ-aminopropyl trimethoxysilane (Union Carbide A-1100 silane). In the examples shown, the MPP concentration was proportional to the mica concentration, equivalent to 2.33 g MPP per 100 g mica. The silane treatment assumed complete reaction and was applied at the rate of 0.5 g aminosilane (A-1100 as supplied) per 100 g mica.

It is apparent that the MPP is more effective with silane-treated mica (Suzorite 200HK) despite the observed similarity in contact angle values reported in *Table 1*. There are additional indications that the maleated waxes differ in their coupling activity with micas from different sources. A parallel behavior was also found with the coarser mica grades (Suzorite 60S) as shown in *Fig 3*. It should be recognized that these results do not always reflect differences in coupling activity but may include other factors such as incomplete dispersion (due to inferior wetting characteristics or unfavorable viscosi-

ties). Note the large contact angle of polypropylene on untreated mica for example (*Table 1*).

The strength properties of the mica-filled polypropylene are sensitive to the molar ratios of MPP and A-1100 silane and appear to reach maximum efficiency near equimolar proportions. This is illustrated in *Fig. 4*. The stoichiometry of the system was determined by the modified titration technique used for the determination of resin acid numbers.

The corresponding modulus values are compiled in *Fig. 5* for the complete set of measurements and indicate a general trend which is only slightly influenced by the wax coupling agent. In a previous investigation (29) it was confirmed that the modulus was primarily dependent upon the flake aspect ratio and that the modulus and the mean aspect ratio both decline on prolonged or repeated processing of the melt. The presence of the MPP wax tended to produce modulus values near the upper bound of measurements whereas in the absence of added wax the modulus values were near the lower set of measurements at each filler concentration.

Figure 6 documents the observed changes in the notched Izod fracture energies with and without added MPP wax, the observed values falling within the standard deviation although the samples containing MPP wax were marginally greater. The fracture toughness can be more than doubled if a tougher resin is substituted (for example, Hercules Profax 6701PM) with only a small sacrifice in modulus.

Extrusion rheology confirmed that the addition of the MPP wax to an injection grade polypropylene considerably reduced the melt viscosity (*Fig. 7*) so that some compensating increase in the molecular weight of the polypropylene matrix is desirable to restore the optimum melt viscosity.

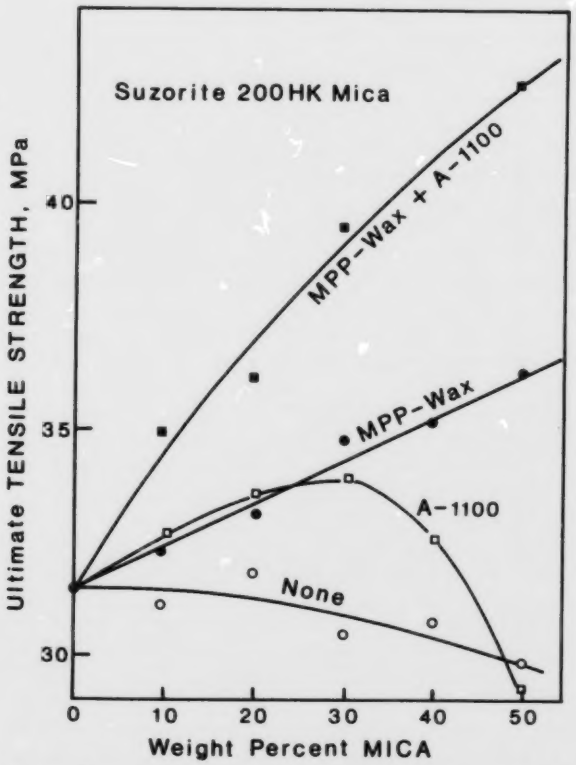

Fig. 2. The maleated wax also increases the tensile strength of polypropylene containing 40 percent Suzorite 200HK mica, with the combined use of aminosilane and wax having an additive effect at all filler concentrations.

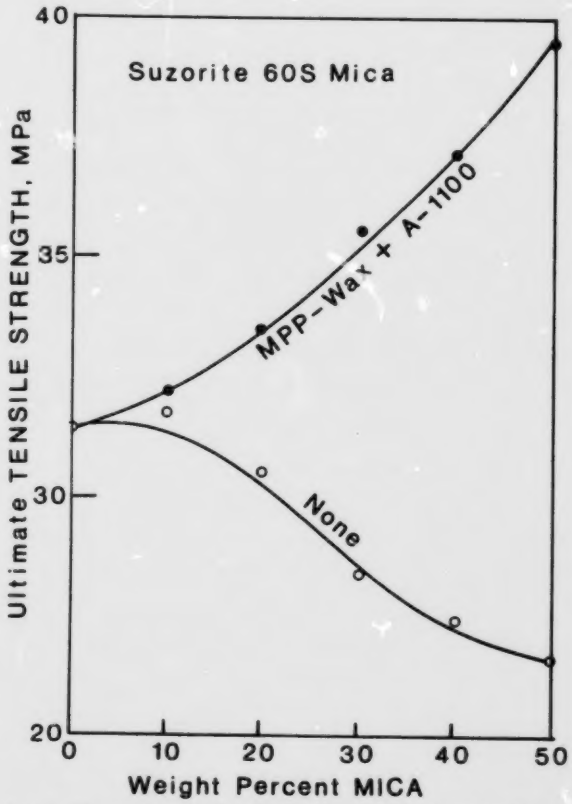

Fig. 3. The combined use of aminosilane and maleated polypropylene wax with 40 percent Suzorite 60S mica shows a similar trend to that of Suzorite 200HK mica.

Table 1. Relationship Between Contact Angle and Ultimate Strength*
(40 percent mica in polypropylene)

Resin	Surface	Contact Angle (°)	Tensile Strength MPa	Flexural Strength MPa
Polypropylene (Hercules 6523 PM)	untreated sheet mica	30.8 ± 2.1	30.8 ± 2.1	61.4 ± 2.8
Maleated polypropylene wax	untreated sheet mica	12.5 ± 2.6	35.3 ± 2.1	67.9 ± 3.7
Maleated polypropylene wax	A-1100 silane treated mica	12.2 ± 1.8	38.2 ± 1.2	74.3 ± 4.0

* Including 95 percent confidence limits.

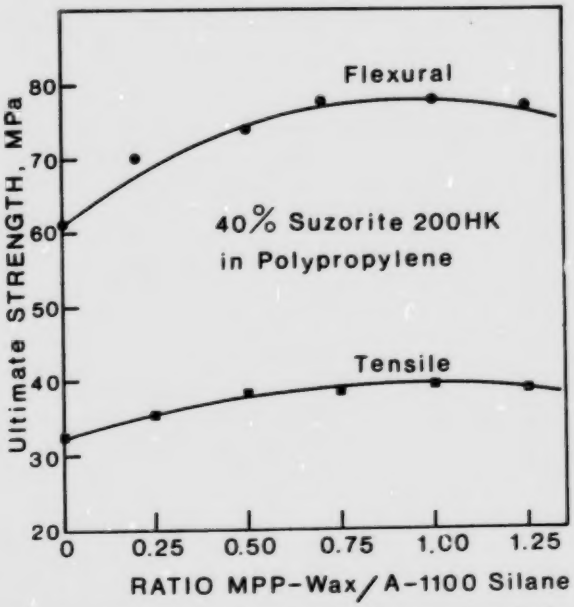

Fig. 4. The maximum increase in strength occurs at equimolar ratios of aminosilane and maleated polypropylene wax.

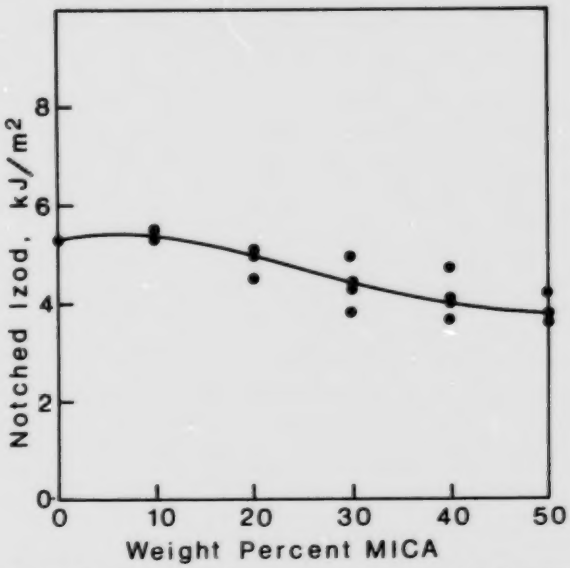

Fig. 6. The notched Izod Fracture energy values tend to decrease slightly as the mica content increases. Samples containing MPP wax are near the upper bound but within standard deviation limits.

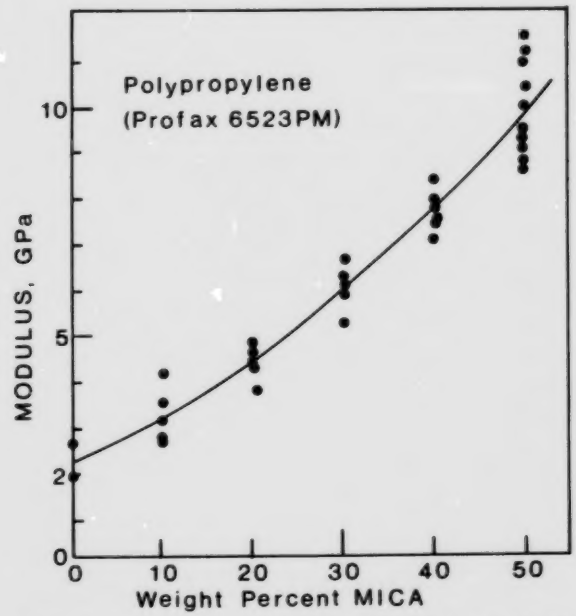

Fig. 5. Flexural modulus values follow the predicted trend with moderate increase in stiffness in the samples containing MPP wax (upper bound).

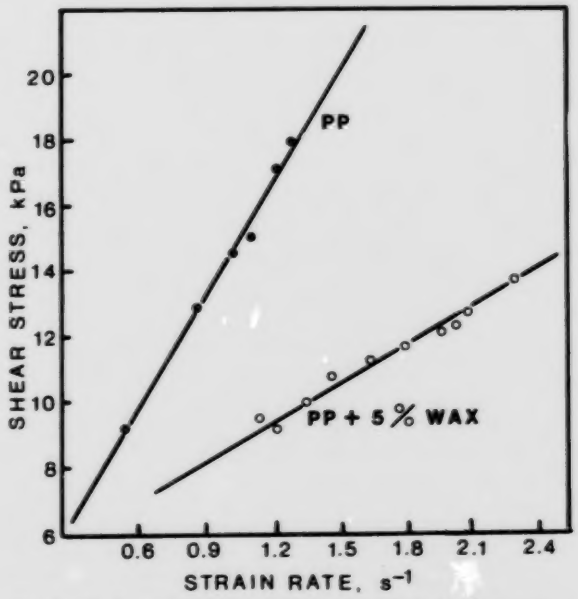

Fig. 7. The low molecular weight of the maleated polypropylene wax (ca ~ 5000 g/mol) reduces the viscosity of the melt.

DISCUSSION

Polypropylene with a surface free energy of 29 mJ/m^2 would be expected to adhere strongly to mica since mica has a much larger surface free energy (~200 mJ/m^2) when perfectly dry (19). However, inorganic materials such as mica strongly adsorb water molecules from the air so that the surface free energy is considerably reduced, often to values less than 30 mJ/m^2 (20). This monolayer of water is tenaciously retained up to temperatures of 440°C (21). The contact angle of polypropylene on mica was reduced from 61 to 12.5°C after maleation, evidence that the polar maleate group has a much greater affinity for the hydrated mica surface. This improved adhesion was reflected in the greater tensile and flexural strength values of the mica-filled polypropylenes containing the maleated wax. Further gains in the composite strengths were obtained using aminosilane-treated micas. This was attributed to the chemical reaction which presum-

ably occurred between the basic amino group of the silane and the acidic functionality of the maleate group, viz.

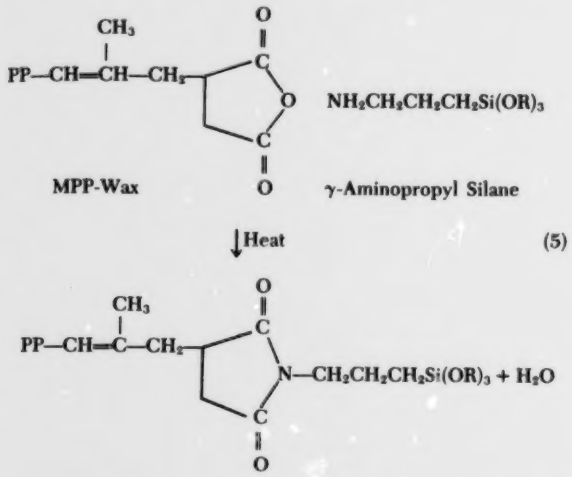

Evidence for this reaction was inferred from the observed maximum strength which occurred near the molar equivalence point.

Although it is common practice in industry to preblend filled thermoplastics prior to injection molding, the use of maleated waxes allows the powder blends to be directly molded without any significant sacrifice in performance. A typical example is reproduced in *Table* 2 which illustrates the slight difference in properties between the same compound directly injection molded from a simple powder mixture and after melt compounding in a Gelimat mixer. Eliminating the compounding step can have significant cost savings for the fabricator. In many applications, the additional strength afforded by silane treatment of the filler is not warranted so that lower cost untreated micas can be substituted. The surface treatment of finely ground micas with emulsified waxes helps to reduce dust formation during handling while aiding filler dispersion during subsequent melt compounding.

Functional polypropylene waxes apparently adsorb at the filler interface, perhaps forming a ductile zone around each particle which contributes to improved stress transfer between the rigid filler and the polymeric matrix, a region which can be manipulated by the choice of polar wax to change its thickness or its chemical composition to meet various design requirements (27). At processing temperatures the low melt viscosity of the wax contributes to faster mixing and dispersion. The high melting point (ca ~160°C) of the maleated wax also helps to retain elevated heat deflection temperatures and aids dimensional stability in molded components.

For many applications which do not require virgin materials, reclaim or scrap polypropylene can be conveniently converted into maleated waxes for added material cost savings. Although as much as 10 percent MPP may be incorporated into filled resins, care must be taken to compensate for the reduction in melt viscosity and fracture toughness by choosing a base resin with a correspondingly larger molecular weight. In practice, however, 1 percent MPP (relative to the mass of mica) has been found adequate for injection molded products.

Maleated polypropylene waxes are efficient dispersing aids and coupling agents for other inorganic and organic fillers. A parallel study revealed that MPP is an efficient coupling agent for polypropylene resins filled with wood pulp (22). The small contact angle of MPP on a variety of inorganic substrates suggests that these waxes should also have broad utility with many other types of fillers in polypropylene resins.

Note that the coupling action with the matrix is dependent upon intersegmental crystallization, a type of interaction that is specific to isotactic polypropylene structures. Although MPP waxes may have utility as dispersing aids in other polymers, the lack of any cocrystallization may limit the cohesive forces and attendant coupling ability unless significant interpenetration occurs at the interface (23).

The use of maleated polypropylene waxes as coupling agents in filled polypropylene has been covered by patent (28).

Table 2. Direct Injection Molding of Powder Blends*

	Powder Blend	Melt Compounded
Tensile strength, MPa	32.5	34.2
Flexural strength, MPa	63.8	67.1
Flexural modulus, GPa	5.8	5.2
Notched Izod, J/m	34.6	32.8

* Compound formula: 75 parts Hercules Profax 6523; 25 parts Suzorite 608 mica; 0.2 parts stabilizer.

CONCLUSION

Maleated polypropylene waxes aid dispersion and promote coupling in mica-filled polypropylene resins. The addition of 1 to 5 percent maleated wax increased the tensile and flexural strength values without significantly altering the modulus or fracture toughness. Although these carboxylated waxes can substitute for silane coupling agents, aminosilane treatment of the filler further increases the strength. The powder blending technique permits direct injection molding without the need for a preliminary melt compounding stage when the MPP wax is used as an additive, without any serious sacrifice in performance. Maleated polypropylene waxes seem to provide similar advantageous increases in mechanical properties afforded by the use of chlorinated paraffin waxes without the undesired corrosive behavior or delayed action. The strong cohesive forces at the filler interface were attributed to intersegmental crystallization between the isotactic wax and the polypropylene matrix. The evidence suggests that such waxes should provide coupling with most inorganic fillers in crystalline polypropylene resins. The relatively low cost of mica and the large specific stiffness of mica-containing thermoplastics is of particular interest in

automotive applications (such as fan shrouds) which require molded parts having improved dimensional stability at elevated temperatures, minimum weight, and resistance to fracture.

ACKNOWLEDGMENTS

The influence of polypropylene wax on the extrusion rheology of mica-filled polypropylene was contributed by L. P. Hébert while a visiting scientist from the Industrial Materials Research Institute, Montreal. The authors also wish to express appreciation to the Natural Sciences and Engineering Research Council of Canada (NSERC) (Grant A4873) and to General Motors of Canada for supporting these investigations.

REFERENCES

1. S. Newman and F. J. Meyer, *Polym. Compos.* **1**, 37 (1980).
2. E. P. Plueddemann and G. L. Stark, 35th Ann. Tech. Conf., SPI RP/C Inst., Section 20-B, 1980.
3. D. Stevenson, D. Windrath, and R. Burge, 36th Ann. Tech. Conf., SPI RP/C Inst., Section 9-B, 1981.
4. P. W. Erickson, A. A. Volpe, and E. R. Cooper, 19th Ann. Tech. Conf., SPI RP/C Inst., Section 21-A, 1964.
5. N. G. Gaylord and A. Takahashi, ACS Reprints 183rd Meeting, Organic Coatings and Applied Polymer Science, Vol. 26, pp. 95–99 (1982).
6. I. Sasaki and F. Ide, *Kobunski Ronbunski*, **38**, 67 (1981).
7. N. G. Gaylord and M. Mishra, *J. Polym. Sci. Polym. Lett. Ed.*, **21**, 23 (1983).
8. Mitsubishi Petrochemical Co., Japanese Pat. 76,041 (1981).
9. C. Shedd, SPE NATEC, Bal Harbour, Fla., Oct. 26, 1982.
10. P. J. Ludwig, *Mod. Plast.*, **1**, 73 (1983).
11. J. E. Guillet and H. W. Coover, *SPE J.*, **16**, 311 (1960); U. S. Pat. 2,835,659 (1958), 2,828,296 (1958), and 3,243,395 (1966).
12. Eastman Chemical Products Inc., Industrial Chemicals Division, Kingsport, Tenn. 37662.
13. R. Simha, L. A. Wall, and P. J. Blatz, *J. Polym. Sci.*, **5**, 615 (1950).
14. T. E. Davis, R. L. Tobias, and E. B. Peterli, *J. Polym. Sci.*, **56**, 485 (1962).
15. T. Sawaguchi, S. Niikumi, T. Kuroki, and T. Ikemura, *Am. Chem. Soc., Div. Polym. Chem. Polym. Prepr.*, **20**, 925 (1979).
16. F. B. Joyner and R. L. McConnell, U. S. Pat. 3,480,580 (1969).
17. F. R. Benn, J. Dwyer, and I. Chappell, *J. Chem. Soc. (London), Perkins Trans. II*, **533**, (1977).
18. I. Chun, M.A.Sc. Thesis, Department of Chemical Engineering and Applied Chemistry, University of Toronto (1981).
19. I. Skeist, "Handbook of Adhesives", p. 40, 2nd Ed., Van Nostrand Reinhold Pub., (1972).
20. W. A. Zisman, *J. Paint Technol.*, **44**, 564 (1962).
21. G. C. Hawley and S. R. Locke, High Aspect Ratio Mica Composites, Proceed. 32nd Ann. SPI Conf. (Canada), 1974.
22. G. Thomas, D. Rogers, and R. T. Woodhams, Wood Fiber Composites, Proceed. Canadian Fracture Conference 8, p. 104, Alton, Ontario, 1982.
23. E. P. Plueddeman and G. L. Stark, 35th Ann. SPI Tech, Conf. RP/C Inst., Sect. 20-B, 1980.
24. P. T. von Bramer and W. D. McGillen, Soap and Chemical Specialties, Dec. 1966; available from Ref. 26.
25. L. P. Johnson and W. E. Draper, 61st Chemical Manufacturers Association Meeting, Chicago, Ill., May 13, 1975; available from Ref. 26.
26. Publication F-260, Eastman Chemical Products Inc., Industrial Chemicals Division, B-280, Kingsport, Tenn. 37662, Dec., 1976.
27. K. K. Mathur and S. B. Driscoll, *J. Vinyl Technol.* **4**, 81 (1982).
28. R. T. Woodhams and I. Chun, U. S. Pat. 4,442,243 April 10, 1984.
29. C. Busigin, G. M. Martinez, and R. T. Woodhams, *Polym. Eng. Sci.*, **23**, 766 (1983).

DISCUSSION

N. L. Brockman: You mentioned that in some examples the mica was pretreated with aminosilanes. Did you make any attempt to prereact the aminosilanes with maleated polypropylenes?

R. T. Woodhams: Not in this study. Current research will explore the feasibility of prereacting aminosilanes with maleated wax to synthesize a silanol-tipped oligomer.

C. Setterstrom: Have you had an opportunity to compare the properties of maleated waxes with higher molecular weight isotactic polypropylene, such as Hercules Profax PC-072? A second question: What is the molar ratio of polypropylene to maleic anhydride?

R. T. Woodhams: The addition of a small proportion of maleated wax to a regular grade polypropylene homopolymer produces mica composites having mechanical properties essentially the same as the acrylic modified polypropylenes such as Hercules Profax PC-072. In fact this research was prompted by our attempts to find a cheaper route than through the use of relatively expensive modified polypropylenes.

Chemical analysis revealed the presence of approximately one maleate group per molecule.

B. D. Favis: I would be interested to see more mechanical test data on these samples after exposure to humidity. Can you provide further details on this? Have you submitted the samples to an accelerated water boil test or other accelerated water exposure test to show what the long term effect of humidity would be on mechanical properties? This may be interpreted as an indication of whether there is an actual chemical reaction at the interface.

R. T. Woodhams: No. The effect of boiling water on the mechanical properties of the injection molded specimens was not determined. Contact angle measurements at temperatures near 100°C in saturated steam, however, indicate that the adhesion is retained on a wide variety of substrates including mica, glass, and limestone. While this is true for maleate functionality, it may not hold true for isolated carboxylic substituents due to differences in chelating ability.

S. Naik: I have two questions: 1. What is the cost of the maleated wax? And, secondly, do you think that addition of 3 to 5 percent of this material (to obtain optimum properties) is beneficial when compared with conventional silane treatment?

R. T. Woodhams: Maleated polypropylene wax is currently sold in the United States at a price near $3.00/lb so that depending upon the concentration employed, it will increase compound costs by less than 5 percent. Major cost savings are possible if

powder blends can be used, by-passing the normal melt compounding and pelletizing stages. Experience has shown that equivalent performance can be achieved compared to the silane treated micas, which are considerably more expensive than the untreated grades.

S. Naik: How did you apply the combination of silanes and waxes?

R. T. Woodhams: The silanes were applied to the mica surfaces from solution using the supplier's recommended technique. The waxes were added to the powder resin grades in either granular or powder form and mixed by normal compounding procedures with the treated micas.

S. Naik: Is there any particular reason why the aminosilane was selected? Usually, aminosilanes are not effective coupling agents with polyolefins.

R. T. Woodhams: The amino group is reactive towards the maleate end group so that a monolayer of isotactic polypropylene wax becomes chemically bonded to the surface of the mica. Coupling with the resin matrix then occurs through segmental crystallization at the interface.

A Novel Technique for the Study of Coupling Agent Phenomena

ANDREW GARTON

Division of Chemistry
National Research Council of Canada
Ottawa K1A OR6 Canada

A modification of the Internal Reflection Spectroscopy (IRS) technique for infrared (IR) spectroscopy is described, where the surface of the IRS element is modified by a thin (100 to 1000 Å) layer of metal oxides, silanes or Kevlar so as to model the surface of reinforcements in composite materials. The modified IRS element is then brought into contact with the matrix material and chemical changes in the first 2000 to 3000 Å of matrix examined by IR spectroscopy. Examples of the technique include a study of the effect of various surfaces on the crosslinking of an anhydride-cured epoxy resin. The kinetics of the crosslinking process and the final ester crosslink concentration are shown to be significantly affected by, for example, a silica or Kevlar surface. The advantages and limitations of this modified IRS technique are discussed relative to other surface characterization techniques.

INTRODUCTION

It is now established wisdom that the interface (or, more correctly, the interphase) between the reinforcement and the matrix material plays a crucial role in the properties of composite materials. This realization has prompted the development of a range of characterization techniques (with their attendant acronyms from AEPS to XRD) to examine the chemical and physical nature of the surfaces of the reinforcements and matrix materials (1). In particular, a variety of high vacuum techniques, involving the use of electron beams or X-rays, have made it possible to examine contaminants on these surfaces at fractions of a monolayer coverage. One such class of "contaminants", in this case added intentionally, is known as coupling agents. For example, organofunctional silanes, as well as a range of other organometallic or wholly organic compounds, are used to promote adhesion between organic polymers and inorganic reinforcements (2).

Despite the variety of surface characterization techniques available, it remains difficult to examine the interphase in situ, i.e., with the adhesive bond between the matrix and the reinforcement intact. Vibrational spectroscopy is the most successful technique in this regard because of its nondestructive nature, but conventional spectroscopic techniques (e.g., obtaining transmission spectra of thin samples or KBr discs) are insensitive to the small amount of interphase material because the total composite is sampled. For this reason we decided to modify and exploit the well established technique of internal reflection spectroscopy (IRS). The major advantage of IRS is that the region of the specimen which is sampled by the spectrometer is restricted to a thin layer (~1500 to 20000 Å) adjacent to the IRS element (3). This "depth of penetration" is determined by the optical constants of the element and of the sample, the angle of incidence, and the wavelength of the radiation. In the work described here, the depth of penetration is 3000 to 4000 Å, and so any interfacial effects will be averaged over this sampling depth, although the averaging process preferentially weights those regions of the sample closest to the element surface (the evanescent wave decreases in intensity going away from the element surface).

IRS has been used for at least twenty years, particularly for infrared (IR) spectroscopy, and its advantages and limitations are relatively well understood (3–5). The refinement of the technique, which is reported here, is to modify the IRS element surface by, for example, humid aging or the application of thin layers of silanes, metal oxides, or polymers, so as to model a variety of surfaces likely to be encountered in composite materials. The modified surface may then be brought into contact with the matrix material (thermoset or thermoplastic) and any chemical or physical changes which occur in the interphase can be examined by IR spectroscopy (*Fig. 1*). This approach is similar to that of Jakobsen, *et al* (6) for the study of biocompatibility and of Linde (7) for the study of polyamic acid-silane interactions but with the difference that the IRS element becomes an integral part of the

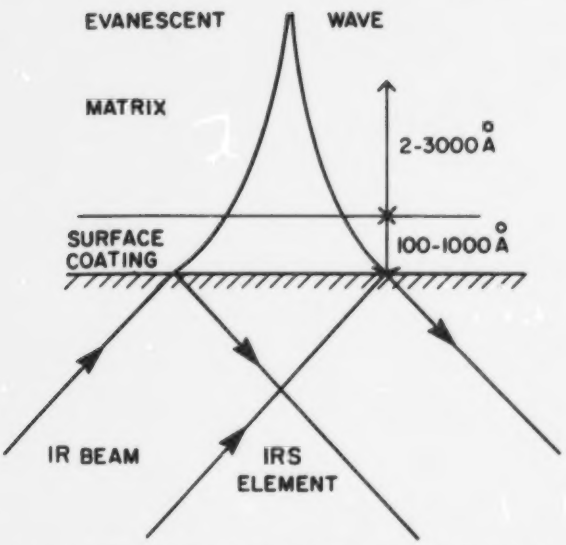

Fig. 1. A schematic representation of the internal reflection phenomenon using a surface-modified IRS element.

composite structure, so making it possible to correlate chemical changes with the performance of the adhesive bond.

EXPERIMENTAL

IR spectra were obtained at 4 cm^{-1} resolution using a Nicolet 7199 Fourier Transform (FT) IR spectrometer, equipped with a mercury-cadmium telluride detector and a Wilks Model 10 IRS attachment. Germanium and silicon reflection elements (50 × 20 × 2 mm, 45 or 60° incidence, Harrick Scientific Corp.) were used to obtain IRS spectra. Before use, the elements were optically polished (Synthetic Gem Materials B-5125), washed with distilled water, and dried in a vacuum oven at 120°C. On completion of each experiment, the element was cleaned by burning off the matrix material in a furnace, followed by coarse polishing with alumina to remove the oxide layer so produced (8).

The IRS element surfaces were modified by the following treatments: (a) *humid aging*—a germanium element was exposed to 100 percent relative humidity air at 26°C for two hours, (b) *SiO_2 coating*—a silicon element was heated in an air oven to 320°C for 30 minutes, (c) *GeO_2 coating*—a germanium element was heated in air to 440°C for 10 minutes, (d) *silane coating*—a germanium element was spray coated with 1 percent aqueous 3-aminopropyltriethoxysilane (APS, Aldrich) then vacuum dried at 90°C for 40 minutes, (e) *Kevlar coating*—a germanium element was dip-coated with a 0.4 percent solution of Kevlar 49 (Dupont) in concentrated sulphuric acid, then washed in water at 50°C for 40 minutes and dried in vacuum at 110°C for 30 minutes. The thicknesses of the modified surface layers produced by the above techniques were estimated by IR spectroscopy.

The matrix materials described here are an anhydride-cured epoxy resin (8) [Epon 828 (Shell) + Nadic Methyl Anhydride (NMA, Fisher, methylbicyclohept-5-ene-2,3-dicarboxylicacid anhydride) + benzyldimethylamine catalyst (BDMA, Ciba-Geigy)] and polypropylene [25 μm film made from Hercules isotactic resin, Soxhlet extracted with acetone to remove processing aids]. Compositional changes in the epoxy resin during the crosslinking process were followed by monitoring changes in the peak height of characteristic absorptions (1780 cm^{-1} for anhydride, 1740 cm^{-1} for ester groups, and 1509 cm^{-1} for phenyl groups) (8). Anhydride and ester concentration *indices* were obtained by ratioing their characteristic absorptions to the phenyl absorption at 1509 cm^{-1} (which should not vary greatly during the crosslinking process) and correcting the IRS spectra for the wavelength dependence of the depth of penetration (3).

RESULTS

Figure 2 shows the IRS spectra of thin layers of APS (~400 Å in *Fig. 2a*, *b*, ~300 Å in *Fig. 2c*) on a germanium reflection element, either alone (*Fig. 2a*), with a covering of polypropylene (*Fig. 2b*), or with a covering of the uncured epoxy resin/NMA mixture (*Fig. 2c*). Sufficient "windows" are present in the spectrum of the silane to allow information to be obtained about the chemical state of the overlaid polymer. Conversely, the IR absorptions

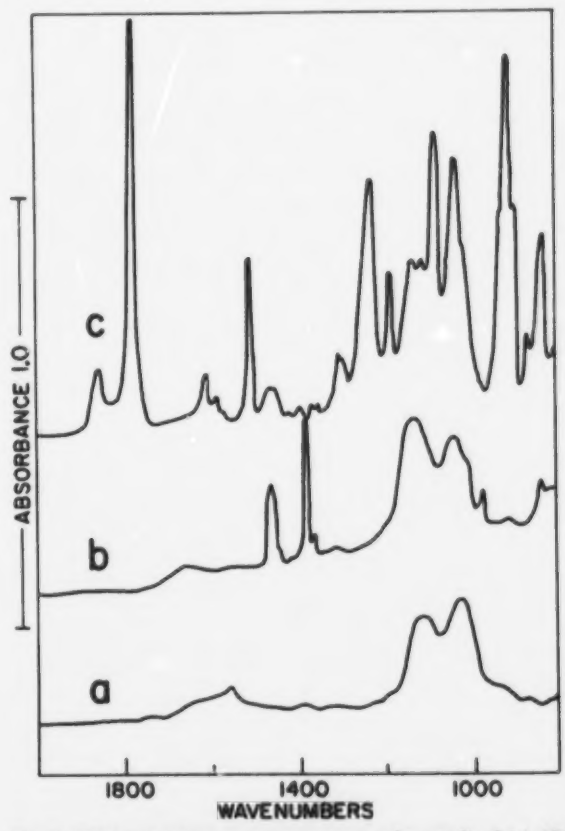

Fig. 2. IRS spectra (germanium spectrum subtracted) of (a) APS coated germanium element, (b) (a) with an overlayer of polypropylene, and (c) (a) with an overlayer of the epoxy resin/NMA mixture in the uncured state.

of the silane frequently are distinguishable from those of the polymer overlayer, allowing examination of chemical changes in the silane.

A detailed study of the effect of various surface treatments on the crosslinking kinetics of the epoxy resin is presented elsewhere (8) and some of the results are summarized in *Fig. 3*. Either humid aging or silane treatment of the surface increases the subsequent rate of anhydride consumption and reduces the residual anhydride level on completion of the cure cycle. Humid aging of the germanium also produces a slight decrease in the yield of ester products and this decrease is more pronounced after APS treatment of the surface. IRS data obtained with 60° incidence refer to a depth of penetration of about 3000 Å at 1700 cm^{-1} while 45° incidence refers to a depth of penetration of about 4000 Å.

A layer of germanium dioxide (GeO_2, several hundred Angstoms thick) produces a moderate IR absorption at 800 to 1000 cm^{-1} (*Fig. 4*) but the remainder of the spectrum is unobscured and so the effect of the oxide surface on the crosslinking process can be examined. *Figure 5* shows that the oxide film accelerates the consumption of NMA and reduces the yield of ester compared to the freshly polished germanium surface. Silicon IRS elements have less of a useful spectral window (opaque below 1200 cm^{-1}) but the effect of the SiO_2 surface on the crosslinking process could still be followed. On completion of the cure cycle, the matrix adjacent

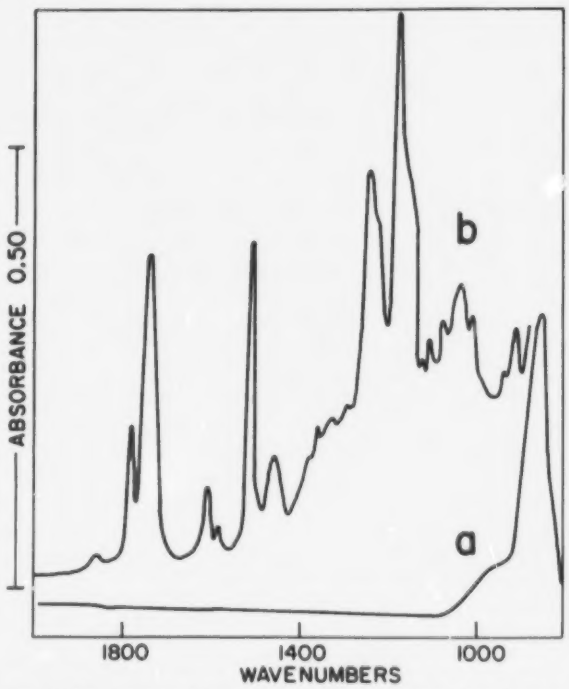

Fig. 4. IRS spectra of (a) thin layer of germanium dioxide on a germanium IRS element (germanium absorptions subtracted), (b) (a) with an overlayer of epoxy resin/NMA cured for 3 hours at 100°C and 3 hours at 150°C.

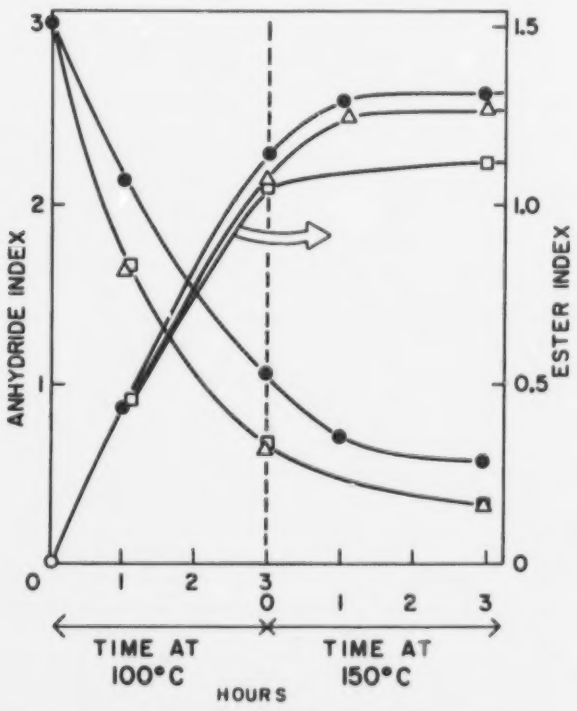

Fig. 3. A comparison of the kinetics of anhydride consumption and ester production for the crosslinking of epoxy resin/NMA on various surfaces. ●—● freshly polished germanium, 45° IRS, △—△ humid-aged germanium, 60° IRS, and □—□ APS treated germanium 45° IRS.

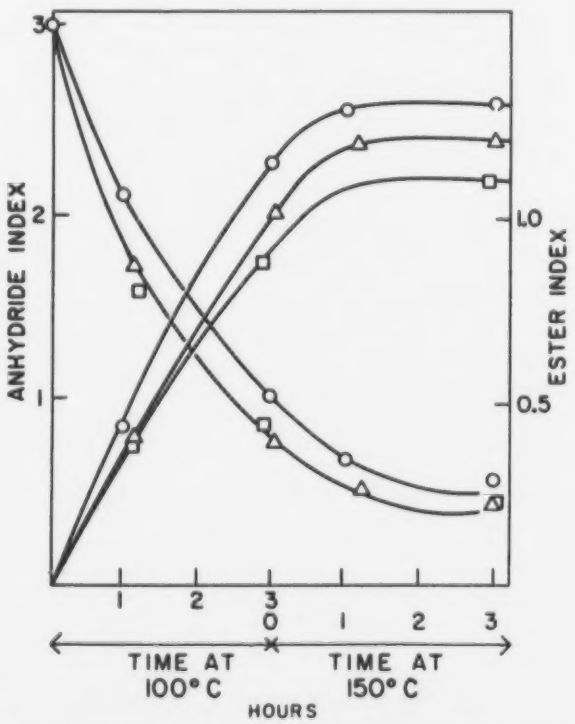

Fig. 5. A comparison of reaction kinetics for the curing of epoxy resin/NMA ○—○ on freshly polished germanium, 45° IRS, △—△ on germanium dioxide coated element, 45° IRS, and □—□ on silicon dioxide coated silicon element, 45° IRS.

to the SiO_2 surface had a ester-crosslink concentration almost 20 percent less than adjacent to the germanium control (*Fig. 5*).

The range of possible surface treatments is not restricted to inorganics. *Figure 6* shows the IRS spectrum of germanium covered with about 1000 Å of Kevlar. This important reinforcing material is known to require special care to ensure adequate interfacial bonding, and the spectrum of the overlaid matrix polymer (*Fig. 6*) shows that the crosslinking of the NMA/epoxy system is significantly affected by the aromatic polyamide surface. Quantifying the spectra, in this case, was complicated by the overlap of the Kevlar spectrum with the 1509 cm^{-1} reference band. This difficulty was resolved by the use of spectral subtraction to remove the Kevlar spectrum and also, as a check, by using the initial anhydride absorption as an internal reference. Both techniques led to the same conclusion that the yield of ester crosslinks is about 22 percent less in the ~3000 Å adjacent to the polyamide surface than adjacent to freshly polished germanium. The significance and possible causes (adsorbed water, traces of sulphuric acid solvent?) of this observation currently are being examined in more detail.

Finally, the usefulness of the "spectral subtract" facility of modern IR instrumentation should be emphasized. It is well known that IRS spectra are prone to distortions in band shape (3) and so spectral subtraction should be approached with some caution. However, subtraction of an IRS spectrum obtained with an untreated IRS element from a spectrum obtained with, for example, a silane treated element, allows rapid visual examination of how the surface treatment modified the chemical and physical structure of the overlaid polymer. *Figure 7* shows such a "difference" spectrum for the epoxy/anhydride system cured on the surface of a germanium IRS element, with and without APS silane treatment. The negative anhydride (1780 cm^{-1}) and ester (1740 cm^{-1}) absorptions (after scaling the spectra to eliminate the phenyl absorption at 1509 cm^{-1}) indicate that the silane treatment resulted in a decrease in residual anhydride and in the yield of ester crosslinks. The positive absorptions at ~1650 and 1550 cm^{-1} are consistent with the production of amide groups in the interphase by reaction of the aminosilane with NMA.

DISCUSSION

A detailed discussion of the mechanisms by which various surface treatments affect the crosslinking of the epoxy resin/NMA system is given elsewhere (8). Briefly, the majority of the observations were consistent with the reaction of adsorbed water with the NMA and reactions between the amino group of APS and either the epoxy resin or the NMA. The purpose of this manuscript is to describe the potential and limitations of this interphase characterization technique.

The major advantages of this technique are its nondestructive nature, the wide range of interphases which can be examined, and the fact that only the interfacial region is sampled by the IR beam. In principle, the technique is much more flexible than has been demonstrated here. For example, variable temperature IRS accessories are available commercially, so chemical changes in the interphase may be followed either as a function of temperature or as a function of time at an elevated temperature. One practical problem with high tem-

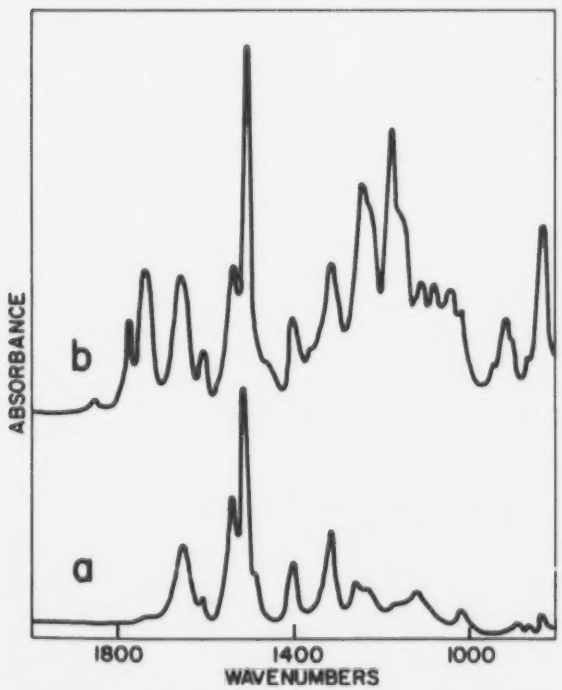

Fig. 6. IRS spectra of (a) thin layer of Kevlar on a germanium IRS element, (b) (a) with an overlayer of epoxy resin/NMA cured for 3 hours at 100°C and 3 hours at 150°C.

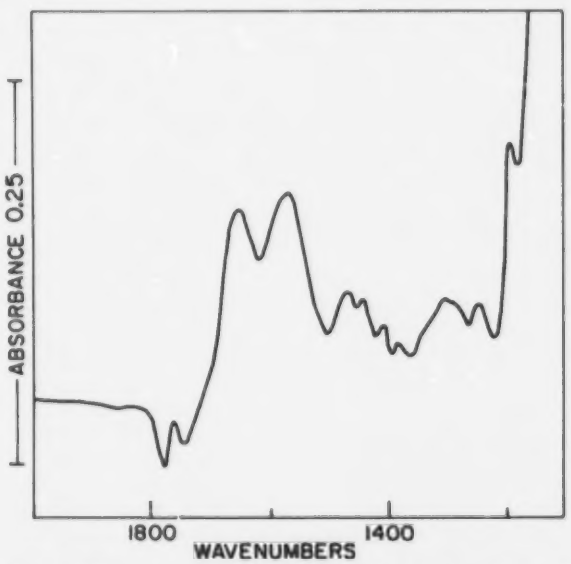

Fig. 7. Difference spectrum obtained by subtracting spectrum of epoxy resin/NMA cured on freshly polished germanium from spectrum of resin cured on APS treated germanium. Spectra scaled to eliminate phenyl absorption at 1509 cm^{-1}.

perature studies, however, is that the low frequency lattice modes of germanium move to higher frequencies at elevated temperatures, progressively obscuring the useful spectral region. The interphase may also be studied in aggressive environments, such as after immersion in boiling water, provided some care is taken to protect the uncoated germanium surfaces which experience slight pitting on prolonged exposure to boiling water.

In situations where a specific chemical species is formed by reaction in an interphase, e.g., amide groups in the APS/epoxy/anhydride system (*Fig. 7*), it is possible to use the modified IRS technique at least in a semi-quantitative fashion. Direct conversion of absorption intensity to a number of absorbing species (analagous to Beers Law in transmission spectra) is not possible from a single IRS spectrum in systems such as this, because the absorption intensity depends upon the spatial distribution of the absorbing species (i.e., their average distance from the IRS element surface) as well as their average concentration over the sampling depth. It is necessary, therefore, to obtain IRS spectra over a series of angles of incidence, and hence depths of penetration, (3) so as to set up a concentration profile of the interphase. Otherwise, it is necessary to assume a reasonable concentration profile (e.g., all amide groups are located within 1000 Å of the surface) and make concentration estimates accordingly.

The major disadvantages of the technique are its larger-than-desirable penetration depth and the fact that the modified IRS element may not satisfactorily model the desired reinforcement. IRS will detect relatively thin layers (<50 Å) of surface contaminants (9) but when used, as is described here, as one component of an adhesive joint, the spectrum of the surface contaminant will be "diluted" by the spectrum of overlaid material. Similarly, if chemical changes occur only in the first 100 Å of the matrix material, their detection will be difficult with a technique which has a penetration depth of 3000 Å. The technique is therefore most useful for situations where moderately thick (>100 Å) surface layers are studied or when chemical changes extend at least 100 Å into the matrix material. This limitation is not as restrictive as might first be imagined, however, because coupling agents are generally used in practice at multilayer coverage and interfacial reactions, e.g., oxidation or the acceleration of crosslinking, are frequently autocatalytic in nature and so their effects will extend some distance from the element surface. Several options are available to reduce the depth of penetration of the IRS technique but all involve some sacrifice. For example, silicon IRS elements can be used at higher frequencies than those reported here (>4000 cm^{-1}, the "overtone" region) and the depth of penetration will decrease with the wavelength. The disadvantage is that IR absorptions in this region generally are rather weak and this, coupled with the lower penetration depth, may lead to instrumental problems in reliably detecting such small absorptions. Internal reflection Raman spectroscopy is also possible (10) and since visible light is used, the depth of penetration potentially is less than with IR spectroscopy. However, the effect of reduced wavelength is counteracted to some degree by the low refractive indices (<2.0) of useful Raman IRS elements (e.g., sapphire). The low intensity of the collectable Raman scattering from such a system may also lead to problems with fluorescence and spectral signal-to-noise under many conditions.

One aspect of work currently in progress not mentioned here is the necessity to correlate observed chemical changes with the performance of the interphase. Germanium and silicon are sufficiently durable that some mechanical and environmental testing of the interphase bonding is possible on the same sample as was characterized spectroscopically. Clearly, a complete understanding of the nature of the interphase in composite materials cannot be obtained with one technique alone.

SUMMARY

Internal reflection spectroscopy in the infrared was one of the first surface characterization techniques to be developed. With certain refinements and the use of modern IR instrumentation, IRS still has a considerable role to play in characterizing the interphase in composites.

REFERENCES

1. W. L. Baun, *Applications of Surface Science*, **4**, 291 (1980).
2. E. P. Plueddemann, in "Composite Materials", Vol. 6 Ch. 6 Academic, New York, (1974).
3. N. J. Harrick "Internal Reflection Spectroscopy", Wiley, New York (1967).
4. P. A. Flournoy and W. J. Schaffers, *Spectrochim Acta*, **22**, 5 (1966).
5. W. N. Hansen, *Spectrochim Acta*, **21**, 815 (1965).
6. R. J. Jakobsen, S. Winters, and R. M. Gendreau, *Proc. SPIE—Int. Soc. Opt. Eng.* **289**, 469 (1981).
7. H. G. Linde, *J. Polym. Sci., Polym. Chem. Ed.*, **20**, 1031 (1982).
8. A. Garton, *J. Polym. Sci., Polym. Chem. Ed.*, in press.
9. W. Bascom, *Macromolecules*, **5**, 792 (1972).
10. R. Iwamoto, M. Miya, K. Ohta, and S. Mina, *J. Chem. Phys.*, **74**, 4780 (1981).

DISCUSSION

P. Cielo: Do you think that your technique could be used to monitor real life changes in a composite by, for instance, embedding an optical fiber in the matrix and making the spectroscopic measurements during the normal aging process of the composite? In particular, I am thinking of the moisture absorption during the real life.

A. Garton: Yes, this is feasible. Silicon or germanium are probably the best optical materials for this purpose. It is possible to buy "double pass" IRS elements which have the IR beam entering and leaving through the same end of the element. The other end could then be embedded in the composite.

L. Piché: How do you define the depth of the penetration? If you have a non-even surface, the radiation will not come back. It seems to me that

you are measuring the impedence of the surface, therefore you have to define the penetration in a clear mathematical term.

A. Garton: The penetration depth, d_p, is defined as a depth at which the intensity of the standing wave diminishes by a factor of e, i.e., to ~37 percent. The coupling of the sample to the wave diminishes with the square of the intensity, i.e., at d_p the coupling has diminished to about 13 percent of the value at the element surface.

L. A. Utracki: As you know, we are very much interested in polymer blends. Your comment about the possibility of spectroscopic analysis of polymer-A/polymer-B interphase is very exciting. You showed that with metal oxides, germanium or silicon oxides, you have a wide "window" in the spectrum, so you can see what is happening across this layer. When you deposit a thin layer of the polymer-A on the reflection element and then polymer-B, in order to see the interphase, you must not obscure it by the first layer, i.e., polymer-A. In other words, you must be very careful selecting your pairs of polymers and place them judiciously in a proper sequence.

A. Garton: Certainly you must have a "window" in the spectrum of the first polymer in order to see the second polymer.

L. A. Utracki: Do you have any idea which pairs you are going to look at?

A. Garton: I know that you are particularly interested in the polyester/polyamid interphase. Since nylon has the simpler IR spectrum, it might be possible to lay down a thin film of nylon and observe the polyester and the interphase through its windows (2000-1680 cm^{-1} and 1200-750 cm^{-1}).

L. A. Utracki: Marvelous. So we are going to have a presentation during the "Polyblend-'84" Symposium, on April 17th.

A. Garton: Why not!

Mechanical Degradation of Mica During Processing with Polypropylene

B. FISA, B. SANSCHAGRIN, *and* B. FAVIS

Industrial Materials Research Institute
National Research Council of Canada
75, boul. De Mortagne, Boucherville, Québec J4B 6Y4

Mechanical degradation of reinforcing fillers during processing is a problem that has been seldom studied due to a lack of particle size determination techniques. Using phlogopite mica as an example, a method allowing a rapid and accurate characterization of flake size and aspect ratio will be described. The influence of several parameters on the mechanical degradation of mica flakes in a mica/polypropylene system has been studied using a laboratory roller blade mixer. The degradation was found to occur in two stages. The first stage takes place immediately after the addition of mica, where the average flake size decreases very rapidly by as much as 20 percent. In the second stage, the particle size remains essentially constant with the time of mixing at low concentrations (2 percent wt); at higher concentrations (40 percent wt) there is a slow reduction in the flake size. The influence of other parameters such as system viscosity, mode of mica addition, silane treatment, and the initial particle size is also discussed.

INTRODUCTION

Reinforced thermoplastics are usually produced by incorporating a reinforcing filler such as glass fiber, mica, etc. into a molten resin. It is well known that filler particles are mechanically degraded during compounding, i.e., their dimensions are reduced as a result of stresses in the melt. This particle breakdown is highly undesirable as it reduces their reinforcing capacity.

The phenomenon of mechanical degradation is difficult to study due to a lack of fast and reliable particle size determination methods. Practically all the work published on this subject was carried out with glass fiber where the problem is reduced to the measurement of fiber length distribution curves on fibers recovered from processed polymer. Dry (1) or wet (2) sieving, microscopic (2–4) or image analysis (5) methods are usually used. The common conclusion of work on glass fiber filled thermoplastics is that the fiber length degrades considerably during compounding and processing. Von Turkevich and Erwin (5) for example, studied fiber length degradation during extrusion and injection molding of glass filled polypropylene, polystyrene, and thermoplastic polyester. These authors found that the amount of degradation was independent of fiber concentrations in the melt: an indication that the fiber-polymer rather than the fiber-fiber interaction is the principal cause of breakdown. The initial fiber length (before processing) was found to have little effect on the final fiber dimensions.

With mica or other planar fillers the problem is compounded by even greater difficulties in the particle size characterization. Unlike glass fiber, where the fiber diameter remains constant, with mica one needs to monitor two characteristic dimensions. The first is related to flake size, the other to its thickness. Woodhams and Xanthos (6) have reviewed the methods of flake size and aspect (i.e., diameter/thickness) ratio determinations and pointed out the need for automatic particle sizing methods. Regarding the mica flake degradation during processing very little is known. Okuno and Woodhams (7) measured the reduction of flake sizes during extrusion of mica filled polypropylene. Marked reduction was observed with all three mica particle sizes studied. Bataille and Bui (8) studying PVC-mica compounds also observed a significant reduction in average particle size resulting from blending in a high shear powder mixer. In these cases, microscopy (7) or sieving (8) was used to measure the particle size distribution.

Two types of interactions can be considered as possible causes of flake size degradation in the mica-filled polymer melt:

Flake-Polymer Interactions

If stresses induced by viscous drag on a particle exceed its strength the particle will break. For an aggregate of two spherical particles in contact with

with mica density $\rho = 2840$ kg/m^3 (W is the total mass of the sample). For monodispersed circular flakes $\Psi = 2p/3$, where p is the aspect ratio defined as $p = d/h$ (h is the flake thickness); for square ones $\Psi = \pi p/6 = 0.52p$.

The characteristics of mica are given in the first row of *Table 2*.

Sample Preparation

The samples were prepared on Brabender roll mill (Model PM 2000), (30 percent difference in speed between the two rolls) at 200°C. First, the "master batch", sample PP-60, was prepared. Its formulation was:

40 wt percent of PP (containing 0.2 wt percent of antioxidants)
60 wt percent of screened mica.

Antioxidants Inorganox 1010 and Inorganox 1024 (Ciba-Geigy) in a 1:1 ratio were used. First, the resin and antioxidants were compounded, then mica gradually added. The mixing time (following addition of mica) was 10 min. After cooling the compound was granulated.

The remaining samples: PP-5, PP-10, PP-25, and PP-40, containing respectively $c = 5$, 10, 25, and 40 wt percent of mica, were prepared by dilution of PP-60 with pure PP resin. First, PP was compounded with antioxidants, then the desired amount of granulated PP-60 was added. It took about 2 minutes to melt the granules. Afterwards, the samples were compounded for 5 minutes, chilled and granulated. The PP sample used in the tests was also roll-mill compounded with the antioxidants. During preparation, an effort was made to keep all the variables (except the mica content) constant: sample volume was 250 ml, temperature 200°C, rolls speed 40 rpm, gap 3 mm and the total milling time (calculated for PP) 15 minutes.

For RMS measurements the granulated samples were compression molded at 170°C for 5 minutes under 20 Mg of loading. For ICR the granules were used directly.

Rheological Measurements

The Rheometrics Mechanical Spectrometer, RMS, Model 605, was used in the dynamic mode in parallel plate geometry at 180°C. Both 2.5 and 5 cm diameter plates, polished as well as serrated, were used. Following the established procedure (5, 6, 8, 9) first the strain and time dependence of the storage, G', and loss, G'', moduli were examined at two frequencies $\omega = 1$ and 10 rads/sec. Next, the frequency sweeps at constant (for all samples) strains $\gamma = 10$, 30, and 50 percent were carried out. The tests were done in air as well as in nitrogen.

The Instron Capillary Rheometer, ICR, Model 3211, was used to measure the steady state viscosity, η, at higher rates of deformation. Using a series of capillaries (listed in *Table 3*) the rates of shear $\dot{\gamma} = 5$ to 2×10^4 sec^{-1} were obtained. The results $\eta = \eta(\dot{\gamma})$ were computed taking into account the Bagley and Rabinowitsch corrections (8). In a special series of measurements, using capillary No. 4, the samples were extruded at three speeds and the steady state extrudates were collected in hot fluorosilicone oil (Dow 1265), the diameter, D, measured and the extrudate swell ratio, $B = D/D_o$, (D_o is the capillary diameter) was calculated (9). The results are listed in Table 4.

Morphological Tests

The specimens sheared in RMS or IRC were observed under optical and in scanning electron (SEM, JFOL Model JSM-35CF) microscopes. Selected results are shown in *Figs. 1* and *2*.

RESULTS

Mica Dimensions

The mica flake sizes are listed in *Table 2*. It can be seen that incorporation of the flakes into the master batch PP-60 reduces the average flake diameter by 15 percent and the shape factor by 16 percent. The subsequent compounding of PP-60 into the other PP-samples further reduced d_o by 7 percent and Ψ by 11 percent. However, for $c < 60$ percent the flake dimensions are independent of c and only slightly affected by the ICR (see *Table 2*): $d_o = 137 \pm 3$ μm, $\Psi = 60.4 \pm 3.0$.

Table 2. The Geometry of Mica Flakes.

No.	Operation	d_o (μm)	Ψ
1.	Before incorporation in PP[a]	174.3 ± 0.5	82.4 ± 1.7
2.	After compounding in PP-60	148.3	69.2
3.	After re-compounding in PP-5	138.6	66.3
	After re-compounding in PP-10	139.7	63.1
	After re-compounding in PP-25	136.3	59.1
	After re-compounding in PP-40	136.3	56.9
4.	After ICR test[b] of PP-5	138.0 ± 3.3	61.1 ± 2.5
	After ICR test[b] of PP-25	134.4 ± 4.2	58.5 ± 0.8
	After ICR test[b] of PP-60	143.1 ± 2.0	59.3 ± 2.3

[a] Average values of three tests and their standard deviations.
[b] The average values from three samples extruded at $\dot{\gamma} = 16$, 173, and 2938 sec^{-1} with their standard deviations.

Table 3. Dimensions of ICR Capillaries (in cm).

Capillary No.	Diameter, D_o	Length, L	L/D_o
1	0.1278	5.0993	39.9006
2	0.1330	1.3000	9.7744
3	0.1310	0.1510	1.1527
4	0.0775	2.5438	32.8232
5	0.0747	0.1500	2.0080
6	0.0762	0.0434	0.5696

Table 4. The Extrudate Swell Ratio B for PP-Mica Samples at the Three Apparent Rates of Extrusion, $\dot{\gamma}_a$, at 180°C.

No.	Sample	$B \times 10^2$ at $\dot{\gamma}_a$ = 52	156	520	Density at 180°C ρ(kg/m^3)
1	PP-0	170 ± 2	179 ± 6	221 ± 4	764
2	PP-5	145 ± 6	159 ± 3	180 ± 1	792
3	PP-10	137 ± 1	143 ± 3	164 ± 3	824
4	PP-25	117 ± 1	120 ± 1	133 ± 1	935
5	PP-40	103 ± 1	104 ± 1	121 ± 1	1080
6	PP-60	96 ± 3	97 ± 2	100 ± 1	1361

each other, the maximum force, F_{max} which tends to separate them is equal to (9):

$$F_{max} = 3\pi\eta\dot{\gamma}r_1r_2 \quad (1)$$

where η is the polymer viscosity, $\dot{\gamma}$, the rate of shear; r_1 and r_2 are the radii of the spheres. This equation underlines the importance of the shear stress, $(\dot{\gamma}\cdot\eta)$, and of the particle size.

Flake-Flake Interactions

Some of the flake-flake collisions in the flowing polymer melt result in flake breakdown. This process can be considered analogous to the orthokinetic flocculation for which Smoluchowski (10) derived the following equation

$$-dn/dt = 4\alpha\phi\dot{\gamma}n/\pi \quad (2)$$

where n is the particle number concentration; $\dot{\gamma}$, the shear rate; ϕ, particle volume fraction, and α is the fraction of collisions ending in flocculation. This equation shows that the number of collisions in a sheared suspension is proportional to the shear rate $\dot{\gamma}$ and to ϕ. By analogy we can consider α to be the fraction of collision leading to flake fracture. This probability of fracture is likely to be related to the forces acting on colliding particles, i.e., to the shear stress and to the particle size.

It is obvious that the complexity of interactions in flowing filled polymer melts is such that these concepts (Eqs *1* and 2) are useful only for qualitative interpretation of flake size degradation.

The objective of this work is to study the mechanical degradation of mica flakes during compounding on the laboratory equipment and to relate it to common processing parameters such as: mica concentration and particle size, mixing time, polymer viscosity, mode of mica addition to the polymer, effect of silane treatment, etc. A recently developed method (11) based on the HIAC particle size analyzer which permits rapid and accurate determination of both particle size and shape factor is used in this work. The shape factor is closely related to the aspect ratio.

EXPERIMENTAL

Materials

Polypropylene

Three resins of different melt viscosities were used. All were in the powder or "as polymerized" form. Their properties are summarized in *Table 1*.

Table 1. Characteristics of Polypropylene Resins*

Name	Melt Index, g/10 min. (ASTM D 1238)	Intrinsic Viscosity (Decahydronaphthalene, 135°C)
Profax** 6301	12	1.7
Profax 6501	4	2.25
Profax 6701	0.8	3.1

* Data provided by the supplier.
** Trademark of Hercules Inc.

Table 2. Characteristics of Mica Used

Nominal Sieve Cuts, Mesh	Upper and Lower Sieve Opening	d_w,* μm	ψ*	Particle Count, (>3 μm)/g
84–120	213–147	257.2	82	6.6×10^6
120–230	147–73	174.3	82	21.8×10^6
230–400	73–38	113.3	68	75×10^6

* See the section on particle size analysis.

Mica

Phlogopite mica was used throughout this study. The Suzorite 200 HK grade was separated into three fractions by wet sieving using the Sweco Vibro-energy separator—Model LS18C33. The sieve cuts were 84 to 120, 120 to 230, and 230 to 400 mesh. Flakes larger than 84 mesh and finer than 400 mesh were discarded. Each fraction was subsequently washed on the Sweco separator to remove as much of the fines as possible. *Table 2* summarizes the characteristics of these three fractions and their flake size distribution curves are shown in *Fig. 1*.

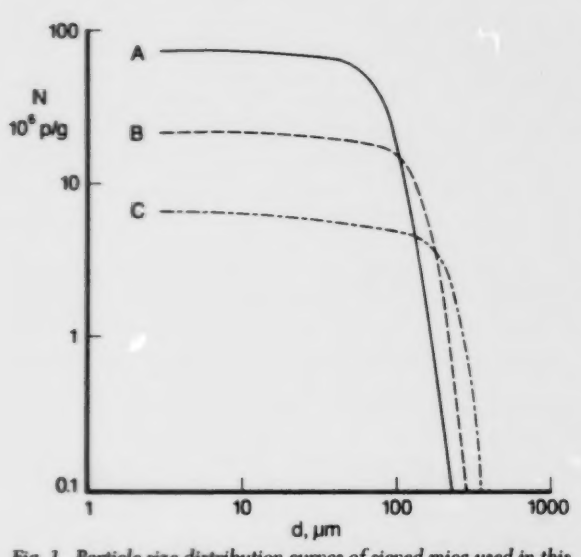

Fig. 1. Particle size distribution curves of sieved mica used in this study. N is the cumulative number of particles greater than d per 1 g of mica. A: 230 to 400 fraction; B: 220 to 230 mesh, C: 84 to 120 mesh.

Silane Treatment

The silane used was a cationic vinyl benzyl silane from Dow Corning Inc. (Trade name Z-6032). Its molecular formula is $(CH_3O)_3\ SiCH_2CH_2CH_2\ NHCH_2CH_2NHCH_2(C_6H_4)CH = CH_2\cdot HCl$. The mica samples were treated for 2 hours with a 0.5 percent (g silane/g H_2O) aqueous solution of the above silane. The pH of the aqueous silane solution prior to the addition of mica was adjusted to pH 4.5 with acetic acid. The treated mica was filtered and washed. The quantity of silane on the surface of mica was determined by carbon analysis (12) to be 0.5 percent (g silane/g mica).

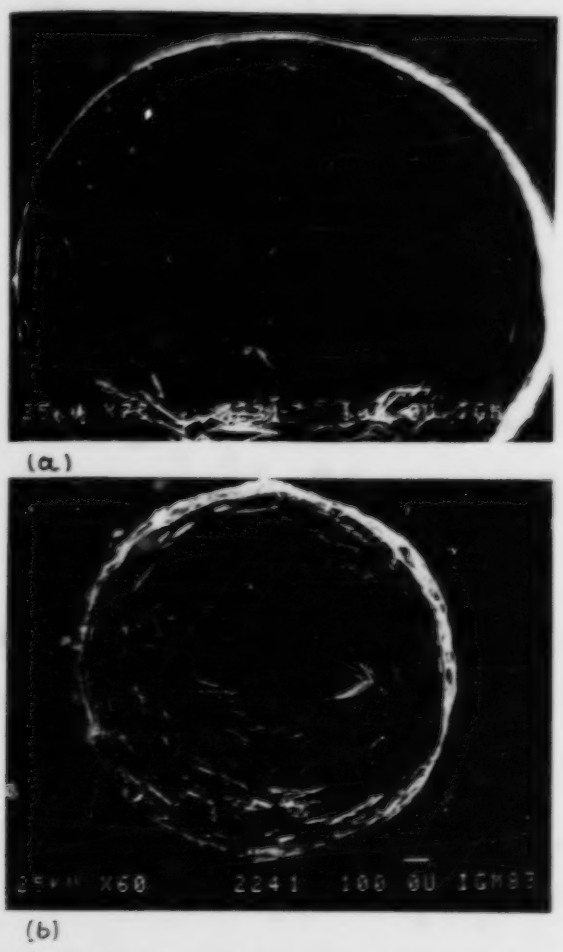

Fig. 1. The SEM micrographs of the cross-section of ICR extrudate of (a) PP-10 and (b) PP-40 ($\dot{\gamma}$ = 10 sec^{-1}, D = 1.278 mm, L/D = 39.9).

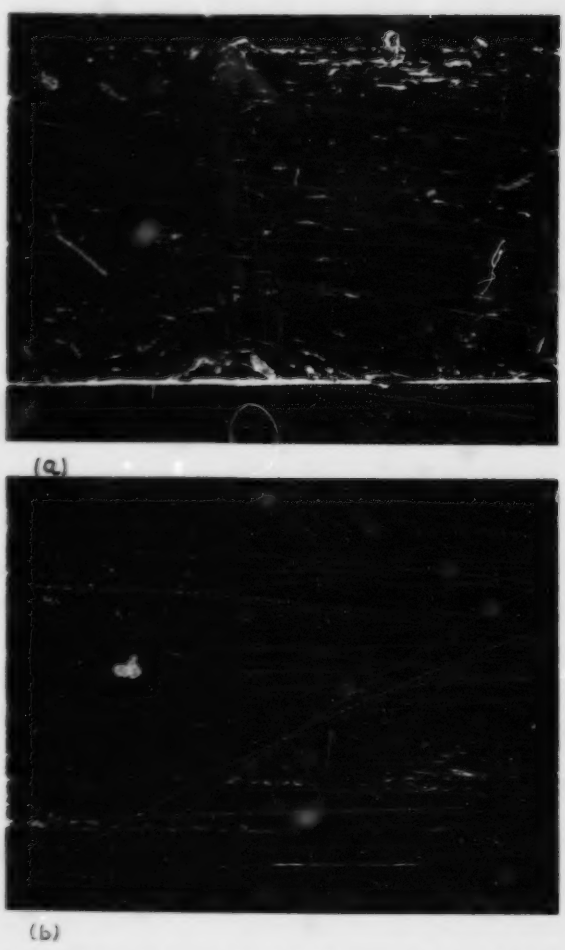

Fig. 2. The SEM micrographs of the edge cross-section of the RMS samples (a) PP-10 and (b) PP-40 after testing at ω = 10 rad/sec for 30 min.

Dynamic Measurements

Time Sweep

Two hours time sweep for PP at 180°C at γ = 10 percent and ω = 10 rads/sec is shown in *Fig. 3*. As usual, the most sensitive parameter is G' which decreased by 3.48, 2.16, 1.79, and 1.78 percent during the consecutive four 30 minute periods. The decreases in G'' were about half as large. Since the normal time of measurements varies from 7 to 20 minutes the sample was considered to be thermally stable and the above effects were neglected in the calculations.

To compare the effect of mica on the thermal stability of the samples the semi-log plot: G' *vs.* t (*Fig. 4*) was constructed. In these coordinates the constant slope indicates a first order reaction (10). It is quite apparent that while this behavior is observed for PP, it is not so for the samples containing mica. Here there are clearly two processes, one relatively rapid, dominant during the first $t \leq 40$ minutes, increasing in magnitude with mica content, and the second, slower, occurring at approximately the same rate for all samples. Since the first mechanism strongly depends on frequency (for PP-10 it is barely detectable at ω = 1 rad/sec), it may be postulated that its origin is associated with an ordering of mica flakes in the sample.

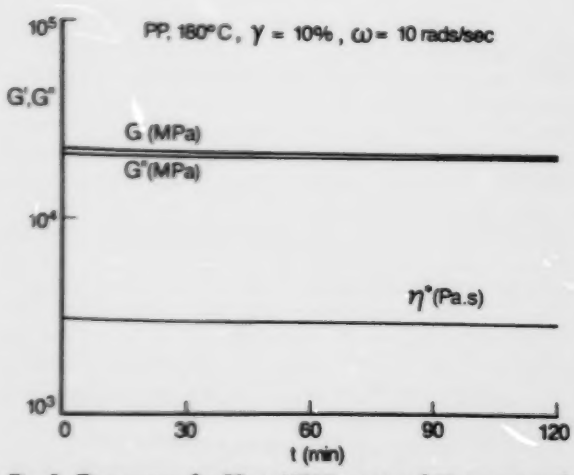

Fig. 3. Time sweep for PP at 180°C, strain of 10 percent and frequency of 10 rads/sec.

Compounding

Equipment

The compounding was carried out on the Plasticorder torque rheometer—Model EPL-V5501 fitted with the roller blade batch mixer from C. W. Brabender Inc. The roller blade mixer is commonly used with materials requiring strong shear forces.

Compounding Procedure

For each run, the weight of ingredients was calculated to keep the batch volume constant at 50 ml at the compounding temperature. The values of 0.75 g/cm^3 (13) and 2.84 g/cm^3 were used as densities of polypropylene and mica respectively.

Two modes of addition of mica to polypropylene were used:

- Addition to molten resin. Mica was added gradually to the molten resin with the mixer running. For concentrations up to and including 25 percent (wt), it took 1 minute to incorporate all the mica; 40 and 60 percent blends required 2 minutes. Three minutes were needed for blends containing 70 percent mica. The mixing times mentioned below do not include this time. The work of mixing, W, was calculated using the formula (14)

$$W = 2\pi BA$$

  where B is the mixer speed in rpm, A is the value of the area under the torque-time curve as supplied by the torque integrator. The values of W used throughout this work include the mixing work performed on the blend between the time of first mica addition and the end of the experiment.
- Blending of mica with polypropylene powder prior to compounding. The mica and polypropylene blends were loaded into a hot running mixer. After about 1 minute as the polymer started to melt the torque increased, passed through a maximum, and stabilized after another 60 seconds. After an additional period of 5 minutes the mixer was stopped and the melt was discharged. The work of mixing related to this procedure includes all the work between the time of addition of mica/polypropylene powder and the end of the run.

Recovery of Mica from Processed PP/Mica Blends

Between 100 and 500 mg of polypropylene/mica blend was placed into a small ceramic crucible which was introduced into a cold furnace. The temperature was gradually increased by approximately 100°C/hr until it reached 600°C where it was kept for 2 hours. The mica powder recovered from the crucible was then ready for analysis. Blank experiments where undegraded mica was blended with polypropylene powder were performed to verify that the pyrolysis does not affect the particle size distribution.

Particle Size Analysis

Equipment

The particle size distribution was determined with the HIAC-PA720 particle size analyzer manufactured by Pacific Scientific Co., Montclair, CA. This instrument utilizes the so-called light blockage principle (15). Particles to be counted are suspended in a fluid having a refractive index different from that of the particles. The suspension is then pumped through a sensing zone consisting of collimated light. When a particle traverses the light beam it momentarily blocks a given amount of light from reaching the photodetector. The flow in the sensing zone is turbulent causing the particles to tumble. This makes the amount of light lost directly proportional to the greatest projected area of the particle. The pulses produced by particles are sorted into 23 sizes and counted. The overall range covered is 45 to 1 divided into 23 equal percentage width increments of $45^{1/23}$ or 1.18. The CMH 300 sensor used in this work covers a nominal range between 5 and 225 μm.

Calibration

The particle size analyzer is factory calibrated using monodisperse polystyrene spheres, and a secondary calibration is required for analysis of other materials (16). To perform such calibration the Suzorite 200 HK mica was wet-sieved by hand using standard ASTM sieves (17). Seven fractions were obtained and their average flake sizes were determined microscopically with the micrometric attachment of the microhardness tester—Model M-400 manufactured by Leco Corp., St. Joseph, MO. Feret's diameters of 100 flakes were measured for each fraction. The Feret's diameter (*Fig.* 2) is the distance between two tangents on opposite sides of the particles, parallel to some fixed direction (18).

Mica standards were suspended in demineralized and filtered water (0.22 μm filter) and passed through the particle size analyzer; the particle concentration was adjusted by trial and error to about 500 particles/ml of suspension. The number average diameter thus obtained was corrected by eliminating from the count the fine particles remaining in suspension despite extensive washing. For example, for the 70 to 100 mesh fraction the HIAC generated a distribution curve shown in the *Fig.* 3 and a number average diameter, d_n, of 63.6 μm. By

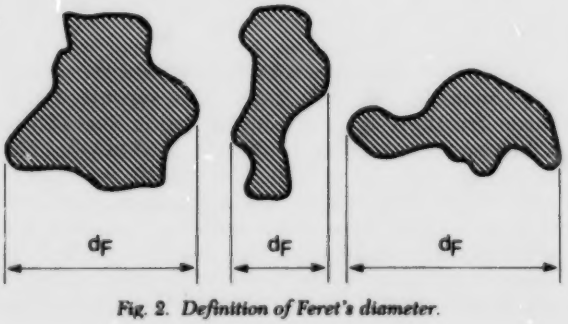

Fig. 2. Definition of Feret's diameter.

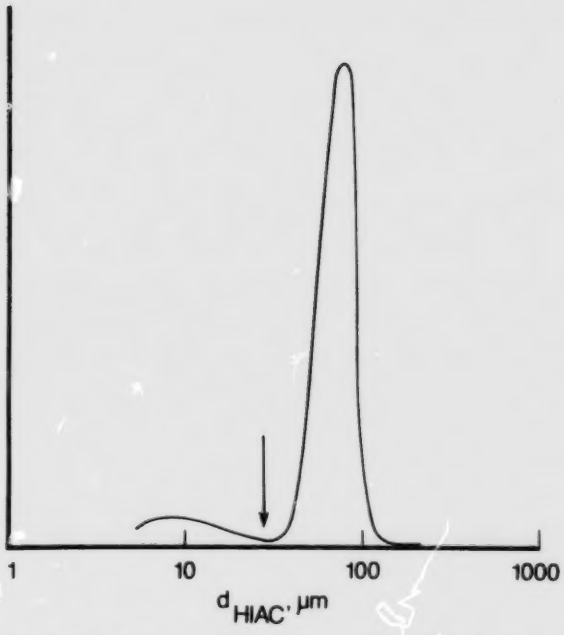

Fig. 3. Particle size distribution (by number) of the 70 to 100 mesh mica standard. Particles finer than 28.4 μm (indicated by the arrow) were excluded from the calculation of $d_{n,HIAC}$.

Table 3. Characteristics of Mica Standards

Nominal Sieve Cuts, Mesh	Upper and Lower Sieve Opening, μm	$d_{n,HIAC}$, μm	$d_{w,F}$, μm
70–100	210–149	70.7	250
100–120	149–125	61.4	217
120–170	125–88	48.7	174
170–200	88–74	37.5	127
200–270	74–532	30.1	96.5
270–325	53–44	26.9	85.8
325–400	44–37	24.5	72.7

eliminating from the count fine particles with a nominal (HIAC) diameter of 28.4 μm and below a corrected value of $d_n = 70.7$ μm was obtained. The characteristics of standards are shown in *Table 3*. The calibration curve (*Fig. 4*) obeys the equation

$$d_{n,F} = 3.830\ d_{n,HIAC} - 17.878 \qquad (R^2 = 0.998) \quad (3)$$

where $d_{n,F}$ is the number average Feret's diameter of each fraction (determined microscopically) and the $d_{n,HIAC}$ is the number average flake diameter as generated by the HIAC instrument. For further flake size calculations, the HIAC diameter corresponding to each of the 23 size channels was replaced by the Feret's diameter obtained from the calibration equation.

Experimental Procedure with Mica Powders

About 1 mg of mica powder was weighed on the Sartorius—Model 4431 ultramicroanalytic balance set to work with a precision of 1 μg. The powder was then suspended in about 220 ml of demineralized and filtered water and under constant agitation

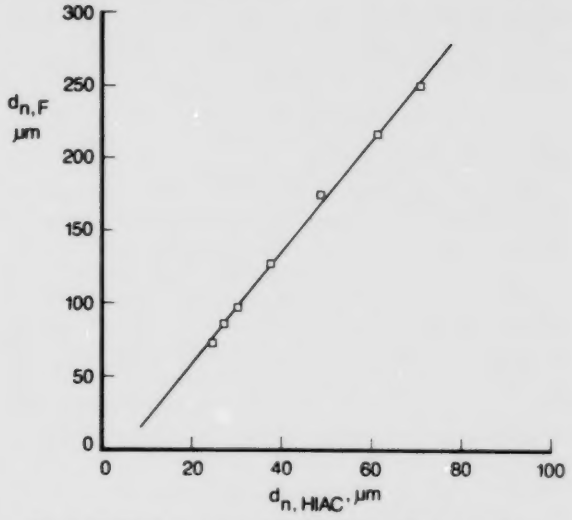

Fig. 4. Calibration curve of the HIAC particle size analyzer.

passed through the particle size analyzer. The amount of suspension used was determined by weighing. Usually about 170 ml was used. It was found that the start of the particle count does not coincide exactly with the start of pumping; a certain volume of suspension passes through the sensor before the count begins. This "dead volume" was determined and used to correct the suspension volume corresponding to the particles counted. Depending on the extent of mica degradation between 15,000 and 150,000 particles were counted during each test.

Calculation of Average Diameter and Shape Factor

The number average diameter is useful only when the size distribution is relatively narrow (e.g., well fractionated and washed mica). In the case of polydisperse materials such as commercial or degraded mica some other average has to be used. We chose the so called "moment mean diameter" (19) defined as

$$d_v = \frac{\sum n_i d_i^4}{\sum n_i d_i^3} \quad (4)$$

where n_i and d_i are the number of particles and the Feret's diameter corresponding to the fraction i respectively ($i = 1, 2, 3, \ldots 23$).

To characterize the aspect ratio, we use the shape factor, ψ, defined as

$$\psi = V_h/V_r \quad (5)$$

where V_h is defined as

$$V_h = \tfrac{1}{6}\pi \sum n_i d_i^3 \quad (6)$$

V_h is the hypothetical volume the sample would have, if all the particles were spherical and V_r is defined as

$$V_r = w/\rho \quad (7)$$

V_r is the real volume of the sample: w is the sample weight, $\rho = 2.84$ g/cm^3 is the density of mica. It is

worth noting that for simple systems such as a monodisperse assembly of discs ψ is directly proportional to the aspect ratio, P

$$\psi = 2P/3 \quad (8)$$

Reliability of the Method

Most of the work in this study was performed with either 2 and 40 percent weight concentrations. Repeat experiments on some samples gave results summarized in *Table 4*. Overall reproducibility is excellent. Increasing scatter at the 2 percent concentration is undoubtedly caused by the presence of some foreign matter in the mica (catalyst residue from the resin, metallic particles from the machine, etc.). This is easily understood considering the amount of resin that had to be burned away to obtain the required amount of mica.

RESULTS AND DISCUSSION

Mixing Time

The dependencies of the average diameter, d_v, and of the shape factor, ψ, on the total work of mixing, W, are shown in *Fig. 5* for mica concentrations of 2 and 40 percent (wt). The work of mixing was varied by simply increasing the mixing time. At 2 percent (volume fraction, $\phi = 0.0054$) one observes a very slow decrease of both d_v and ψ. This can be, at this stage, attributed either to flake-flake collisions or to interactions between the flakes and the polymer. The 40 percent sample ($\phi = 0.15$) exhibits a more complex behavior. Up to a mixing work of about 2×10^4 J which corresponds to a mixing time of 5 minutes there is a rapid drop of d_v and ψ followed by a region of less pronounced degradation. The shape of these curves can be interpreted in terms of flake-flake collisions in the melt:

- In the initial period, before the melt is fully homogenized, one can visualize a high degree of flake-flake interactions in particular in the regions where local mica concentration is high.
- As the flakes break, the flake size distribution becomes broader, thus increasing the maximum packing volume fraction, ϕ_{max} (20). This reduces the probability of flake-flake collisions.
- The shape factor decreases as a result of attrition. Flakes with lower shape factor (i.e., less nonspherical) are likely to be more resistant to fracture in the event of flake-flake collision.

Useful insight into the flake degradation can be gained by studying the differences between particle size distributions of processed and initial (unprocessed) mica powders. *Figures 6* and *7* show the evolution of the particle size distribution with time of mixing for 2 and 40 percent mica concentrations. On the Y-axis we plot the function ΔN, defined as

$$\Delta N(d) = |N(d)_{t=t} - N(d)_{t=0}|$$

where $N(d)$ is the number of particles of diameter d and greater present in 1 g of mica powder. The peak on the right side of each curve in *Figs. 6* and *7* represents the particles that have disappeared as a result of attrition whereas the curves on the left are in fact particle size distributions of newly

Table 4. Reliability of the Particle Size Analysis Method

Mica Concentration in Polypropylene	n	d_v (μm)	±σ(%)	ψ	±σ(%)
Unprocessed mica	4	174.3	0.2	82.4	1.9
2	7	170.7	1.1	77.6	3.1
40	4	138.8	0.7	68.9	1.9
40	4	151.2	0.8	55.0	1.3

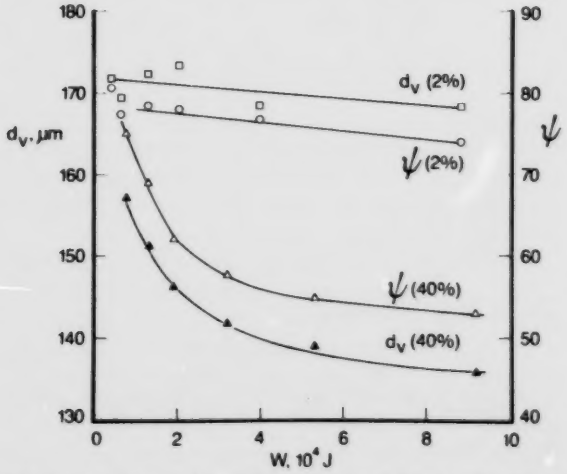

Fig. 5. Dependence of d_v and ψ on the work of mixing for blends containing 2 and 40 percent of mica. The points on each curve correspond to mixing times of 1, 2, 5, 10, 20, and 40 minutes. Profax 6501, 120 to 230 mesh mica, 45 rpm, 200°C.

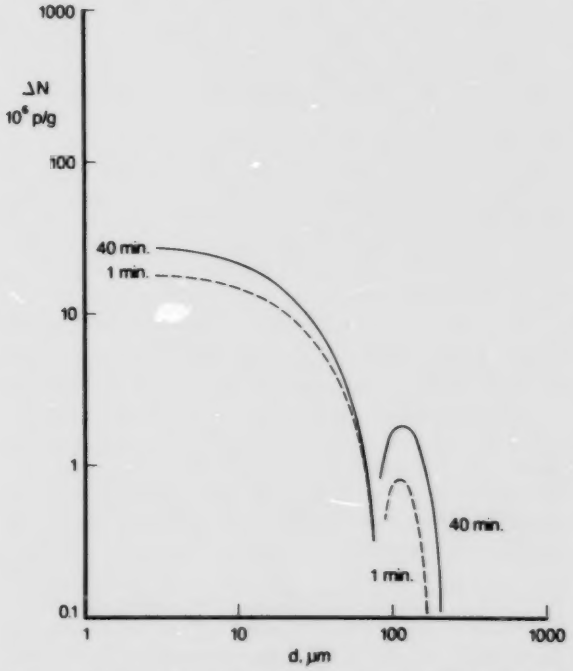

Fig. 6. ΔN vs. d, obtained with the 2 percent blend for times of mixing of 1 and 40 minutes. Process conditions were those of Fig. 5.

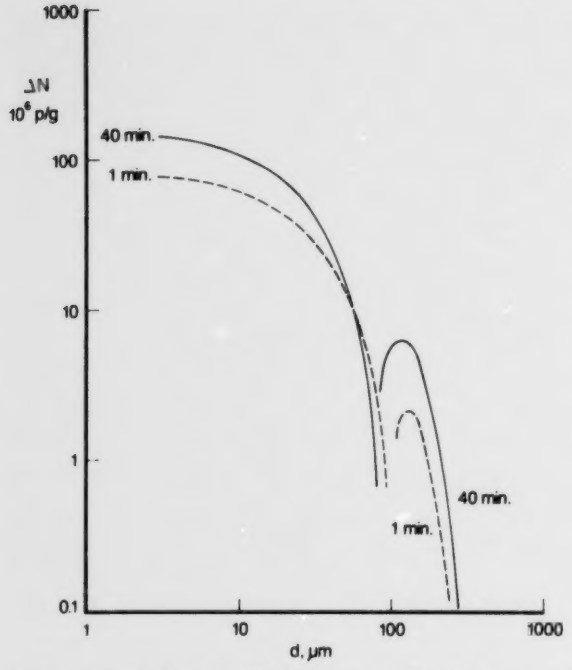

Fig. 7. ΔN vs. d obtained with the 40 percent blend, for times of mixing of 1 and 40 minutes. Process conditions were those of Fig. 5.

formed flakes. *Figure 6* shows that after 1 minute of compounding at 2 percent mica concentration the number of newly generated particles in the measured range (i.e., greater than ~ 3 μm) is almost equal to the number of particles originally present in the unprocessed mica powder. Comparison between the left and the right side of the ΔN function clearly shows that, at this stage, the degradation proceeds by formation of small fragments rather than by random breaking into flakes of similar sizes. This is also in agreement with the relatively small changes in both d_v and ψ (*Fig. 5*). The amount of degradation which has occurred between 1 and 40 minutes of compounding is surprisingly small: only about 10×10^6 additional particles/g of mica were counted. It seems that the unprocessed mica has some weak flakes, the flakes themselves may have thin, brittle edges, etc. that break rapidly and the rate of degradation then slows down to a constant rate. The flake-flake collisions are again more likely before a fully homogeneous melt is obtained.

Turning now to the ΔN *vs.* d dependence for the 40 percent sample (*Fig. 7*), similar observations are made except that the rate of degradation is much more rapid. After 1 minute of compounding (following the 2 minutes it took to incorporate all the mica into the melt) the particle count has already increased by 70×10^6 p/g. Forty minutes of mixing produced a mica powder containing 140×10^6 p/g more than the initial powder (see *Table 2*). This means that an average mica flake has now given rise to 7 additional particles (in the measured particle size range). Since the d_v and ψ have decreased only by 22 and 35 percent respectively, we can conclude that these new particles are on the average much smaller than the "mother" particles which, albeit reduced in size by attrition still provide most of the weight in the calculation of the overall average particle size and shape factor.

Figure 8 provides a visual insight into the degradation process. *Figure 8a* shows the original unprocessed mica. The relative uniformity in the flake size and the absence of fines are clearly visible. Forty minutes of compounding at a mica concentration of 2 percent (*Fig. 8b*) does not seem to have produced a significant effect although small fragments can be observed. In the case of 40 percent blend (*Fig. 8c* and *8d*), the effect of compounding can now be qualitatively followed by microscopy; small fragments as well as "mother" particles are now present.

Mica Concentration

The effect of mica concentration on the final particle size and shape factor for mixing times of 2 and 20 minutes is shown in *Fig. 9*. The d_v *vs.* ϕ and ψ *vs.* ϕ curves exhibit two interesting features. First as the zero concentration is approached all curves tend to intercept the Y axis at values of d_v and ψ which are very close to those of virgin mica—the influence of compounding time decreases as the ϕ decreases. This indicates that the mica-polymer interactions do not contribute in any significant way to the flake size degradation. If the mica-polymer interactions were important, a contribution of mixing time to flake degradation should be observed. It is to be noted that other data in this work (*Fig. 5*–2 percent concentration) support this argument as well.

The second interesting feature of these curves is related to the d_v and ψ *vs.* ϕ dependencies at high concentrations. The 40 and 60 percent samples ($\phi = 0.15$ and 0.28 respectively) have similar values of d_v and ψ for both mixing time. The 70 percent sample ($\phi = 0.38$) underwent a similar amount of attrition as the one containing only 25 percent of mica ($\phi = 0.08$). This is also illustrated in *Fig. 10* where ΔN *vs.* ϕ dependencies of samples containing 2, 25, 60, and 70 percent after 20 minutes of compounding are shown. The ΔN functions of the 25 and 70 percent samples are essentially identical. The shape of the curves in *Fig. 9* suggests that as the mica concentration increases beyond $\phi \simeq 0.1$ the frequency of the flake breakage starts to decrease. Certainly, at high mica concentration, the relative freedom to rotate or even to oscillate in the flow must be hindered by neighboring flakes. The flakes probably orient along the flow streamlines resulting in a sort of aligned structure (21) in which there is little flake to flake movement and, consequently, little flake degradation. It is interesting to note that similar d_v *vs.* ϕ dependence was also observed with polyethylene-commercial polydisperse mica blends made on a two-roll mill (22).

Polymer Viscosity

The effect of polymer viscosity on the degradation of mica flakes was studied by using three different resins (*Table 1*) and by varying the temper-

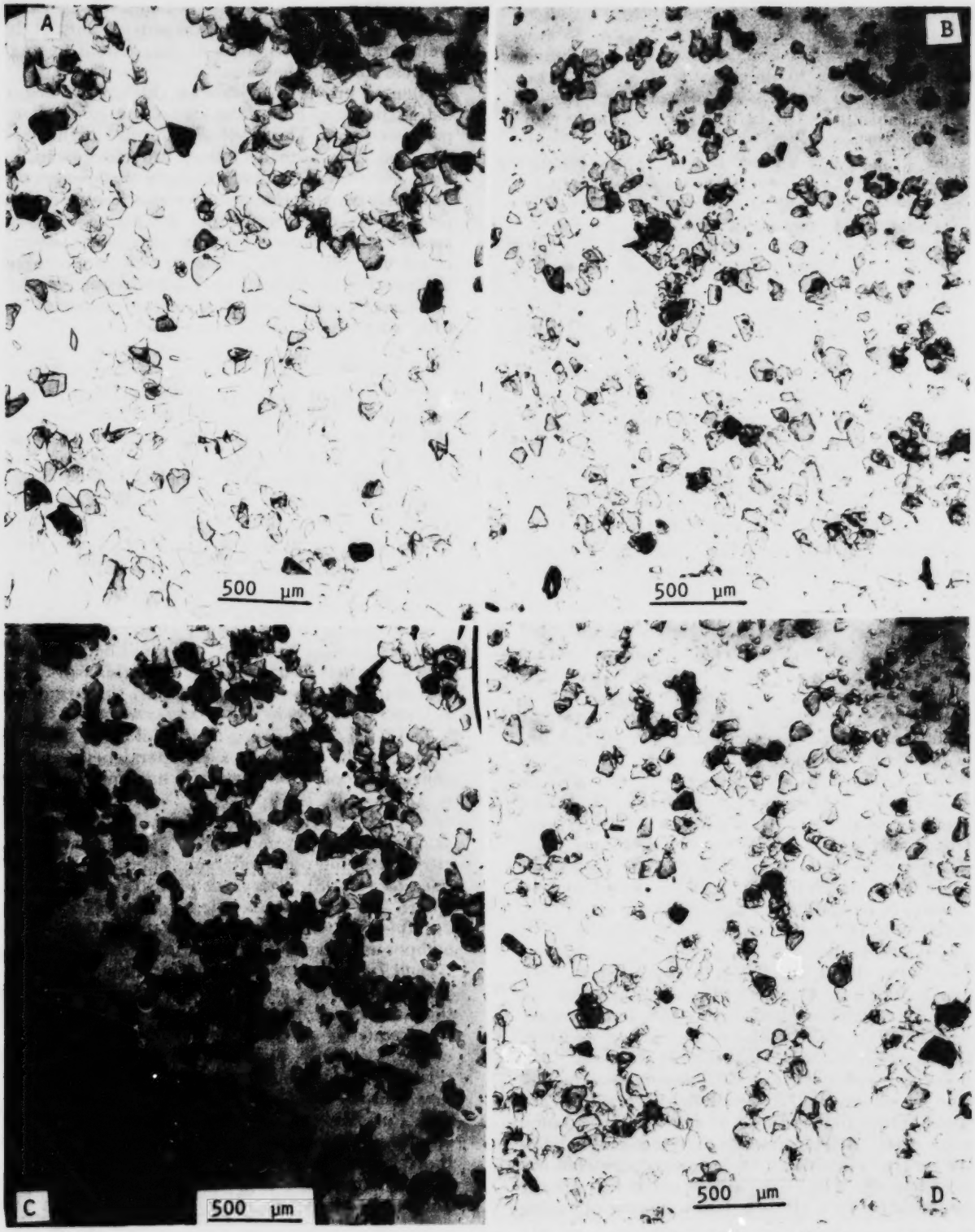

Fig. 8. Mica particles as seen in an optical microscope. A: unprocessed mica. B: mica recovered from the 2 percent blend compounded for 40 minutes. C: 40 percent blend, 1 minute compounding. D: 40 percent blend, 40 minute compounding. Process conditions were those of Fig. 5.

ature: each resin was compounded at 180 and 200°C. *Figure 11* shows the d_v and ψ as functions of work of mixing for blends containing 2 percent of mica and compounding times of 2 and 20 minutes. Both d_v and ψ decrease moderately as the blend viscosity increases. Since the polymer viscosity is

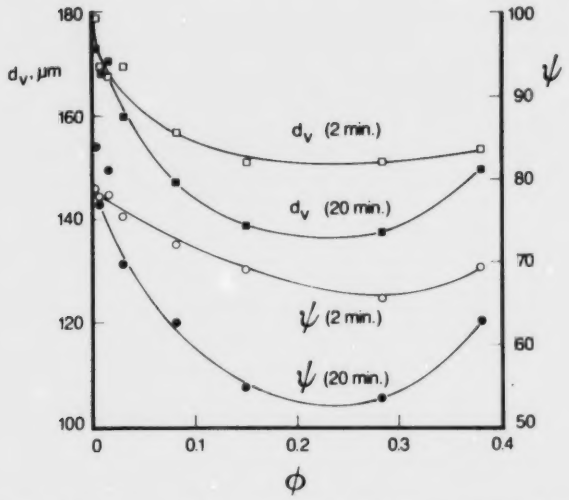

Fig. 9. Dependence of d_v and ψ on the flake volume fraction, ϕ, for mixing times of 2 and 20 minutes. Profax 6501, 120 to 230 mesh mica, 45 rpm, 200°C.

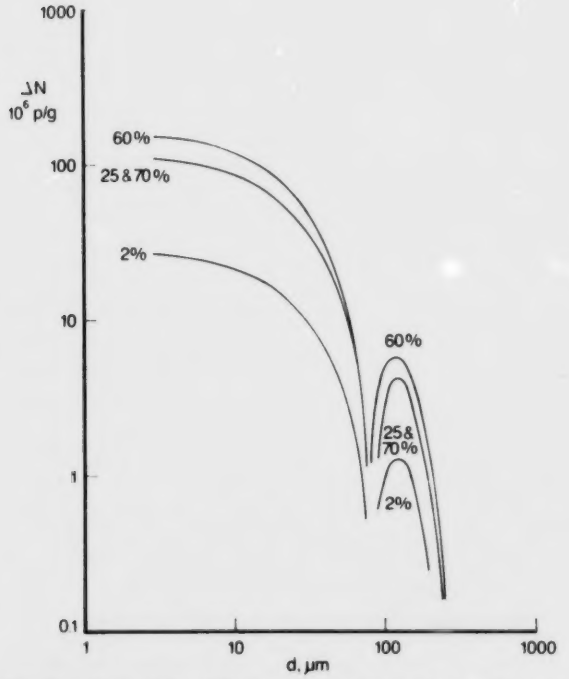

Fig. 10. ΔN vs. d for different concentrations of mica. Time of mixing 20 minutes, process conditions were those of Fig. 9.

the only variable, each sample has received a similar amount of shear: compounding time, rotor speed, and batch volume were all kept constant. Assuming then that the number of flake-flake collisions stays approximately constant, the observed decline in d_v and ψ may be attributed to an increasing probability of flake fracture with increasing polymer viscosity. This is easily understood since in similarly sheared suspensions of mica in low viscosity liquids such as water or paraffin oil flakes do not degrade despite frequent flake-flake collisions (23).

When the mica concentration is raised to 40 percent, both d_v and ψ decrease very rapidly with the increasing viscosity of the melt (*Fig. 12*). This is particularly pronounced for the 2 minute compounding time where the reductions in d_v and ψ were only 8 and 9 percent respectively for the least viscous blend but reached 21 and 25 percent for the most viscous one. This again illustrates the great stresses to which the flakes are subjected in the initial period of compounding when the mica is being incorporated into the melt. For the compounding time of 20 minutes the curves show a further decline in d_v and ψ. However, below the d_v of 135 μm and ψ of about 55 the attrition rate slows down substantially: the probability of flake breakage is reduced, possibly because of lower ψ and of higher ϕ_{max}.

Figure 13 shows how ψ changes with d_v as the

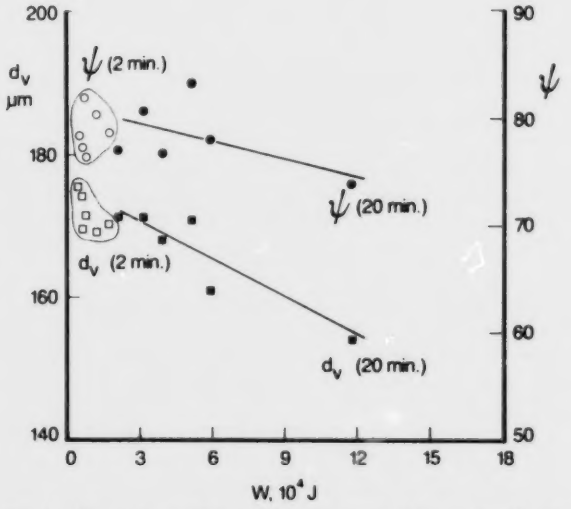

Fig. 11. Dependence of d_v and ψ on the work of mixing for blends containing 2 percent mica. Times of mixing were 2 and 20 minutes. The points on each curve were obtained by using each resin (Table 1) at temperatures of 180 and 200°C. 120 to 230 mesh mica, 45 rpm.

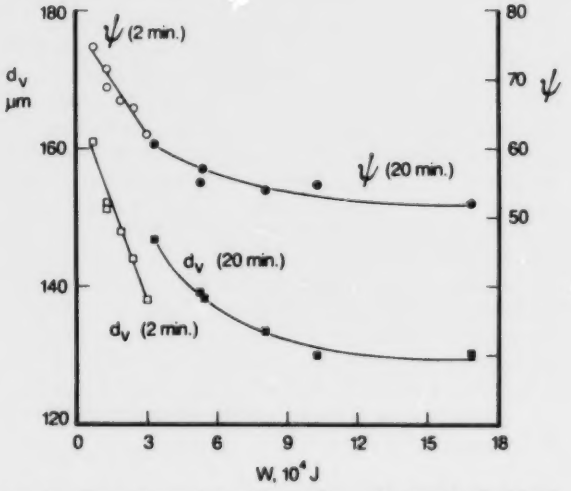

Fig. 12. Dependence of d_v and ψ on the work of mixing for blends containing 40 percent mica. Other process conditions were those of Fig. 11.

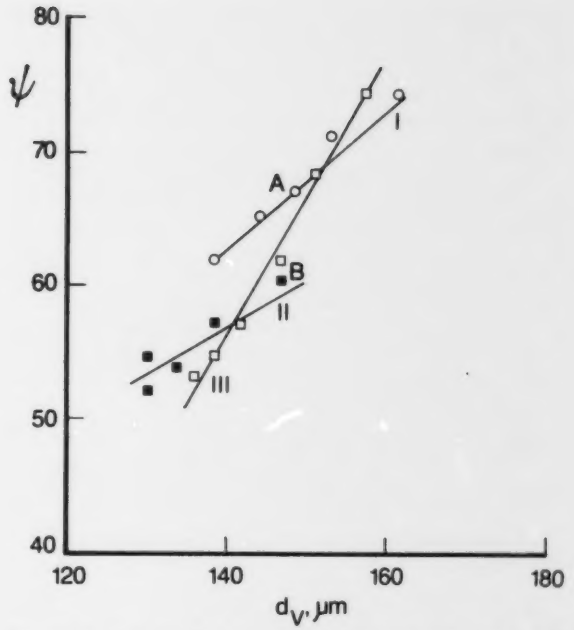

Fig. 13. ψ vs. d_v for 40 percent blends. Lines I and II: 2 and 20 minute compounding with different viscosity resins. Line III: compounding with the Profax 6501 resin at 200°C for different times.

polymer viscosity is increased. Lines I and II correspond to compounding times of 2 and 20 minutes. For comparison the ψ *vs.* d_v dependence of one of the blends with increasing compounding time is also shown (line III). The extent of damage for the high viscosity blends is again clearly seen. *Figure 13* illustrates how different flake size distributions are generated under different compounding conditions. Let us consider the points A and B in *Fig. 13*. Samples corresponding to these points have approximately the same d_v (147.9 and 146.8 μm) and particle count (134×10^6 and 132×10^6 p/g). However, there is about 10 percent difference in ψ between them. Sample A was made with the medium viscosity resin at a temperature of 180°C; the compounding time was 2 minutes and the work of mixing was 1.9×10^4 J. Sample B was made using the low viscosity resin at 200°C; compounding time and work of mixing were 20 minutes and 3.3×10^4 J respectively. The ΔN *vs.* d functions of these two samples reveal significant differences (*Fig. 14*). Sample A (i.e., higher viscosity, shorter compounding) shows lower values at the right side than for sample B but higher values on the left side in particular in the region between 10 and 50 μm. This means that, compared to sample B, a smaller number of "mother" flakes gave rise to a larger number of larger flakes. These curves (*Fig. 14*) are indicative of the differences in flake fracture during the initial period and during the steady state when the mica is fully dispersed in the melt.

Mode of Mica Addition

It is generally accepted that an incorporation of reinforcing fillers such as glass fiber and mica into a molten polymer is preferable to blending of components prior to compounding. This reduces the machine wear and it is also believed to reduce the filler degradation (24). *Figure 15* illustrates the results obtained with the mica/polypropylene system. The points on the d_v and ψ *vs.* W curves come from three sets of experiments carried out with a

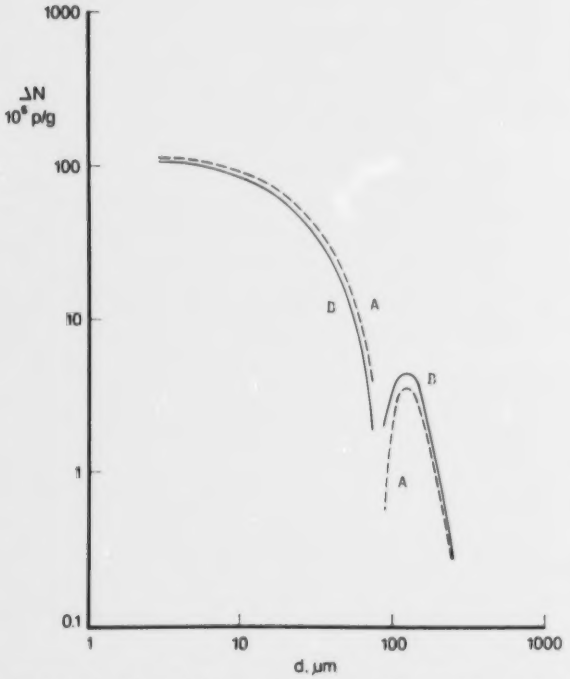

Fig. 14. The ΔN vs. d for samples corresponding to points A and B of Fig. 13.

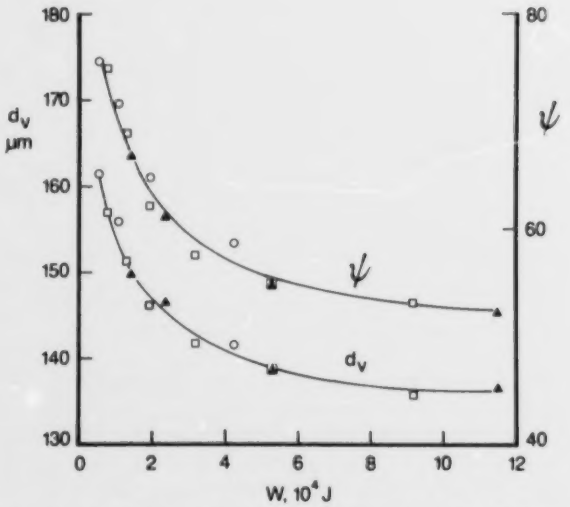

Fig. 15. d_v and ψ dependence on W-40 percent mica. Symbols: □: mica added to the melt, constant rpm, times of mixing between 1 and 40 minutes. ▲: mica added to the melt, compounding time was kept constant at 20 minutes. Rotor speed varied between 15 and 90 rpm. ○: mica blended with PP powder prior to compounding, rotor speed varied between 15 and 90 rpm, compounding time 5 minutes following the torque stabilization. Profax 6501, 120 to 230 mesh mica, mixer temperature 200°C.

mica concentration of 40 percent and a mixer temperature of 200°C.

- Mica was blended with the polypropylene powder prior to compounding; rotor speed was varied.
- Mica was incorporated into the molten polypropylene; rotor speed was varied.
- Mica was incorporated into molten polypropylene, compounding time was varied (same data as in *Fig. 5*).

All the points fall on the same curve—the degradation is the function of work of mixing only. This indicates that degradation causing stresses to which the flakes are subjected must be of similar magnitude for both modes of mica incorporation. These results again confirm that it is during the dispersing stage when most degradation occurs. From this point of view both modes of mica addition are likely very similar. When mica is added to a molten polymer the first stage of compounding consists of a formation of striations or "pockets" of mica powder in the melt. This situation may be similar to blending of mica and polypropylene powder prior to compounding. The approximate size of an average polypropylene particle is about 300 μm and these "as polymerized" particles are known to have a porosity of about 30 percent (25). This gives a particle count of $\sim 5 \times 10^4$ p/g. Comparing this with the mica count of 2×10^7 p/g one obtains a ratio of about 300 mica flakes that have to be dispersed in each polypropylene particle once it has become molten. Parallel experiments during which 40 percent mica-60 percent polypropylene powder blends were mixed at room temperature in the roller blade mixer as well as the high speed Waring blender revealed an absence of measurable flake degradation after mixing times of 5 and 10 minutes.

Different behavior is observed when experiments parallel to those of *Fig. 15* are performed with the 2 percent mica blend (there are only about 8 mica flakes for each polymer particle). Incorporation of mica into the melt gives the now familiar slow decrease in d_v and ψ which depends only on the work of mixing (*Fig. 16*). Compounding of the mica/polymer powder produces a much sharper decrease in the average flake size. Surprisingly, the shape factor remains almost constant and independent of d_v. This shows that the particles generated by degradation under these conditions have shape factors similar to those of unprocessed mica. The ΔN *vs.* d function for one of these samples is shown in *Fig. 17*. The right side peak is narrower and the minimum occurs at a higher value of d ($\sim$110 μm) confirming that the newly generated particles are larger than in other cases ($\sim$90 μm, see *Figs. 6, 7, 10,* and *13*). The differences observed at mica concentration of 2 percent between addition to the melt and blending prior to compounding are difficult to explain. Possibly by gradually adding the small amount of mica powder to molten polypropylene ($\phi = 0.0054$) the frequency of flake-flake collisions during the dispersing stage is reduced.

The results of *Figs. 15* and *16* are at variance with those of Burns (26) who has studied the compounding of glass fiber bulk molding compounds in a Z-blade mixer. With this system he found that the fiber length degradation was much slower at low rotor speeds (the amount of shear was kept constant). This and the above mentioned work by Von Turkevich and Erwin (5) illustrates the differences in particle size degradation between glass fiber and mica filled polymers.

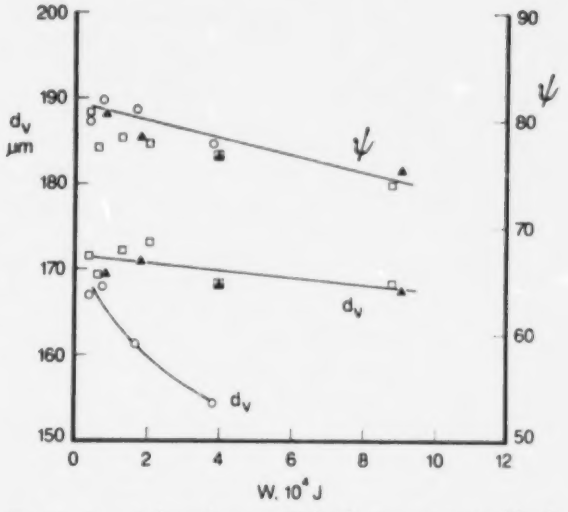

Fig. 16. d_v vs. ψ dependence on W for the 2 percent mica blends. Symbols are identical to those in Fig. 15.

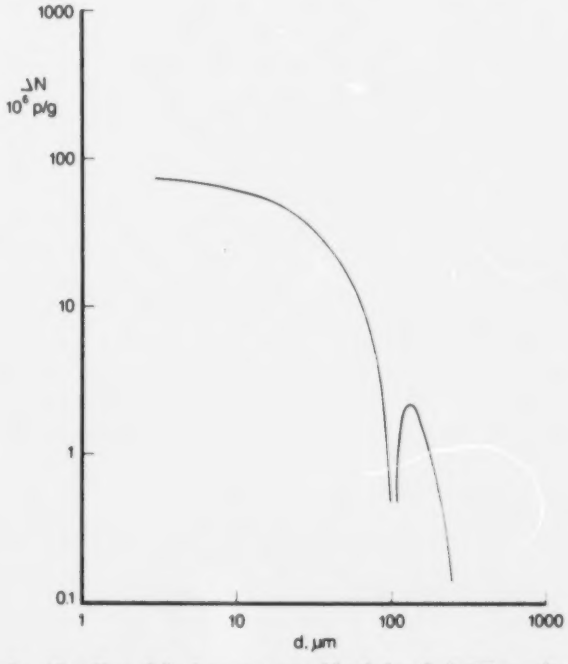

Fig. 17. ΔN vs. d for 2 percent mica blended with the PP powder prior to compounding. Rotor speed—90 rpm. Process conditions were those of Fig. 15.

Silane Treated Mica

Silane and other coupling agents are mainly used to promote filler-polymer adhesion which is important for an efficient reinforcing effect (27). As an

added benefit, coupling agents reduce the surface energy and facilitate the filler dispersion during compounding (28). In order to study the effect of silanes on the mechanical degradation of mica, we chose to treat the mica using a procedure similar to that described by Favis, *et al.* (11). The use of this method avoids possible interference of other factors such as internal or external lubrication by unattached coupling agent (25) which is removed by washing.

In these experiments mica flakes were blended with the polypropylene powder prior to compounding; the mixing work was varied by changing the temperature of the mixing chamber. Results analogous to those in the preceding section were obtained (*Fig. 18*). At mica concentration of 2 percent, the d_v decreases while ψ remains almost constant. With the 40 percent blend moderate decreases of d_v and ψ were observed (*Fig. 19*). In all cases the curves for untreated and treated mica run parallel to each other, the latter exhibiting higher values of d_v and ψ. The differences are particularly significant for the 40 percent treated mica blends which have shape factor values higher by about 10 percent than the untreated mica. The data available here (*Fig. 19*) unfortunately do not show the shapes of the d_v and ψ *vs.* W curves at low W. However, comparing *Figs. 19* and *15* it seems reasonable to assume that initial rapid decrease of d_v and ψ at low work of mixing is less pronounced with the silane treated mica/PP blend. The slower degradation of the easier-to-disperse silane treated mica is then consistent with the ideas suggested by this work i.e., that the most severe flake degradation occurs during the dispersing stage.

It is worth noting that in all experiments with the silane treated mica the mixer torque was always identical to that measured with the equivalent untreated mica/polypropylene blends. This confirms the absence of a lubrication effect.

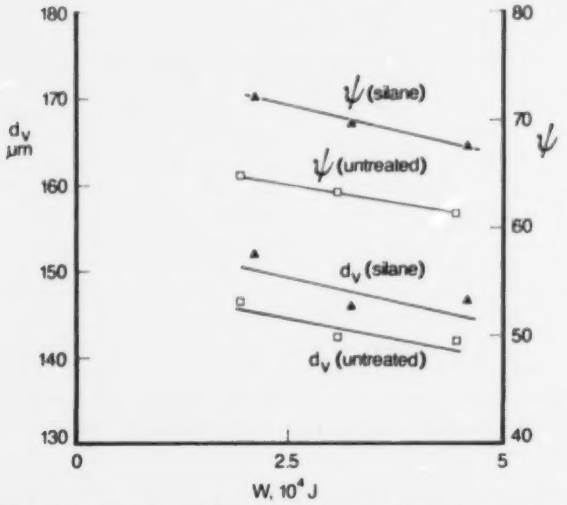

Fig. 18. d_v and ψ dependence on the work of mixing; 2 percent of mica was blended into the PP powder prior to compounding. The work of mixing was varied by varying the mixer temperature (170, 180, and 200°C). Profax 6501, 120 to 230 mesh mica.

Particle Size

Figure 20 shows the effect of the initial particle size on the mechanical degradation. As the particle size decreases the decline between the initial and final flake size also decreases. With the shape factor exactly the opposite happens. The decrease is largest for the smallest particle size. The data in *Table 5* show that the particle counts in the processed mica samples increased by approximately the same number (135×10^6 p/g) regardless of the initial particle size and count. This means that the total number of flake fractures is independent of the initial particle size. Furthermore the ΔN *vs.* d functions (*Fig. 21*) overlap in the range below 30 μm

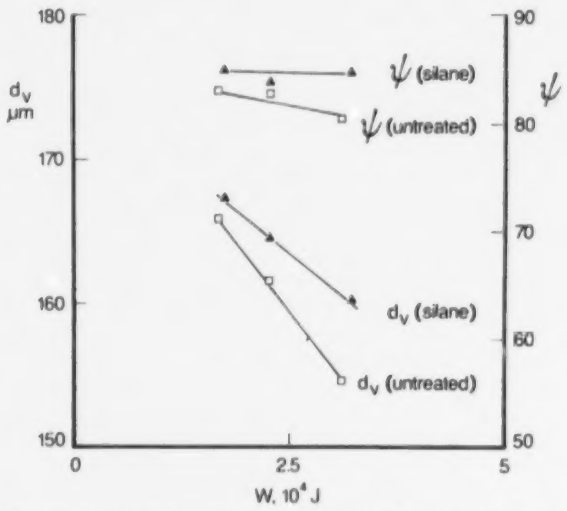

Fig. 19. d_v and ψ dependence of the work of mixing. 40 percent mica blend; process conditions were those of Fig. 18.

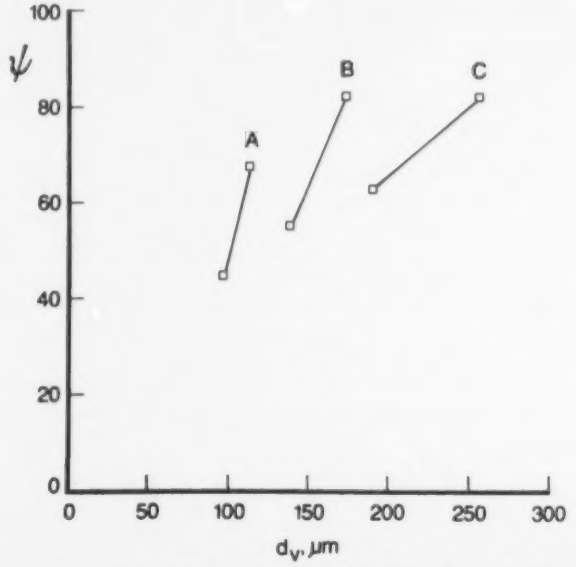

Fig. 20. ψ vs. d_v change for identical compounding conditions with different particle size mica. A: 230 to 400 mesh. B: 120 to 230 mesh. C: 84 to 120 mesh. Mica was incorporated into molten PP, mixing time 20 minutes, T = 200°C, 45 rpm, Profax 6501.

Table 5. Influence of the Initial Flake Size on Degradation

Nominal Sieve Cuts, Mesh	W, J	d_v (μm)		ψ		Particle Count (>3 μm)/g	
		Before	After	Before	After	Before	After
84–120	55100	257.2	190.6	82	63	6.6×10^6	136×10^6
120–230	53000	174.3	138.8	82	55	21.8×10^6	156×10^6
230–400	54600	113.3	97.1	68	45	75×10^6	214×10^6

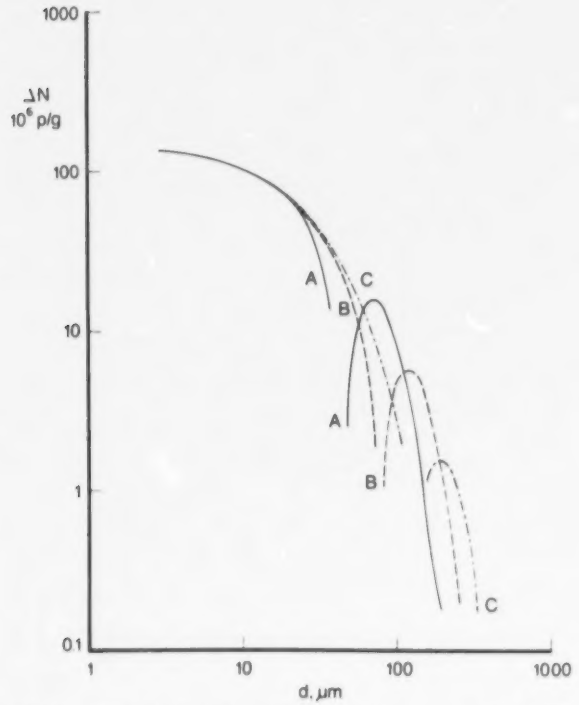

Fig. 21. ΔN vs. d for different particle size micas. A: 230 to 400 mesh B: 120 to 230 mesh C: 84 to 120 mesh. Process conditions were those of Fig. 20.

indicating that the particle size distributions of newly formed particles are very similar in this region.

SUMMARY AND CONCLUSIONS

Mechanical degradation of mica during compounding with polypropylene occurs principally via a gradual attrition of larger flakes to form small flakes rather than by random breakdown into flakes of comparable sizes. This results in a reduction of the average flake size and shape factor.

The most rapid degradation occurs in the very first stage of compounding i.e., when the mica is being incorporated into the molten resin. Silane treated mica is less degraded probably because of easier dispersion during this initial period. The mode of mica addition to the polymer (mica addition to the melt *vs.* to polypropylene powder prior to compounding) was found to have little effect except at low (2 percent) mica concentration.

Concentration dependencies of flake size and shape factor suggest that the degradation results primarily from the flake-flake collision; the flake-polymer interaction do not appear to play a significant role. The size reduction is most severe in the 40 to 60 percent wt concentration range; the degradation of the 25 and 70 percent samples was found to be very similar. Polymer viscosity plays a major role especially in the initial stages of compounding: the less viscous the polymer the easier the dispersion—hence less degradation.

The study of the effect of initial particle size revealed that the number of flake fractures during compounding was very similar: samples containing initially between 6.6×10^6 and 75×10^6 particles/g all generated about 135×10^6 additional particles/g under identical compounding conditions.

Overall the observed flake degradation is relatively moderate under the most severe conditions d_v and ψ decreased by only 22 and 35 percent respectively. Work currently underway at our Institute deals with flake degradation in processing machinery and its effects on physical and mechanical properties of mica-reinforced resins.

ACKNOWLEDGMENTS

The work reported here would not have been possible without the contribution of Mr. J. Dufour whose determination has played a decisive role in the development of the flake size analysis method.

REFERENCES

1. W. Filbert, *SPE J.*, **25**, 65 (1969).
2. J. B. Shortall and D. Pennington, *Plast. Rubb. Process Appl.*, **2**, 33 (1982).
3. L. Czarnecki and J. L. White, *J. Appl. Polym. Sci.*, **25**, 1217 (1980).
4. B. A. Knutsson, J. L. White, and K. B. Abbas, *J. Appl. Polym. Sci.*, **26**, 2347 (1981).
5. R. Von Turkevich and L. Erwin, *Polym. Eng. Sci.*, **23**, 743 (1983).
6. R. T. Woodhams and M. Xanthos in "*Handbook of Fillers and Reinforcements for Plastics*", J. V. Milewski and H. S. Katz, Eds., Van Nostrand Reinhold, New York (1978).
7. K. Okuno and R. T. Woodhams, *Polym. Eng. Sci.*, **15**, 308 (1975).
8. P. Bataille and T. W. Bui, *Polym. Compos.*, **2**, 8 (1981).
9. Z. Tadmor and C. G. Gogos, "Principles of Polymer Processing," J. Wiley & Sons, New York (1979).
10. M. Smoluchowski, *Z. Phys. Chem.*, **92**, 155 (1917).
11. B. Fisa, B. Sanschagrin, and B. D. Favis, *Powder Technology*, submitted for publication.
12. B. D. Favis, L. P. Blanchard, J. Léonard, and R. E. Prud'homme, *J. Appl. Polym. Sci.*, **28**, 1235 (1983).
13. B. Wunderlich, "Macromolecular Physics," Vol. 1, Academic Press, New York, (1973).
14. Plasti-corder Operating Manual, C. W. Brabender Instruments Inc. South Hackensack, N.J.
15. H. A. Kupfer, *Powder Metall. Int.*, **10**, 96 (1978).
16. G. G. West, *Hydraulics and Pneumatics*, **8**, 1 (1975).
17. R. R. Irani and C. F. Callis., "Particle Size: Measurement, Interpretation and Application," J. Wiley & Sons, New York (1963).
18. R. D. Cadle in "Testing and Characterization of Powders

and Fine Particles". J. K. Beddow and T. Meloy, Eds., Heiden, London (1980).
19. T. Allen, "Particle Size Measurement", Chapman and Hall, London (1981).
20. J. V. Milewski, *Polymer-Plast. Technol. Eng.*, 3, 101 (1974).
21. L. A. Utracki, B. D. Favis, and B. Fisa, this symposium.
22. B. Fisa and L. A. Utracki, *Polym. Compos.*, 5, 36 (1984).
23. B. Fisa, unpublished results.
24. B. M. Walker in "Handbook of Fillers and Reinforcements for Plastics", J. V. Milewski and H. S. Katz, Eds., Van Nostrand Reinhold, New York (1978).
25. J. Wristers, *J. Polym. Sci., Polym. Phys. Ed.*, 11, 1619 (1973).
26. R. Burns and D. Pennington, *SPI R.P.C. Inst. Annu. Conf. Proc. 34th*, New Orleans, LA, Sect 7-D.
27. E. P. Plueddeman in "Additives for Plastics," Vol. 1, R. B. Seymour, Academic Press, New York (1978).
28. L. A. Utracki and B. Fisa, *Polym. Compos.*, 3, 193 (1982).

DISCUSSION

F. K. Lautenschlaeger: There is some interest in metal coated mica for conductive systems. How would you look at it from the point of view of mica degradation? This may be also an indirect method of measurement.

B. Fisa: I would say that the total coated surface would be nearly constant, independent of the attrition.

D. G. Fesko: Do you think that it would be worthwhile to carry out another compounding experiment in a very low shear system? For instance, as a suspension in a low viscosity oil.

B. Fisa: We have done that in a paraffin oil and in water. In this case, there was no degradation. I want to stress that the amount of degradation we observe during the processing with polymer is surprisingly large. We also tried to see the effect of ball-milling. It would take several hours of dry ball-milling to get a similar amount of degradation to that which we observe after 2 min. compounding with polypropylene. Degradation of mica flakes during the compounding with polymer is a very rapid, severe process.

D. G. Fesko: Once the mica is dispersed in these low viscosity liquids, then if you applied mechanical energy there was very little attrition. Is this true?

B. Fisa: We have done some exploratory work where we would mix mica with paraffin oil and we did not see any degradation as a result of dispersion in the low viscosity medium. What you are asking, as I understand, is that one should optimize the initial step of compounding by pre-dispersing in low viscosity medium to bypass the first stage of the process, during which the flake-flake collision results in a rapid degradation. That makes sense but we have not yet tried to do this.

Dynamic and Steady State Flow of Polypropylene/Mica Systems

L. A. UTRACKI, B. D. FAVIS, *and* B. FISA

Industrial Materials Research Institute
National Research Council of Canada
75 De Mortagne Blvd., Boucherville, Quebec J4B 6Y4

Six compositions containing commercial polypropylene, PP, and monodispersed, untreated phlogopite mica were prepared. Their rheological properties were determined at 180°C in dynamic and capillary flows. The results are discussed in terms of strain-induced orientation of mica flakes. Two critical volume fractions were found to affect the flow: ϕ_c defined as a concentration of flakes overlap and ϕ_m as a concentration of maximum packing of freely sedimenting particles. At $\phi > \phi_c$ yield stress and at $\phi > \phi_m$ non-linearity in dynamic response were observed.

INTRODUCTION

There is a growing interest in technology of filled systems (1). The flow properties and processability of plastics filled with anisometric particles were recently reviewed (2–4). It must be stressed that in order to get full benefit from this type of composite, well-oriented, high aspect ratio particles are required (5, 6). The current use of mica in North America is about 17 Gg per annum, incorporated into about 1500 million pounds of plastics products (primarily polyolefins).

In our previous publications (2, 3, 5–7) the properties of injection molding grade high density polyethylene, HDPE, compounded with a commercial, silane treated phlogopite mica were studied. The interpretation of data was difficult due to the presence of a coupling agent, the broad distribution of flake sizes and the concentration dependent effects of attrition.

In the present work these difficulties have been reduced; uncoated, well-characterized mica fractions were used, the lower concentration samples were prepared by dilution of a "master batch" and the changes in flakes dimensions were determined at each stage of the measurements. The main goal was to compare the steady-state viscosities with the results of dynamic testing under different strains. There was an attempt to correlate the rheological responses with the orientation of flakes during the testing. The paper should be considered only as a "progress report" on the flow, processability and properties of plastics filled with anisometric particles (1–7).

EXPERIMENTAL

Materials

The characteristics of the polypropylene, PP, (Hercules Inc., PRO-FAX 6501) used in this study are given in *Table 1*.

The mica was the commercial high aspect ratio, untreated Suzorite 200 HK supplied by Marietta Resources Intl. Ltd. This material was dispersed in water and screened through a series of Sweco Vibro-energy Separator sieves. The fraction used in this study was collected between Nos 120 and 230 mesh screens, i.e., screen openings varied between 63 and 125 μm.

The particle size distribution was determined in HIAC-PA720 (Pacific Sci. Co.), calibrated using specially prepared mica standards (6). The volume average Feret's diameter:

$$d_v = (\Sigma n_i d_i^4)/(\Sigma n_i d_i^3) \tag{1}$$

and the shape factor:

$$\Psi = \Sigma n_i V_{H,i}/V_R \tag{2}$$

were computed. In *Eq 2* the $V_{H,i}$ is the encompassed (spherical) volume of the particle "i":

$$V_{H,i} = \pi d_i^3/6, \tag{3}$$

and V_R is the total volume of the sample:

$$V_R = W/\rho \tag{4}$$

Table 1. Characteristics of PP Resin.

No.	Parameter	Value
1.	Melt Index—ASTM 1238 (g/10 min)	4
2.	Molecular Weights: Number Average $M_n \cdot 10^{-3}$	250
	Weight Average $M_w \cdot 10^{-3}$	325
3.	Intrinsic viscosity [η] (m^3/kg) at 135°C in decahydronaphthalene	0.225
4.	Zero-shear: viscosity $\eta_o \cdot 10^{-4}$ (Pa·s)	1.95
	normal stress difference coefficient $\Psi_o \cdot 10^{-5}$ (Pa·s^2)	1.15
5.	Density (after annealing) (kg/m^3) at 23°C	906
	at 180°C	764
6.	Melting point (°C)	167

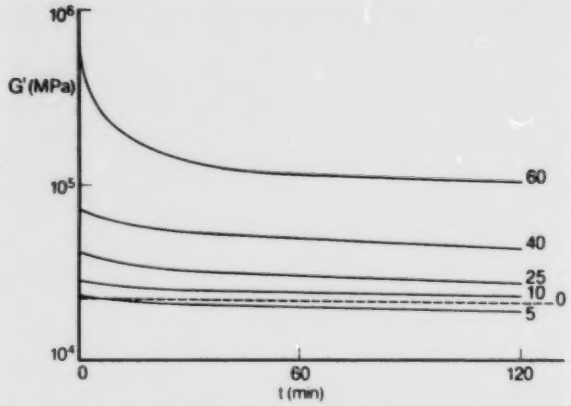

Fig. 4. Time dependence of G′ for PP/mica samples at 180°C, stain 10 percent, and frequency 10 rads/sec. The numbers indicate mica content in wt percent.

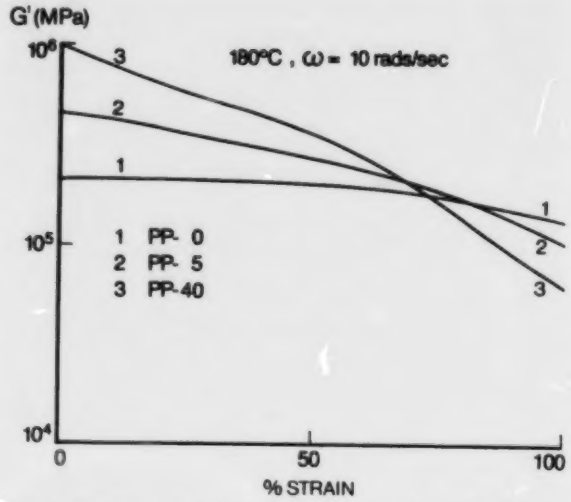

Fig. 5. Strain sweep at 180°C and ω = 10 rads/sec for PP/mica samples; γ = 0 to 100 percent with 2 percent per step.

Strain Sweep

The effect of strain, γ, on G' at 180°C and ω = 10 rads/sec is presented in *Figs.* 5 and 6; in the first case γ = 0 to 100; in the second γ = 0 to 15 percent. Since, in these tests, each change of γ takes 2.73 minutes, it is possible to independently vary the strain and time spans. This is quite useful for materials whose properties depend on these two variables. In *Fig.* 7, G' and G'' vs. γ are shown. Two rates of strain increases were used, resulting in total elapsed times of 4.1 and 39.7 minutes for the upper and lower sets of data respectively. Additional strian sweep data will be presented discussing the mechanisms responsible for G' variability with time and strain (see **DISCUSSION**).

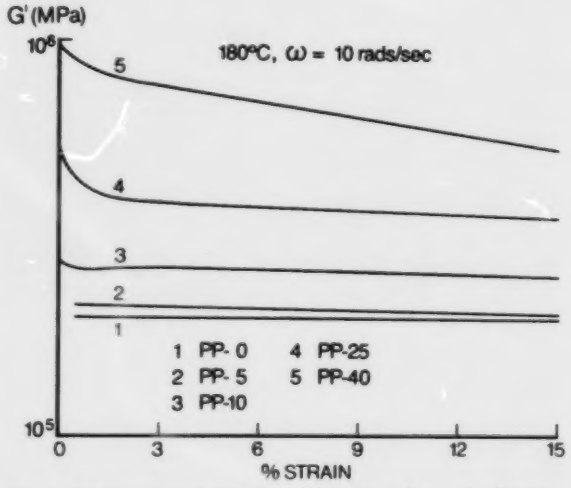

Fig. 6. Strain sweep at 180°C and ω = 10 rads/sec for PP/mica samples; γ = 0 to 15 percent with 0.5 percent per step.

Frequency Scan

An example of these results is shown in *Fig.* 8. Two loadings of PP samples were done, one starting at frequency $\omega = 10^{-1}$ and increased to $\omega = 10^{2}$, the second starting at ω = 1 and decreased to $\omega = 10^{-2}$ rads/sec. An excellent overlap of data points within one decade of frequency was always obtained.

An example of the results of frequency scans for PP-mica systems are presented in *Fig.* 9 in form of G', G'' dependence on ω for PP-25 at the three selected values of strain γ = 10, 30, and 50 percent. The strain induced differences in G' (and G'') were observed at higher frequencies, $\omega > \omega_c$ (*c*, γ), for all samples. The critical value of ω depends on both *c* and γ. Even for PP ω_c (0, 30) = 40 and ω_c (0, 50) = 10 rads/s. For PP-10 ω_c (10, 50) < 0.1.

The PP-60 samples between serrated plates fractured even at the lowest γ = 10 percent and ω = 0.1 rads/s. For this reason, the frequency scan was performed using the torsion-rectangular fixtures for solid specimens at γ = 0.05 percent and ω = 0.1 to 100 rads/s. The response was a smooth, nearly linear (log-log plot!) increase of both: $G' \cdot 10^{-6}$ from 4.3 to 24 Pa and $G'' \cdot 10^{-6}$ from 7.3 to 18 Pa.

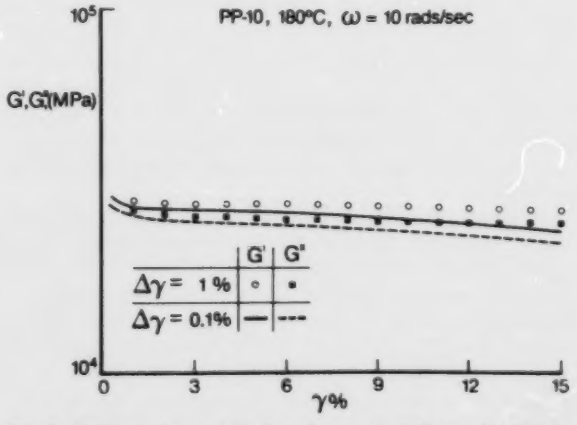

Fig. 7. Strain sweep at 180°C and ω = 10 rads/sec for PP-10, γ = 0 to 15 percent in steps of 1 percent (points) and 0.1 percent (curves).

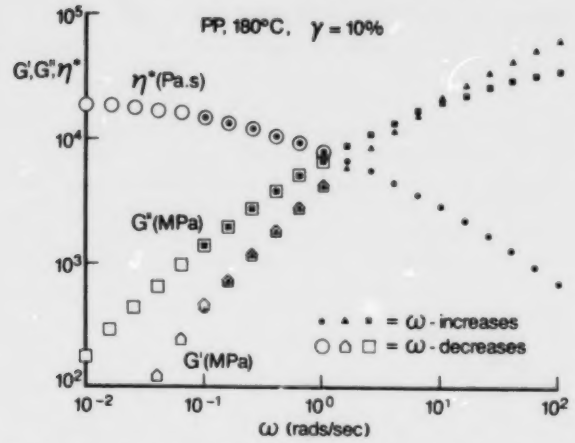

Fig. 8. Frequency sweep for PP at 180°C and γ = 10 percent. Two samples were tested at ω = 0.1 to 100 and ω = 1 to 0.01 respectively.

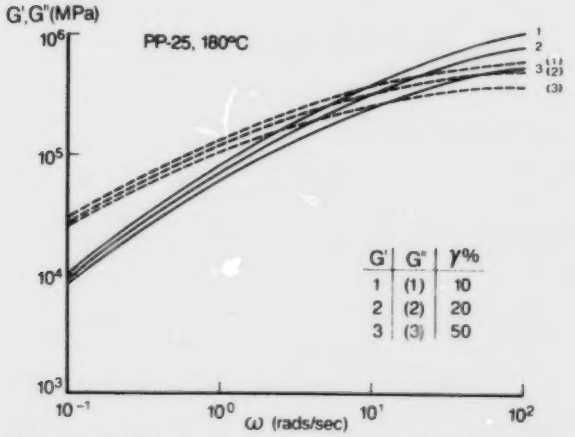

Fig. 9. G′ and G″ vs. ω at 180°C and γ = 10, 30, and 50 percent for PP-25.

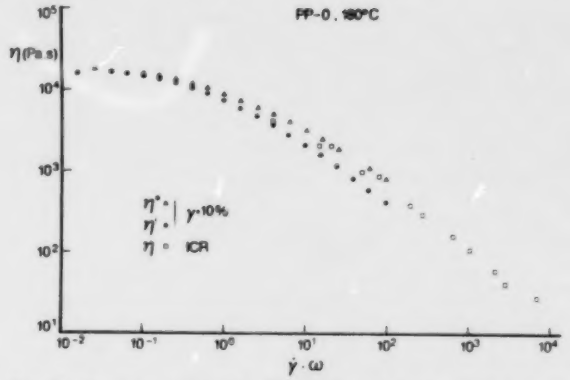

Fig. 10. Comparative results from ICR and RMS (strain γ = 10 percent) for PP-0 at 180°C.

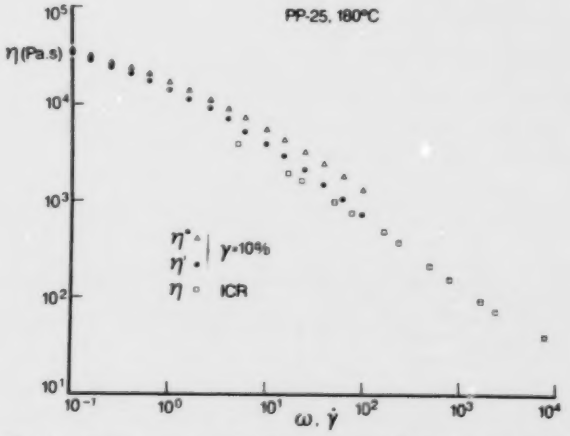

Fig. 11. Comparative results from ICR and RMS (strain γ = 10 percent) for PP-25 at 180°C.

ICR Data

Viscosities

In all cases at least 3 capillaries, in each of the two diameter categories, were used. The results followed one single curve indicating no slip on the wall and no need for Mooney correction. With increasing concentration of mica there was a systematic decrease in both melt fracture and extrudate swell. No pressure oscillation was observed.

Examples of correlations between the complex, η^*, dynamic, η', and the steady-state (capillary), η, viscosities are shown in *Figs. 10* and *11* for PP-0 and PP-25 respectively. Note that in the latter case the η^* and η' are measured within the strain-dependent region ($\omega = 10$). The data are summarized in *Fig. 12* where η for PP-0 to PP-40 is compared with η' measured at the three values of strain: γ = 10, 30, and 50 percent. For clarity, the dynamic data points are omitted and the curves consecutively, for each polymer, displaced vertically by one decade. It is quite apparent that η does not increase with c nearly as much as η'.

This point is further illustrated in *Fig. 13* where the ICR values for all samples are plotted *vs.* rate of shear, $\dot{\gamma}$. For clarity, the data for PP-0 and PP-60 are represented by solid and broken lines, respectively. The standard error of these measurements is $\sigma = \pm 6.4$ percent; within this range, the viscosities of the samples containing $c = 0$ to 25 wt percent of mica are the same. The viscosities of PP-40 and PP-60 are respectively about 40 and 100 percent larger than that of PP-0. There is the same tendency toward a lower Newtonian plateau at $\dot{\gamma} > 10^3\ s^{-1}$.

Entrance/Exit

In *Fig. 14*, the Bagley correction, P_e, is plotted as a function of corrected shear stress for three samples: PP-0, PP-10, and PP-60. The other data for PP-5, PP-25, and PP-40 follow the dependence for PP-10. In all cases the data from two different capillary diameters followed the same dependence. As can be seen, at lower shear stress $\sigma_{12} < 7.10^4$(Pa) the P_e is proportional to σ_{12}, whereas above this limit $P_e \propto \sigma_{12}^m$, where $m = 1$ for PP-60, $m = 1.7$ for PP-10, and $m = 2.67$ for PP-0.

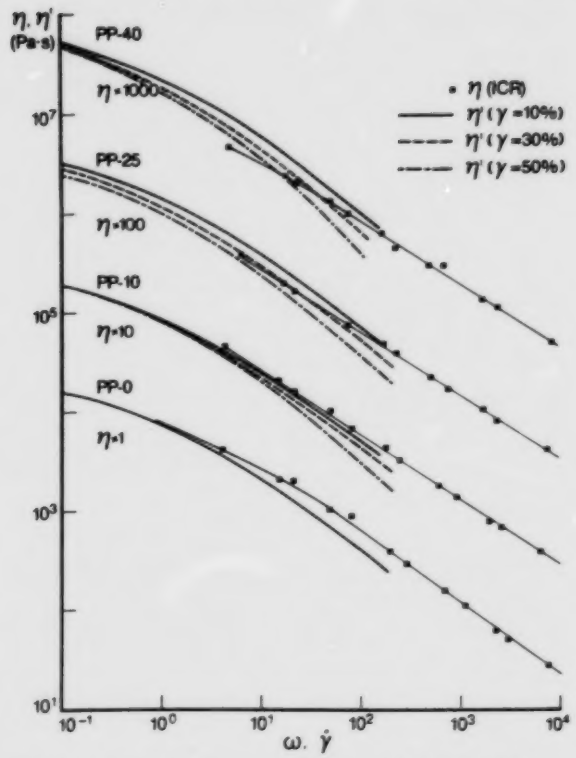

Fig. 12. Comparison between η(ICR) and η' determined at three strain levels γ = 10, 30, and 50 percent for PP-0, PP-10, PP-25, and PP-40. The data for each subsequent composition are multiplied by ten.

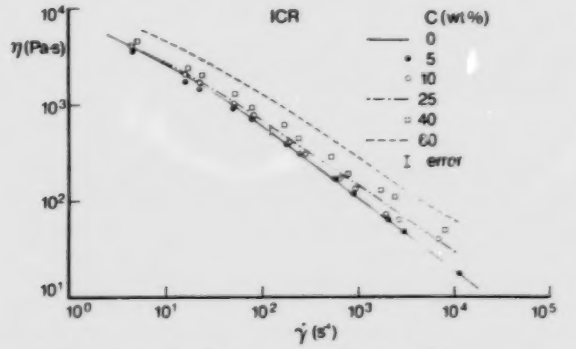

Fig. 13. Summary of η(ICR) vs. γ̇ results for all PP/mica samples (c = 0 to 60 wt percent) at 180°C. The standard error of measurements is indicated.

Extrudate Swell

The results of extrudate swell measurements from the capillary No. 4 at three apparent rates of shear are presented in *Table 4*. Since for this capillary $L/D_o = 32.8$, the swelling may be higher than its equilibrium value at $L/D_o \rightarrow \infty$. During the measurements, the strands were collected in hot silicone oil of density ρ (180°C) = 1087 kg/l. The densities of the samples (listed in *Table 4*) indicate that only for PP-60 the negative buoyancy effect can cause reduction of B; the values $B \ll 1.0$ are most likely due to the gravitational pull.

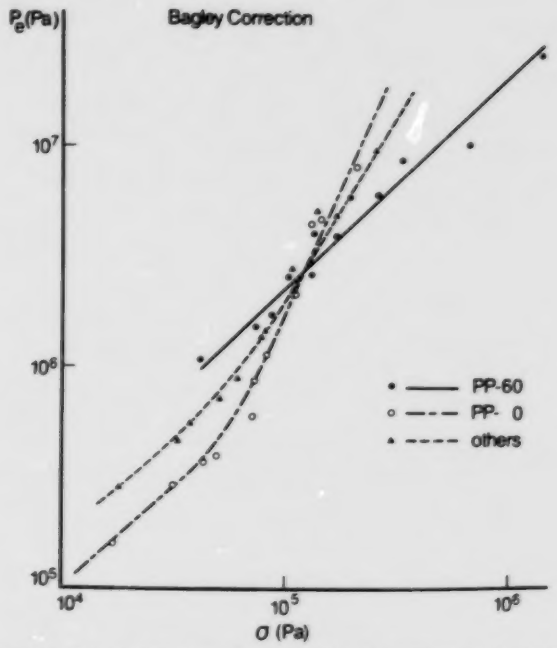

Fig. 14. The Bagley correction P_e vs. the shear stress σ_{12} for PP/mica samples at 180°C.

MORPHOLOGY

ICR

Examples of the orientation of mica flakes in PP are presented in SEM (*Fig. 1*). It can be seen that extrusion at relatively low speed through a long capillary results in nearly perfect circumferencial alignment. The surface of these extrudates is also quite smooth although at $c = 40$ percent the flakes are quite visible under a thin skin of PP. The reason for this is the 20 percent reduction of PP volume between 180°C and ambiant temperature. The stresses during cooling are too small, $\sigma_{11} < \sigma_y$, to cause displacement of interacting mica flakes. Much poorer orientation and surface smoothness were observed extruding at the same rate through shorter, $L/D_o = 10$, capillary; only the first layer near the wall was oriented. This observation contradicts the previous reports on orientation of glass fiber-filled plastics (4); in the latter case only the converging flow at the entry to the die was responsible for orienting the fibers. It was observed that shear flow through long dies decreased the orientation. Here, in the flow of mica flakes, the orientation seems to occur in two steps: at the capillary entrance the flakes are oriented with long axis in the flow direction but randomly in respect to the capillary wall; only in the shear flow is the second orientation accomplished. When the rate of extrusion was increased by a factor of 130 the flake orientation (in extrudates from both long and short capillaries) was much poorer but their surface gloss improved. The reason for this apparent contradiction is the increased rate of PP crystallization on the surface. Due to this quenching effect the extru-

dates were found to be full of voids/holes especially near the centerline of the strands.

RMS

Examples of flakes orientation in RMS samples are shown in SEM, *Fig. 2* for PP-10 and PP-40. In all samples containing $c < 25$ wt percent of mica, the flake orientation parallel to the surface was observed. In this case, there was no apparent effect of (dynamic) testing on flake orientation. For the two highest concentration samples, PP-40 and PP-60, the flakes were mutually oriented in large "stacks", but these were randomly oriented (at different locations) in respect to the sample surface. PP-40 after testing (see *Fig. 2*) showed improved orientation of the flakes near the sample edge.

DISCUSSION

As indicated in *Table 2* the compounding of mica into PP-60 lowered both d_v and Ψ by about 15 percent, i.e., the diameter of flakes was reduced without reduction of their thickness. The incorporation of PP-60 into the remaining samples and subsequent ICR testing further reduced d_v and Ψ by about 10 percent. In *Fig. 15* these values are compared with those reported previously (5). It is apparent that using a master-batch method one may obtain samples of much more uniform particle diameter than by individual compounding of each sample, as done before. However, the relative amount of attrition for heavily loaded materials is similar in both cases. In the subsequent discussion the diameter and aspect ratio of mica will be assumed to be the same for all PP-compositions.

Using the recently proposed empirical relation (11) obtained by sedimentation of crushed glass fibers:

$$1/\phi_m = 1.38 + 0.0376 p_w^{1.4}; \qquad p_w = 3\Psi/2 \quad (5)$$

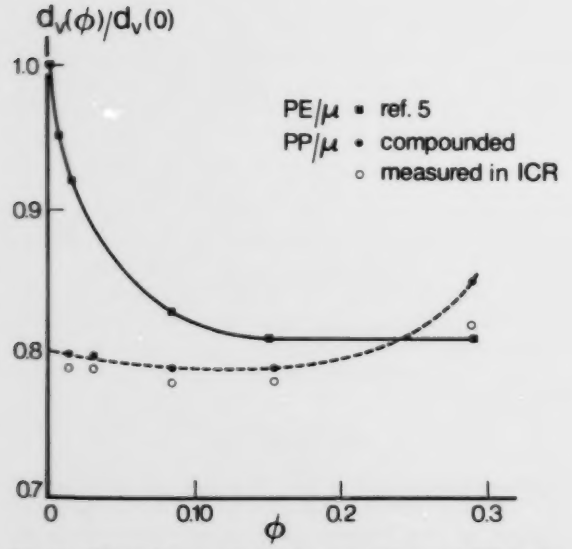

Fig. 15. Effect of the methods of compounding and ICR testing on the relative mica flake diameter; see text.

the maximum packing volume fraction $\phi_m = 0.0429$ may be cal ulated. Correcting this for flake geometry (2–4), $\phi_m = 0.0472$ is found; i.e., the PP-25, PP-40, and PP-60 may flow only if the flakes are mutually oriented.

In the region of dilute suspension, $\phi \ll \phi_c \doteq 1/\Psi = 0.0166$, the period of rotation of a flake may be calculated as (4):

$$t_p = 2\pi\,(p + 1/p)/\dot{\gamma} \qquad (6)$$

Substituting: $p = 3\Psi/2$ the value $t_p = 569/\dot{\gamma}$ (sec) is found. This means that for dilute systems, with mica content $c < 5.9$ wt percent at low $\dot{\gamma}$ the tumbling process is rather slow; even for $\dot{\gamma} = \omega = 10$ it takes about a minute to rotate an average flake.

The prepared PP/mica samples are quite thermally stable for about 1.5 hour at 180°C. During this time the most sensitive rheological function, G', decreases by about 6 percent. In RMS tests the time/strain sweeps indicate two simultaneous processes: first, the slower one observed at long times for all samples with a constant rate of $D_T = (\partial \ln G'/\partial t) = -2.35.10^{-5}$ (sec^{-1}), and the second, the rate of which increases with ϕ. Using a decay function:

$$G' = G_o' \exp(-t/\tau) \qquad (7)$$

the first process can be expressed in terms of the relaxation time $\tau_1 = 42{,}553$ sec and the second:

$$\tau_2 = 76 \exp\{-12.5\phi\}; \qquad \phi > 0 \qquad (8)$$

The τ_2 calculated from *Eq 8* is quite similar to the t_p values derived from *Eq 6* at corresponding frequency. In consequence, the observed time/strain decrease in the rheological signals may be explained by a slow thermal degradation and relatively rapid orientation of flakes. The second process strongly depends on ϕ, indicating that, at higher concentrations, flakes are pre-oriented and the imposed shear field causes rather rapid readjustment of flake orientation relative to the shear plane.

One of the most interesting areas of dynamic flow involves the strain dependence of the rheological functions. Variation of G' is of particular interest. In *Fig. 7*, for PP-10, the strain sweep at $\gamma = 0$ to 15 percent using two different steps are shown. The dependence is complex due to compressive yielding (see below), thermal degradation and strain dependence. These measurements were repeated with different steps as well. The numerical data were analyzed by subtracting the thermal degradation effect and plotting the normalized $\ln(G'/G_o')$ *vs.* γ (G_o is the initial value of G' at $t = 0$). The resulting plot was found to be independent of the rate of strain increase (size of the step). There were three clearly defined zones of behavior:

(1) for $\gamma < 2$ percent, initial compressive yielding,
(2) for $2 < \gamma < 5.5$, a flat, strain independent response, and
(3) for $\gamma < 5.5$, a second-order type decrease of $\ln(G'/G_o')$.

In short, for PP-10 at $\omega = 10$ rads/s, the strain dependence is observed at $\gamma > 5.5$ percent. This observation was further confirmed by repeating the strain sweep in the range of $\gamma < 1$ percent using 0.01 percent as a step. The measurements at $\omega = 10$ rads/s under a blanket of N_2 were repeated in two directions—increasing and decreasing the γ. By pre-compressing the samples, the compressive yield was eliminated. The resulting data showed an excellent strain and the direction of strain changes independent response down to 0.15 percent, limited by the sensitivity of the instrument. Similar results were obtained for PP-25, but not for PP-40. In the latter case, G' was found to decrease in the whole experimentally accessible range of $\gamma > 0.1$ percent.

It is not a coincidence that for PP samples with $\phi > \phi_m$, or containing $c > 25$ wt percent of mica, the strain scans do not show any strain independent plateau and that their flow parameters depend on the direction of the rate of shear changes. Here pre-shearing at higher rates causes improved orientation of flakes and lower viscosity at low rates in comparison to the non pre-sheared sample. This phenomenon is also responsible for yield.

The calculation of the yield stress was performed using the modified Casson relation, written in the form (4):

$$(G'')^{1/2} = \sigma_y^{1/2} + a(G''_{PP})^{1/2} \qquad (9)$$

where the sample G'' and matrix G''_{PP} loss moduli are taken as measures of the shear stress at the same frequency, ω = const. An excellent linearity with the correlation coefficient squared $r^2 \geq 0.9996$ was obtained. The results are shown in *Fig. 16* and in the third column of *Table 5*.

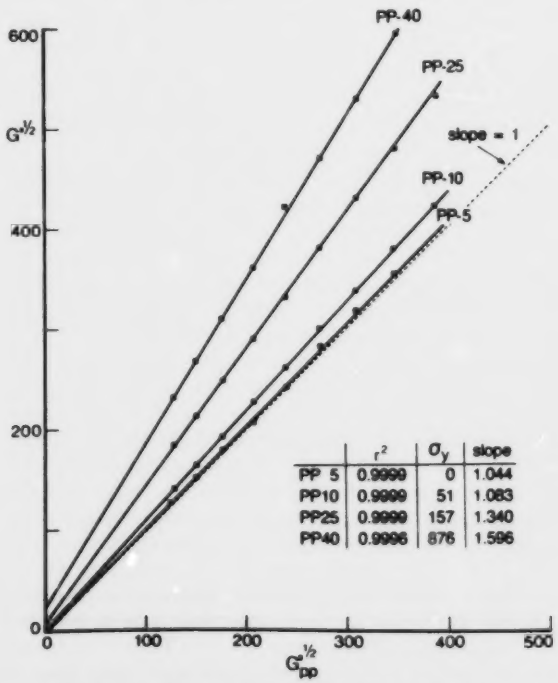

Fig. 16. Modified Casson plot for PP/mica. See text.

Table 5. Yield Stress in Compression and Zero Shear Viscosity for PP/Mica Samples.

Sample	ϕ	σ_y	$\sigma_{y,c}$	$\eta_o \times 10^{-4}$	η_r^o	$G' \times 10^{-6}$
PP-0	0.0000	0[a]	—	1.95	1.00	2.850[b]
PP-5	0.0140	0	50	2.45	1.18 ± 0.09	3.485
PP-10	0.0290	51	100	3.28	1.38 ± 0.12	3.862
PP-25	0.0823	157	199	6.14	2.81 ± 0.60	4.449
PP-40	0.1520	876	749	7.85	6.93 ± 1.07	4.796
PP-60	0.2874	—	12,000	—	—	

[a] Computed from modified Casson Eq 9.
[b] G' at γ = 50 percent, ω = 40 rads/s.

The dynamic testing in RMS should start when a loaded and trimmed sample has completely relaxed. This is evidenced by the gradual decrease to zero of the normal stress meter. For PP/mica systems this signal was seen to exponentially decrease to a stable positive value of thrust, proportional to the yield stress in compression, $\sigma_{y,c}$. The values of this parameter, also listed in *Table 5*, can be approximated by an empirical dependence:

$$\sigma_{y,c} = 22 \exp\{19.19\phi\}; \qquad \phi > 0.014. \quad (10)$$

It may be a coincidence but the yield stress in elongation, $\sigma_{y,e}$, calculated (4) for HDPE/mica system has the same exponential form:

$$\sigma_{y,e} = 1.88 \exp\{19.2\phi\}; \quad \phi > 0,$$

but with about 12 times smaller pre-exponential factor. This is most likely due to the fact that the mica previously used was highly polydispersed and silane treated and that HDPE was of low molecular weight.

Comparing $\sigma_{y,c}$ with σ_y, it is surprising to see their relative agreement. First of all, for unoriented particles von Mises criterion for plastic flow of solids should be obeyed, i.e., $\sigma_{y,c} = \sigma_y \times 3^{1/2}$. Indeed, for the low concentration systems $\sigma_{y,c} > \sigma_y$. However, for samples with $\phi > \phi_m$ $\sigma_{y,c} \simeq \sigma_y$ indicating that the compressive yielding occurs via the shear mode, i.e., the flakes exist in an oriented state.

In *Table 5* the zero shear viscosities, η_o, are also given. These were calculated from the Cole-Cole plot (5), corrected for σ_y. Using these values the relative viscosity at zero deformation rate can be calculated:

$$\eta_r^o = \eta_o(\phi)/\eta_o(\phi = 0) \mid_{\dot{\gamma} \to 0} = f(\phi). \qquad (11)$$

The dependence (11) is presented in *Fig. 17* for PP/mica as well as for the previously studied (5) HDPE/mica system. The similarity of these two curves (Nos 1 and 2 in *Fig. 17*) give a confidence to the developed method of treatment. Both curves show a very rapid initial increase of η_r^o with ϕ, much steeper than prediced by the Einstein hard sphere equation:

$$\eta_r^o = 1 + 2.5\phi \qquad (12)$$

represented by curve No 4 in *Fig. 17*. The slope $[\eta]_c = d \ln \eta_r^o / d\phi$ is a measure of the hydrodynamic volume of the suspended particle, dependent on the aspect ratio and its ability to rotate. By virtue of the lower slopes for PP/mica dependence one

has to postulate an increased hindrance of rotation of these larger, more uniform sized flakes dispersed in more viscous matrix. For both systems, the initial concave curves change to convex at around $\phi \doteq \phi_m$, i.e., the higher loading of mica drastically reduces the freedom of rotation of flakes, especially in the PP/mica suspensions.

The straight line dependence in *Fig. 17* (curve 3):

$$\eta_r = \eta(\phi, G'')/\eta(\phi = 0, G'')\,|_{G''=\text{const.}} \qquad (13)$$

was calculated via a modified Kitano, *et al.* (12) method. These authors observed that for low ϕ the ratio of suspension viscosity to matrix viscosity at the same shear stress level, σ_{12} = const., is nearly constant. As ϕ increases the plot of log η_r *vs.* log σ_{12} shows a decrease of η_r to a plateau level at high σ_{12}. The decrease was explained by yield and/or orientational effects at higher deformation stresses. For low aspect ratio suspensions, $p < 28$, the authors observed a concaved shape of log η_r *vs.* ϕ dependency.

Using the data presented in *Figs. 10* to *12*, η_r was computed at constant value of G'', using both dynamic and complex viscosity ratios. Within the range of $G'' = 10^4$ to 10^5 Pa there was no systematic variation of η_r with G'' and the average values (quoted in the last column in *Table 5*) were plotted *vs.* ϕ in *Fig. 17*. The dependence:

$$\eta_r = \exp\{12.7\phi\}, \qquad (14)$$

with the correlation coefficient squared $r^2 = 0.9996$ was obtained. It can be seen that at a constant value of stress the hydrodynamic volume of mica flakes is constant, $[\eta]_c = 12.7$, within the investigated range of G'' and ϕ.

Lingard and Whitmore (13) measured the relative viscosities of suspensions of plastics discs in aqueous media. Their results are presented in *Fig. 18* along with the $[\eta]_c$ value determined by the Kitano method for mica. The data can be represented by a straight line dependence:

$$[\eta]_c = 2.51 + 0.1127p; \quad r^2 = 0.9960 \qquad (15)$$

For $p \to 1$, $[\eta]_c \to 2.62$ in a small variance with the Einstein theoretical prediction.

To complete the discussion on η_r, it is worth returning to *Fig. 13*. Using, e.g., the Spencer and Dillon extrapolation method (14), one can estimate η_o for each composition and calculate η_r. Its value: $\eta_r = 1.0 \pm 0.1$, does not depend on c up to 60 wt percent. This clearly indicates that ICR, in which the shear stress and the shear rate depend on the properties of material adjacent to the capillary wall, is not an appropriate tool for multiphase systems. In the case of composites, as the system studied in this work, the particle migration toward the center of the stream can occur and the measured properties are grossly those of the matrix. In polymer blends, there is a well documented tendency for the lower viscosity phase to move toward the wall; again the measured properties are not representative of the sample but of its single phase.

In *Figs. 10* to *12* the dynamic viscosities η' are compared with the viscosities from ICR. It should be stressed that a good superposition from the different diameter sets of capillaries was obtained, indicating neither slip in the die nor the shear crystallization. At the same time in the dynamic testing, especially at larger strains, a slip between sample and oscillating plate was observed for $c >$ 10 wt percent of mica. For this reason, the dynamic data were collected using the serrated 5 cm diameter plates. Under these conditions good, reproducible within ±4 percent, results were obtained for all but PP-60 samples. In the latter case, a planar fracture inside the samples was observed.

The η(ICR) *vs.* $\dot{\gamma}$ for linear viscoelastic polymer melts (8, 9) usually follows $\eta = \eta^*$ dependence at high deformation rates and $\eta = \eta'$ at low ones. This tendency is also observed for PP-0 in *Fig. 10*. However, as mica content increases the η(ICR) depend-

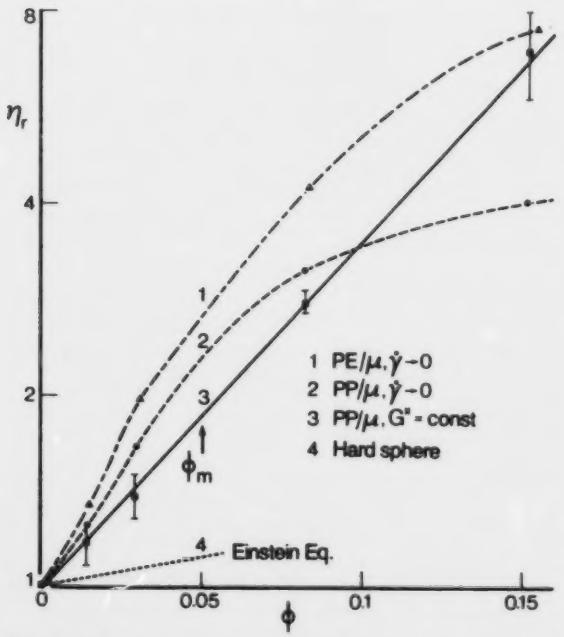

Fig. 17. Relative viscosity vs. volume fraction of mica in HDPE (5) and in PP. The dependence for hard sphere suspensions is also shown.

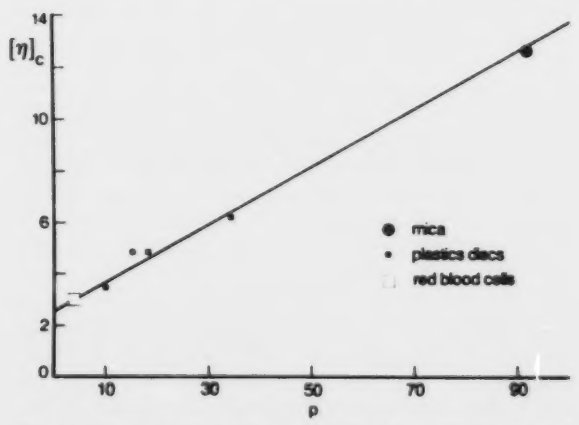

Fig. 18. The intrinsic viscosity, $[\eta]_c$, vs. the aspect ratio p, for mica, plastics discs and blood cells (13).

ence progressively drifts lower and lower with respect to the dynamic results. This tendency is caused by the mismatched strains in these two types of measurements leading to the shear fractionation in capillary flow. Numerous examples of this effect were presented before (2, 4).

Onogi and Matsumoto reported (15) that the steady state data of polystyrene, PS, solution filled with crosslinked PS-spheres could be approximated by η' at $\gamma \doteq 20$ percent. The results in *Figs. 10* to *12* indicate that η(ICR) may be approximated by η' only for $c < 25$ percent and if η' is determined at strains which increase with ϕ; for $c = 0$, 5, 10, and 25 wt percent the required strains should be approximately 10, 15, 30, and 50 percent, respectively. There are two possible reasons for this, both related to the wall effect in capillary flow: the increasingly important (1) orientation of mica flakes, and (2) the shear depletion of particles in the skin area. Note that in comparing the dynamic and capillary data the attempt is to correlate a relatively uniform, low strain behavior of the material, firmly attached to the serrated RMS plates with a highly non-uniform plug-flow result, determined by shearing of a thin "skin" layer, adjacent to the capillary wall. The concentration is constant within the plug, but not in the "skin" (4).

The extrudate swell *vs.* c behavior, presented in *Table 4*, is another evidence of the differences between the capillary and dynamic type of deformation. If B is to be related to the elastic component of the flow tensor (16) then its value should increase with c, to parallel the G' behavior (see *Fig. 6* or *Table 5*). Instead, addition of mica systematically decreases B toward zero swelling at $40 < c < 60$ wt percent.

The correlation between B and the recoverable shear strain, s, has been frequently discussed (16). Assuming $s = G'/G''$, one can calculate the values of B_o for a uniform capillary flow. If the difference between B and B_o is due to a plug flow, then the reduction in B should be proportional to the relative size of plug, P (in percent); for PP-0 though to PP-60 the values of P change respectively from 0 to 35, 49, 75, 97, and 100 percent. These approximate calculations indicate a significant amount of non-Poiseuille flow already for the sample containing 5 percent of mica. This is easy to understand (4) noting the relative diameters of the mica flake ($d_v = 139$ μm) and of the capillary ($D_o = 775$ μm). The effect of the relative size of filler particle on the flow profile was discussed in detail by Mason, *et al.* (See Refs. 4 and 17). For hard sphere suspension in Newtonian liquid at the 33 vol percent of loading upon increase of the d_v/D_o ratio from 0.056 to 0.112, P increased from about 25 to 100 percent.

SUMMARY

(1) The method of preparation of samples by dilution of a highly concentrated "master batch" provides uniform mica size in all samples.

(2) Slow thermal degradation of PP and faster, theoretically predicted flake orientation complicate the dynamic measurements.

(3) The slip on the upper platen in RMS tests was observed for the PP/mica system, but there was no slipping in ICR capillary flow.

(4) The strain dependence of G' and G'' was found to depend on mica content and test frequency. At $\omega = 10$ rads/s the limiting strains for linear responses for $c = 0$, 5, 10, 25, and 40 wt percent were respectively 58, 28, 5.5, 1.5, and <0.1 percent.

(5) If the Bagley correction, P_e, is taken as a measure of the elastic component in flow then three dependencies P_e *vs.* σ_{12} describe the system; one for PP, another for PP-60, and the third for all remaining samples. The crossover point for these three relations is at $\sigma_{12} = 1.2 \times 10^5$ Pa and $P_e = 2.5 \times 10^6$ Pa.

(6) An agreement between capillary and dynamic test results can be obtained for samples containing $c \leq 25$ wt percent of mica only if γ increases with ϕ.

(7) Capillary rheometry is an unreliable test method for multiphase systems.

(8) The yield stress for uniform size, untreated mica flakes is 12 times higher than that for treated, polydispersed flakes of about three times smaller aspect ratio.

(9) Comparison of the compressive and shear yield stresses provides an insight into filler orientation.

(10) The intrinsic viscosity of platelets varies linearly with the aspect ratio.

ACKNOWLEDGMENT

The authors wish to thank Mr. P. Sammut for his excellent measurements of the dynamic properties reported in this paper.

NOMENCLATURE

a	= Parameter in *Eq* 9.
B	= Extrudate swell (D/D_o).
c	= Mica concentration (wt percent).
d, d_i, d_v	= Mica particle diameters, monodisperse/circular, individual and Feret's average, respectively (μm).
D	= Extrudate diameter (mm).
D_o	= Capillary diameter (mm).
D_T	= Thermal degradation rate (s^{-1})
G', G''	= Shear storage and loss moduli, respectively (MPa).
G_o'	= G' at $t = 0$.
h	= Flake thickness (μm).
L	= Capillary length (mm).
M_n, M_w	= Number and weight average molecular weights, respectively.
n_i	= Number of flakes of diameter d_i in *Eqs 1* and *2*.
p, p_w	= Aspect ratio and weight average aspect ratio, respectively.
P_e	= Bagley correction (pressure drop) in capillary flow (Pa).
r^2	= Correlation coefficient squared.

t, t_p = Time and flake period of rotation, respectively (s).
$V_{H,i}$ = Encompassed volume of an individual mica flake.
V_r = Volume of a mica sample in the test; *Eqs 2, 4*.
W = Weight of a mica sample in the test; *Eq 4*.
γ = Strain (percent).
$\dot{\gamma}$ = Strain rate (s^{-1}).
η, η_o = Viscosity and zero shear viscosity, respectively (Pa.s).
η_r, η_r^o = Relative viscosity and zero-shear relative viscosity, respectively.
η', η^* = Dynamic and complex viscosity, respectively (Pa.s).
$[\eta]$, $[\eta]_c$ = Intrinsic viscosity and its value at non-zero c, (m^3/kg).
ρ = Density (kg/m^3).
σ_{12} = Shear stress (Pa).
σ_y, $\sigma_{y,e}$, $\sigma_{y,c}$ = Yield stress in shear, elongation and compression, respectively (Pa).
τ, τ_i $(i = 1,2)$ = Relaxation time in *Eq 7*, (s).
ϕ, ϕ_c, ϕ_m = Volume fraction of mica flakes and its value at a flake overlapping concentration and at the maximum packing, respectively.
Ψ = Mica flake shape factor, *Eq 2*.
Ψ_o = First normal stress difference coefficient at the zero rate of shear limit (Pa.s^2).
ω = Frequency in dynamic tests, (radians/s).
ω_c = Critical value of ω above for which strain dependence in G' is observed.

REFERENCES

1. Proceedings of NRCC-IMRI mini-symposia: "Composites-'81", Montreal, Dec. 8, 1981, *Polym. Compos.*, **3**, No. 4, (1982); "Composites-'82", Montreal, Nov. 30, 1982, *Polym. Compos.*, **5**, No. 1, (1984); "Composites-'83", Boucherville, Nov. 29, 1983, *Polym. Compos.*, this issue.
2. L. A. Utracki and B. Fisa, *Polym. Compos.*, **3**, 193 (1982).
3. L. A. Utracki, Proceed. 74th AICHE Meeting, Los Angeles, CA, Nov. 15–18, 1982.
4. L. A. Utracki, Proceed. A.C.S., Rubber Division 124th Meeting, Houston, Texas, Oct. 25–28, 1983; Rubber Chem. Technol., *57*, 507 (1984).
5. B. Fisa and L. A. Utracki, *Polym. Compos.*, **5**, 36 (1984).
6. B. Fisa and L. A. Utracki, Proceeds., SPE-NATEC, Detroit, Michigan, Sept. 20–22, 1983.
7. L. A. Utracki and J. Lara, *Polym. Compos.*, **5**, 44 (1984).
8. L. A. Utracki and R. Gendron, Proceeds, CSCHE Meeting, Toronto, Ontario, Oct. 3–7, 1983; J. Rheol., *28*, (1984).
9. L. A. Utracki, A. M. Catani, G. L. Bata, M. T. Kamal, and V. Tan, *J. Appl. Polym. Sci.*, **27**, 1913 (1982).
10. L. A. Utracki, Z. Bakerjian, and M. R. Kamal, *Trans. Soc. Rheology*, **19**, 173 (1975).
11. M. M. Cross, A. Kaye, J. L. Stanford, and R. F. T. Stepto, *ACS Polym. Mater. Sci. Eng. Div., Preprints*, **49**, 531 (1983).
12. T. Kitano, T. Kataoka, and T. Shirota, *Rheolog. Acta*, **19**, 764 (1980); *ibid.* **20**, 207 (1981).
13. P. S. Lingard and R. L. Whitmore, *Chemeca*, 11–24 (1970).
14. R. S. Spencer and R. E. Dillon, *J. Colloid Sci.*, **3**, 163 (1948); *ibid.* **4**, 241 (1949).
15. S. Onogi and T. Matsumoto, *Polym. Eng. Rev.*, **1**, 45 (1981).
16. L. A. Utracki, Z. Bakerdjian, and M. R. Kamal, *J. Appl. Polym. Sci.*, **19**, 481 (1975).
17. H. L. Goldsmith and S. G. Mason, in "Rheology", F. R. Eirich, Ed., Vol. 4, Ch. 2, Academic Press, New York, (1967).

DISCUSSION

M. R. Kamal: You were saying that the capillary viscosities were nearly independent of the mica concentration. You also showed some micrographs. Did you see the layer near the capillary wall to be enriched in polypropylene? Is there any particle migration toward the center during the flow?

L. A. Utracki: I want to emphasize that the results we presented were determined with great care and with excellent reproducibility; all the necessary corrections have been applied throughout. There is a series of fundamental differences between ICR and RMS data! In ICR, using 3 capillaries in two diameters each, the behavior of the mica-containing samples was very similar to that of polypropylene; there was no slip on the wall, the flow was of the power law type with the power exponent $n \doteq 1/3$, the numerical values of the true viscosity at the wall (within the whole range of rates of shear from about 5 to 10^4 sec^{-1}) increased by about 20 percent in the whole range of mica concentration (from 0 to 60 wt percent). By contrast, in RMS, all samples containing mica showed a slip on the oscillating platten (this is why we had to use the serrated plates), all samples at higher strains and frequencies showed $d \log G''/d \log \omega = n \rightarrow 0$, and the values of η^* for the sample containing 40 percent of mica were about three times higher than for polypropylene. This is powerful though indirect evidence that what we are measuring in ICR is only the matrix; possibly with some wall scraping by the mica flakes at the entrance to the die. This is confirmed by the microscopy; the strands have a continuous sheet of the polymer of at least 15 μm thick. Beneath this, there are clearly visible broken fragments not flakes, well-aligned parallel to the surface. All three elements: presence of the polymer layer, visible attrition of flakes, and the alignment indicate that in the capillary flow it is not the average rheological response of the material that is being measured but rather that of a highly modified layer, adjacent to the wall.

M. R. Kamal: Are you saying that you observed a plug flow? If this is so, how do you explain the development of flake orientation during the capillary flow?

L. A. Utracki: I am certain that we have a plug flow. There are two reasons for it: (1) the very low value of log G'' *vs.* log ω slope, which mathematically translates into virtually flat flow profile, and (2) existence of the yield stress. The development of orientation in the capillary flow is probably a relaxation phenomenon. At the entrance to the capillaries, the flake lines are folded like draperies with very large stresses acting at the bends. The stress relaxation gradually pushes the flakes into a regular

orientation. That the time is a crucial parameter is evidenced by poorer orientation of flakes in the bulk of strands at higher rates of shear.

M. R. Kamal: How do these results from capillary rheometer translate into the orientation of flakes and surface roughness during processing of mica-filled polypropylenes? In particular, did you observe a similar behavior during sheet extrusions?

L. A. Utracki: This is the main subject of the presentation of B. Favis later in the day. In general, there should be a direct correlation between these two. However, in screw extrusion of plug-flowing material the pre-orientation in the barrel has to be taken into account.

Elongational Behavior of Short Glass Fiber Reinforced Polypropylene Melts

*M. R. KAMAL *and* A. T. MUTEL

Department of Chemical Engineering, McGill University, Montreal, Canada, H3A 2A7

and

L. A. UTRACKI

Industrial Materials Research Institute, National Research Council, Boucherville, Que., J4B 6Y4 Canada

The Rheometrics Elongational Rheometer was employed to study the uniaxial extensional flow of glass fiber filled polypropylene melts, in which the fiber concentration, c, varied between zero and 40 weight percent. The constant strain rate mode was used for strain rates, $\dot{\epsilon}$, between 0.003 and 0.6 s^{-1}. Steady state elongational viscosities were observed in most cases for fiber filled polypropylene melts, even at rates at which the stress continued to increase for unfilled polypropylene. The rate of relative stress growth increased with $\dot{\epsilon}$ and was affected by the addition of fibers. The steady elongational viscosity of the fiber reinforced melts was found to decrease with increasing $\dot{\epsilon}$ and to increase with increasing c. Yield stresses were observed in elongational flow at high concentrations, although there was no clear evidence of yield in steady shear.

INTRODUCTION

Interest in fiber reinforced thermoplastics has continued to increase during the last decade. This is due to the enhancement achieved in the mechanical and thermal performance of these materials, at reasonable cost. The optimal processing of fiber reinforced thermoplastics requires a detailed knowledge of their thermal and rheological properties. However, due to the complexity of these materials, only a few useful studies have been reported on their rheological behavior, especially in elongational flows. Some of the more significant reports have been related to the behavior of small particle filled melts.

Mewis and Metzner (1) studied the rheological properties of fiber suspensions at low concentrations (0.1 to 1.0 percent by volume) in Newtonian fluids subjected to an elongational deformation. A device based on the concept of melt spinning was used. Extensional viscosities, (η_l), for the fiber suspensions were found to be independent of strain rate. Incorporation of fibers raised the elongational viscosity to a level as much as 260 times greater than that of the suspending fluid. Nazem and Hill (2) measured both the elongational viscosities, at constant stress, and the shear viscosities of glass bead filled styrene-acrylonitrile composites in the rubbery flow region. Elongational viscosities were found to be independent of strain rate, and Trouton ratios, $R_T = \eta_l/3\eta_0$ close to 1 were observed for concentrations less than 20 percent by volume.

Equilibrium viscosities in elongational flow for small particle filled polystyrene melts, measured with an Ide-extensiometer (3) at constant strain rate, were found to decrease with increasing strain rate, even at strain rates at which the elongational viscosity was independent of strain rate for unfilled polystyrene (4–7). Yield stresses were observed, both in shear and extensional flow, for the small particle filled melts. The ratio of the tensile to the shear yield stress was generally found to be close to the von Mises criterion of $\sqrt{3}$. Equilibrium elongational viscosities were observed at low elongational rates for the filled melts. These were found to be as much as 10 times larger than the elongational viscosity for the unfilled polymer melt at the same rates. Equilibrium viscosity increased with increasing filler content, and the effect of particles decreased with increasing strain rate.

Utracki and Lara (8) studied the elongational flow behavior of mica filled high density polyethylene,

* To whom all correspondence should be addressed.

employing a Rheometrics Elongational Rheometer, both at constant strain rate and constant stress. Equilibrium elongational viscosities were found to depend on elongation rate, even at the lower end of the strain rate range covered ($10^{-3} - 3\ s^{-1}$). The Trouton ratio was found to increase with mica content up to the value of 6.7. Subsequently, the ratio decreased with increasing strain rate, as observed in other studies with small particle filled polystyrene (4–7).

The only study of the elongational flow behavior of fiber reinforced thermoplastic melts has been reported by White, *et al* (9, 10) on glass fiber reinforced high density polyethylene and polystyrene melts. The Trouton ratio for the unfilled polymer melt was found to be about 1, while those for the glass fiber filled melts were of the order 10 at low rates. The Trouton ratios for fiber filled melts decreased with increasing strain rate, and the ratio became lower than unity at the higher end of the strain rate range covered ($2 \times 10^{-3} - 1\ s^{-1}$). The rate dependence of elongational viscosity was in qualitative agreement with Goddard's theory (11–13). The effect of fiber concentration was not clearly indicated.

In this paper, we summarize the results of an exploratory study to evaluate the elongational behavior of fiber reinforced polypropylene melts. Emphasis is placed on the qualitative observations made and the phenomena that appear to be associated with the elongational flow of these materials. Although the quantitative aspects of the data should be of interest, detailed discussion of these will be reserved for a future paper.

EXPERIMENTAL

Materials

Injection molding grade polypropylene (PP) compounds filled with 0, 10, 30, and 40 percent by weight glass fibers supplied by the Fiberfill Division of Dart Industries were used in the experiments. The volume percent of glass fibers and average fiber length for each formulation are given in *Table 1* (18). The compound was available in the form of pellets with fiber lengths up to 3 mm and a diameter of 10 μ. Fiber length was reduced during transfer molding, which was employed to prepare the specimens for the tests. Specimens in the shape of cylindrical rods with a diameter of approximately 6.25 mm and a length of 24.0 mm were prepared by transfer molding in sets of 15 at 200°C and 2000 psi. Antioxidant Irganox B-215 supplied by Ciba-Geigy Corporation was used at a concentration of 0.2 percent by weight. The specimens were left to relax and solidify in the mold and later were cut to the proper length. After annealing at 175°C for 3 hours, one specimen from each set was tested at 200°C in the silicon oil used for the elongational experiments, in order to check for deformation due to frozen stresses. Later, the specimens were glued to T-clips, using an epoxy resin, and cured overnight at room temperature.

Table 1. Fiber Content and Dimensions in the Different Formulations

Nominal Weight Fraction of Glass Fibers	Nominal Volume Fraction of Glass Fibers	Average Length of Glass Fibers (mm)
10%	3.8%	1.54
30%	12.8%	0.80
40%	18.3%	0.60

Two kinds of silicon oil were used for the experiments: Dow-1265 for the 30 and 40 percent filled melts and Dow-210H silicon oil for the unfilled melt and the 10 percent filled polypropylene melt. Two different types of oil were required in order to match the densities of the different formulations. Samples were immersed in the oil at 200°C up to 24 hours to evaluate the effect of oil on the polymer. Weight losses of less than 2 percent were observed in 24 hours for Dow-1265. On the other hand, with Dow 210H, in the first 15 minutes an increase in the weight of the polymer up to 2 percent was observed, indicating swelling. This was followed by degradation of the polymer, as indicated by a loss of weight. However, the ratio of elongational viscosity to zero shear viscosity for the unfilled PP was found to be 3.2 which is close to the expected value of 3.0. This result and the superposition of stress growth results with different experimental time histories indicate that there is no appreciable effect of the oil on η_l.

Apparatus

A RER-9000 Rheometrics Extensional Rheometer was used in the constant strain rate mode. Two double beam leaf springs, 1 N and 0.1 N full scale, were used during the experiments. The instrument was calibrated by using standard weights. The sensitivity of the transducer is specified as 0.1 percent of the full scale. The oil bath temperature was controlled to within ∓ 0.2°C. Stress growth and stress relaxation experiments were carried out at 180°.

RESULTS AND DISCUSSION

Stress Growth

Stress growth experiments in uni-axial extensional flow for unfilled polypropylene and glass fiber reinforced polypropylene melts were carried out at constant strain rates between 0.003 and 0.6 s^{-1}. The stress signals for different fiber concentrations are compared in *Fig. 1*, at approximately the same force level. The signal obtained with fiber filled melts shows fluctuations at a level of about ±5 to 15 percent of the mean stress value. The noise level on the stress growth curve for pure melt (note that the scale was expanded 10 times) is much smaller, $\leq \pm 2$ percent. This indicates that the fluctuation of the stress for filled samples is not an artifact but a property of the material itself. These are thought to be related to the fiber motions and fiber-fiber interactions during the flow. Fiber-fiber interactions could be more dominant, considering that the amplitude of fluctuations increases with increasing fiber content.

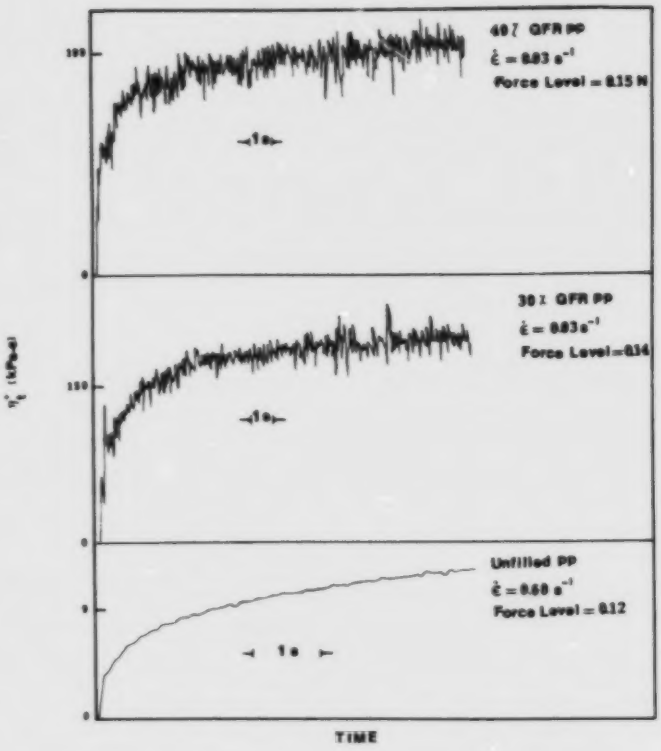

Fig. 1. Stress growth for polypropylene melts filled with 30 and 40 percent glass fibers; 180°C.

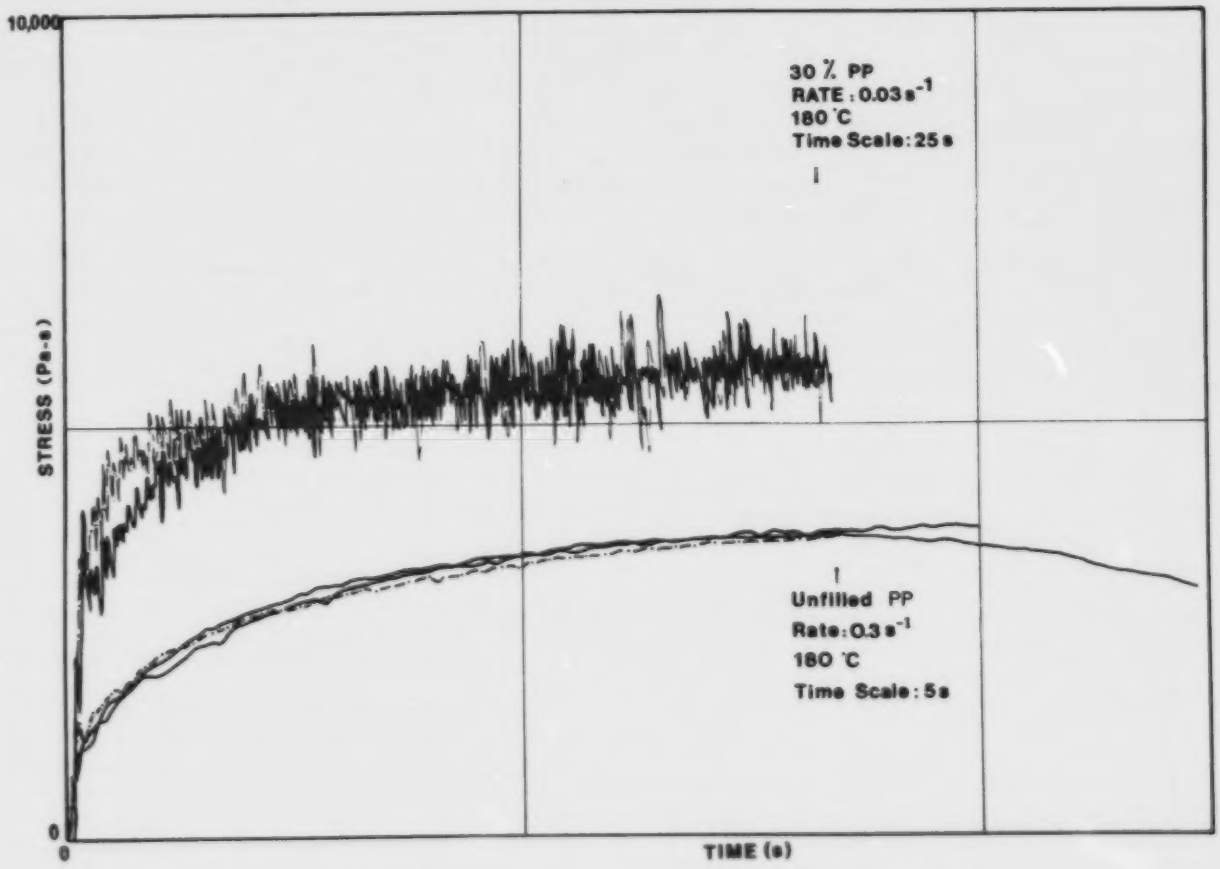

Fig. 2. Reproducibility of the stress growth results for unfilled and filled polypropylene; 180°C.

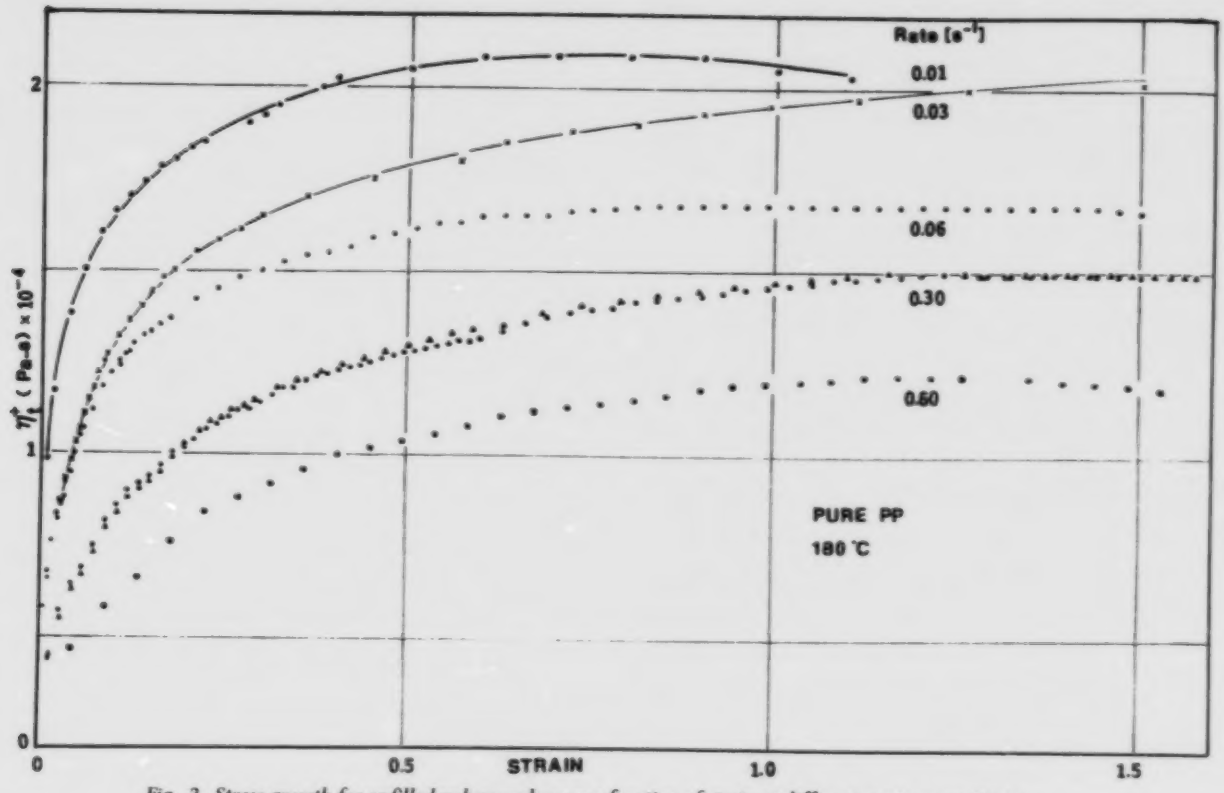

Fig. 3. Stress growth for unfilled polypropylene as a function of strain at different strain rates; 180°C.

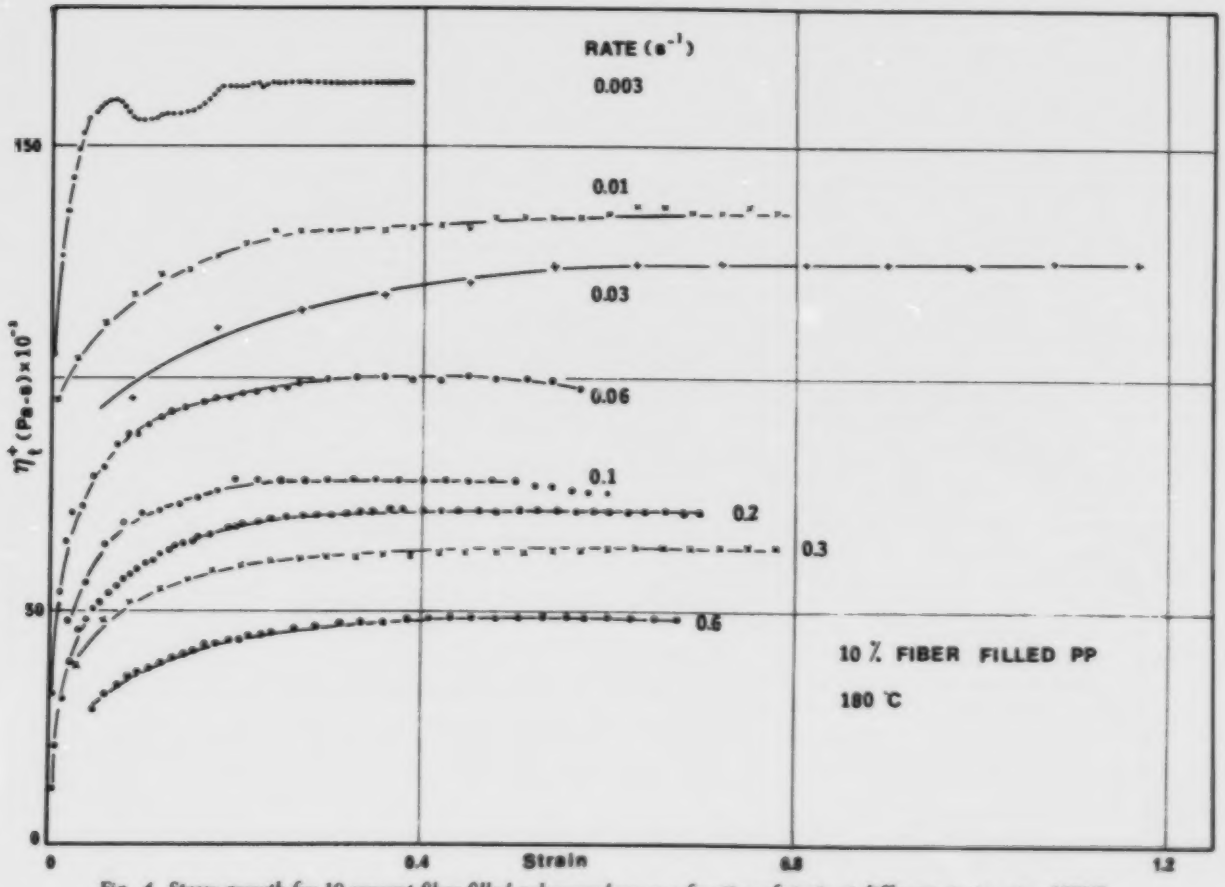

Fig. 4. Stress growth for 10 percent fiber filled polypropylene as a function of strain at different strain rates; 180°C.

The stress growth tests were repeated three times for most of the cases investigated. Reproducibility was found satisfactory. Typical results, both in Dow 1265 and Dow 210H, are shown in *Fig.* 2.

Stress growth was followed up to Hencky strain, ϵ, of 1.5 and 0.5 for the unfilled polymer and for the filled melts, respectively. In earlier experiments, it was found that, for the unfilled PP, there was no necking at $\epsilon \leq 1.8$, while necking became evident at strain levels between 0.6 and 1.0 for the filled melts. As seen in *Fig.* 3, the stress continuously increased with strain up to the maximum allowed strain level, $\epsilon = 1.5$, for the unfilled polymer. At the lowest strain rate, the stress showed a decline for $\epsilon \geq 0.8$ ($t \geq 80$ s), which was due to the onset of flow instabilities. On the other hand, an equilibrium value for fiber filled melts was obtained at strain rates $\dot{\epsilon} \leq 0.1\ s^{-1}$ and strain levels $\epsilon = 0.2$ to 0.4 (*Figs.* 4 and 5). The flow was unstable at $\dot{\epsilon} \geq 0.1\ s^{-1}$.

The data for unfilled and 40 percent fiber filled polypropylene are replotted on a double logarithmic scale in *Fig.* 6. For unfilled PP, the stress growth data coincide on the same line, as reported elsewhere (11). At the highest rate, 0.6 s^{-1}, the data start to deviate at $\epsilon \geq 1.5$ from the main curve due to necking. This result indicates linear viscoelastic behavior for the PP used in this study. Ide and White (3), and Ishizuka and Koyama (14, 15) have reported data on elongational flow of polypropylene melts, showing strain hardening behavior. This phenomenon has not been observed in the present experiments. It should be pointed out that the polypropylene used in Ishizuka and Koyama's work has a zero shear viscosity approximately one order of magnitude higher than the polypropylene used in this work. For filled polymer melts (see *Fig.* 6), the stress growth function depends not only on time, but also on rate. The stress buildup becomes slower with increasing strain rate. Only at very short times, $t \leq 1$ sec, the data for different strain rates superimpose. For $t \geq 1$ sec, the stress growth curves separate from each other, showing a non-linear behavior at low elongation rates as well as at high rates. These same highly filled materials were found to show non-linear behavior even at very low strains in dynamic shear experiments (16).

Linear plots of normalized stress growth data were prepared to observe the rate of approach to the equilibrium value or to the value at the maximum strain used in cases where no equilibrium was reached. At all concentrations, the equilibrium stress was approached faster at higher strain rate. A comparison of the relative stress growth rate for unfilled and filled melts shows that the equilibrium stress is approached faster in fiber filled melts than in pure PP (*Fig.* 7). This indicates that the stresses created by the fibers or fiber structure develop much faster than the stresses associated with the polymer matrix. The rate of stress buildup is comparable at all levels of loading for the filled melts.

The equilibrium viscosities or, in the cases where equilibrium values were not observed, viscosities at the maximum strain, have been plotted in *Fig.* 8.

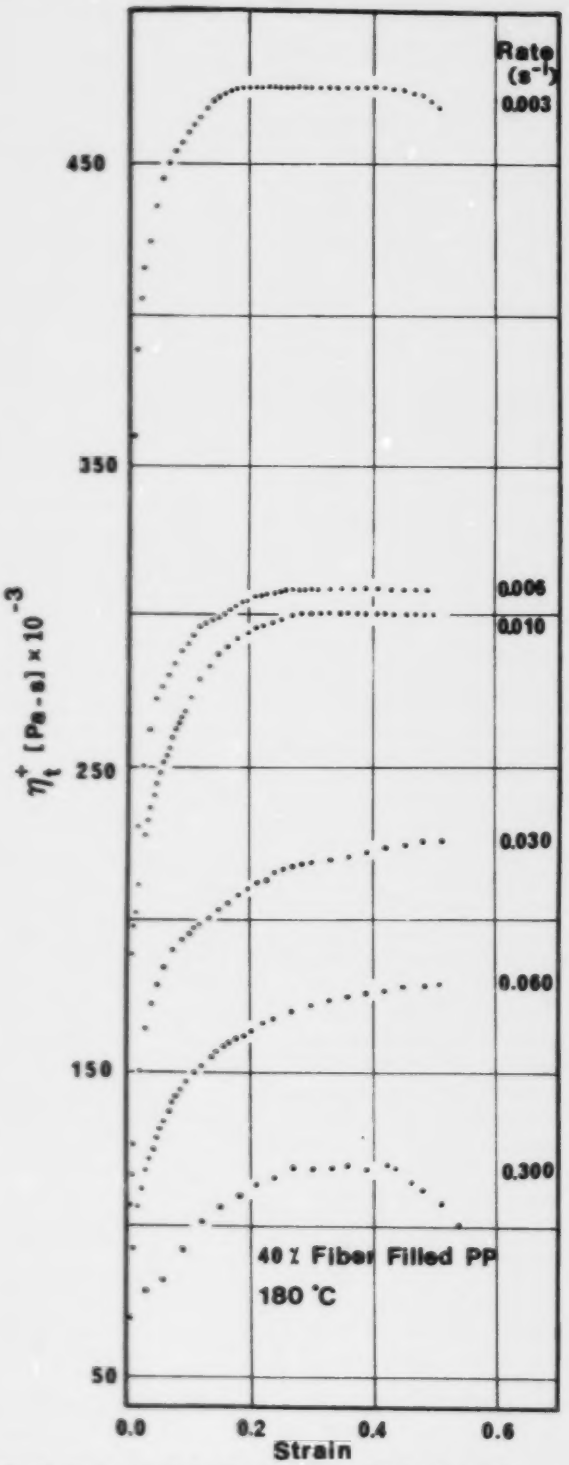

Fig. 5. Stress growth for 40 percent fiber filled polypropylene as a function of strain at different strain rates; 180°C.

For the unfilled melt, the equilibrium viscosity continued to increase with decreasing strain rate, even at the lowest rate covered. This result seems to contradict the linear viscoelastic behavior observed in stress growth experiments for unfilled PP. How-

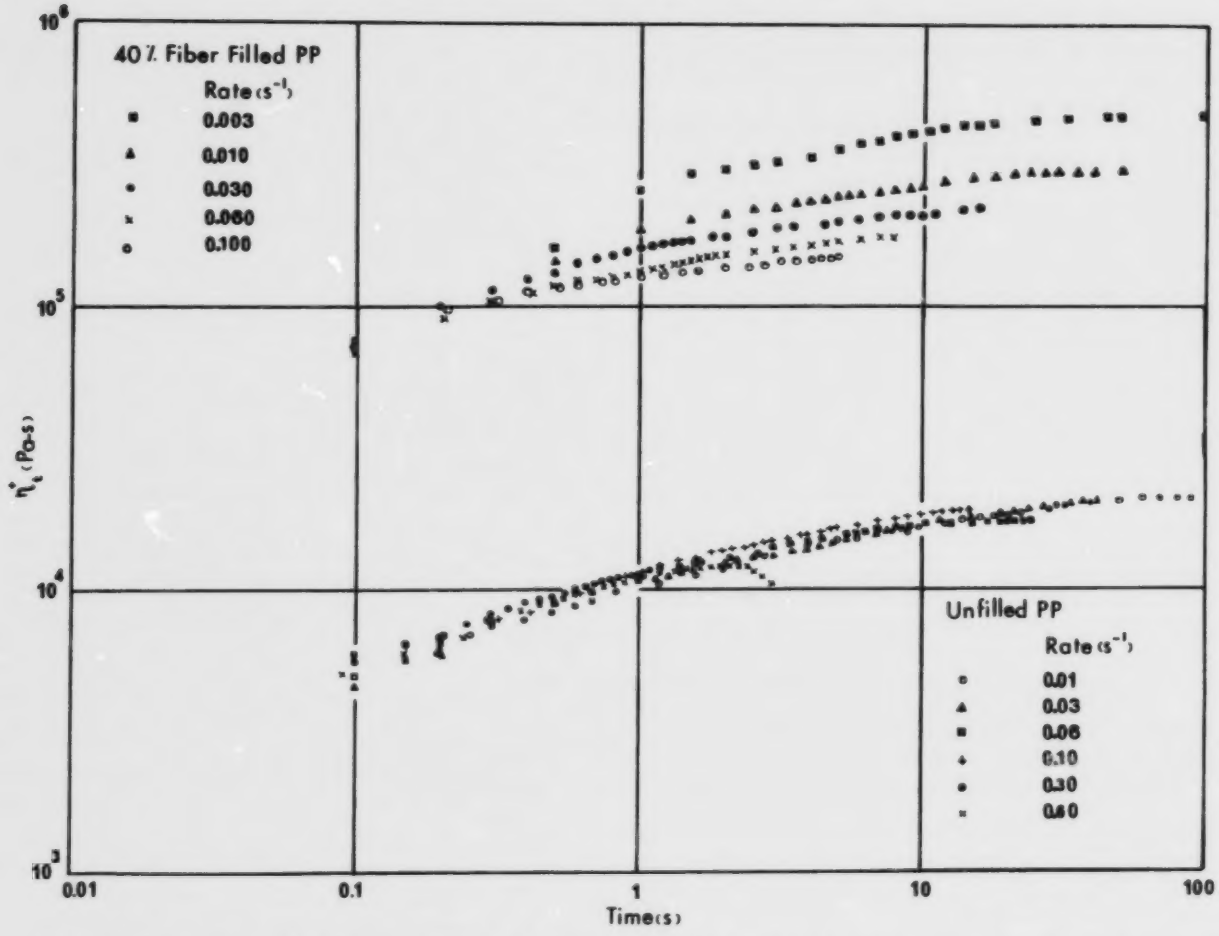

Fig. 6. Stress growth for unfilled polypropylene and 40 percent fiber filled PP as a function of time at different strain rates; 180°C.

ever, as indicated above, no equilibrium viscosities were observed for the unfilled PP up to a Hencky strain of $\epsilon \leq 1.5$. In fact, the elongational viscosity values for PP used in *Fig. 8* were transient elongational viscosities at 1.5 Hencky strain, corresponding to different times on the single stress growth curve (more specifically to shorter times with increasing strain rate). At the lowest strain rate, the ratio of elongational viscosity to zero shear viscosity is 3.2, which is quite close to the expected value of 3.0.

Fiber reinforced melt viscosities decreased with increasing strain rate. in the whole strain rate range covered. This is in agreement with the results of Chan, *et al* (9, 10) for glass fiber filled polyethylene and polystyrene melts. Also, this behavior has been reported for small particle filled melts (4, 6, 8). These results agree qualitatively with the theory of Goddard (11–13) for the tensile behavior of power law fluids containing oriented slender fibers. A steep increase in viscosity at low stresses for 30 and 40 percent glass fiber filled melts indicates yield behavior. Shear experiments between rotating parallel plates have not shown any indication of a yield stress (16). There is no indication of yield stresses

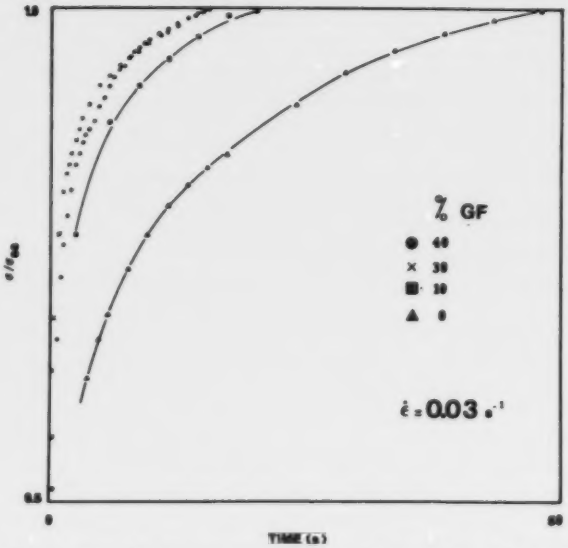

Fig. 7. Normalized stress growth for unfilled and fiber filled PP at $\dot{\epsilon} = 0.03\ s^{-1}$.

in extension for the 40 percent filled melt, although the viscosity continues to increase with decreasing

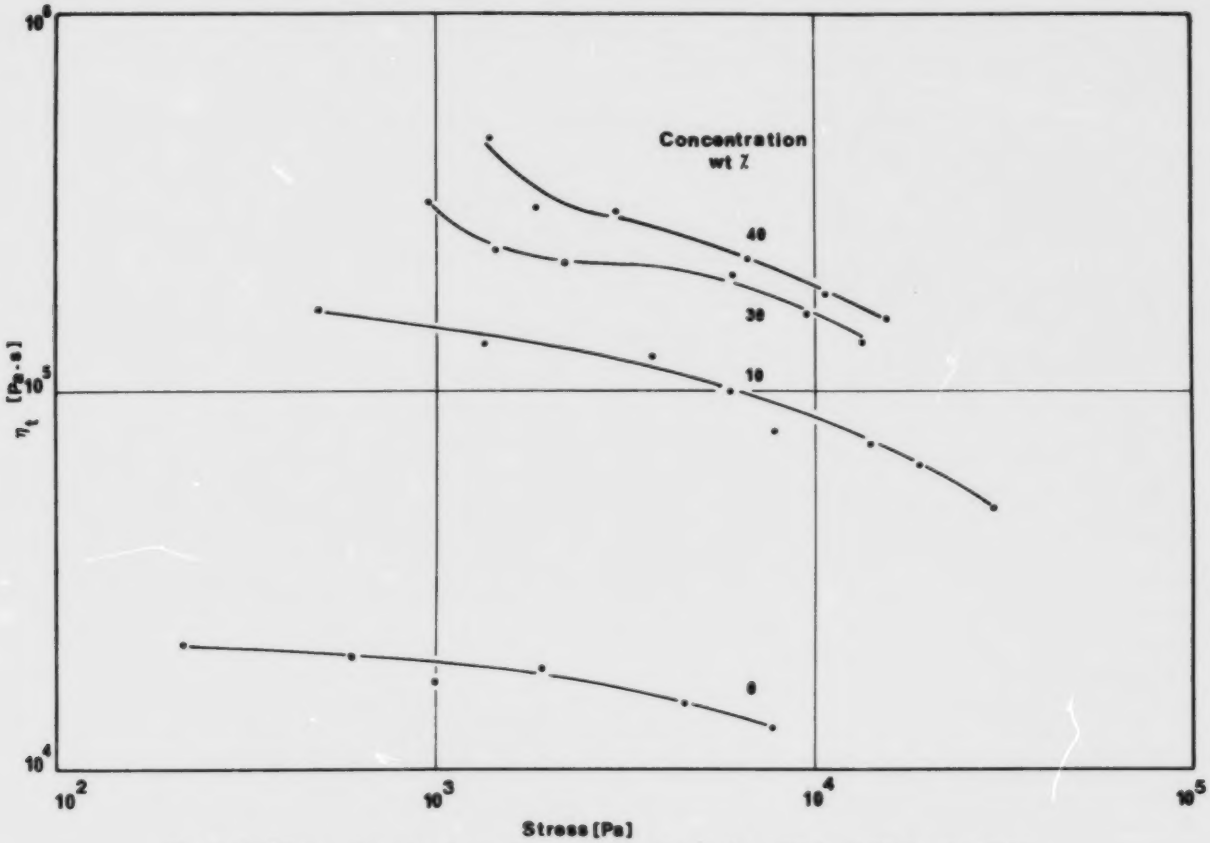

Fig. 8. Equilibrium elongational viscosity as a function of stress for unfilled and filled melts; 180°C.

stress at the lowest elongation rates or stresses. Modified Casson plots are given in *Fig. 9* (17). Yield stresses are observed for 30 and 40 percent filled PP melts. In modified flow curves obtained by subtracting the yield stresses from the total stress, the elongational viscosity continues to increase at very low strain rates, indicating the possibility of a change in structure through the orientation of fibers. The only data available in the literature for fiber filled polymer melts in elongational flow are those of Chan, *et al.* (9, 10). Unfortunately, they plot the equilibrium viscosities as a function of strain rate, and there is no indication of yield stresses, although viscosities continue to increase with decreasing strain rate at the lowest rates studied.

The effect of concentration on the equilibrium viscosity is given in *Fig. 10*, at different strain rates. At all rates, the elongational viscosity increases 4 to 6 times with 10 percent fiber addition. Viscosity increases less rapidly at higher concentrations. This might be explained by the decrease in the free volume available for fiber motion, resulting in a broader distribution of orientations around the perfect alignment with the flow direction and by the shorter fibers at high fiber loadings. All fiber concentrations used in this study are above the overlapping concentration. Hence, the rotation of a fiber is hindered by the presence of other fibers in the vicinity, which might prevent perfect alignment with the flow, as expected in extensional flows. An increase in concentration means an increase in the particle-particle interactions, resulting in a broader distribution around the perfect alignment orientation. The effect on viscosity of adding more fibers above that of the overlapping concentration is offset by the effect of deviation from perfect orientation with flow. This result is in accordance with the findings of Utracki and Lara (8) for mica-filled polyethylene.

Addition of fibers up to 40 percent by weight increases the elongational viscosities 4 to 12 times with respect to the unfilled polymer. These results are in accordance with those of White, *et al.* (9, 10), which give values between 2 and 10, for glass fiber filled high density polyethylene, and between less than 1 and 7 for glass fiber filled polystyrene melts.

Stress Relaxation

Stress relaxation experiments were conducted after the cessation of elongational flow at a strain $\epsilon = 1.5$ for the unfilled polymer and $\epsilon = 0.5$ for the filled melts. An exponential-type decay of stress was observed for the unfilled melt, as shown in *Fig. 11*. However, in the case of 30 and 40 percent filled polymer, an unexpected phenomenon was observed. In all cases, the stress decayed rapidly and fell below zero, indicating compression. After-

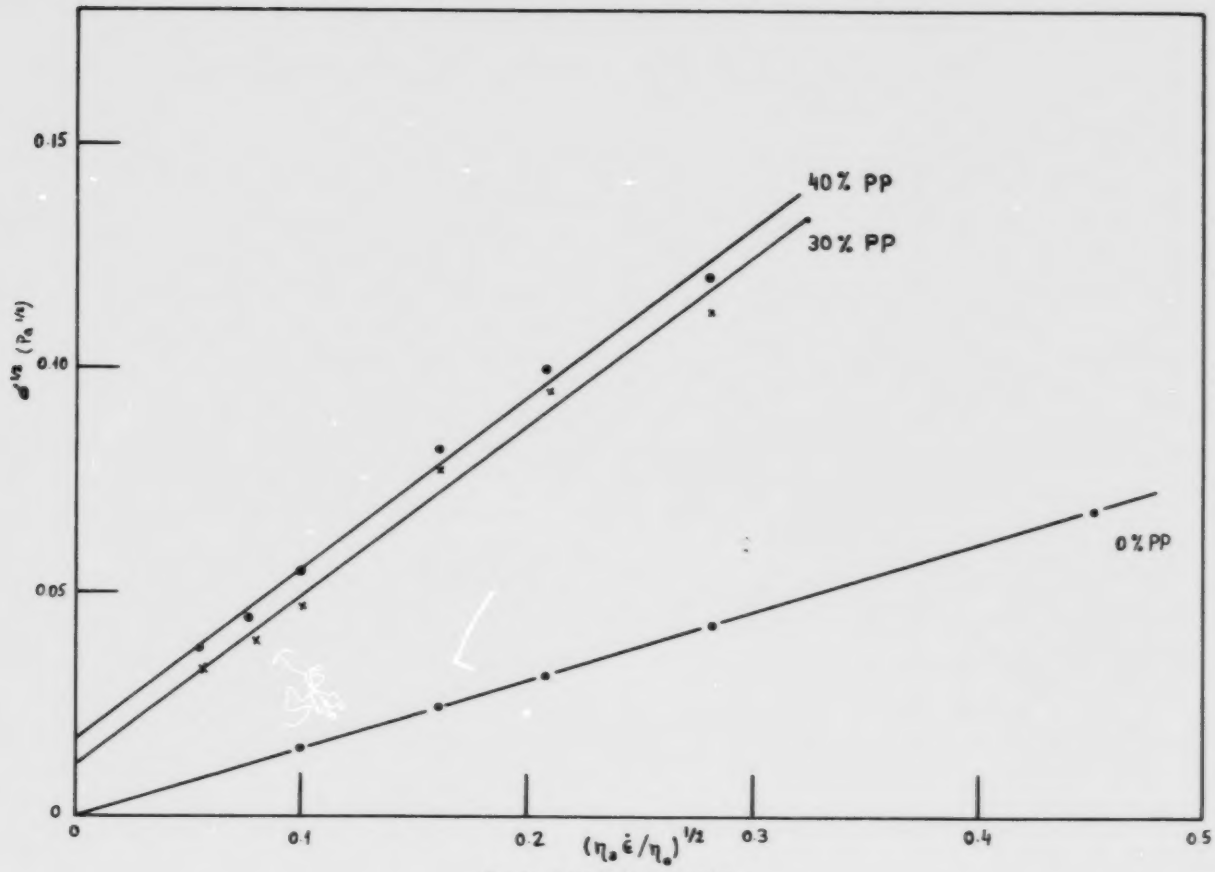

Fig. 9. Modified Casson plot.

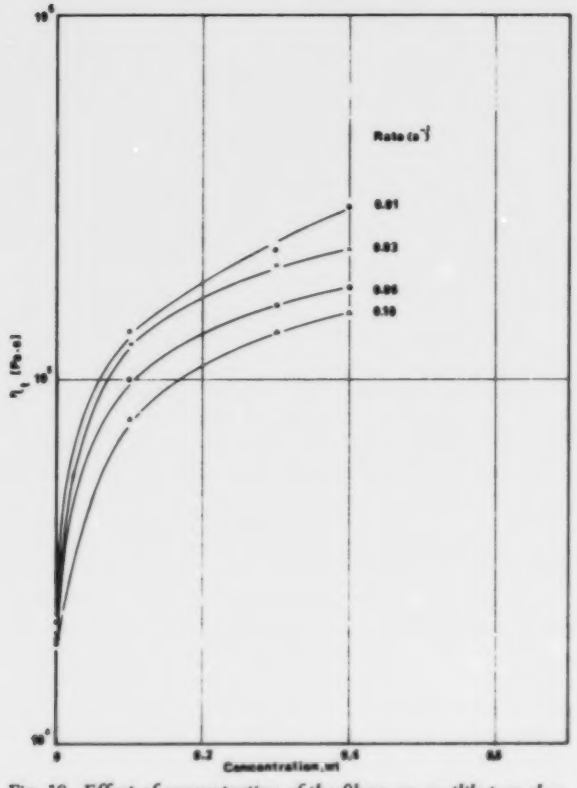

Fig. 10. Effect of concentration of the fibers on equilibrium elongational viscosity; 180°C.

wards, stress recovered partially reaching approximately 15 to 30 percent of the original stress. This was followed by an exponential-type decay, as seen in *Fig. 12*.

Upon further inspection of the apparatus, it has been found that, upon cessation of sample extension, the stretching rod falls ~0.1 percent of the total strain, resulting in compression of the sample before it is locked into a constant strain position. This behavior is manifested in stress data only at low strains with very stiff materials like fiber filled polymer melts. In view of this situation, discussion and analysis of stress relaxation data must await the resolution and clarification of the above problem.

CONCLUSIONS

Stress growth during elongational flow was measured for glass fiber filled polypropylene melts. The stresses during elongation were found to fluctuate by about ±5 to 15 percent of the mean stress value for the fiber filled melts. Equilibrium elongational viscosities were observed with fiber filled melts, even at rates for which the stresses continue to increase at much higher strains for the unfilled polypropylene. Stress buildup was faster for the filled polypropylene melts compared to the unfilled polypropylene, indicating that the stresses caused by the fibers developed at a faster rate. As expected, equilibrium elongational viscosities increased by the addition of fibers, reaching 4 to 12 times the

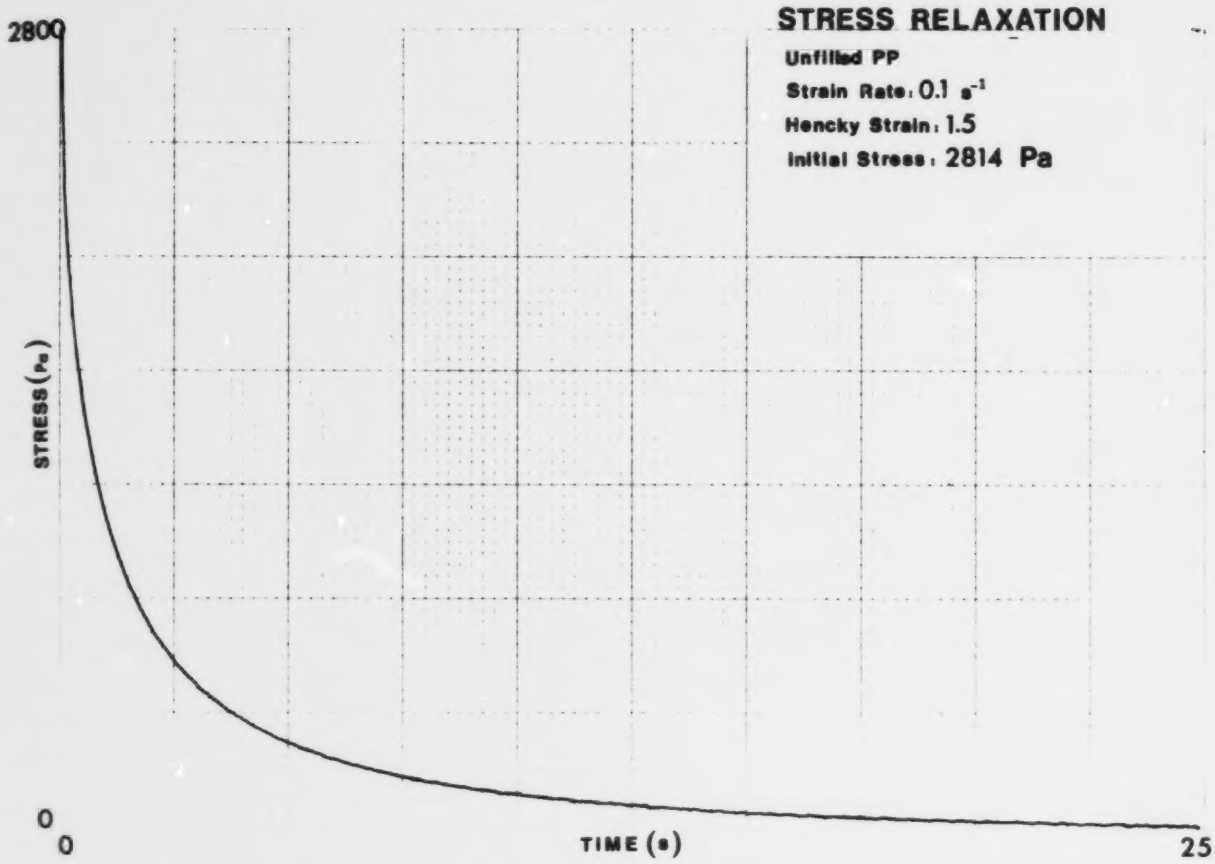

Fig. 11. Typical stress relaxation data for unfilled polypropylene at 180°C.

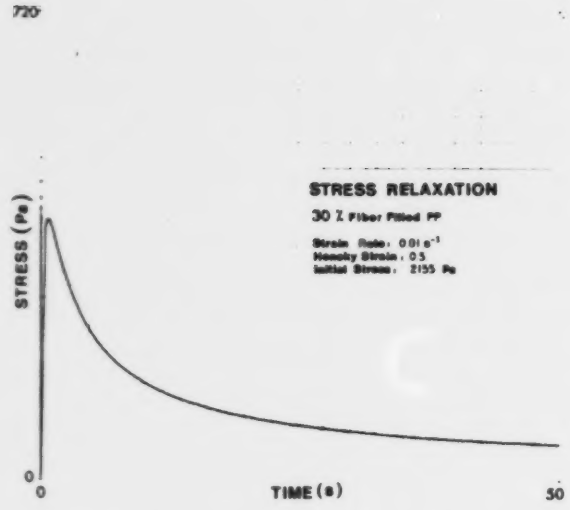

Fig. 12. Typical stress relaxation data for 30 percent filled polypropylene at 180°C.

values of the elongational viscosities for the unfilled polypropylene melt, at the same strain rate. Equilibrium elongational viscosities for the fiber reinforced polypropylene decreased with increasing strain rate. Yield stresses were observed for the highly filled melts, although no clear evidence for yield stresses was found in steady shear experiments.

ACKNOWLEDGMENTS

The authors would like to acknowledge financial support from the following organizations: Engineering Mechanics Department of General Motors Corporation, Natural Sciences and Engineering Research Council of Canada, and Ministère de l'Education of the Government of Quebec.

NOMENCLATURE

c = Concentration of fibers, wt percent.
R_T = Trouton ratio, $\eta_t/3\eta_o$.
$\dot{\epsilon}$ = Strain rate, s^{-1}.
η_o = Zero shear viscosity, Pa-s.
η_a = Apparent shear viscosity, Pa-s.
η_t = Equilibrium elongational viscosity, Pa-s.
η_t^+ = Transient elongational viscosity, Pa-s.
σ = Stress, Pa.
σ_{ss} = Equilibrium stress, Pa.
ϵ = Hencky strain.

REFERENCES

1. J. Mewis and A. B. Metzner, *J. Fluid Mech.*, **62**, 593 (1974).
2. F. Nazem and C. T. Hill, *Trans. Soc. Rheol.*, **18**, 87 (1974).
3. Y. Ide and J. L. White, *J. Appl. Polym. Sci.*, **22**, 1061 (1978).
4. V. M. Lobe and J. L. White, *Polym. Eng. Sci.*, **19**, 617 (1979).
5. H. Tanaka and J. L. White, *Polym. Eng. Sci.*, **20**, 949 (1980).
6. J. L. White and H. Tanaka, *J. Appl. Polym. Sci.*, **26**, 579 (1981).
7. J. L. White, L. Czarnecki, and H. Tanaka, *Rubber Chem. Technol.*, **53**, 823 (1980).
8. L. A. Utracki and J. Lara, NRCC-IMRI Mini-Symposium "COMPOSITES-82", Montreal, Nov. 30th, 1982; *Polym. Compos.*, **5**, 44 (1984).
9. Y. Chan, J. L. White, and Y. Oyanagi, *J. Rheology*, **22**, 507 (1978).
10. J. L. White and L. Czarnecki, *J. Rheology*, **24**, 501 (1980).
11. J. D. Goddard, *J. Non-Newt. Fluid Mech.*, **1**, 1 (1976).
12. J. Goddard, *J. Fluid Mech.*, **78**, 177 (1976).
13. J. D. Goddard, *J. Rheology*, **22**, 615 (1978).
14. O. Ishizuka and K. Koyama, *Polymer*, **21**, 164 (1980).
15. O. Ishizuka, K. Koyama, and H. Nokubo, *Polymer*, **21**, 691 (1980).
16. A. T. Mutel and M. R. Kamal, *Polym. Compos.*, **5**, 29 (1984).
17. S. Onogi and T. Matsumoto, *Polym. Eng. Rev.*, **1**, 46 (1981).
18. M. J. Sudlow, M. Eng. Thesis, McGill University (1982).

VI. DISCUSSION: A. T. MUTEL

M. Grmela: I would like to know if you have done similar measurements in shear flow also. In particular, whether you have observed these fluctuations and the unusual stress relaxation in the steady shear

A. T. Mutel: We made the measurements in steady shear between rotating parallel plates using RMS. The fluctuations were observed also in this mode of deformation, although they were not as pronounced as in the case of elongational flow. However, you have to remember that in elongational flow the viscosity increased with concentration by a factor of 12, whereas in steady shear it increased by 2. The "unusual" behavior in stress relaxation was not observed in relaxation of normal stresses in RMS. I would like to add that in RMS, the inertia of the plates is much larger than the arrangement used in RER, which might have a damping effect.

C. L. Beatty: Did you notice any critical concentration for the transition from linear to non-linear viscoelastic behavior?

A. T. Mutel: Excepting pure polypropylene, our lowest concentration of glass fibers was 10 percent. Even at this concentration, the non-linearity appeared. I expect that if we would go down to about 2 percent, i.e., below the particle overlapping region, then we would see the linear behavior. We are planning to test this in the near future.

D. G. Fesko: I recall some work done at the University of Delaware on the squeeze flow of polymers between the parallel plates. They also reported oscillation similar to these you presented today. This was shown both in experimental data and theoretical calculations.

M. R. Kamal: At the University of Delaware the work was done with pure polymers; they observed the oscillations even in this case. Although there may be some similarity between their and our results, I want to stress that we did not see any fluctuation in flow of neat polypropylene. We feel confident that the origin of stress fluctuation in flow of the glass fiber filled material is due to some sort of fiber-fiber interaction, friction or slippage.

Factors Affecting the Surface Texture in Extruded Mica-Polypropylene Composites

B. D. FAVIS, B. FISA, *and* B. SANSCHAGRIN

Industrial Materials Research Institute
National Research Council of Canada
75 De Mortagne Blvd., Boucherville, Quebec J4B 6Y4

A Taylor-Hobson Talysurf instrument was used to quantify the surface roughness of phlogopite mica-polypropylene extrudates. The rate of feeding and the speed of rotation of the screw were found to have a significant effect on the surface texture. Under the appropriate conditions of extrusion the roughness of 40 percent (by weight) mica-filled polypropylene extrudates could be reduced by a factor of three. This effect was found to be independent of the extrusion rate.

INTRODUCTION

The use of filled polymer materials has gained considerable interest in recent years. The so-called reinforced composites have many properties far superior to the virgin polymer and represent ideal systems in the trend towards stronger and lighter materials.

Woodhams, *et al.* have shown that mica, when suitably delaminated and oriented in a polymer matrix, was able to impart a significant degree of reinforcement (1–3). The use of mica increases rigidity, lowers warpage, reduces permeability, and improves electrical resistance. Mica is an abundant and relatively inexpensive mineral which can be readily delaminated to yield high aspect ratio flakes. Mica also possesses the advantage that it is a silicate material and rapidly interacts with the standard coupling agents used for glass fiber to improve interfacial phenomena (4–6). Hence, as an added advantage much of the chemistry developed for glass fibers can be readily applied to mica.

To date, injection molding has been the most widely used process with mica-filled thermoplastics. The high pressures used and low polymer viscosities result in well dispersed and highly-oriented materials especially at the surface. The properties tend to be relatively homogeneous and surface finish is excellent. Extrusion processes, on the other hand, have seen much less use and have been less studied. Such basic problems as surface roughness are difficult to overcome with highly filled extruded materials.

The analysis of surface roughness in polymeric materials is typically described in a qualitative manner. Sharkskin is a term which is often used to indicate the onset of surface roughness. Rough and smooth porcupine skin are also expressions (7) which have been used to describe varying degrees of surface roughness in glass fiber-filled composites. To date there has not been a comprehensive study nor a quantitative method considering surface roughness in extruded objects.

The surface roughness of reinforced polymeric composites is determined by the degree of orientation of the reinforcing agent. Knutsson, *et al.* (8), in studying polycarbonate reinforced with glass fiber, have shown that fiber orientation increases and surface roughness decreases with increasing extrusion rate. They noted an increase in the fiber orientation ratio occurring at a shear rate of 100 s^{-1}. Wu (7) has shown that glass fiber-filled poly (ethylene terephthalate) undergoes transitions from a smooth porcupine surface to a rough porcupine surface and then to a shorn porcupine surface with increasing rate of shear. He also noted a radial migration of the fibers towards the axis at high shear rates.

Some work on the effect of calendering on the final properties of extruded polypropylene mica sheet (9) have shown that the resulting extensional flow produced a large increase in the tensile and flexural properties. This increase was related to both the greater degree of parallel alignment of the mica flakes and the increased molecular orientation in the direction of the flow. Okuno and Woodhams (10) studied the extrusion of mica-polypropylene through a cylindrical orifice with an L/D value of 8.9. Their results showed (for 40 percent by weight mica) that the flakes near the outer surface are oriented parallel to the surface while the flakes in the center are perpendicular. Fisa and Utracki (11) have shown that in polyethylene containing 25 percent mica, the mica flakes are oriented throughout in the direction of flow. The above sample was extruded through a capillary with an L/D of 33 in an Instron Capillary Rheometer. Their samples showed significant surface roughness.

In this paper, it will be shown that under the appropriate conditions mica-polypropylene com-

positions may be extruded with a very smooth surface texture and high mica orientation. A method for measuring surface roughness quantitatively is also presented.

EXPERIMENTAL

The polymer used in this study is an extrusion grade polypropylene from Hercules Inc. known as Profax Polypropylene 6501. Its properties are shown in *Table 1*.

The mica used was of the phlogopite variety supplied by Marietta Resources International Ltd. (trade name Suzorite mica). In this study, the 200 HK and 200 NP types were used. 200 refers to the nominal mesh size of the flakes and HK refers to its classification as being highly delaminated. The NP grade has been surface treated with a silane particularly for use with non-polar polymers. These commercial micas have, in actual fact, a wide distribution of particle size and a typical distribution for a sample of 200 HK is shown in *Fig. 1*. The 200 NP grade has an essentially identical particle size distribution. A method using HIAC particle size analyzer has been developed in our laboratories to measure both the size distribution and aspect ratio of mica flakes (12). The mechanical degradation of these flakes in extrusion and in mixing processes in general will be considered in a subsequent publication (13).

The extrusion studies were carried out on a Brabender Plasticorder Model EPL-V5501. A three-quarter inch two-stage screw was used with an L/D of 25. A non-adjustable slit die was employed with an L/D of 50 at its narrowest part and its dimensions are given in *Fig. 2*. In these studies, the polypropylene powder and the mica were dry-blended, the blend was then fed into the extruder using a screw feed hopper (Model 05-30-000) recommended for the processing of non-free flowing powders such as the 40 percent mica/polypropylene blend. The output of the feeder can be controlled by the feeder screw speed. The feeder output, q, determined with the feeder removed from the extruder is always higher than the true feeding rate. The latter, which, under stationary state conditions, is equal to the extrusion rate is a function of the feeder output, extruder screw speed and other factors related to the geometry of the inlet zone. During the course of the extrusion process, the pressure, temperature, torque, and flow rate were measured. Various temperature profiles were considered and the lowest torque values were obtained with a descending profile from 240 to 200°C as suggested by Trotignon, *et al.* (14). The temperature profile used was 240°C in the first zone, 230°C in the second zone, 215°C in the third zone, and 200°C in the die. In a typical run, the material was added to the hopper and the torque was given time to stabilize. Once stabilization was achieved, a full hopper was passed through. The volumetric flow rate was calculated by using densities of 2.86 $g \cdot cm^{-3}$ for mica and 0.755 $g \cdot cm^{-3}$ for polypropylene at 200°C (10).

The technique used to measure the surface roughness of the extrudates was a Taylor Hobson Talysurf 4. The instrument consists of a finely balanced arm which at its end possesses a shoe and a stylus. The shoe is meant to ride at the top of the crests and provides a point of reference while the stylus is displaced by the fine structure of the surface (see *Fig. 3a*). A certain stroke or traverse is applied and the deflection of the stylus is amplified and recorded. A typical trace is shown in *Fig. 3b*. A center line is calculated by the instrument through the trace such that the sum of the areas above the line is equal to that below the line (15). A center line average value (CLA) which is the average

Table 1. Characteristics of PP Resin

No.	Parameter	Value
1.	Melt index—ASTM 1238 (g/10 min)	4
	Molecular weights:	
	Number average $M_n \cdot 10^{-3}$	250
	Weight average $M_w \cdot 10^{-3}$	325
	Intrinsic viscosity $[\eta]$(m^3/kg)	0.225
2.	(at 135°C in decahydronaphthalene)	
	Zero-shear viscosity $\nu_0 \cdot 10^{-4}$ (Pa·s)	1.95
	Normal stress difference coefficient $\Psi_0 \cdot 10^{-5}$ (Pa·s^2)	1.15
3.	Density (after annealing) (kg/m^3) at 23°C	906
4.	Melting point (°C)	167

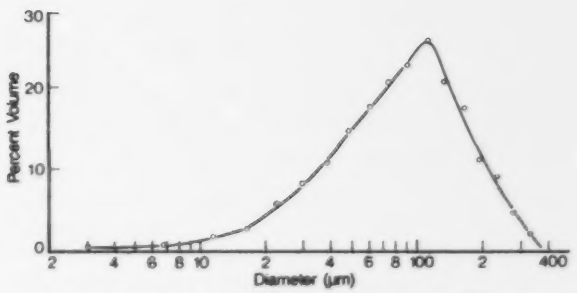

Fig. 1. Particle size distribution of Suzorite mica 200 HK.

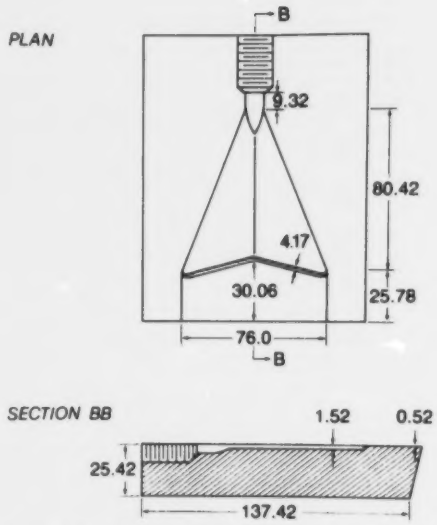

Fig. 2. Plan and section of slit die used in extrusion experiments. Dimensions are shown in millimeters.

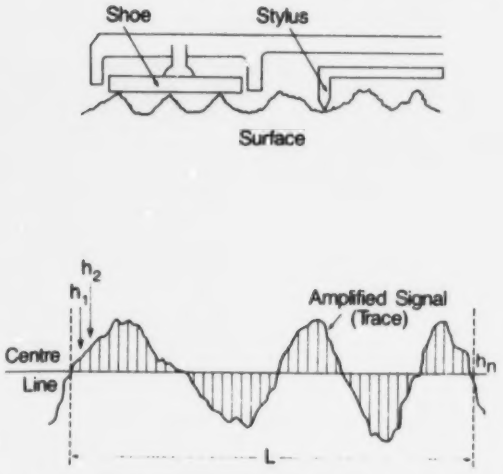

Fig. 3. a) Idealized representation of a portion of the Talysurf arm on a surface. b) Amplified signal from stylus divided by a center line. Unit height divisions used in calculating the CLA value are also shown.

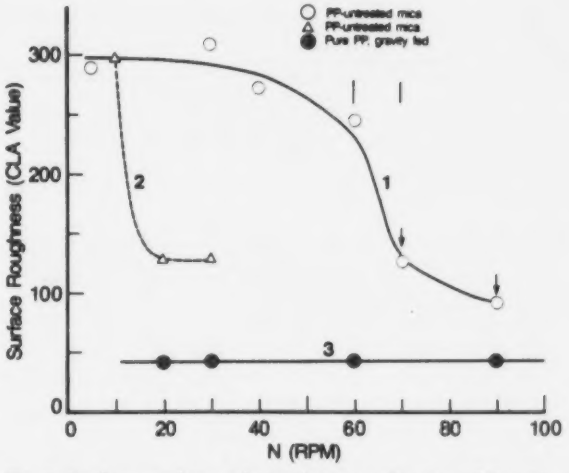

Fig. 4. Surface roughness of extrudates as a function of the screw speed, N. Curve 1 represents 40 percent mica in polypropylene fed at a feeder output of 75 g min^{-1}. Curve 2 represents 40 percent mica in polypropylene fed at a feeder output of 38 g min^{-1}. Curve 3 represents pure polypropylene, gravity fed. Arrows indicate smooth surface.

height of the trace above and below the center line is then calculated by integration as follows.

$$\text{CLA} = \frac{h_1 + h_2 + h_3 + \ldots h_n}{L}$$

$$= 1/L \int h_n \, dL$$

where h is the height of the trace above or below the center line at unit distances apart and L is the sampling length (see *Fig. 3b*). The Talysurf instrument therefore calculates a dimensionless quantity which may be related to the average height of the asperities on the surface; the higher this CLA value, the rougher the surface.

Each reported surface roughness value is the average taken from 4 to 6 runs on the Talysurf. Half of the runs were taken parallel to the direction of extrusion and the other half perpendicular. The average error per run was ±14 CLA units. The error of the reported values is, of course, further reduced by the averaging.

The photos of the extrudate surface and the fracture surface were taken on a JEOL 35 CF Scanning Electron microscope. The samples were fractured after immersion in liquid nitrogen.

RESULTS AND DISCUSSION

1. Surface Finish

The effect of the screw speed, N (at two feeder outputs) on the surface roughness of 40 percent by weight mica-filled polypropylene is shown in *Fig. 4*. At a feeder output, q, of 75 g/min and for low values of N, the surface texture is very rough, as indicated by the high CLA value obtained from the Talysurf instrument. At higher screw speeds the surface becomes gradually smoother with the most critical change taking place at 60 to 70 rpm. The CLA value at 90 rpm and for a feeder output rate of 75 g/min is less than one third the value observed at 5 to 30 rpm. This result represents a remarkable reduction in the surface roughness. The dispersion was also improved. At a lower q of 38 g/min, a significant decrease in surface roughness is also observed (*Fig. 4*). The transition, however, shifts to lower rpm values. The surface roughness of gravity-fed pure polypropylene is shown for comparison. Surface treated mica, added at a q of 75 g/min, showed similar behavior with respect to the reduction in surface roughness. Surface roughness values using treated mica obtained at screw speeds of 30 and 90 rpm are shown in *Table 2*.

Figure 5 shows the reduction in surface roughness as observed by scanning electron microscopy. The samples were obtained at a feeder output of 75 g/min and extruded at screw speeds of 30 and 90 rpm. The surface of the extrudate produced at 30 rpm is discontinuous and mica flakes protruding from the surface are evident. In contrast, the surface of the extrudate produced at 90 rpm is very smooth and continuous.

The fracture surfaces of the same extrudates as above are shown in *Fig. 6*. It is apparent that the mica flakes are much more highly oriented at 90 than at 30 rpm. It is significant, in the latter case, that the flakes are organized parallel to the direction of extrusion throughout the thickness of the ribbon. It is clearly this highly organized structure which imparts the remarkable observed surface characteristics. It can also be expected that the mechanical properties of this organized structure would be different.

2. Extrusion Analysis

In *Fig. 7*, the corresponding change in pressure with N for gravity fed polypropylene and 40 percent treated and untreated mica in polypropylene with the feeder output of 75 g/min is shown. The continual pressure increase for the pure gravity fed

Table 2. Surface Roughness of Polypropylene-Silane Treated Mica Extrudates

Screw Speed (RPM)	Feeder output (g min^{-1})	Surface Roughness (CLA)
30	75	241
90	75	113

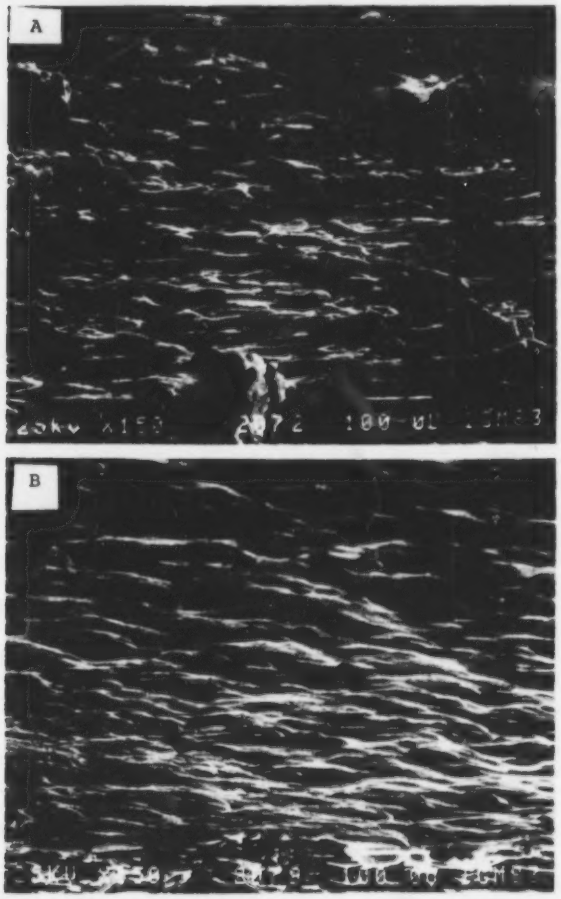

Fig. 5. SEM photomicrographs showing surfaces of 40 percent mica-polypropylene extruded with a screw speed of a) 30 rpm, b) 90 rpm with the feeder output of 75 g min^{-1}.

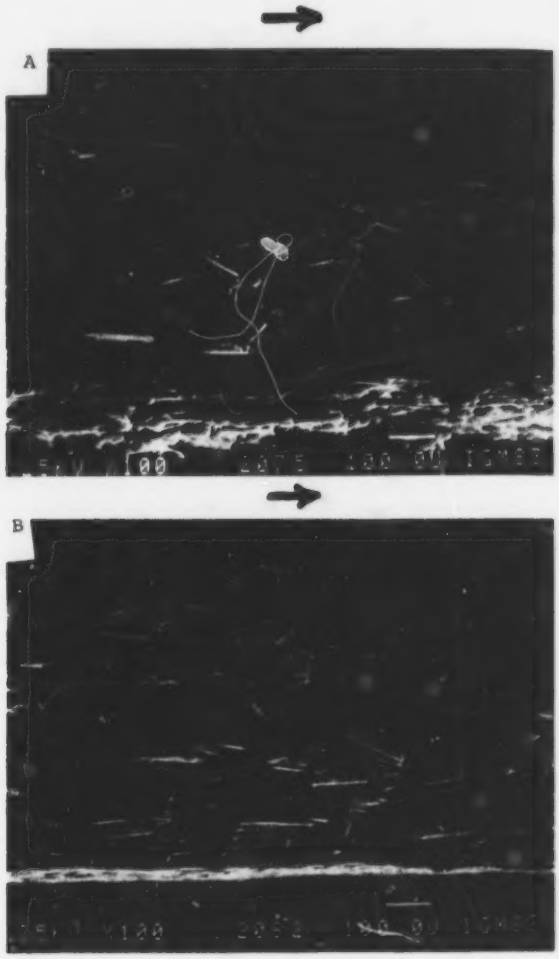

Fig. 6. SEM photomicrographs showing fracture surfaces of 40 percent mica-polypropylene. The direction of extrusion is indicated by the arrow. Samples were extruded at screw speeds of a) 30 rpm, b) 90 rpm, the feeder output was 75 g min^{-1}.

polypropylene with N is evident and is the normal behavior for this type of material. For the filled materials, the pressure in the die is higher due to their increased viscosity (10, 11, 16), with the silane treated mica the less viscous of the two as would be expected for a silane treated silicate (17–19). In both cases, the pressure increases up to 60 rpm, but then begins to drop at higher values of N.

In *Fig. 8*, the dependence of the flow rate *vs.* N is shown. For gravity fed pure polypropylene, the flow rate increases steadily with rpm. For the filled samples with the feeder output at 75 g/min, the flow rates up to 60 rpm superimpose well with the data obtained for pure polypropylene. At N greater than 60 rpm, the flow rates for both treated and untreated mica in polypropylene begin to level. For mica-polypropylene fed at a $q = 38$ g/min, the flow rate begins to level off at 10 rpm.

In *Fig. 9*, it can be seen that the torque for the treated and untreated mica in PP decreases steadily with N and approaches a plateau at approximately 60 rpm. The torque for polypropylene stays approximately constant at 16 NM.

Figures 7 and *8* indicate that the sudden decrease in surface roughness observed in *Fig. 4* may be correlated with a corresponding drop in the pressure and the flow rate. The critical value of N, at a feeder output of 75 g/min, occurs at a screw of 60 rpm. 60 rpm also represented the point where the torque value for the filled samples levels and approaches the value for pure polypropylene.

3. *Starve Feeding*

The discontinuities in the pressure and the flow rate at higher N indicate that the highly oriented mica-polypropylene extrudates are possibly being produced under conditions of starve feeding. Starve feeding may be defined as the state where solid feed is metered into the extruder at a rate less than

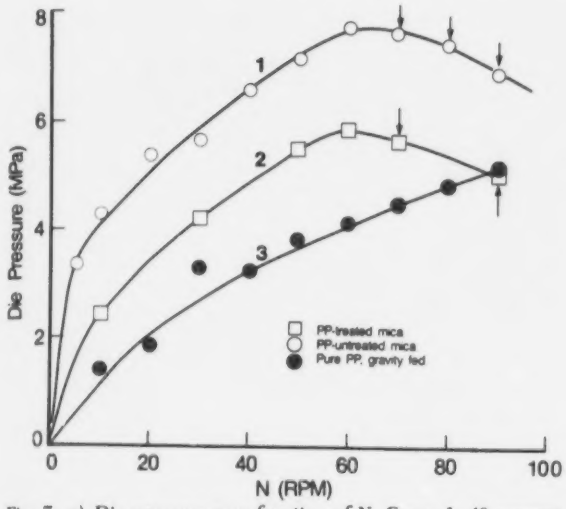

Fig. 7. a) Die pressure as a function of N. Curve 1: 40 percent untreated mica in polypropylene fed at 75 g min^{-1}; Curve 2: 40 percent treated mica in polypropylene fed at q = 75 g min^{-1}; Curve 3: pure polypropylene, gravity fed. Arrows indicate smooth surface.

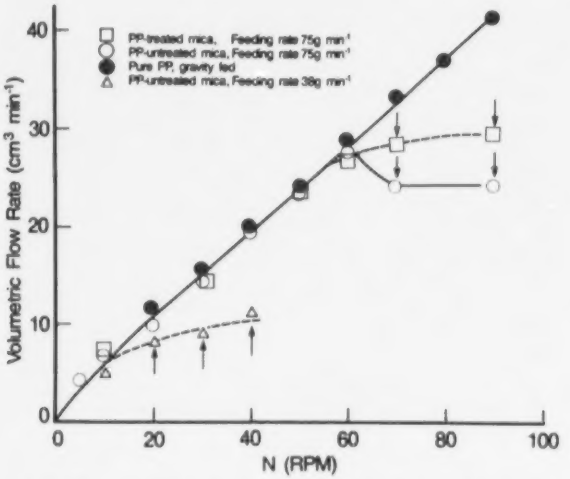
Volumetric Flow Rate (cm^3 min^{-1})
N (RPM)
PP-treated mica, Feeding rate 75g min^{-1}
PP-untreated mica, Feeding rate 75g min^{-1}
Pure PP, gravity fed
PP-untreated mica, Feeding rate 38g min^{-1}

Fig. 8. The volumetric flow rate, Q, as a function of the screw speed and feeding rate. Arrows indicate smooth surface.

the extrusion capacity of the screw. The degree of starve feeding, S, is defined as:

$$S = 1 - (Q/Q_o)$$

Q_o represents the extrusion rate under flood feed conditions (screw is full) at any screw speed, N, and Q is the rate at the same speed under starved-fed conditions (20). If the curve for gravity-fed polypropylene in *Fig. 8* is considered as indicative of the volumetric flow rates obtained when the screw is full then it can be seen that the onset of starve feeding for the mica-poly propylene samples corresponds to the point at which smooth surfaces were obtained. In order to show the effect of starve feeding conclusively, the extrusion process was stopped suddenly and the material in the barrel and

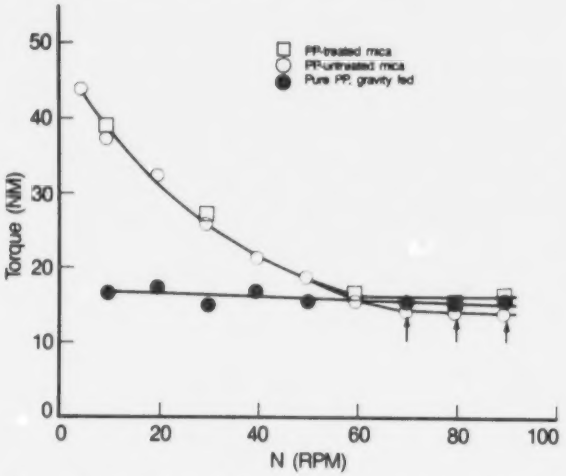

Fig. 9. The torque as a function of the screw speed. Arrows indicate smooth surface.

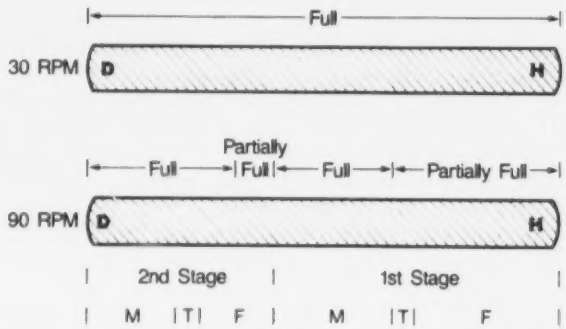

Fig. 10. Illustration of the effect of starve feeding on the quantity of material on the screw at 30 and 90 rpm. M, T and F refer to the metering, transition, and feeding zones respectively. H indicates hopper and D is the die.

die was cooled. The two-stage screw was then removed and observed. This was carried out at 30 and 90 rpm for a feeder output of 75 g/min^{-1}. The results are depicted in *Fig. 10*. At 30 rpm, the entire length of the screw is full. At 90 rpm, the screw contains much less material and is full only in the metering zone *M* and *T* respectively and transition zone of the second stage and the metering zone of the first stage. To further illustrate the direct dependence of starve feeding on surface roughness, the feeder output in an extrusion experiment at 90 rpm and 75 g/min was doubled to 142 g/min. Within a few minutes, which represents a normal stabilization period, there was a transition from a smooth to a rough surfaced extrudate. From the above data, it is quite conclusive that highly oriented and very smooth surfaced extrudates of 40 percent mica in polypropylene are obtained under conditions of starve feeding.

3. *Effect of Flow Rate*

In *Fig. 11*, the flow rate *vs.* the die pressure is shown. For pure polypropylene Q increases contin-

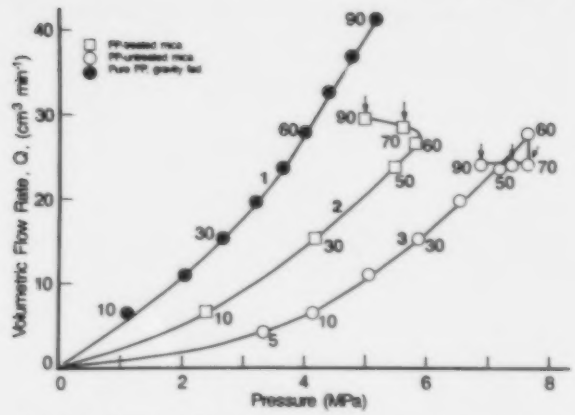

Fig. 11. Volumetric flow rate vs. the die pressure. The N values are shown. Feeder output $q = 75$ g min^{-1}.

uously with P, however, treated and untreated mica in PP show abrupt discontinuities at 60 rpm as previously discussed. It is interesting to note from *Fig. 11* that curve 3 between 80 and 90 rpm, which resulted in highly oriented and smooth surfaced extrudates, falls exactly in the region observed for 50 rpm which gave a poorly oriented and rough surfaced sample. This indicates that the apparent shear stress (which may be directly correlated with the pressure, P) and the apparent shear rate (directly related to the flow rate, Q) in the die, alone are not responsible for controlling the observed change in the orientation of the mica flakes.

As a complement to this work, the effect of the flow rate on surface roughness was also considered. The same system was used (40 percent by weight mica in polypropylene) except that the materials were pre-compounded on the roll mill. The granules were then fed by gravity into the Brabender equipped with the same slit die as used in all previous experiments. The results are shown in *Table 3*. It can be seen that when the flow rate is increased by a factor of 3, there was 20 percent reduction in surface roughness. This reduction however was much less pronounced than that obtained by starve feeding. Electron micrographs of the surface and fracture surface of the extrudate at 90 rpm and at high flow rate are shown in *Fig. 12*. It is evident that this surface can be considered as rough when compared to the smooth surfaces extruded by starve feeding. The fracture surface of the extrudate also indicates poorer orientation.

These data suggest that the critical phenomena controlling orientation by starve feeding are occurring before the die. In order to verify this, portions of cooled extrudate taken after the breaker plate and before the die were examined. Two cases were considered: samples extruded at 30 rpm and at 90 rpm with a feeder output of 75 g/min. The two samples visually were very different even though their composition was identical. The sample taken at 30 rpm (which resulted in rough surfaced extrudates) was dark with a flat-lustre finish while that at 90 rpm (smooth surfaced extrudates) was very smooth, light colored, and had a highly reflective

Table 3. Effect of the Flow Rate on Surface Roughness

Screw Speed (RPM)	Feeding	Flow Rate (cc/min)	Surface Roughness (CLA)
30	gravity-fed	17	258
90	gravity-fed	46	206

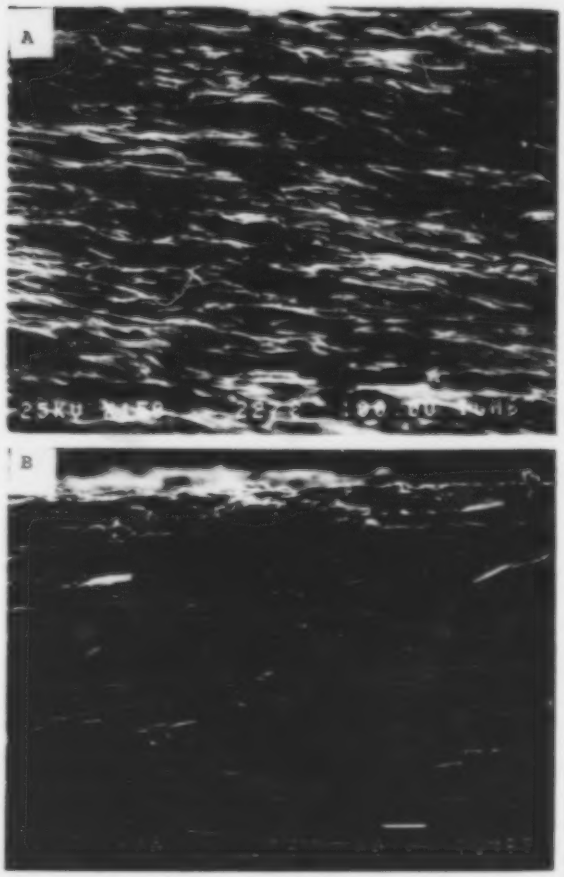

Fig. 12. a) SEM photomicrograph showing the surface of 40 percent mica-polypropylene extrudate gravity-fed and extruded at 90 rpm, not starve fed. b) Fracture surface of sample in a).

surface. Scanning electron micrographs (*Fig. 13*) of the two surfaces at a magnification of 100 times give an indication of the significant differences in surface texture observed. These data suggest major differences in the orientation of the mica flakes near the surface and indicate that the critical phenomena controlling the orientation phenomena studied occur in the barrel of the extruder.

Some questions remain to be answered:

1. To what extent are the material properties (e.g., concentration and particle size) contributing to surface roughness?
2. Can the observed orientation phenomena caused by conditions of starve feeding be extended to fibers, other reinforcing agents, and different polymers?

Work is underway to respond to the above questions and will be reported soon.

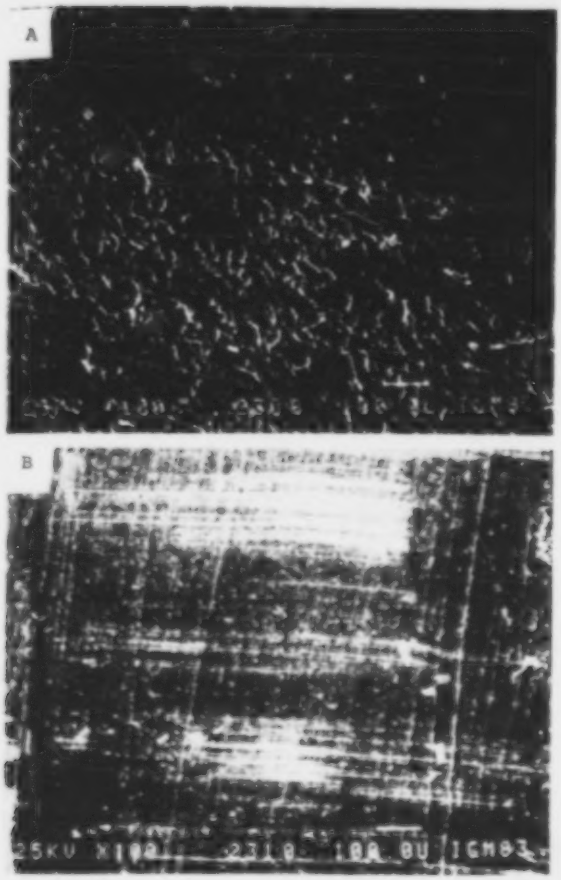

Fig. 13. SEM photomicrograph showing surfaces of cooled samples taken from between the barrel and the die. The magnification is 100 times. The feeder output was 75 g min^{-1} and the screw speed just prior to cooling was a) 30 rpm, b) 90 rpm.

CONCLUSIONS

The surface roughness of ribbon extrudates containing 40 percent by weight mica in polypropylene are significantly reduced under conditions of starve feeding. By controlling the rate of feeding, this effect may be produced independent of the extrusion rate. Furthermore, these smooth extrudates show a high orientation of mica flakes in the direction of extrusion throughout their entire thickness.

The Talysurf surface analysis technique can be used to quantitatively measure the surface roughness of polymeric extrudates.

ACKNOWLEDGMENTS

The authors would like to express their appreciation to Dr. L. A. Utracki for interesting discussions, and to Mr. Michel Thibodeau for his excellent assistance with the scanning electron microscope.

REFERENCES

1. J. Lusis, R. T. Woodhams, and M. Xanthos, *Polym. Eng. Sci.*, 13, 139 (1973).
2. H. S. Katz and J. V. Milewski, "Handbook of Fillers and Reinforcements for Plastics", Ch. 20, Reinhold, Toronto, (1978).
3. R. T. Woodhams, Can. Pat. 89163 (1972).
4. B. D. Favis, L. P. Blanchard, J. Léonard, and R. E. Prud'homme, *J. Appl. Polym. Sci.*, 28, 1235 (1983).
5. B. D. Favis, L. P. Blanchard, J. Léonard, and R. E. Prud'homme, *Polym. Compos.*, 28, 1235 (1983).
6. B. D. Favis, M. Leclerc, and R. E. Prud'homme, *J. Appl. Polym. Sci.*, in press.
7. S. Wu, *Polym. Eng. Sci.*, 19, 638 (1979).
8. B. A. Knutsson, J. L. White, and K. B. Abbas, *J. Appl. Polym. Sci.*, 26, 2347 (1981).
9. I. Lee, S. Turner, and R. T. Woodhams, *Polym. Compos.*, 3, 212 (1982).
10. K. Okuno and R. T. Woodhams, *Polym. Eng. Sci.*, 15, 308 (1975).
11. B. Fisa and L. A. Utracki, *Polym. Compos.*, 5, 36 (1984).
12. B. Fisa, B. Sanschagrin, and B. D. Favis, *Powder Technology*, submitted for publication.
13. B. Fisa, B. Sanschagrin, and B. D. Favis, *Polym. Compos.*, 5, 264, 1984.
14. J. P. Trotignon, B. Sanschagrin, M. Piperaud, and J. Verdu, *Polym. Compos.*, 3, 230 (1982).
15. Taylor Hobson Talysurf 4 Operations Manual.
16. L. A. Utracki and B. Fisa, *Polym. Compos.*, 3, 193 (1982).
17. E. P. Plueddemann, "Silane Coupling Agents", pp. 186–188. Plenum Press, New York, (1982).
18. M. S. Boaira and C. E. Chaffey, *Polym. Eng. Sci.*, 17, 715 (1977).
19. C. D. Han, T. Van den Weghe, P. Shete, and J. R. Haw, *Polym. Eng. Sci.*, 21, 196 (1981).
20. J. M. McKelvey and S. Steingiser, *Plast. Eng.*, 45 (June, 1978).

VII. DISCUSSION: B. D. FAVIS

A. N. Wright: From the industrial point of view, this is very important work. All our joint projects with Ray Woodham's group on mica/polypropylene composites use injection molding, not extrusion. The program we have with IMRI where we focus on the eventual use of extrusion of rigid PVC and mica will be affected by these results.

P. D. Frayer: Two questions: (1) Have you seen these effects in a single-stage screw? and (2) Why did you have a two-stage screw completely filled with gravity fed polypropylene? The two-stage screw is only used for venting, so it should never be completely filled.

B. D. Favis: We had difficulties extruding this material with a single-stage screw. As a matter of fact, we could not obtain any output; the material simply stayed in the barrel. Apparently, the back pressure flow term was equal to the drag flow term. Next, we tried the two-stage screw in a non-vented barrel and we were able to achieve an output. The screw filled only with gravity-fed polypropylene was not analyzed. The screw containing polypropylene-mica may have been full also as a result of the high pressure flow term.

A. Samak: Would you please comment on the mechanical properties of the material extruded from the same compound but under different processing conditions. I expect that not only do you have a different degree of flake orientation but also a difference in matrix elongation. Maybe the improved orientation during starve feeding is due to an in-

crease in matrix elongation.

B. D. Favis: We have not done any measurement of the mechanical properties on these materials. This is something which obviously has to be done. Certainly, with improved mica orientation one should expect an improvement of the mechanical performance. Matrix elongation would be expected to increase with the rate of shear, the observed mica orientation reported here was independent of the shear rate.

The Effect of Silica on the Crystallization of Isotactic Poly(Propylene Oxide)

M. A. KENNEDY, G. R. BROWN, *and* L. E. ST-PIERRE

Department of Chemistry
McGill University
Montreal, Quebec, Canada H3A 2K6

The addition of one part, by weight, of fine particle silica to one hundred parts isotactic poly(propylene oxide) causes a retardation in the rate of radial growth of spherulites at all temperatures between 268 and 313 K. The results have been fitted empirically by use of the Hoffman-Lauritzen equation suitably modified to account for effects due to the presence of the silica. At certain temperatures the presence of the silica also causes a change in the morphology of the spherulites.

INTRODUCTION

Fillers, either powders or fibers, are introduced into a broad range of polymers to modify their mechanical properties thus giving them new applications and commercial value. Their effect on melt viscosities and on viscoelasticities during processing are marked but are expected on the basis of both theory and experience. However, their effect on the crystallization behavior of polymers such as poly(ethylene terephthalate) is not fully understood. Consequently, great difficulties are experienced in selecting proper molding temperatures and times. This, in turn, has resulted in shrinkage and warping of parts.

Silica, carbon fibers, and glass fibers have all been shown to act as nucleants for the crystallization of composites. As such they can serve the useful purpose of diminishing processing cycles, as in the case of indigo in polypropylene. However, in concert with their nucleating behavior, which is a function of the melt-filler interfacial energy, they can affect viscosity and thus influence the transport of crystallizable polymer segments to the crystal face. In certain cases this latter factor can become sufficiently large to supercede the accelerating effect of increased numbers of nuclei and result in a retardation of the overall rate of crystallization.

Such a retardation was first reported by us in silica-filled isotactic polystyrene (1) and more recently in silica-filled poly(ethylene terephthalate) (2). An explanation was offered that is based on the experimentally observed retardation in the radial growth rates of spherulites in the presence of filler (3, 4). The experimental observations were in turn rationalized on the basis of the Hoffman-Lauritzen theory of spherulitic growth.

In the present paper a new system, isotactic poly(propylene oxide) (PPO) filled with silica, is treated and the previously observed retardation in the radial growth rates in the presence of filler is seen once again. Furthermore, morphological changes not previously reported are also shown to occur as a consequence of the presence of the silica.

EXPERIMENTAL

Isotactic poly(propylene) oxide was prepared by polymerizing propylene oxide (Aldrich) at 80°C (353 K) in the presence of ferric chloride/propylene oxide catalyst according to methods described by Price and Osgan (5). The isotactic portion was recovered as the precipitate by cooling a hot acetone solution of the crude polymer to −30°C (243 K). The tacticity was confirmed by X-ray diffraction. Gel permeation chromatography measurements, using THF as solvent, revealed a number average molecular weight of 1.73×10^4 and a weight average molecular weight of 8.56×10^4 yielding a polydispersity of 4.9. The equilibrium melting point, the glass transition temperature, and percentage crystallinity, as determined by DSC (Perkin-Elmer DSC-2C), were 48°C (321 K), −71°C (202 K), and 86 percent (based on a heat of fusion of 8.36 kJ/repeat unit (6)), respectively.

Fine particle silica (Cab-O-Sil M5) with a surface area of 200 square meters per gram was used as the filler. The composites were prepared by adding the required weight of silica, previously dried at 110°C (383 K) in a vacuum oven, to a 10 percent solution of PPO in CCl_4 (dried over molecular sieves). After the suspensions had been stirred the solvent was removed under vacuum.

Polymer samples to be used for the measurement of radial growth rates by photomicroscopy were prepared by pressing samples, while heating, into thin films between a microscope slide and the cover glass. For the unfilled PPO aluminum spacers of 20 μ thickness were used. The samples were melted at 125°C (398 K) for 20 min. on a Mettler FP52

Hotstage. Temperature calibrations of the hotstage were made from the melting points of benzoic acid, naphthalene, and benzophenone. After melting, the samples were cooled to the desired crystallization temperature, somewhere between −5 and 40°C (268 and 313 K), which could be achieved by passing a stream of nitrogen previously cooled by liquid nitrogen through the hotstage. Photographs of the growing spherulites were taken at appropriate time intervals with an Olympus OM1 35 mm camera, using Ilford 400 ASA black and white film, on a Leitz HM-LUX microscope. For each crystallization temperature diameters of 5 to 10 different spherulites were measured at 5 to 10 different growth times. All growth rates were linear in time and were determined from the measured diameters (in the range 0.038 to 0.815 mm) using a linear least squares program.

RESULTS AND DISCUSSION

Spherulitic growth—no nucleant added

We have previously shown that crystallization of PPO occurs in the form of spherulites but at that time only limited analysis was made of radial growth rates (7). That study also showed that the nucleation density in the crystallization of PPO is increased by approximately an order of magnitude by the addition of fine particle silica.

Measurement of spherulitic growth patterns of un-nucleated PPO as a function of crystallization temperature shows the radial growth rates to be very sensitive to temperature (*Fig. 1*). The maximum in the growth rates is in the region of 285 K (*Fig. 2*). The effect of temperature on the radial growth rates follows the usual pattern and can be analyzed in terms of the classical Hoffman-Lauritzen theory (8). They showed that the growth rates can be described by

$$\ln G = \ln G_o - \frac{C_1}{R(C_2 + T - T_g)} - \frac{4b_o\sigma\sigma_e T_m^{\,0}}{k\Delta HT\Delta T} \quad [1]$$

where G is the spherulitic growth rate, G_o is a pre-exponential factor which is temperature independent, R is the ideal gas constant, and k is the Boltzmann constant. The effect of temperature on the rate of transport in a polymer melt is described by the term $C_1/[R(C_2 + T - T_g)]$, where C_1 and C_2 are constants derived from the WLF constants describing viscous flow in polymers, T is the crystallization temperature, and T_g is the glass transition temperature. The last term $4b_o\sigma\sigma_e T_m^{\,0}/k\Delta HT\Delta T$ relates to the secondary nucleation energy which depends on the crystallite plane monomolecular thickness b_o, the side and end interfacial energies σ and σ_e, respectively, the heat of fusion ΔH, the equilibrium melting temperature $T_m^{\,0}$ and the supercooling ΔT.

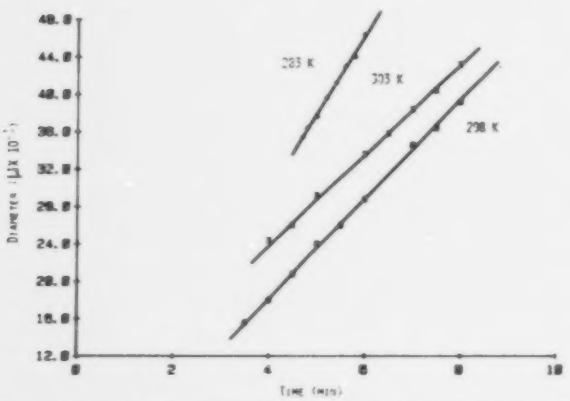

Fig. 1. The effect of temperature on the radial growth rates of spherulites of unfilled poly(propylene oxide).

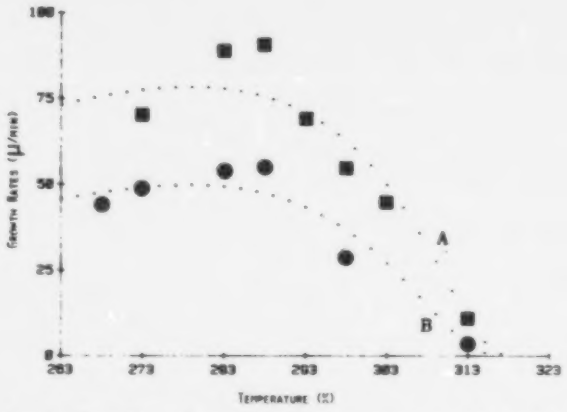

Fig. 2. The effect of crystallization temperature on the radial growth rates of spherulites of poly(propylene oxide). A—Unfilled ■—Experimental, . . .—Calculated by Eq 5; B—One part silica in 100 parts polymer ●—Experimental, . . .—Calculated by Eq 7.

The transport, or WLF, term accounts for the temperature dependence characterizing the motion of amorphous chains in viscous flow (8). The transport process is controlled by the mobility of the polymer segments which, in turn, is related to the viscosity of the melt. Any factor that can influence the mobility, e.g., increase in molecular weight or presence of filler (9–11), will affect the rate in transport. As a polymer is cooled the quantities in the WLF equation that relate to the rate of transport of polymer units to the crystallizing site become the dominant factors. From the point of view that the bulk viscosity in an amorphous polymer is governed by its free volume (12), the constant C_1 in *Eq 1* can be expressed in terms of the WLF universal constants

$$C_1 = 2.303RC_1^{\,0}C_2^{\,0} \quad [2]$$

with

$$C_1^{\,0} = B/2.303f_g \quad [3]$$

$$C_2^{\,0} = f_g/\alpha_f = C_2 \quad [4]$$

where f_g is the fractional free volume at T_g, α_f is the thermal expansion of the free volume relative to the total volume, and B is a constant close to unity. If it is assumed that $B = 1$ and that the fractional free volume at the glass transition temperature is 0.025 (12), the constants C_1 and C_2 have the values 1.72×10^4 J/mol (4120 cal/mol) and 51.6 K, respectively. However, the values of the constants C_1 and C_2 (in *Eq 1*) that apply to the crystallization

process need not be identical to those applied to bulk fluidity (13, 14), the reason being that in the crystallization process these values probably refer to motions near and within a physically adsorbed layer of molecules at the crystal face.

To analyze the present data a plot was made of $\ln G + C_1/\{R(C_2 + T - T_g)\}$ as a function of $1/T\Delta T$ (*Fig. 3*). Curve A results when the classical values of C_1 and C_2 are used with a T_g of 202 K and a T_m^0 of 321 K. A straight line can be obtained by readjusting C_2 from 51.6 to 319 K (curve B, *Fig. 3*) while leaving the constant C_1 at its classical value of 1.72×10^4 J/mol. The shift in C_2 is extraordinarily high. However, since this constant is related to segment transport it is possible that the wide distribution in molecular weights, as demonstrated by a polydispersity of almost 5, is a factor in this behavior.

When these new values are used *Eq 1* becomes

$$\ln G = 10.25 - \frac{2073}{319 + T - 202} - \frac{7.67 \times 10^3}{T(321 - T)} \quad [5]$$

which yields points that approximate to the observed temperature dependence of the growth rates of the spherulites (*Fig. 2*).

Spherulitic growth-silica added

As mentioned previously, we have shown in earlier work that the presence of fine particle silica in PPO increases the number of nuclei per unit volume of crystallizing polymer (7). We have also determined the heat of adsorption of dioxane, a model compound for PPO, on Cab-O-Sil M5 to be (36.4 ± 0.82) kJ/mol (15) which indicates a strong attachment of the polymer segments to the silica particles. The result would obviously be a quasicrosslinked system with a marked increase in the viscosity of the composite melt. This would, in turn, diminish the rate of segment transport at any given temperature and thus decrease the rate of growth of any given spherulite.

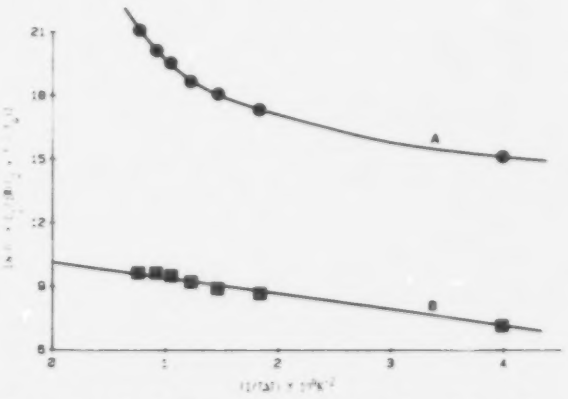

Fig. 3. Fit to the Hoffman-Lauritzen equation for poly(propylene oxide). A—Using classical values for C_1 and C_2, B—Using adjusted values for C_2.

Precisely this effect is observed in *Fig. 2* where the addition of one part of fine particle silica, by weight, in 100 parts polymer is seen to inhibit the growth rate of the spherulites at all temperatures for which measurements were made. It is of interest that in the case of isotactic polystyrene the decrease in the rate of spherulitic growth was noticeable predominantly at higher temperatures. An explanation for this difference is not available at the present time. For PPO, the temperature at which the maximum growth rate is observed is affected only minimally, if at all, by the addition of silica.

These data were also analyzed by Hoffman-Lauritzen techniques. For this analysis the transport term in *Eq 1* was modified to take into account the effect of adsorption in the presence of filler so that it becomes

$$(C_1 + \emptyset\Delta H_{ads})/\{R(C_2 + T - T_g)\} \quad [6]$$

where $\emptyset$ is a "fitting parameter".

In the numerator of *Eq 6* the classical C_1 value of 1.72×10^4 is used. To it has been added the heat of adsorption per segment of PPO onto silica, 3.64×10^4 kJ/mol multiplied by a "fitting factor" $\emptyset$. These operations are in effect a modification of C_1, a term related to the fractional free volume in the composite. This is done to obtain a fit to the experimentally measured growth rates. It should be recalled, perhaps, that the C_1 and C_2 values in the original WLF development were also obtained by curve fitting. When the classical value of 2073 is used for C_1/R together with 330 K for C_2, 36.4 kJ/mol for ΔH_{ads} and 0.022 for $\emptyset/R$ a straight line is obtained from the plot of $\ln G + (C_1 + \emptyset\Delta H_{ads})/\{R(C_2 + T - T_g)\}$ as a function of $1/T\Delta T$. Thus, the final form of *Eq 1* for silica-filled PPO is

$$\ln G = 11.89 - \frac{2073 + 0.022\ (3.64 \times 10^4)}{(330 + T - 202)} - \frac{1.03 \times 10^4}{T(321 - T)} \quad [7]$$

A plot, *Fig. 2*, of growth rates at various temperatures calculated with this equation yields points which follow the experimentally measured radial growth rates. The fact that the values required for C_1 and for C_2 in the Hoffman-Lauritzen treatment of the nucleated system are different from those for the bulk polymer is not surprising since the nature of the material being transported in the composite has undergone considerable modification.

Morphology

As shown in *Fig. 4A*, when an un-nucleated sample of PPO is crystallized at 283 K the usual spherulites are obtained which produce the regular Maltese cross when viewed through crossed polarizers on a microscope. Under identical experimental conditions a dramatic change is seen for spherulites formed from PPO containing 1 part silica per 100 parts polymer (*Fig. 4B*). The presence of the silica results in a much coarser morphology showing a tendency towards a dendritic structure. This

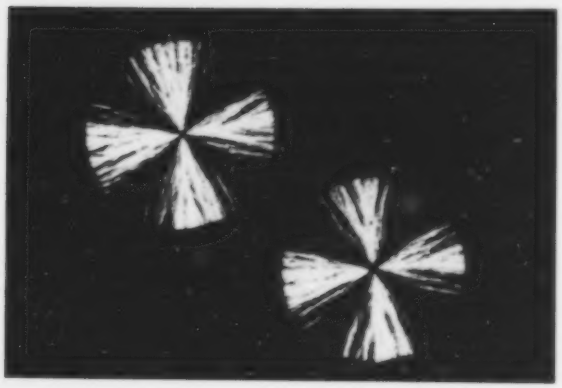

A

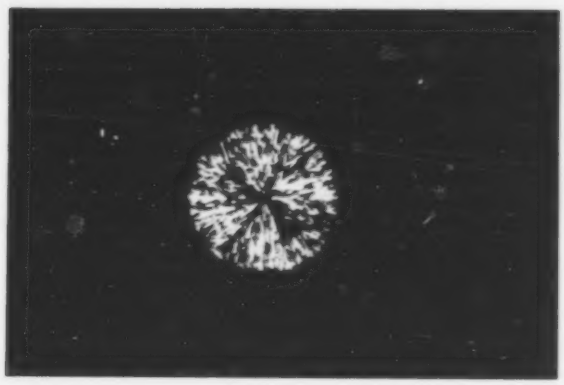

B

Fig. 4. Spherulites of poly(propylene oxide) crystallized at 283 K. A—Unfilled. B—one part silica in 100 parts polymer.

change in structure is also indicated by a change of the last term of the Hoffman-Lauritzen equation from 7.67×10^3 for the unfilled PPO (*Eq 5*) to 1.03×10^4 for the silica-filled PPO (*Eq 7*). The presence of the filler evidently causes quasicrosslinking, due to strong adsorption of the polymer onto the silica surface. This tends to reduce the diffusion coefficient, D, hence the ratio D/G, where G is the radial growth rate of the spherulite. This is known to decrease the frequency of branching and results in coarser spherulites (16). Similar changes in the structure of spherulites are known to result from changes in the crystallization temperature (17). However, there are apparently no previous reports of such changes resulting from the addition of filler material.

SUMMARY

Although silica acts as a nucleant for crystallization of PPO from the melt, it also reduces the rate of radial growth of spherulites at any given crystallization temperature. This retardation results from strong adsorption of polymer segments to the silica particles with a concomitant increase in the viscosity of the melt. This adsorption also causes the spherulites to become coarser in structure.

ACKNOWLEDGMENTS

Financial support from the Faculty of Graduate Studies and Research, McGill University; from the Natural Science and Engineering Council of Canada; and from the Quebec Ministry of Education in the form of operating grants and scholarships (for MAK) is gratefully acknowledged. We would also like to express our appreciation to Prof. R. St-J. Manley for helpful discussions.

REFERENCES

1. G. Turturro and L. E. St-Pierre, *J. Colloid Interf. Sci.*, **67**, 349 (1978).
2. G. Turturro, G. R. Brown, and L. E. St-Pierre, *Polymer*, **24**, in press.
3. M. Kennedy, G. Turturro, G. R. Brown, and L. E. St-Pierre, *Nature*, **287**, 316 (1981).
4. M. A. Kennedy, G. Turturro, G. R. Brown, and L. E. St-Pierre, *J. Polym. Sci., Polym. Phys. Ed.*, **21**, 1403 (1983).
5. C. C. Price and M. Osgan, *J. Am. Chem. Soc.*, **78**, 4787 (1956).
6. C. Booth, C. J. Devoy, and G. Gee, *Polymer*, **12**, 327 (1971).
7. J. H. Cole and L. E. St-Pierre, *J. Polym. Sci. Polym. Symp.*, **63**, 205 (1978).
8. J. D. Hoffman and J. I. Lauritzen, *J. Res. Natl. Bur. Stand. Sec. A*, **A65**, 297, (1961).
9. R. S. Chahal and L. E. St-Pierre, *Macromolecules*, **2**, 193 (1969).
10. G. J. Howard and R. A. Shanks, *J. Macromol. Sci. Phys.*, **B19**, 167 (1981).
11. G. J. Howard and R. A. Shanks, *J. Appl. Polym. Sci.*, **26**, 3099 (1981).
12. J. D. Hoffman, G. T. Davis, and J. I. Lauritzen, in "Treatise on Solid State Chemistry", p. 3, Plenum, New York, (1976).
13. J. Boon, G. Challa, and D. W. Van Krevelen, *J. Polym. Sci. A-2*, **6**, 1791 (1968).
14. T. Suzuki and A. J. Kovacs, *Polym. J.*, **1**, 82 (1970).
15. J. H. Cole, Ph.D. Thesis, McGill University, 1971.
16. B. Wunderlich, "Macromolecular Physics", Vol. 1, p. 324, Academic Press, New York, (1973).
17. H. D. Keith and F. J. Padden, Jr., *J. Appl. Phys.*, **35**, 1270 (1964).

VIII. DISCUSSION: L. E. ST-PIERRE

L. A. Utracki: I do not understand what you mean by slowing down the crystallization rate upon addition of $c > 0.5$ percent of the nucleating agent. Which mechanism are you proposing? In the presence of the silica, the rate seems to be especially low during the initial part of the crystallization. Are you implying a sort of epitaxial crystallization with a very slow initial crystal growth, followed by transformation to another, "normal" crystal morphology? Are you saying that upon addition of an amount of silica larger than 0.5 percent the density of nucleating sites is too high?

L. E. St-Pierre: Let us say that you added these small nucleating particles to an atactic polymer, and then determined the viscosity. You would find a significant change, an increase of viscosity above that of pure polymer. Now, if you add these to a crystallizable polymer at a temperature above its melting point, the particles will play two roles: (1) they will cause an increase of viscosity, and (2) on lowering

of the temperature, they will nucleate. There is some balance here. In no case, until we went to the coated filler, did we ever see anything but an increased rate of crystallization, even though we have known since Einstein:

$$\eta = \eta_o(1 + 2.5\phi + \ldots)$$

that we are restricting the viscous flow and making it more difficult for the liquid to crystallize. In the net, however, we usually have so many more nuclei that the total crystallization rate is faster than that of a non-nucleated system. But at some point, and we have seen this mostly with the coated fillers with diminished nucleating ability you have halved it or maybe reduced it to one-third, so you have more nuclei than in pure polymer but less than in the normal nucleated system. Independently of the number of active nuclei, the viscous effect is elevated enough so you offset the overall crystallization rate; you have more nuclei growing but because of the higher viscosity they grow more slowly, lowering the overall rate. The net result is retardation as discussed for isotactic polystyrene.

L. A. Utracki: Since you quoted Einstein, I have to point out that in his derivation, addition of particles does not influence the viscosity of the medium. In your discussion of matrix crystallization, mobility of polymer segments, not the bulk response of the suspension, should be considered. There are some rheological purists who do not like to use the term "viscosity" in relation to a multiphase system; in these systems, there is no continuity in the stress lines nor in the velocity profile and the ratio of these two loses its intended meaning. Here, one measures higher bulk stresses at the same imposed rates of deformation, but in all cases the matrix viscosity, and this is what crystallizes, stays constant.

L. E. St-Pierre: I do not know what you call the medium because we can get into an argument here as to what viscosity we are looking at. Whether we are looking at the viscosity in the interphase, where you are forming the crystal, or another I would not know. All that I am saying is that the transport is sharply diminished on addition of nucleating particles. There is no other way to explain the observed behavior. Consider: first fact, you see that your crystallinity develops more slowly in the nucleated than non-filled sample. Fact number two: the spherulite, when you look at this microscopically, grows more slowly at the same temperature than when the nucleant is absent. The only conclusion I come to is transport. So, you can put any kind of viscosity or rheological interpretation you like, but this is what it is.

M. R. Kamal: I assume that your DSC kinetics, which you showed for the poly(ethylene terephthalate) is based on calories per gram of resin; or is it per gram of mixture?

L. E. St-Pierre: We always normalize. That is usually around 0.98, so we are adding a small amount. When we did our original work with silicones we went up to 40 to 50 percent. There we were looking at a slug of quasi-solid stuff.

The Dynamic Mechanical Method for the Characterization of Solid Composite Polymers

JOHN W. E. GEARING

Polymer Laboratories Ltd.,
New Campus, Ashby Road,
Loughborough, U. K.

and

MARGÔT R. STONE

Polymer Laboratories Inc.,
Amherst Fields Research Park,
Amherst, Mass., 01003

Information and parameters obtainable from the dynamic mechanical thermal analysis test method are defined. The sensitivity of the technique in detecting the presence of separate phases is emphasized. The Polymer Laboratories DMTA instrumentation is briefly described and its various modes of operation, such as frequency multiplexing, discussed. The theory of the mechanical response of two phase systems is presented via the Takayanagi model approach. Series and parallel coupling constants are derived for a few systems as examples of the definition of phase morphology. Examples are given of the results for ethylene-propylene random copolymer, block copolymer elastomers, rubber toughened poly(styrene), carbon fiber reinforced expoxies with different orientations of fiber, and carbon black filled rubbers. The engineering properties of composites are available directly from the PL-DMTA, which provides sensitive detection of non-linear mechanical behavior, frequently found in multi-phase polymer systems.

INTRODUCTION

The principle of the mechanical test method is to impart a small sinusoidal mechanical strain onto a solid or visco-elastic liquid, and to resolve the stress into real and imaginary components. Changes in these components then detect the variations in the state of molecular motion in the material as temperature is scanned. It is thus a powerful technique for studying the effect of not only molecular structure, but also phase morphology and filler addition on the physical properties required for component design.

The torsion pendulum technique in particular has been used extensively to investigate grain boundary and crystal dislocation motion in metals (1). In the polymer field Alexandrov and Lazurkin (2) measured the frequency dependence of the moduli of rubbers as early as 1940. The first workers to use the technique for the dynamic mechanical thermal analysis of polymers were Schmieder and Wolf (3), who used a torsion pendulum device. The advent of microprocessor control of instrumentation has led to the availability of commercial systems which are as simple to operate as Differential Thermal Analysis instruments.

The dynamic mechanical technique is largely complementary to DSC/DTA. These latter techniques give quantitative measurements of heat changes during first order thermodynamic transitions (e.g., melting and crystallization). Resolution of pseudo second order transitions, T_g is rather poor, particularly in the case of minor components, and detection of secondary transitions is impossible. The Dynamic Mechanical method detects molecular relaxations such as those occurring at T_g with a factor of approximately 1000 higher sensitivity than DSC/DTA and measures secondary relaxations quantitatively. The response to first order transitions is however complex and non-specific as it is related to the precise morphology involved.

The examples given in the present paper cover phase separated and non-phase separated copolymers, rubber toughening, filler reinforcement of rubbers, and carbon fiber reinforcement of epoxy resins. Finally, frequency multiplexing is discussed

for the rapid generation of relaxation spectra and activation energies.

THEORY

When a sinusoidal stress is applied to a perfectly elastic solid, the deformation and hence the strain occurs exactly in-phase with the stress. In extension or bending after allowance for the correct geometrical factors the dynamic Young's modulus (E^*) is given basically as (stress amplitude)/(strain amplitude). In shear deformation the dynamic rigidity modulus (G^*) is obtained. However, when some internal molecular motion is occurring in the same frequency range as the impressed stress the material responds in a visco-elastic manner and the strain response lags behind the stress.

It is then convenient to resolve E^* or G^* into elastic and viscous components, called the storage (E', G') and loss components (E'', G''). A more useful parameter is the dimensionless ratio, $\tan \delta = E''/E'$, often referred to as the damping factor.

A relaxation process (onset of some new degree of motional freedom) may be scanned by changing frequency at constant temperature (frequency plane data) or changing temperature at constant frequency (temperature plane data). Although the former is purer in that no structural changes will occur, experimentally accessible frequency ranges are so limited that even a single relaxation process cannot conveniently be encompassed. The "Dynamic Mechanical Thermal Analysis" (or DMTA) technique is thus to scan temperature over a wide range, typically from −150°C to above the material's glass transition. In this way secondary processes (β and γ) due to limited chain or side group motion can be seen as well as main T_g processes (α) in a "thermal spectrum".

Damping peaks shift to higher temperatures with an increase of measurement frequency. The shift allows the activation energy for the process to be determined as $\Delta H^* = -R[d\ln f/d(1/T)]$.

Mechanical Properties of Composites

Multiphase materials respond to stress as a "sum" of its components. However the "sum" will be via a mixing rule which in general will be complex.

The simplest cases are when the phases exhibit strains either in parallel or in series (4). These cases can be represented as seen in *Fig. 1A* and *1B* and represent the upper and lower bounds of modulus.

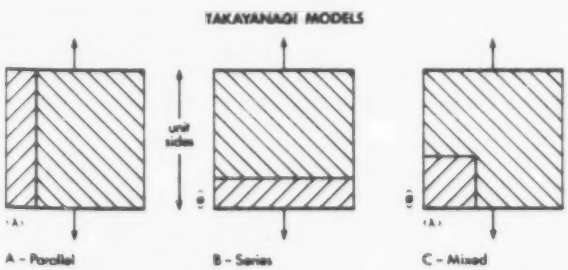

Fig. 1. Takayanagi Model, cubic cross-sections, with unit depth, showing parallel, series, and mixed strain responses. λ and ϕ are the parallel and series coupling parameters.

Surprisingly, these simple models do provide a good representation of real composite materials. Unidirectional composites, for example with rigid fibers oriented parallel to each other and to a sample axis, will respond approximately as a parallel model giving

$$E_c = \lambda E_F + (1 - \lambda)E_M \qquad (1)$$

where E_c, E_F, and E_M are the moduli of the composite, the fiber, and the matrix material respectively and $\lambda = v$, the volume fraction of fiber.

In the series case compliances (J) replace the moduli (E) throughout in the relation with $\phi = v$.

For non-specified arrangements of phases, the modulus can be fitted by adjusting the series (λ) and parallel (ϕ) coupling constants

$$E_c^* = \left[\frac{\phi}{\lambda E_F^* + (1 - \lambda)E_M^*} + \frac{1 - \phi}{E_M^*}\right]^{-1} \qquad (2)$$

This approach should strictly be applied only to the complex dynamic moduli ($E^* = E' + iE''$) of each phase rather than the resolved parts. It provides a useful empirical description of the stress coupling between the phases of two-phase material.

Theories of composite materials (5–7) particularly insofar as they apply to rigid fibers in a polymer matrix give predictive relations of the composite modulus as a function of aspect ratio of the fibers.

INSTRUMENTATION

After a number of decades of work with home made equipment there are now a number of commercial instruments on the market. The PL-DMTA has a standard frequency range of three and a half decades as well as giving rapid accurate data in thermal scanning. All data presented in this paper has been acquired with this instrumentation.

The Polymer Laboratories DMTA is shown schematically in *Fig. 2*. In this instrument stress is proportional to the level of ac current fed to the drive coil from the analyzer module. The frequency of oscillation is selectable from 0.033 to 90Hz and does not depend on sample stiffness. Strain is proportional to the displacement of the drive clamp and is monitored by a non-contacting eddy current

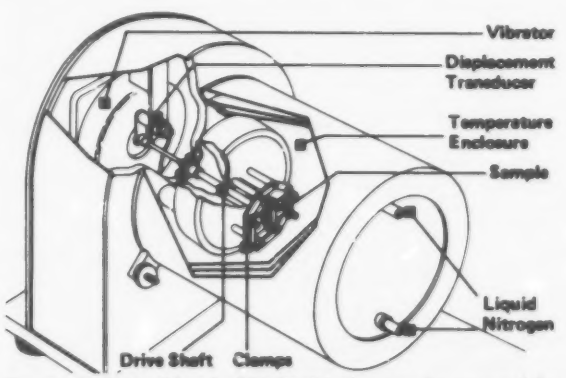

Fig. 2. Mechanical head of PL-DMTA showing the essential features of sample mounting, vibrator system, and transducer.

transducer. The analyzer unit compares the stress and strain signals and by using refined counting circuits resolves the strain into its in-phase (storage) and out-of-phase (loss) components. When the sample geometry constant is dialed into the instrument log E' and tan δ are computed.

The sample temperature is controlled in the range −150 to +300°C by a temperature programmer such that it can be ramped up/down at controlled rates (up to 15°C/min. for measurement) or held at any desired temperature. Use of a microcomputer and the IEEE interface allow frequency to be multiplexed during a slow thermal scan with all data stored for subsequent manipulation.

The normal mode of deformation geometry is by bending small bars as dual or single cantilevers. In the single cantilever mode considerable thermal expansion, such as occurs through a melting point, can be accommodated because of the lateral compliance of the drive. Alternative geometries such as shear sandwich can be used, with tensile mode available on a separate head.

RESULTS AND DISCUSSION

Phase Structure Measurements

In random copolymers two inherently incompatible polymer sequences are forced to co-exist in a single phase. The polymer exhibits a single α-relaxation process intermediate between that of the parent homopolymers. *Figure 3* illustrates this for poly(ethylene-ran-vinyl acetate) at two different frequencies. Sharpening of loss peaks of random copolymers can occur because of improved compatibility between sequences. However, in this case a decrease in ethylene sequence crystallinity occurs with increasing temperature of measurements. The decrease of constraints on the amorphous chains gives a more homogeneous phase and a narrower distribution of relaxation times. In contrast incompatible sequences in block copolymers, in general, phase separate. This can be assessed by DMTA via the observation of two separate α processes. *Figure 4* shows this for effectively a block copolymer of poly(styrene) (PS) and random butadiene-styrene

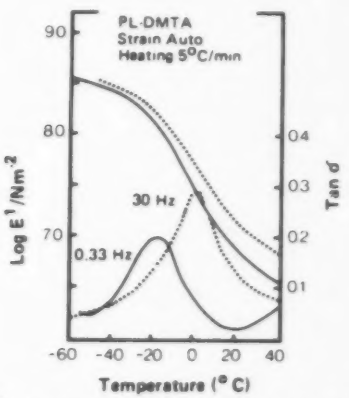

Fig. 3. Ethylene-ran-vinyl acetate copolymer at two different frequencies on the Polymer Laboratories DMTA. A single phase polymer exhibits a single T_g relaxation between that of the parent polymers.

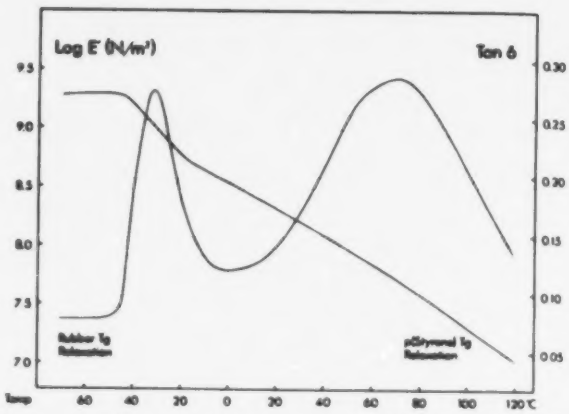

Fig. 4. PL-DMTA scan of block copolymer of butadiene with SBR at 1 Hz and 5°C/min. heting rate. The two loss peaks clearly show phase separation but with considerable phase boundary mixing

polymer. However, the PS peak in particular is occurring at a lower temperature than homo PS of the same molecular weight, indicating some mutual solubility and phase boundary mixing. The modulus level in the region between the two T_g processes allows an assessment of the phase structure from *Eq 2*. If the glassy phase is continuous the modulus will be high but if the rubber phase is continuous it will be low. In the Takayanagi model equation the glassy state modulus of the PS phase, obtained from separate measurements of pure PS, is given by $E_s' = 2 \times 10^9$ N/m^2. The modulus of the SBR rubber phase can again be taken as the parent material before modification, $E_B' \approx 10^7$ N/m^2 and as this value is only about one hundredth that of the matrix, its exact value is not significant. The volume fraction $v_B = \phi$, $\lambda = 0.3$, thus the modulus of the two phase system at 0°C, $E_c = 4 \times 10^8$ N/m^2, is matched by $\phi = 0.32$, $\lambda = 0.92$.

This high level of parallel coupling indicates the morphology is predominantly lamellar in nature. A related material is the Shell SBS, thermoplastic elastomer, in which the resulting room temperature modulus of cast films depends on the nature of the solvent used. Toluene is a good solvent for both phases and allows an equilibrium structure to be achieved with poly(butadiene) (PB) as continuous matrix and PS as the disperse phase. This material has a low, rubbery modulus at room temperature. However, casting from methylene chloride, because of its greater compatibility with the PS, encourages this to be the continuous phase. The PS content of this polymer is 27 percent so that it cannot be the major matrix phase, but it is drawn out to be a non-discrete phase. The evidence for this lies largely in its high room temperature modulus.

The modulus, $E_c = 10^8$ N/m^2 at −40°C and this and the whole modulus curve through the PB relaxation is adequately fitted using *Eq 2* with:

$$\phi = \lambda = 0.52 \text{ for toluene cast SBS}$$

For the methylene chloride cast material, $E_c = 7 \times 10^8$ at −40°C and the whole PB relaxation region is now fitted using $\phi = 91$ and $\lambda = 0.30$.

The toluene cast sample with equal series and parallel coupling constants is close to the ideal result for dispersed spheres.

Rubber toughening of glassy polymers such as PS and poly(methyl methacrylate) is a common commercial practice. DMTA measurements allow a characterization of the phases present from the modulus of the resulting material. An example is given in *Fig. 5* for ABS polymer in which the phase separation of the rubber domains is seen via the PB α-relaxation at low temperature. Further examination shows additional features below the main T_g characteristic of the forming operations.

Thermosets

The curing of epoxy resins and similar materials from the liquid state is extremely difficult to follow. The approach we normally use is to coat an inert substrate (such as a 50 micron steel foil) and to follow the cure of the resulting composite. *Figure 6* shows the increase in modulus with time during a room temperature cure of a two component epoxy. The tan δ damping peak occurs as the system is driven into the glassy state by the cross-linking reaction. If a symmetrically coated strip is used, a reasonable evaluation of the matrix parameters can be made via:

Apparent E' for composite bar E_c'

$$= E_2' + [t_1/(t_1 + t_2)]^3 E_1' \quad (3)$$

where E_1' and E_2' are the dynamic storage moduli of the steel and the coating respectively and t_1 and t_2 their respective thicknesses.

Fiber reinforced composites are of growing importance particularly for aerospace use where their high stiffness to weight ratio is very attractive. As predicted by the model equations this high stiffness only occurs in the fiber direction and efforts have to be made to bring the transverse stiffness up to an acceptable level. Interesting property variations are seen in these materials as a result of the extremely high fraction of stress borne by the fibers. *Figure 7* compares a uniaxially oriented carbon fiber/epoxy composite to a biaxial system (an impregnated woven mat). The test direction in each case was indexed to a fiber axis. Despite being the same resin the relaxation spectra look very different. The explanation is believed to be as follows.

The low temperature damping peak at 130°C is actually reflecting the T_g of the resin and this peak arises from the matrix polymer stressed perpendicular to the fiber direction. The unidirectional sample matrix must also soften in the same range, but because the fibers carry all the stress, the stiffness does not decrease until longitudinal shear can occur between fibers along their length.

Frequency Multiplexing

Recent advances in computer control have led to new, more rapid and in some ways more accurate methods of data acquisition. If during a slow thermal scan, typically at 1°C/min., frequency is continually changed (multiplexed) by and external computer, the data can be sorted and displayed as a series of single measurement frequencies *vs.* temperature. *Figure 8* shows this for an epoxy, multi-

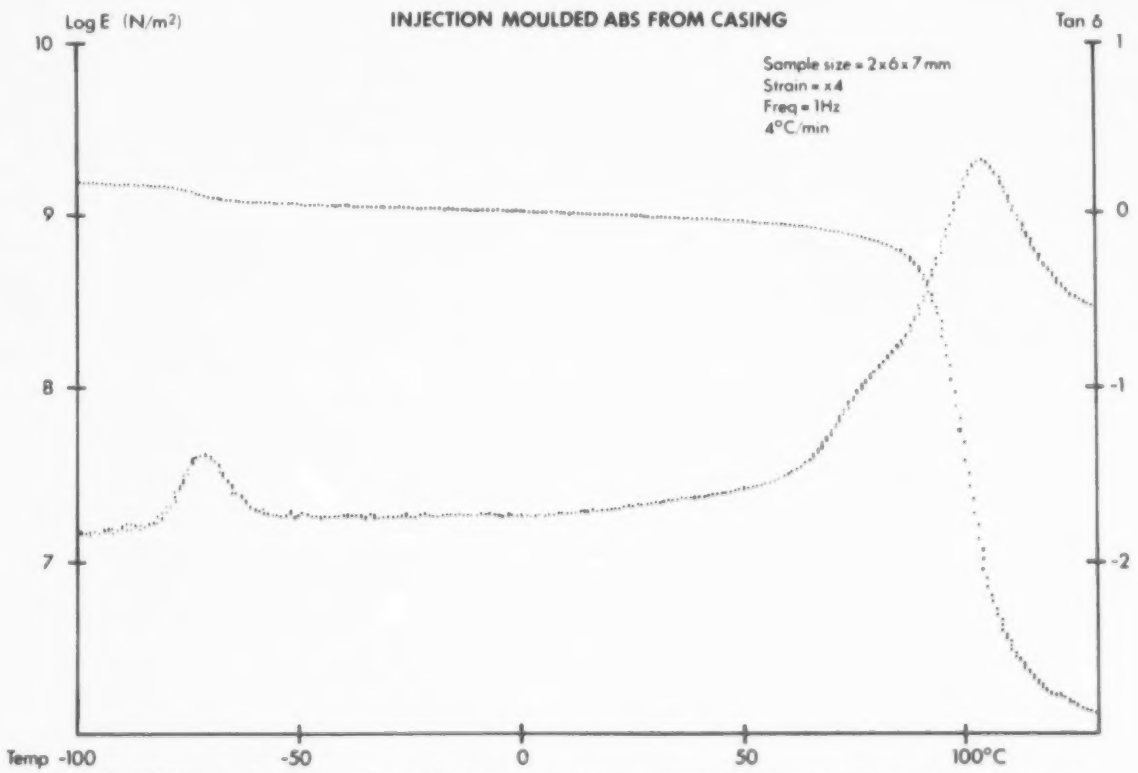

Fig. 5. PL-DMTA scan of rubber toughened ABS showing phase separated poly(butadiene) relaxation at low temperature.

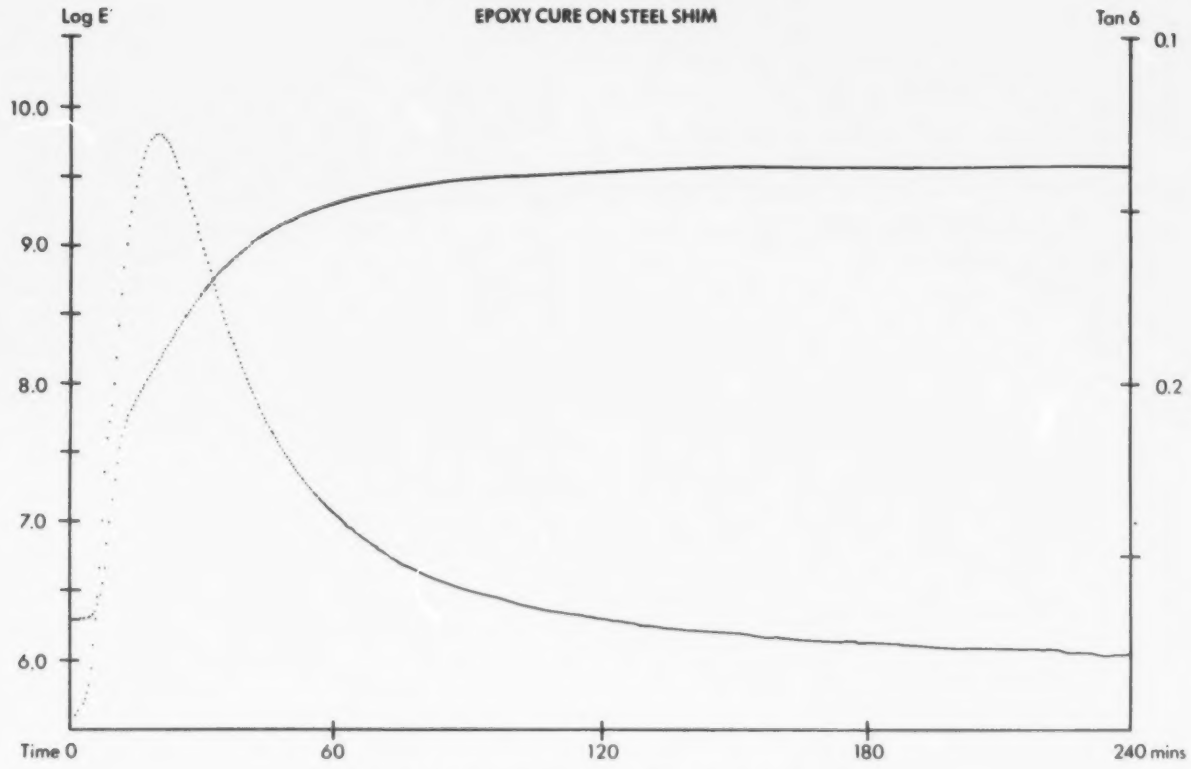

Fig. 6. Curing of an epoxy matrix with time, showing tan δ peak.

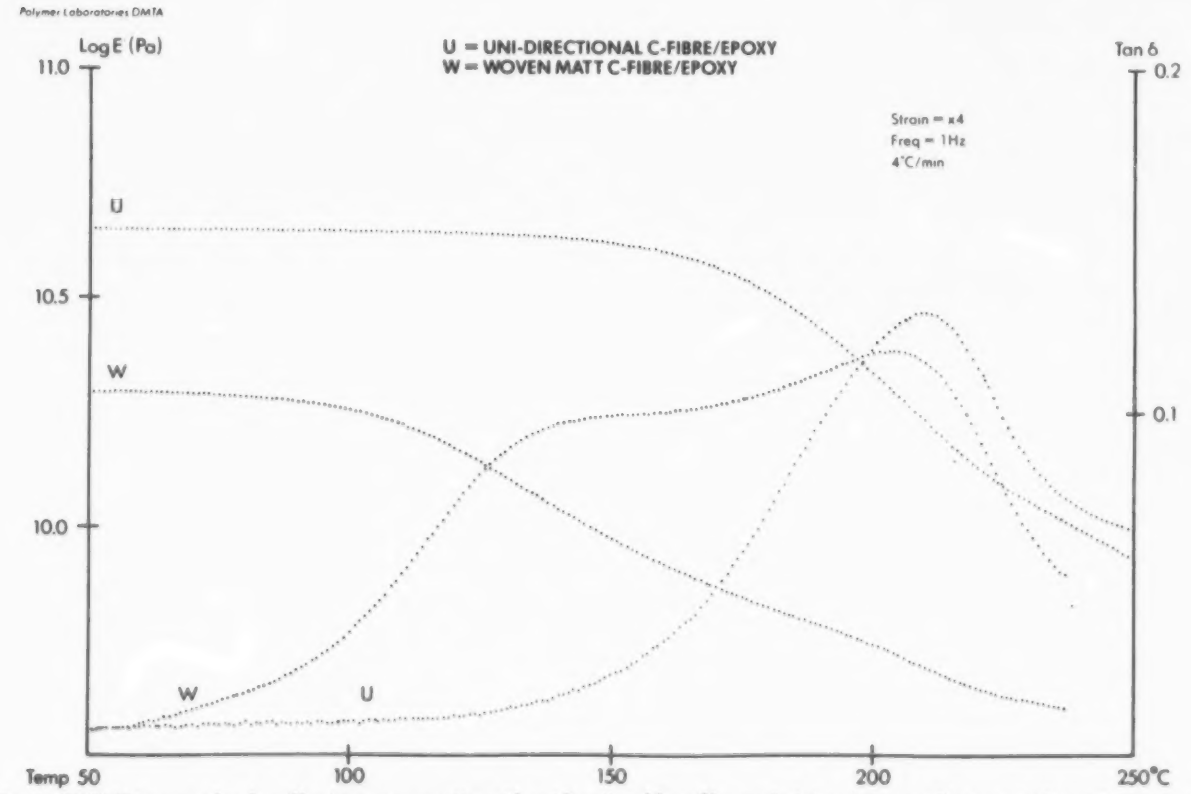

Fig. 7. PL-DMTA scans of carbon fiber/epoxy composites with unidirectional long fibers only (u) and a woven fiber mat with equal transverse and longitudinal fibers (w). The resin is the same in each case. The tan δ curves (right axis) show maxima.

plexed. The peak shift is plotted *vs.* reciprocal temperature in *Fig. 9*, giving the activation energy of 383kJ/mol. Rather complete rheological characterization is given by this technique and besides the time saving advantages over isothermal work, two main benefits accrue: (1) any temperature error is exactly the same for every frequency because the temperature is increasing linearly with time, and (2) clamping during heating stays positive, as there is a tendency for the sample to expand into the clamps. During isothermal measurements most normal samples tend to relax away from clamping pressure with time. Thus rather complete and accurate viscoelastic characterization can be achieved by this new approach.

Filler Rubbers; Non-Linear Behavior

The PL-DMTA turns out to be a very sensitive instrument for picking out non-linear viscoelastic behavior. Whereas single phase homopolymers such as PS or unfilled elastomers are linear materials at low strains, most two phase systems seem not to be. Thus many crystalline polymers between T_g and T_M are non-linear and many polymer blends are non-linear. The most extreme and well documented example is that of carbon black-filled rubbers. It seems that reversible filler-filler structures are the main cause of this phenomenon which is illustrated by frequency plane data in *Fig. 10*. This information is of prime importance in the design of engineering components such as car tires and belting.

CONCLUSIONS

The DMTA technique always provides rapid qualitative characterization of multi-phase composite polymers. When only two phases are present

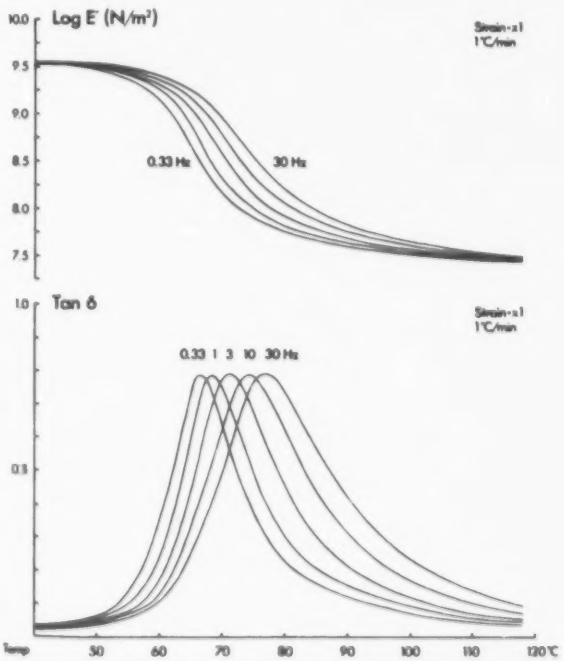

Fig. 8. Frequency multiplexing with the PL-DMTA. The sample was a moderately cross-linked epoxy. This data was acquired at 1°C/min. giving a total measurement time of 80 minutes.

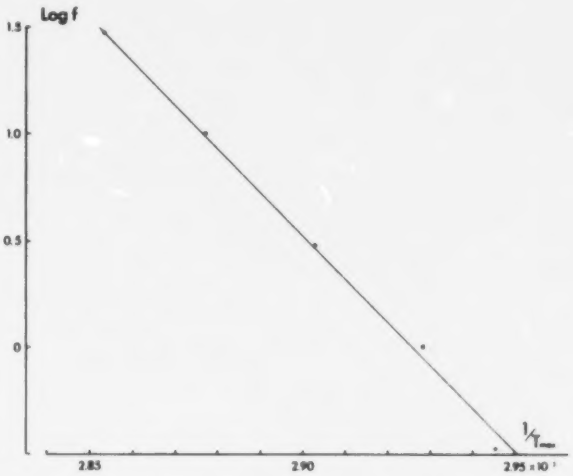

Fig. 9. Loss peak positions plotted as log f vs. reciprocal temperature to determine the activation energy of the relaxation process shown in Fig. 10.

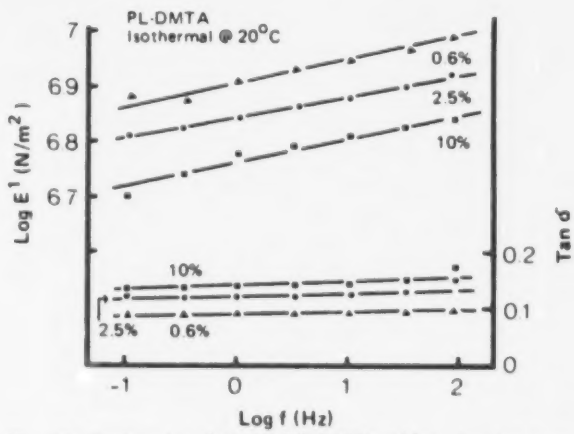

Fig. 10. Engineering data on filled SBR rubber showing non-linear viscoelastic behavior. Upper lines— modulus, lower lines— tan δ.

quantitative information can be obtained by modeling the data with, for example, the Takayanagi equations. The technique detects the occurrence of phase separation via observations of relaxation processes characteristic of each phase and it is hence very sensitive.

Frequency multiplexing during a thermal scan is a convenient and rapid method for measuring viscoelastic response and the activation energies of relaxation processes.

Engineering data are obtained directly as absolute modulus and damping are measured. The strain dependence of visco-elastic response is pronounced for most two-phase systems even at low strains and allowance must be made for this in engineering design with composites.

REFERENCES

1. C. Zerner, "Elasticity and Anelasticity of Metals," Chicago Univ. Press (1948).
2. A. P. Alexandrov and Yu. S. Lazurkin, *Acta Physico-chimica URSS*, **12**, 647 (1940).
3. K. Schmieder and K. Wolf, *Kolloid-Zeit*, **134**, 149 (1953).

4. M. Takayanagi, H. Harima, and Y. Iwata, *Mem. Faculty of Eng., Kyushu Univ.*, **23**, 1 (1963).
5. R. M. Jones, "Mechanics of Composite Materials," McGraw Hill (1975).
6. J. D. Ferry, "Viscoelastic Properties of Polymers," 3rd Ed., Wiley, New York, (1980).
7. N. G. McCrum, B. E. Read, and G. Williams, "Anelastic and Dielectric Effects in Polymeric Solids," Wiley (1967).

IX. DISCUSSION: J. W. E. GEARING

J. Minte: Do I understand you correctly that you are changing both temperature and frequency during one test?

J. W. E. Gearing: We can do this. Typically, we take a sample and do a fairly fast scan at a single frequency over a wide range of temperature, typically 10°C/min. Then, when we know the areas of interest, we do a slower run at 2 to 3°C/min., jumping several frequencies, multiplexing as we call it, during the single thermoscan.

J. Minte: I fear that you are mixing these effects when you do both—changing the temperature and changing the frequency. When you increase the frequency, you increase the stiffness, but when you increase the temperature, you decrease it. In any case, when you are doing both at the same time you are getting a mixed effect.

J. W. E. Gearing: If the machine would take too long to record the data, this could be the case. We are typically taking data in 2 to 3 cycles, so as long as we are not scanning at too low frequency, as long as we are using frequencies above 0.3 Hz we do not run into problems. We did a scan at 0.03 Hz multiplexing at 0.4°C/min. thermoscan rate without any apparent difficulty.

J. Minte: How do you judge if you have problem or not?

J. W. E. Gearing: The data which we have produced in instances when we expected them to follow WLF equation, did follow it. In some other instances, for other systems, as expected we have gotten quite different curves at different frequencies. We would like to repeat these measurements at a single frequency and compare the results with those obtained by multiplexing. This we have not done.

L. A. Utracki: You may be right as far as pure single phase materials are concerned. There the relaxation spectrum is regular and relatively sharp. However, once you start using composite systems (filled plastics or multiphase polymer blends) the spectrum becomes complex. In a filled system, the solid particle-matrix interactions add a box-like part to the relaxation spectrum at very low frequency end. This part will be invisible in your recommended rates of thermoscans and frquencies. Multiplexing in these systems may not give you the true picture.

J. W. E. Gearing: You could say that most things in life are compromises. You could stabilize in jumps of 1°C and do the whole frequency scan under isothermal conditions. Not only would this be very laborious, but also in some instances your polymer would change: crosslink, degrade or creep. If we are scanning at 2°C/min. taking the data in 10 to 15 sec at each frequency, since most polymers are very bad heat conductors, you may have some displacement in regard to a very slow, single frequency scan. But multiplexing gives you assurance that the displacement is relatively constant at all multiplexed frequencies. The whole test lasts about 2 hrs.

C. L. Beatty: I think that the question Leszek brought up is very important. In fact, the whole question regarding where the transition is from linear to non-linear viscoelastic behavior becomes extremely important in phase separated systems. This is a major problem in materials science. I have one of three PL-DMTA instruments in my laboratory and I have not seen this particular fact. I have also a Dynostat electronics package coupled with an MTS system, so we can get larger amplitudes of stress and strain. In the latter case, we definitely got into a non-linear viscoelastic region and you see all these effects. You can see the effect of mechanical heating of the sample and other serious experimental and theoretical problems to be concerned about. However, from our preliminary studies with PL-DMTA, if you maintain the strain amplitude sufficiently small you can multiplex without serious error. Of course, you may not be able to measure the whole relaxation spectrum but that is another point.

Evidence of Interaction of Fillers with Matrix Polymers via Transition Maps

CHARLES L. BEATTY

Department of Materials Science and Engineering,
University of Florida,
Gainesville, Florida 32611

Surface modifications of fillers can be detected via dielectric relaxation spectroscopy with surface coatings that interact with the matrix polymer resulting in higher glass transition temperatures of the matrix polymer. Increasing the surface area of filler present by increasing the amount of filler systematically shifts the glass transition temperature of the matrix polymer to higher values. Increasing the surface area of the filler by making the surface microporous improves many mechanical properties but may not immobilize as many matrix polymer molecules if a weak boundary layer is present.

INTRODUCTION

The concept that the combination of two materials to form a new material that has characteristics different than either pure component is the basis for the major thrust of composites in all materials areas. Also, it is generally accepted that the nature and degree of interaction between components of the composite also contributes toward the composite's properties as do the properties of the individual components.

In polymeric composites the interaction between the matrix polymer and the included second phase is referred to as either reinforcing or nonreinforcing dependent upon how the modulus and tensile strength vary with an increasing content of filler. Reinforcement is thought to occur when the filler is bound to the polymer matrix whereas unreinforcing fillers are not as well bonded to the matrix polymer. Since the glass transition temperature, T_g, is the temperature at which the polymer molecules become liquid-like, T_g is often used to document the bonding of the matrix polymer that does occur. The literature (1, 2) is repleat with examples of fillers that serve as reinforcing fillers with one matrix polymer but not with another polymer. The advent and use of both silane and titanate coupling agents to gain more and/or stronger bonding between the matrix polymer and the filler are well-documented routes for providing or accentuating such reinforcement bonding (3, 4).

The exploration of the bonding between the filler and polymer via variation of the excitation frequency in dielectric relaxation spectroscopic measurements and the information gained and/or inferred from these measurements is the topic of this paper.

EXPERIMENTAL

The glass transition temperature of selected polymeric composites was determined via dielectric relaxation spectroscopy. A Hewlett Packard (HP) Model 4274A LCR Bridge controlled by a HP 9845 minicomputer was used to acquire and process the dielectric data (5). A Delta Design Model 5900 programmable temperature oven was used to scan temperature at a rate of 0.35°C/min. Deformation was accomplished with a MTS Corp. Model 901.02 minicomputer controlled electrohydraulic deformation system (5). Dynamic mechanical spectroscopic results were acquired using a IMASS Dynalyzer Scaler and Dynatherm connected to a MTS Corp. Model 917.23 deformation system (6).

The composites studied were prepared by using sieved fractions of particulate fillers. Surface treatments were accomplished on the same sieved fraction, in most cases, so that direct comparisons with the untreated filler composite could be made. The filler particles are in the 75μ size range and the surface modification is <1μ so filler size changes due to surface modification are not large. The surface modification technique used for $CaSO_4$ and $CaCO_3$ particulate fillers was R.F. plasma polymerization. This technique allows the deposition of a crosslinked, thin (<1μ) pinhole free films on irregular surfaces of a variety of monomers (7). Tetrafluoroethylene (TFE) and methylmethacrylate (MMA) were used as monomers as they produce plasma polymerized poly(methylmethacrylate) (PPMMA) and plasma polymerized poly(tetrafluoroethylene) (PPTFE) that are similar to their conventionally polymerized analog as evidenced by their infrared spectra (7). In addition, R.F. plasma treatment in the absence of monomer results in the removal of adsorbed water, oil, and other surface contaminants from the filler surface (7). Poly(methylmethacrylate) (DuPont Corp. Elvacite 2010, M_n 40,000 $M_w \cong$ 82,500) was utilized as the matrix polymer for the $CaSO_4$ and $CaCO_3$ composites.

Glass powder (33 mole percent Li_2O and 67 mole

percent SiO_2) was prepared from reagent grade Li_2CO_3 and SiO_2 powder melted at 1350°C for 24 hours in a closed Pt crucible, cast between graphite blocks annealed at 450°C for 4 hours following by grinding in a ball mill (8). Cation solutions were prepared by dissolving ultra-pure (>99.999 percent) metal chloride in deionized water. The glass powder was treated with these metal chloride solutions for 12 hours at 90°C (8). Surface area and density of the glass powder were measured by a LMFC-4 Model OS-7 BET apparatus and a PY-5 pycnometer respectively.

RESULTS AND DISCUSSIONS

$CaSO_4$-Polymethylacrylate

The surface treatments of $CaSO_4$ prior to incorporation into the PMMA matrix by R.F. plasma took several forms. R.F. plasma treatment was accomplished in the presence of argon to clean the filler surface of adsorbed surface contamination of oil, water ($CaSO_4$ is hygroscopic), etc. In addition TFE and MMA were R.F. plasma polymerized onto the surface of the filler in both packed bed and rotating tube reactors (7). The rotating tube reactor provides continuous mixing during the surface treatment. A twenty weight percent loading of these fillers in PMMA results in rather large changes in stress-strain behavior as illustrated in *Fig. 1*. Note that the stress scale for the untreated and PPTFE treated filler is the right-hand scale in *Fig. 1*. Poor adhesion between the Teflon-like PPTFE coated filler and the matrix polymer and the poor tensile properties of the composite are expected. The nearly equally poor performance of the "as-received" $CaSO_4$ compared to the argon plasma treated $CaSO_4$ or cleaned $CaSO_4$ suggests that the cleaning process (presumably the removal of weakly bound adsorbed water, etc.) converts $CaSO_4$ from a unreinforcing filler to a reinforcing filler. Unfortunately, this cleaning effect of the R.F. plasma is not permanent if the filler is stored at ambient conditions prior to forming the composite. Presumably water can be readsorbed at the filler surface resulting in a deterioration of properties of the composite. On the other hand, the MMA treated $CaSO_4$ filler exhibits reinforcing characteristics analogous to the R.F. plasma cleaned $CaSO_4$ composite. However, the PPMMA coated $CaSO_4$ filler can be stored at ambient conditions prior to incorporation in the matrix polymer with little deterioration of composite properties.

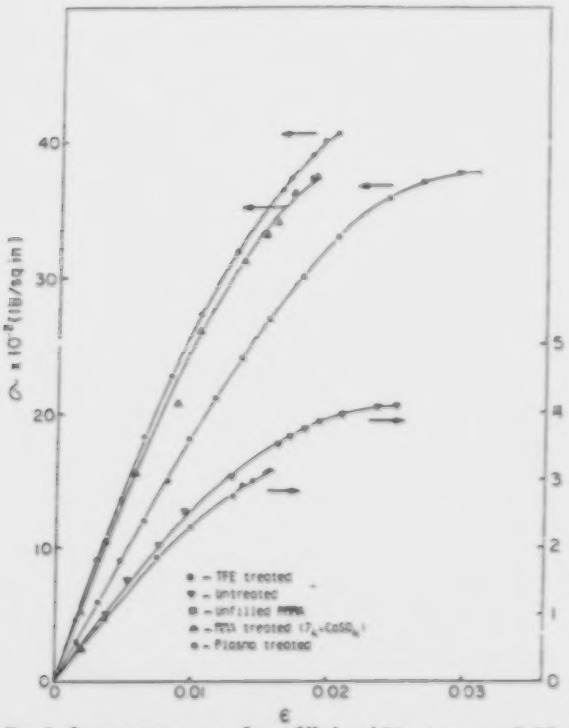

Fig. 1. Stress-strain curves for unfilled and 20 wt. percent $CaSO_4$ filled PMMA films.

Dielectric relaxation spectroscopy of these $CaSO_4$ particulate filled polymers (*Fig. 2*) results in a peak at approximately 30°C whose magnitude decreases with increasing excitation frequency. Also the temperature of this peak is invariant regardless of the frequency used. These characteristics suggest that this phenomena is of the Maxwell-Wagner-Sillars (MWS) type. The MWS effect is more apparent in the TFE and uncoated $CaSO_4$ filled systems presumably because the filler particles are not bound well with the matrix and are therefore quite accessible for charge trapping. The MMA treated and plasma treated filler composites exhibit better bonding which presumably reduces the potential for change trapping at the filler/polymer interface.

Variation of the test frequency results in a systematic shift of the glass transition temperature to higher values. The transition map (*Fig. 3*) is an Arrhenius type plot of the shift in T_g with changes in measurement frequency. This figure clearly shows that at low frequencies the glass transition temperature of the composite can be quite different from the T_g of the unfilled matrix polymer. More

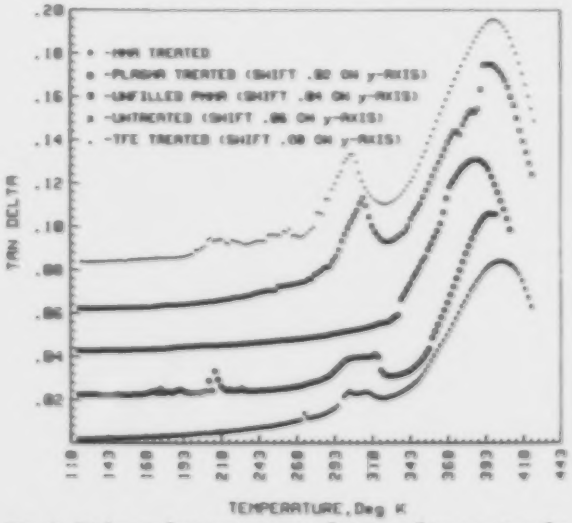

Fig. 2. Dielectric loss tangent as a function of temperature for PMMA and 20 wt. percent $CaSO_4$ filled PMMA film at 100 kHz.

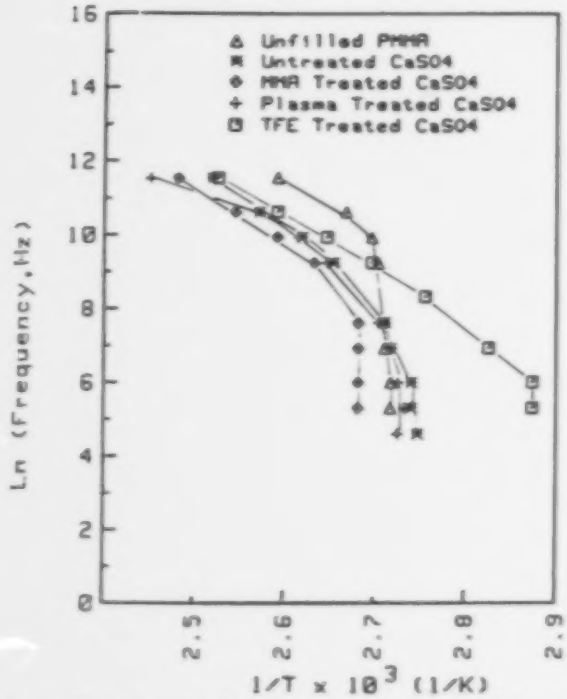

Fig. 3. Transition map of ln (frequency) vs. 1/T for unfilled and $CaSO_4$ filled (20 wt. percent) PMMA films. Polymerization conditions: 125 μ $CaSO_4$ treated for 20 minutes at 100 watts power and 2 torr pressure in dense packed bed reactor.

importantly the type of surface treatment to the same size and type of filler results in a significant shift in T_g of the matrix polymer to either higher values or to lower values. It is not unexpected to observe an increase in T_g of the matrix polymer for the PPMMA coated $CaSO_4$ as better bonding of the filler to the matrix is expected. Recent studies in our laboratory on the changes in relaxational behavior of elastomers (9, 10) and polymeric glasses (6, 9) indicate that deformation of a polymer can significantly shift relaxation processes to higher temperatures. For example, deformation of polycarbonate results in a shift of the lumped broad sub-T_g relaxation processes centered at −100°C into three relaxation processes whose location on the temperature scale is dependent upon the magnitude of the applied stress (*Fig. 4*). Clearly the rate of shift with deformation is not the same for all the relaxation processes. Similarly deformation of a polyurethane elastomer results in the systematic shift of both the sub-T_g and the T_g relaxation processes to higher temperatures as illustrated by the transition map (*Fig. 5*). The activation energies (*Table 1*) increase systematically as the degrees of freedom of the polymer chain are reduced by greater extents of deformation. These results are analogous to the effect of hydrostatic pressure for these relaxation processes (11, 12). Thus, it appears that better bonding and thus immobilization of the polymer matrix chains by the PPMMA coated filler or a reduction in the degrees of freedom to the matrix polymer molecules results in an increase in the apparent T_g of the matrix polymer.

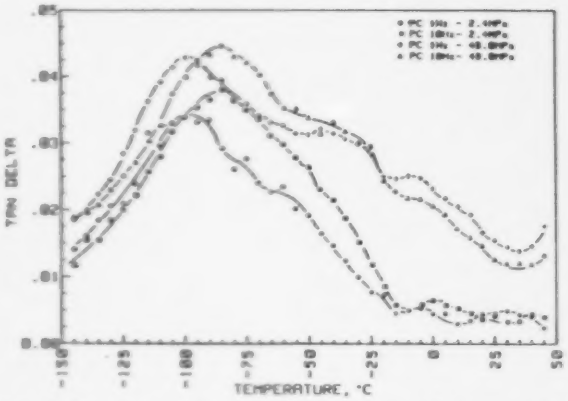

Fig. 4. Tan δ as a function of temperature and measurement frequency at low and high offset stress.

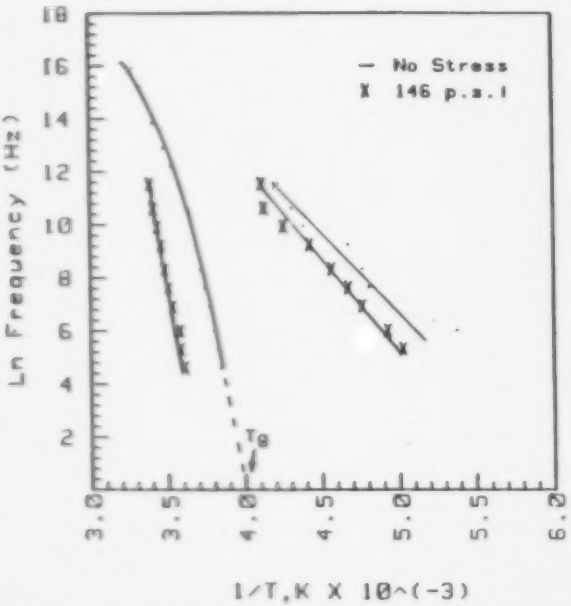

Fig. 5. Transition map for the α (T_g) and β (Sub-T_g) relaxations at zero stress level and 146 psi.

Table 1. Activation Energies as a Function of Stress Levels

No Deformation		With Deformation			
		75 psi (or 0.58 M.Pa)[a]		146 psi (or 1.13 M.Pa)[b]	
Sub-T_g (kcal/mole)	T_g at 10 kHz (kcal/mole)	Sub-T_g (kcal/mole)	T_g at 10 kHz (kcal/mole)	Sub-T_g (kcal/mole)	T_g at 10 K (kcal/mole)
5.65	59.06	8.42	62.86	12.69	67.62

[a] Corresponds to an elongation of approximately 50 percent at 26°C.
[b] Corresponds to an elongation of approximately 100 percent at 26°C.

The decrease in T_g of the PMMA matrix upon inclusion of PPTFE coated $CaSO_4$ was unexpected. Upon reflection it may be reasoned that reduced interaction of the filler with the matrix may be equivalent to providing significantly greater surface area for the PMMA matrix. The PMMA chains in the surface, being less constrained than those in the

bulk may then exhibit a lower T_g. This scenario is similar to that observed by others (14, 15) for the depression of T_g of the polystyrene dispersed phase poly(styrene-co-butadiene) block copolymers compared to the T_g for similar molecular weight undispersed polystyrene.

Also unexpected was the crossover of T_g of the matrix polymer for the composites compared to the unfilled polymer at higher measurement frequencies (*Fig. 3*). As the glass transition temperature is a function of frequency for both the matrix polymer and the composites, the effect of excitation frequency can be illustrated more clearly by plotting the difference of the composite matrix T_g and unfilled polymer T_g *vs.* the measurement frequency (*Fig. 8*). It is worth noting that at high measurement frequencies (i.e., >10 kHz) the addition of filler regardless of surface coating results in an apparent increase in the T_g of the matrix polymer. The variation of the matrix T_g is approximately 30°K for the frequency range studied (i.e., 100 Hz to 100 kHz) for the TFE coated filler whereas it was approximately 10°K for the PPMMA coated $CaSO_4$ filler. Clearly, the frequency of measurement as well as the type of surface modification of the filler are both variables in the apparent T_g of the matrix polymer in the composite. These results suggest that other composite properties should change significantly as the rate of deformation or temperature of deformation is varied.

Analysis of the dielectric behavior of the $CaSO_4$ composites was accomplished by plotting the real component of dielectric constant *vs.* the imaginary component of the dielectric constant (*Figs. 7* and *8*). The PPTFE coated $CaSO_4$ composite can be represented by the Cole-Cole Equation indicating that the dispersion is symmetric similar to the unfilled PMMA which further supports the view that little interaction occurs between the PPTFE coated $CaSO_4$ and PMMA matrix polymer. However, the PPMMA coated $CaSO_4$ composite cannot be represented by such a Cole-Cole plot suggesting that significant interactions occur between the matrix and filler.

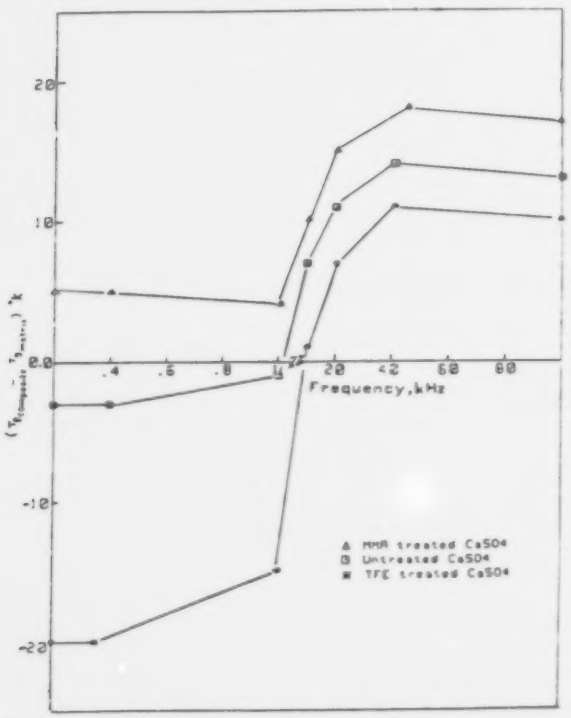

Fig. 6. Plot of ($T_{g_{composite}} - T_{g_{matrix}}$) as a function of frequency for untreated and treated $CaSO_4$ filled (20 wt. percent) PMMA films.

$CaCO_3$-Polymethylmethacrylate

Similar studies were performed on R.F. plasma treated $CaCO_3$ particulate filler dispersed in PMMA. The transition map (*Fig. 9*) illustrates that the T_g of the composites are all lower than the unfilled polymer except at higher frequencies where the R.F. plasma treated $CaCO_3$ composite has a higher T_g than the unfilled PMMA. The origin of this depression in T_g for the composites is unknown. It should be noted that the MWS peak occurs at ~37°C for the $CaCO_3$ composites and may be related to the apparent lowering of the T_g of the composites. The T_g difference plot (*Fig. 10*) again demonstrates that variation of the frequency of measurement results in greatly different T_g's of the matrix in the polymeric composite. Also the major change occurs in the 1 to 20 kHz range although the shape of the T_g difference plot is substantially different from the $CaSO_4$-PMMA composite case. Although the T_g curve is shifted to lower tempera-

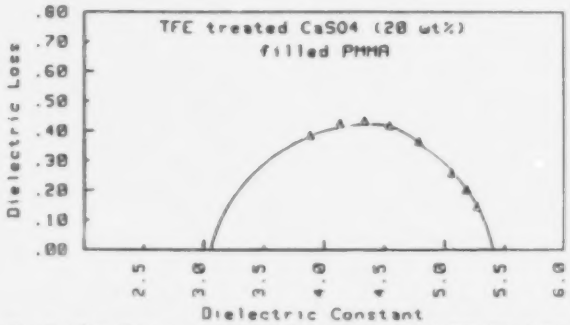

Fig. 7. Plot of ε" vs. ε' at 380°K for TFE treated $CaSO_4$ filled (20 wt. percent) PMMA film. Polymerization conditions: 125 μ $CaSO_4$ treated for 60 minutes at 100 watts power and 2 torr pressure in rotating tube reactor.

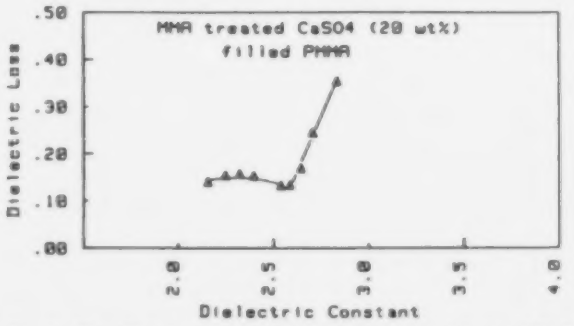

Fig. 8. Plot of ε" vs. ε' at 380°K for MMA treated $CaSO_4$ filled (20 wt. percent) PMMA.

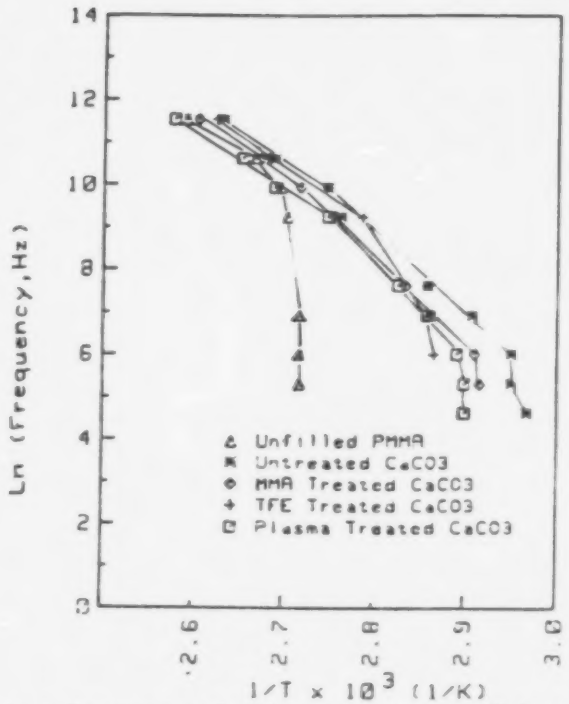

Fig. 9. Transition map of ln (frequency) vs. 1/T for unfilled and filled (20 wt. percent) PMMA films.

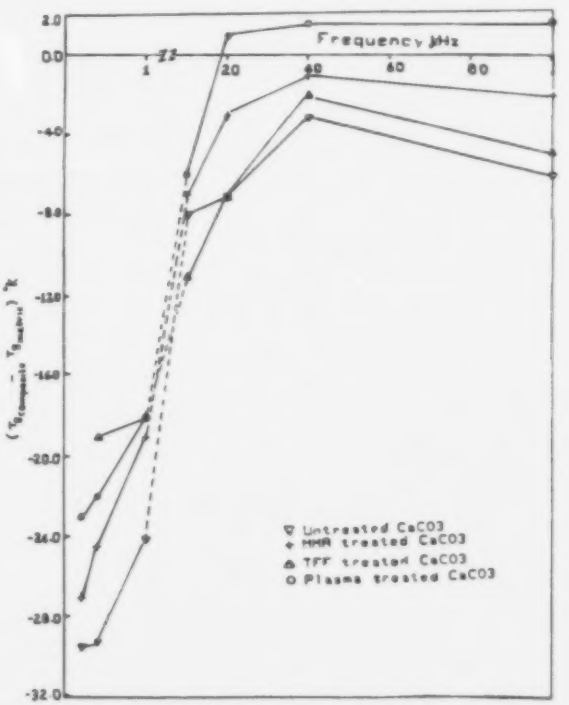

Fig. 10. Plot of $(T^{-}_{g_{composite}} - T_{g_{matrix}})$ as a function of measurement frequency for $CaCO_3$ filled (20 wt. percent) PMMA films.

tures for the composites at nearly all measurement frequencies, the activation energy (*Table 2*) for the glass transition relaxation process varies in a manner consistent with our previous findings. That is, the PMMA in the T_g PPMMA coated filler composite has a higher activation energy for the glass transition relaxation process than the activation energy/ for T_g of the matrix PMMA in the PPTFE coated filler composite.

Inorganic Solution Modified Glass Powder Composites

Corrosion of glass surfaces via exposure to solutions of inorganic ionic compounds can result in changes in surface roughness, porosity, and charge (16–18). The corrosion treatment results in a significant increase in porosity or roughness of the glass powder surface (*Table 3*) with no detectable difference in glass powder size. The tensile strength of composites formed from these glass powders with and without the corrosion treatment and a random copolymer of poly(stryene-n-butylmethacrylate) are shown in *Fig. 11*. The increase in surface area is expected to provide an increased number of bonding sites as well as a gradient in stress distribution across the filler matrix interface. Both effects would presumably yield a higher tensile strength composite. Thus, it is expected that surface rough-

Table 2. Activation Energies[a] for Filled[b] and Unfilled PMMA at Various Frequencies

Frequency (kHz)	PMMA	Filled With Untreated $CaCO_3$	Filled With TFE Treated $CaCO_3$	Filled With MMA Treated $CaCO_3$	Filled With Plasma Treated $CaCO_3$
20	119.1	67.29	63.59	73.6	64.23
60	71.2	56.86	58.88	63.95	55.84
80	41.95	56.82	40.95	55.67	51.2

[a] cal/deg. mol
[b] 20 wt.% loading

Table 3. Surface Areas of Four Hundred Mesh 33 Mole Percent Li_2O-67 Mole Percent SiO_2 Glass Powder Before and After Cation Solution Surface Corrosion

1000 PPM Cation Solution	Surface Area After 90°C, 12 hr. Treatment (m^2/g)
$AlCl_3$	26.36
$MgCl_2$	24.18
$ZnCl_2$	4.73
Untreated	1.47

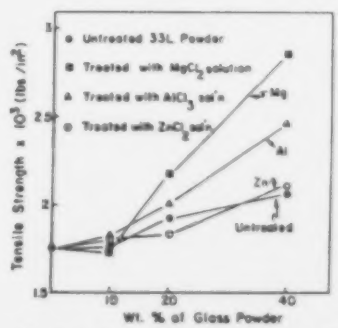

Fig. 11. Tensile strength of 33L glass power filled polymeric composites a function of glass power content, both before and after treatment with $MgCl_2$, $AlCl_3$, and $ZnCl_2$ solutions, respectively.

ening would effectively bond more of the matrix polymer and thereby increase the T_g of the matrix polymer in the polymer composite. As illustrated in *Fig. 12*, the MWS phenomena for the glass powder filled composites occurs at ~47°C. The glass transition relaxation process for PMMA shifts systematically to higher T_g's at high frequencies as more glass powder is added to the composite (*Fig. 13*). The addition of more glass powder included should result in the immobilization of more polymeric matrix material. In this fashion these variations in T_g at high frequency is comparable to the R.F. plasma treated filled composites. Also the crossover in T_g as frequency is varied occurs in approximately the same frequency regime as for the R.F. plasma treated filler composites.

Corrosion of the glass powder provides some interesting and unexpected results as illustrated in *Fig. 14*. Increasing the surface area was expected to raise the T_g of the matrix polymer to higher values in a fashion analogous to adding more glass beads (i.e., creation of more filler surface) to the composite. However, it was observed that at high frequencies the T_g of the matrix polymer is actually depressed compared to the smoother, lower surface area untreated glass powder composite. These results suggest that the polymer is not adhered as well to the corroded glass powder particles as to the untreated glass filler. Upon examination of the treated glass powder in a Scanning Electron Microscope (SEM) it was clear that a film partially covered the treated glass powder. Also it appeared to be weakly bonded as portions of the films were missing and additional areas appeared to be removable by agitating the treated glass powder (8). X-ray diffraction studies of these inorganic coatings (that resulted from corrosion treatment) indicated that they were $Mg(OH)_2$ ZnO, $Al(OH)_3$ for the appropriate ionic corrosion solutions. Thus it appears that these inorganic coatings (which result from the surface roughening treatment) provide a weak boundary layer which minimizes the bonding of the matrix polymer chains despite the significant increase in bonding area. Consequently, the improvement in tensile strength of composite formed from these roughened glass powders is probably due to the increased surface area and not better or increased bonding to the matrix polymer. The roughened or porous surface of the glass filler is thought to provide a gradient of modulus across the matrix-filler boundary thereby minimizing stress concentration at the boundary between the low modulus matrix and the high modulus filler. The step-change in modulus that occurs in many composites results in stress-concentration at the matrix-filler interface that often results in subsequent delamination failure. Current research in these glass composites is focused on substituting a good bonding surface for the weak boundary layer coatings. Thus, it is hoped that the increased surface area and gradient of modulus that is achievable via the corrosion process combined with more adherent filler surface coatings will result in superior composites.

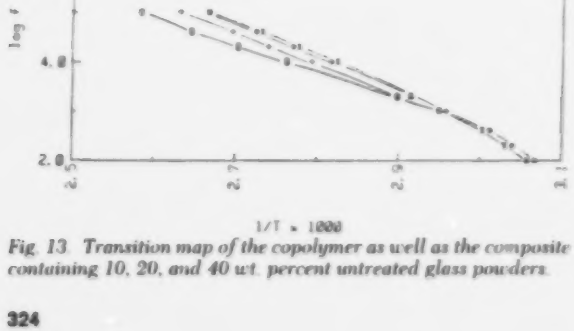

Fig. 12. Dielectric loss factor (tan δ) vs. temperature of the composite containing 20 wt. percent untreated glass powders as a function of frequency.

Fig. 13. Transition map of the copolymer as well as the composite containing 10, 20, and 40 wt. percent untreated glass powders.

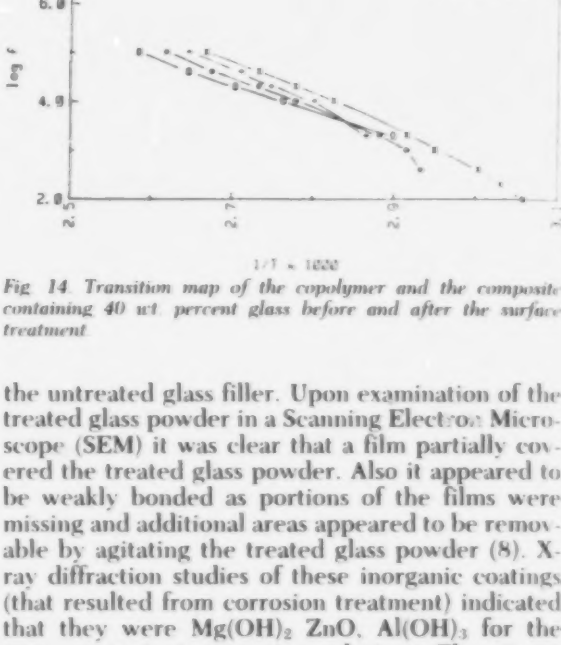

Fig. 14. Transition map of the copolymer and the composite containing 40 wt. percent glass before and after the surface treatment.

SUMMARY

1. Surface modifications of fillers can be detected via dielectric relaxation spectroscopy with surface coatings that interact with the matrix polymer resulting in higher glass transition temperatures of the matrix polymer.
2. Increasing the surface area of filler present by increasing the amount of filler systematically

shifts the glass transition temperature of the matrix polymer to higher values.
3. Increasing the surface area of the filler by making the surface microporous improves many mechanical properties but may not immobilize as many matrix polymer molecules if a weak boundary layer is present.

ACKNOWLEDGMENTS

The author wishes to acknowledge the research efforts of K. Shah, K. Venkataswamy, H. Kolman, K. Shih, and C. Lee as well as the valuable discussions of Drs. J. Pochan and D. Clark. Financial support of the varied research projects by the Air Force Office of Scientific Research—Contract # F49620-80-C-0047, the Microstructure of Materials Center of Excellence and the Engineering and Industrial Experimental Station, University of Florida is greatly appreciated.

REFERENCES

1. J. A. Manson and L. H. Sperling, "Polymer Blends and Composites," Plenum Press, New York, N. Y. (1976).
2. L. E. Nielsen, "Mechanical Properties of Polymers and Composites," Marcel Dekker, Inc., New York, N. Y. (1974).
3. K. L. Mittal, Ed., "Adhesion Aspects of Polymeric Coatings," Plenum Press, New York, N. Y. (1983).
4. E. P. Plueddemann, "Silane Coupling Agents," Plenum Press, New York, N. Y. (1982).
5. K. Venkataswamy, K. Ard, and C. L. Beatty, *Polym. Eng. Sci.*, **22**, 961 (1982).
6. H. J. Kolman, K. Ard, and C. L. Beatty, *Polym. Eng. Sci.*, **22**, 950 (1982).
7. K. Shah and C. L. Beatty, to be published.
8. C. T. Lee, D. E. Clark, K. S. Shih, and C. L. Beatty, *Ceramic Eng. Sci. Proceedings*, **2**, 9–10 (1983).
9. C. L. Beatty, H. Kolman, and K. Venkataswamy, IUPAC Proceedings, Amherst, MA., p. 848 (1982).
10. K. Venkataswamy and C. L. Beatty, to be published.
11. E. N. Dalad and P. J. Phillips, *Macromolecules*, **16**, 890 (1983).
12. D. L. Questad and M. Oskooie-Tabrizi, preprint.
13. K. D. Pae and D. L. Questad, *J. Polym. Sci.*, **21**, 1195 (1983).
14. S. Krause and M. Iskandar, *Adv. Chem.*, **176**, 205 (1979).
15. L. Jean and J. Leblanc, *J. Appl. Polym. Sci., Polym. Chem. Ed.*, **21**, 2419 (1977).
16. M. F. Dilmore, D. E. Clark, and L. L. Hench, *Am. Ceram. Soc. Bull.*, **58**, 1111 (1979).
17. G. A. Hudson and F. R. Bacon, *Am. Ceram. Soc. Bull.*, **37**, 185 (1985).
18. J. M. Horn and G. Y. Onoda, Jr., *J. Am. Ceram. Soc.* **59**, 62 (1976).

X. DISCUSSION: C. L. BEATTY

L. E. St-Pierre: When we were working with poly(dimenthyl silicone) we never saw T_g to go down. We could increase it by as much as 10°C. We did do some work adsorbing the polymer and swelling it. With a surprise, we observed that the polymer adsorbed sometimes swelled more than the free, non-adsorbed, one. We expected that the adsorbed species will behave as a partially crosslinked rubber. But its equilibrium swelling showed a super-loose structure. We have never found a satisfactory explanation for this observation. It still puzzles me. Maybe this is somehow related to the stuff you are talking about.

C. L. Beatty: It is quite evident in the literature, particularly in the Russian literature. They have published T_g data as a function of frequency, but they have not really tried to take the difference of the matrix and the composite. The frequency effect looks very confusing until you start taking into account the actual difference between the pure matrix material and the composite response. Only then do natural patterns start to emerge. The methods we are currently trying to develop is the dynamic-mechanical approach. In this particular technique, we will not have the potential conflict between Maxwell-Wagner-Sillars polarization peak to interfere with the glass transition peak. This was always a potential problem in the dielectric measurements. We think that in our study we eliminated this interference but in all honesty we have to admit that this was a problem.

L. A. Utracki: This is really an exciting work. It is rather amazing to see how much the T_g changes on addition of filler particles—both up and down the temperature scale. By using the WLF-equation, you suggest that the change is due to modification of the free volume around T_g. This makes me quite happy, although I am not in great favor of the WLF-equation. The free volume is such a simple physical concept amenable to interpretation. One can transpose your observations regarding T_g to a statement that addition of fillers coated with different substance, can either increase or decrease the free volume fraction in the composite. In particular, by incorporating the Teflon coated $CaSO_4$, you reduced T_g by nearly 30°C, what must mean a great increase in free volume. If this is so, then the viscosity of your composite should be much lower than that of the matrix polymer at the same temperature and frequency. Since the viscosity-temperature relation is particularly steep near T_g the measurements at a temperature a few degrees higher than the matrix glass transition should give you the largest difference. In our review on rheology of composites (*Polym. Compos.*, **3**, 193 (1982)) we quoted a paper by Prokopenko, who reported a 45 percent reduction of viscosity of polystyrene on addition of a fraction of wt. percent of fine crushed glass. Of course, this is far away from your work, but maybe in both cases the mechanism is similar. It certainly would be very interesting to pursue this line of research. In particular the effect of free volume on extensional flow should be investigated. We will be happy to help you in this work if you so desire.

C. L. Beatty: We have not looked at any of the melt properties; this is something we want to do. I am not certain that the interactions between filler and matrix carry from the solid state to the melt. So far, we studied only behavior of these systems in the solid state. I suspect it does. One thing is very clear—if you add various amounts of the Teflon-coated $CaSO_4$ you can march the low frequency depression of T_g right out; it shifts in a nice, systematic fashion. In other words, it seems to behave in a reasonable manner. The Teflon-coated filler does not disperse terribly well; you really have to work to have it dispersed. The optical properties

change dramatically as a result of degree of dispersion. On the other hand, poly(methyl methacrylate)-coated materials disperse very nicely, resulting in a transparent composite.

L. A. Utracki: Are these coated materials available for testing?

C. L. Beatty: We can not get enough for our own. One needs a lot of material to do the rheological studies. We coat in 10 to 20 g batches. Presently, we are trying to scale-up the process.

The Effect of Aspect Ratio of Inclusions on the Elastic Properties of Unidirectionally Aligned Composites

G. P. TANDON *and* G. J. WENG

Department of Mechanics and Materials Science
Rutgers University
New Brunswick, NJ 08903

This paper examines the influence of aspect ratio α, from zero to infinity, on the effective elastic moduli of a transversely isotropic composite. The reinforcing inclusions, which could be flakes or short fibers, are assumed to be spheroidal and unidirectionally aligned. Of the five independent elastic constants, the longitudinal Young's modulus E_{11} and in-plane shear modulus μ_{12} appear to increase with increasing aspect ratio, while the transverse Young's modulus E_{22}, out-plane shear modulus μ_{23}, and plane-strain bulk modulus K_{23}, generally decrease. It is further noted that E_{11} is more sensitive to α when $\alpha > 1$ but the others are more so when $\alpha < 1$. The present analysis was carried out by the combination of Eshelby's and Mori-Tanaka's theories of inclusions.

1. INTRODUCTION

As lightweight materials of great strength and stiffness, reinforced plastics have emerged as composites of major technological significance in recent years. By a proper combination of, say fibers and a matrix, a wide range of elastic properties can be achieved. In order to fully utilize their potential, a more complete in-depth study is required as to how the bulk properties of the composite depend on the elastic properties and the geometric parameters of its constituents.

The present work is concerned with the theoretical study of the elastic properties of materials containing reinforcing inclusions, which could be flakes or short fibers, aligned unidirectionally. It is assumed that the binder and the inclusion materials are both linearly elastic, isotropic, and homogeneous. The inclusions are taken to be uniformly distributed. Because of the inclusion orientation the composite is macroscopically homogeneous and transversely isotropic; it therefore has five independent elastic constants. The problem, then, is to find expressions for the effective elastic moduli of the reinforced material in terms of the geometry of the inclusions, characterized here by the aspect ratio, and the properties of the two phases at various concentrations.

In this respect, some semi-empirical and numerical approaches (1, 2) have been suggested to derive unidirectional stiffness constants. A well-known example is the Halpin-Tsai equation (3). Unidirectional fiber orientation can also be considered as a limiting case of partial fiber alignment. The subject of biased fiber orientation has been taken up by Fukuda and Kawata (4) for short fibers and by Cox (5) and Cook (6), among others, for continuous fibers.

The variational principle of the theory of elasticity has been applied by Hashin and Rosen (7), Hill (8), and Hashin (9) to obtain upper and lower bounds for the effective moduli of fiber-reinforced composites, in which fibers are assumed to be of infinite length. Also, Hill (10), using the self-consistent theory, gave estimates for the elastic moduli of unidirectionally continuous fiber composites. Laws and McLaughlin (11) and Chou, *et al.* (12) have further applied Hill's self-consistent method to analyze the elastic stiffness of short-fiber composites. The self-consistent method treats both phases on equal footing; it therefore cannot treat one phase as matrix and the other as inclusions. Treating the inclusions and matrix separately, Russel (13) has applied Eshelby's (14) solution of an ellipsoidal inclusion to address the same problem. Due to the neglect of phase interactions, Russel's results, however, are valid only at very dilute concentrations.

At finite concentrations, but not so large as to warrant direct contact between inclusions, the stated problem could be treated by the combination of Eshelby's solution (14) and Mori-Tanaka's average stress (15). The essence of this average stress is the following: Under a given applied stress the average stress in the matrix is perturbed from the applied one due to the presence of inclusions. The volume average of the perturbed parts over both the matrix and the inclusions, however, has to vanish in order to satisfy the equilibrium condition. This theory has been applied by Taya and Chou

(16) and Taya and Mura (17) to calculate the longitudinal Young's modulus of three phase composites, and generalized by Weng (18) to any anisotropic composite containing multiphase, anisotropic inclusions. We now follow this line of inquiry to study specifically the influence of aspect ratio of inclusions on the five independent elastic constants of a transversely isotropic composite. Covering the whole range of variation of aspect ratio from zero to infinity, the results will be applicable to disc-shaped, spherical, or fiber-like reinforcements.

2. THE BASIC THEORY

The composite model is shown in *Fig. 1a*, where the unidirectionally aligned spheroidal inclusions are embedded in the infinite, elastic matrix. The elastic moduli tensor of the matrix is denoted by $C^0_{ijk\ell}$, and that of the inclusions, which are aligned in the x_1-direction, is given by $C^1_{ijk\ell}$. We now prescribe a surface traction on the boundary of the composite to give a uniform stress $\bar{\sigma}_{ij}$. To determine the stress and strain state of the inclusions and the average values of the matrix, we introduce an identically shaped matrix, as shown in *Fig. 1b*, as a comparison material, subjecting to the same boundary stress. If we denote the still unknown elastic moduli tensor of the composite by $C_{ijk\ell}$, the strain of the composite $\bar{\epsilon}_{ij}$ and of the comparison material ϵ^0_{ij} will be related to the applied stress $\bar{\sigma}_{ij}$ by

$$\bar{\sigma}_{ij} = C_{ijk\ell}\bar{\epsilon}_{k\ell}, \tag{1}$$

$$\bar{\sigma}_{ij} = C^0_{ijk\ell}\epsilon^0_{k\ell}, \tag{2}$$

where the usual Einstein summation convention for a repeated index from 1 to 3 is implied. Apparently ϵ^0_{ij} represents the uniform strain state in the matrix of the composite (*Fig. 1a*) when the inclusions are absent.

In general, the average strain in the matrix is not equal to $\epsilon^0_{k\ell}$; a certain average perturbed strain $\tilde{\epsilon}_{k\ell}$ from $\epsilon^0_{k\ell}$ has been introduced due to the presence of inclusions. This perturbed strain corresponds to an average perturbed stress, denoted by $\tilde{\sigma}_{ij}$, in the matrix; through the elastic constants $C^0_{ijk\ell}$

$$\tilde{\sigma}_{ij} = C^0_{ijk\ell}\tilde{\epsilon}_{k\ell} \tag{3}$$

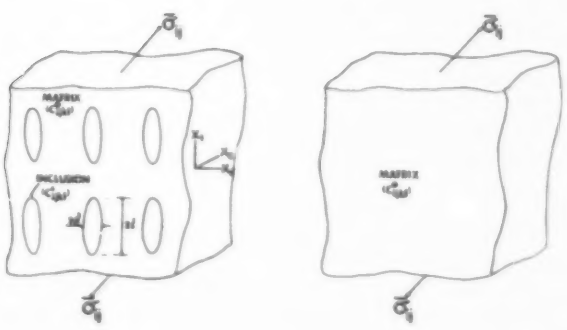

Fig. 1. A composite reinforced with unidirectionally aligned spheroidal inclusions

Thus, under a given $\bar{\sigma}_{ij}$, the average stress in the matrix is now given by $\bar{\sigma}_{ij} + \tilde{\sigma}_{ij}$ and its average strain is $\epsilon^0_{ij} + \tilde{\epsilon}_{ij}$. These quantities are, of course, related to each other by

$$\bar{\sigma}_{ij} + \tilde{\sigma}_{ij} = C^0_{ijk\ell}(\epsilon^0_{k\ell} + \tilde{\epsilon}_{k\ell}). \tag{4}$$

This concept was originally introduced by Mori and Tanaka (15).

To find the average stress and strain in the inclusions, we now apply Eshelby's solution of an ellipsoidal inclusion (14). First of all, let us denote the perturbed stress component in the inclusion from the average stress $\bar{\sigma}_{ij} + \tilde{\sigma}_{ij}$ in the matrix by σ^{pt}_{ij}, and the corresponding perturbed strain by ϵ^{pt}_{ij}. We further denote the "equivalent transformation strain" of the inclusions by ϵ^*_{ij}. According to Eshelby's equivalent principle the stress in the inclusion may be written as

$$\begin{aligned}\bar{\sigma}_{ij} + \tilde{\sigma}_{ij} + \sigma^{pt}_{ij} &= C^1_{ijk\ell}(\epsilon^0_{k\ell} + \tilde{\epsilon}_{k\ell} + \epsilon^{pt}_{k\ell}) \\ &= C^0_{ijk\ell}(\epsilon^0_{k\ell} + \tilde{\epsilon}_{k\ell} + \epsilon^{pt}_{k\ell} - \epsilon^*_{k\ell}),\end{aligned} \tag{5}$$

in terms of its own moduli $C^1_{ijk\ell}$ and of the moduli of the matrix $C^0_{ijk\ell}$, respectively. Eshelby's solution readily renders the relation

$$\epsilon^{pt}_{k\ell} = S_{k\ell mn}\epsilon^*_{mn}, \tag{6}$$

where $S_{ijk\ell}$ is Eshelby's transformation tensor; its components depend on the shape (or aspect ratio in the present case) of the inclusions and the elastic moduli of the matrix.

Since the average of stresses over the matrix and inclusions should give rise to $\bar{\sigma}_{ij}$, one has

$$\tilde{\sigma}_{ij} + c\,\sigma^{pt}_{ij} = 0, \tag{7}$$

where c is the volume fraction of the inclusions. From *Eqs 4* and *5*, we write

$$\sigma^{pt}_{ij} = C^0_{ijk\ell}(\epsilon^{pt}_{k\ell} - \epsilon^*_{k\ell}). \tag{8}$$

Substituting *Eqs 3* and *8* into *Eq 7*, one obtains the average perturbed strain in the matrix

$$\tilde{\epsilon}_{k\ell} = -c(\epsilon^{pt}_{k\ell} - \epsilon^*_{k\ell}), \tag{9}$$

for arbitrary $C^0_{ijk\ell}$.

On the other hand, the strain of the composite $\bar{\epsilon}_{k\ell}$ in *Eq 1* is given by the volume average of strains over its matrix and inclusions. Namely,

$$\bar{\epsilon}_{k\ell} = \epsilon^0_{k\ell} + \tilde{\epsilon}_{k\ell} + c\,\epsilon^{pt}_{k\ell}. \tag{10}$$

Further from *Eq 9* it simply reduces to

$$\bar{\epsilon}_{k\ell} = \epsilon^0_{k\ell} + c\,\epsilon^*_{k\ell}. \tag{11}$$

The equivalent transformation strain $\epsilon^*_{k\ell}$ will have to be found from the second part of *Eq 5*. With *Eqs 6* and *9*, it may be rearranged to

$$\begin{aligned}(C^1_{ijk\ell} - C^0_{ijk\ell})[\epsilon^0_{k\ell} + (1-c)S_{k\ell mn}\epsilon^*_{mn} + c\,\epsilon^*_{k\ell}] \\ + C^0_{ijk\ell}\epsilon^*_{k\ell} = 0,\end{aligned} \tag{12}$$

which allows one to calculate $\epsilon^*_{k\ell}$ in terms of $\epsilon^0_{k\ell}$.

Then, the effective elastic moduli of the composite $C_{ijk\ell}$ may be calculated from *Eqs 1*, *2*, and *11*. Alternately, one may use the principle of equivalent

elastic energy as developed in (16) and (17) to calculate the effective property. It has been proven in the general theory of Weng (18) that these two approaches are entirely equivalent.

3. CALCULATION OF ϵ_{ij}^*

For spheroidal inclusions aligned along the x_1-direction, the nonvanishing components of $S_{ijk\ell}$ are given in the **Appendix**. It is the nature of this tensor that the normal and shear components are always uncoupled. Further, since both $C_{ijk\ell}^0$ and $C_{ijk\ell}^1$ are taken to be isotropic, they may be written as

$$C_{ijk\ell}^0 = \lambda_0\delta_{ij}\delta_{k\ell} + \mu_0(\delta_{ik}\delta_{j\ell} + \delta_{i\ell}\delta_{jk}), \quad (13)$$

$$C_{ijk\ell}^1 = \lambda_1\delta_{ij}\delta_{k\ell} + \mu_1(\delta_{ik}\delta_{j\ell} + \delta_{i\ell}\delta_{jk}), \quad (14)$$

where λ_0, μ_0 and λ_1, μ_1 are the Lamé constants of the matrix and inclusions, respectively, and δ_{ij} is the Kronecker delta, having the property $\delta_{ij} = 1$ when $i = j$ and $\delta_{ij} = 0$ when $i \neq j$.

To find the ϵ_{ij}^* components, let us first set $ij = 11$, 22, and 33 in *Eq 12*. These lead, respectively, to

$$D_1\epsilon_{11}^0 + \epsilon_{22}^0 + \epsilon_{33}^0 + B_1\epsilon_{11}^* + B_2(\epsilon_{22}^* + \epsilon_{33}^*) = 0, \quad (15)$$

$$\epsilon_{11}^0 + D_1\epsilon_{22}^0 + \epsilon_{33}^0 + B_3\epsilon_{11}^* + B_4\epsilon_{22}^* + B_5\epsilon_{33}^* = 0, \quad (16)$$

$$\epsilon_{11}^0 + \epsilon_{22}^0 + D_1\epsilon_{33}^0 + B_3\epsilon_{11}^* + B_5\epsilon_{22}^* + B_4\epsilon_{33}^* = 0, \quad (17)$$

where

$$B_1 = c\,D_1 + D_2 + (1 - c)(D_1S_{1111} + 2\,S_{2211}),$$

$$B_2 = c + D_3 + (1 - c)(D_1S_{1122} + S_{2222} + S_{2233}),$$

$$B_3 = c + D_3 + (1 - c)[S_{1111} + (1 + D_1)S_{2211}],$$

$$B_4 = c\,D_1 + D_2 + (1 - c)(S_{1122} + D_1S_{2222} + S_{2233}),$$

$$B_5 = c + D_3 + (1 - c)\,(S_{1122} + S_{2222} + D_1S_{2233}),$$

and

$$D_1 = 1 + 2(\mu_1 - \mu_0)/(\lambda_1 - \lambda_0),$$

$$D_2 = (\lambda_0 + 2\mu_0)/(\lambda_1 - \lambda_0),$$

$$D_3 = \lambda_0/(\lambda_1 - \lambda_0).$$

Solving *Eqs 15–17* simultaneously, we obtain

$$\epsilon_{11}^* = [A_1\epsilon_{11}^0 - A_2(\epsilon_{22}^0 + \epsilon_{33}^0)]/A, \quad (18)$$

$$\epsilon_{22}^* = [2A_3\epsilon_{11}^0 + (A_4 + A_5A)\epsilon_{22}^0 + (A_4 - A_5A)\epsilon_{33}^0]/2A, \quad (19)$$

$$\epsilon_{33}^* = [2A_3\epsilon_{11}^0 + (A_4 - A_5A)\epsilon_{22}^0 + (A_4 + A_5A)\epsilon_{33}^0]/2A, \quad (20)$$

where

$$A_1 = D_1(B_4 + B_5) - 2B_2,$$

$$A_2 = (1 + D_1)B_2 - (B_4 + B_5),$$

$$A_3 = B_1 - D_1B_3,$$

$$A_4 = (1 + D_1)B_1 - 2B_3,$$

$$A_5 = (1 - D_1)/(B_4 - B_5),$$

and $A = 2B_2B_3 - B_1(B_4 + B_5)$.

Similarly, setting $ij = 12$, and 23 in *Eq 12* one finds, respectively,

$$\epsilon_{12}^* = -\frac{\epsilon_{12}^0}{\frac{\mu_0}{\mu_1 - \mu_0} + c + 2(1 - c)S_{1212}}, \quad (21)$$

$$\epsilon_{23}^* = -\frac{\epsilon_{23}^0}{\frac{\mu_0}{\mu_1 - \mu_0} + c + 2(1 - c)S_{2323}}. \quad (22)$$

The value of ϵ_{13}^* is related to ϵ_{13}^0 and S_{1313} in exactly the same fashion.

4. THE FIVE EFFECTIVE ELASTIC MODULI

With the inclusions aligned along the x_1-direction, there are five independent elastic constants associated with the transversely isotropic composite. These are the longitudinal Young's modulus E_{11}, the transverse Young's modulus E_{22}, the in-plane shear modulus μ_{12}, the out-plane shear modulus μ_{23}, and the plane-strain bulk modulus K_{23}. These constants may be determined from the foregoing theory under appropriate boundary conditions.

1) Longitudinal Young's Modulus E_{11}

To determine E_{11}, let us apply $\bar{\sigma}_{11}$ and set other $\bar{\sigma}_{ij} = 0$. The 11-component of *Eq 1* becomes

$$\bar{\sigma}_{11} = E_{11}\bar{\epsilon}_{11}. \quad (23)$$

The strain components in the comparison material, from *Eq 2*, are

$$\epsilon_{11}^0 = \bar{\sigma}_{11}/E_0, \qquad \epsilon_{22}^0 = \epsilon_{33}^0 = -\nu_0\bar{\sigma}_{11}/E_0, \quad (24)$$

where ν_0 and E_0 are the Poisson's ratio and Young's modulus of the matrix, respectively.

Then from *Eqs 23, 11, 18,* and *24* we have

$$\frac{E_{11}}{E_0} = \frac{1}{1 + c(A_1 + 2\nu_0A_2)/A}. \quad (25)$$

2) Transverse Young's modulus E_{22}

Similarly, we apply $\bar{\sigma}_{22}$ and let other $\bar{\sigma}_{ij} = 0$. Then the corresponding equations are

$$\bar{\sigma}_{22} = E_{22}\bar{\epsilon}_{22}, \quad (26)$$

$$\epsilon_{22}^0 = \tilde{\sigma}_{22}/E_0, \qquad \epsilon_{33}^0 = \epsilon_{11}^0 = -\nu_0\tilde{\sigma}_{22}/E_0. \quad (27)$$

Using *Eqs 26, 11, 19,* and *27* we find

$$\frac{E_{22}}{E_0} = \frac{1}{1 + c[-2\nu_0 A_3 + (1 - \nu_0)A_4 + (1 + \nu_0)A_5 A]/2A}. \quad (28)$$

3) In-Plane Shear Modulus μ_{12}

We apply a pure shear stress $\tilde{\sigma}_{12}$ and $\tilde{\sigma}_{21}$. Then

$$\tilde{\sigma}_{12} = 2\mu_{12}\tilde{\epsilon}_{12}, \quad (29)$$

$$\epsilon_{12}^0 = \epsilon_{21}^0 = \tilde{\sigma}_{12}/2\mu_0. \quad (30)$$

From *Eqs 29, 11, 21,* and *30,* one obtains

$$\frac{\mu_{12}}{\mu_0} = 1 + \frac{c}{\frac{\mu_0}{\mu_1 - \mu_0} + 2(1 - c)S_{1212}}. \quad (31)$$

4) Out-Plane Shear Modulus μ_{23}

In exactly the same way, we apply a pure shear $\tilde{\sigma}_{23}$ and $\tilde{\sigma}_{32}$. The result is parallel to *Eq 31:*

$$\frac{\mu_{23}}{\mu_0} = 1 + \frac{c}{\frac{\mu_0}{\mu_1 - \mu_0} + 2(1 - c)S_{2323}}. \quad (32)$$

5) Plane-Strain Bulk Modulus K_{23}

In this case we apply $\tilde{\sigma}_{22} = \tilde{\sigma}_{33} = \tilde{\sigma}$. We further write $\tilde{\epsilon}_{22} = \tilde{\epsilon}_{33} = \tilde{\epsilon}$. Then

$$\tilde{\sigma} = 2K_{23}\tilde{\epsilon}. \quad (33)$$

In order to maintain the plane strain condition for the composite a stress $\tilde{\sigma}_{11}$ is needed to prevent $\tilde{\epsilon}_{11}$. Since $\tilde{\epsilon}_{11} = (\tilde{\sigma}_{11} - 2\nu_{12}\tilde{\sigma})/E_{11}$, we have

$$\tilde{\sigma}_{11} = 2\nu_{12}\tilde{\sigma}, \quad (34)$$

where ν_{12} is the major Poisson's ratio of the composite (yet to be determined). The corresponding strains in the comparison material are

$$\epsilon_{22}^0 = \epsilon_{33}^0 = \tilde{\sigma}[1 - \nu_0(1+2\nu_{12})]/E_0,$$
$$\epsilon_{11}^0 = 2\tilde{\sigma}(\nu_{12} - \nu_0)/E_0. \quad (35)$$

From *Eqs 33, 11, 19,* and *35,* we arrive at

$$\frac{K_{23}}{\bar{K}_0} = \frac{(1 + \nu_0)(1 - 2\nu_0)}{1 - \nu_0(1 + 2\nu_{12}) + c[2(\nu_{12} - \nu_0)A_3 + [1 - \nu_0(1 + 2\nu_{12})]A_4]/A}, \quad (36)$$

where $\bar{K}_0$ is the plane-strain bulk modulus of the matrix, given by $\bar{K}_0 = \lambda_0 + \mu_0$. The major Poisson's ratio ν_{12} is not an independent modulus; it is related to the others by

$$\nu_{12}^2 = \frac{E_{11}}{E_{22}} - \frac{E_{11}}{4}\left(\frac{1}{\mu_{23}} + \frac{1}{K_{23}}\right). \quad (37)$$

In other words, after finding E_{11}, E_{22}, and μ_{23} from the foregoing equations ν_{12} is directly related to K_{23}. *Equation 36* therefore is an implicit equation and can be solved by a simple iterative procedure. Once K_{23} is solved, ν_{12}, if needed, may be calculated from *Eq. 37.*

It is obvious from *Eqs. 25, 28, 31, 32,* and *36* that when $c = 0$ the effective modulus of the composite is identical to the corresponding value of the matrix. We have also checked that when $c = 1$ each quantity reduces to that of the inclusions.

5. NUMERICAL RESULTS AND DISCUSSIONS

To make the effect of aspect ratio α and volume fraction c of the inclusions more apparent, we now plot the variation of these five independent elastic constants as a function of α and c. The material properties used in the computation are those of glass/epoxy, such that

$$E_0 = 2.76 \text{ GPa}, \qquad \nu_0 = 0.35,$$
$$E_1 = 72.4 \text{ GPa}, \qquad \nu_1 = 0.20.$$

The results are shown in *Figs. 2-6,* respectively.

First of all, it is observed that, among these five constants, E_{11} is especially sensitive to the variation of α when $\alpha > 1$, and that within this range the other four moduli remain relatively insensitive to α. On the contrary, when the inclusions are oblate spheroids, or $\alpha < 1$, the reverse effect becomes evident. Generally speaking, both E_{11} and μ_{12} in-

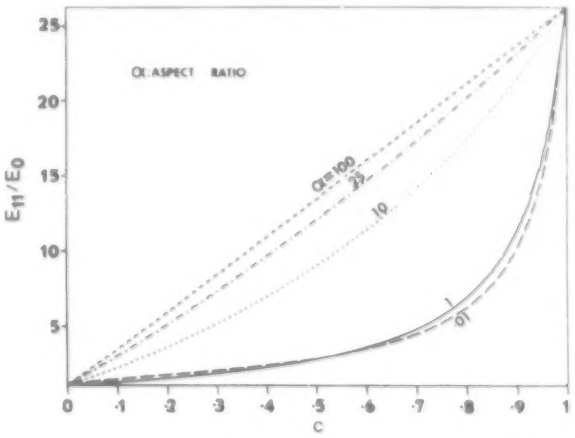

Fig. 2 The variation of longitudinal Young's modulus E_{11}

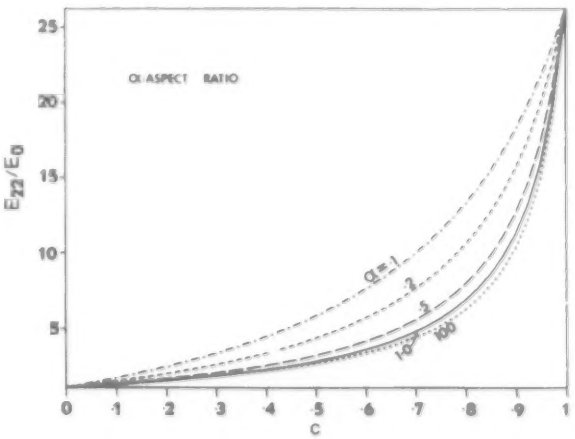

Fig. 3 The variation of transverse Young's modulus E_{22}

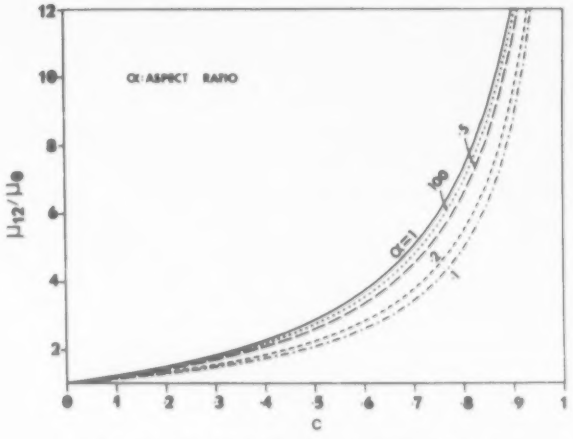

Fig. 4. The variation of in-plane shear modulus μ_{12}

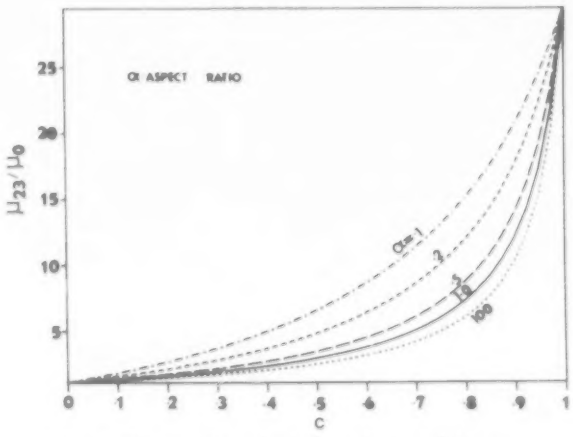

Fig. 5. The variation of out-plane shear modulus μ_{23}

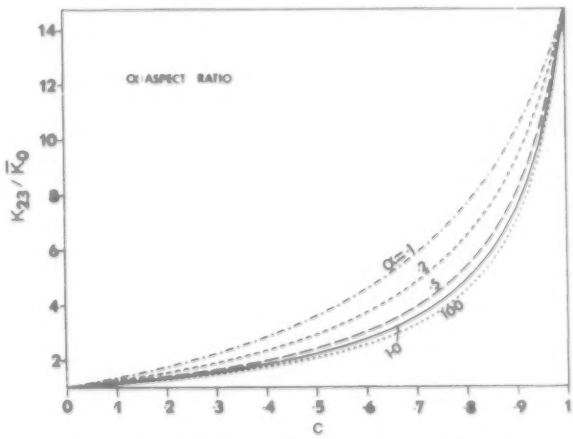

Fig. 6. The variation of plane-strain bulk modulus K_{23}

crease with increasing aspect ratio, whereas the other three decrease with it. An unexpected behavior for μ_{12}, as shown in *Fig. 4*, was noted at $\alpha = 100$; at this aspect ratio the value of μ_{12} is seen to be less than at $\alpha = 1$. We have made several calculations to explore this range of sensitivity further, and found that the value of μ_{12} increases initially with increasing α and then begins to decrease. The variation, however, is usually small. It is further noted that, for practical purposes, we can consider fibers with aspect ratio of about 100 as being infinitely long.

The variation of major Poisson's ratio ν_{12} is also given. As shown in *Fig. 7*, the value of ν_{12}, at a given concentration, tends to increase at low α and then decreases; its maximum was found to occur around $\alpha = 2 \sim 3$.

Finally, to place the present theory in proper perspective, we also compare it to the self-consistent theory (19) and the Halpin-Tsai equation (3). Using the same parameters suggested in (19) ($E_1/E_o = 20$, $\nu_o = 0.35$ and $\nu_1 = 0.3$) the results of the longitudinal Young's modulus at three different aspect ratios 100, 10, and 2 are given in *Fig. 8*. As expected the self-consistent theory gives a higher estimate while the present one generally lies between the two. At very low aspect ratio, however,

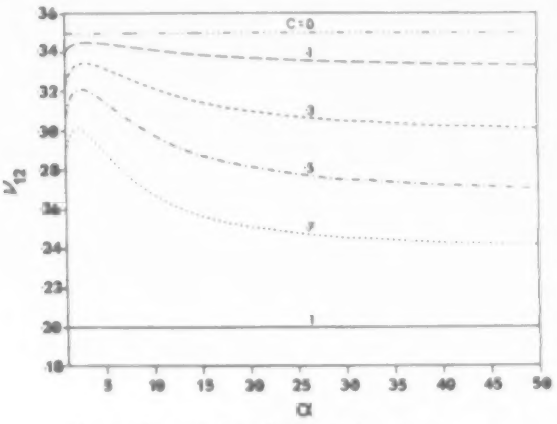

Fig. 7. The variation of major Poisson's ratio ν_{12}

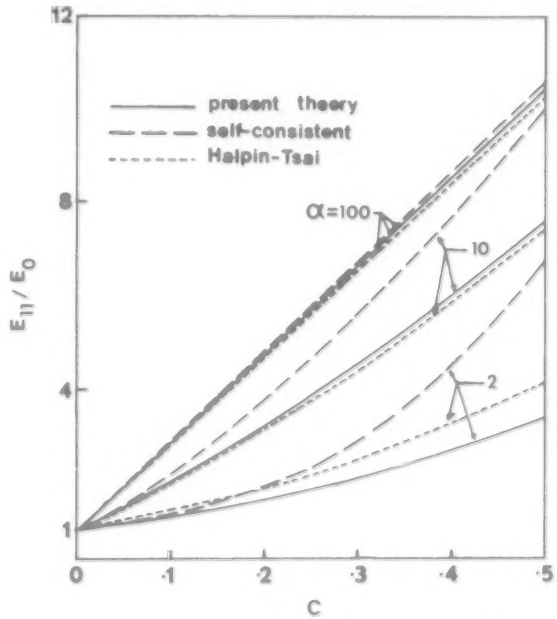

Fig. 8. Comparison of the self-consistent theory and Halpin-Tsai equation

the present one gives the most conservative estimate. To see the validity of the theory it was also applied to predict the isotropic Young's modulus of tungsten-carbide/cobalt (E_o = 206.8 GPa, ν_o = 0.3, E_1 = 703 GPa, ν_1 = 0.22) and glass/polyester (E_o = 1.72 GPa, ν_o = 0.45, E_1 = 70.3 GPa, ν_1 = 0.21). The theoretical curves, together with the experimental data of Nishimatsu and Gurland (20) and of Richard (21), respectively, are also depicted in *Fig.* 9; the agreement is seen to be very good indeed.

ACKNOWLEDGMENT

This work was supported by the U.S. Department of Energy under Contract AS 05-81ER10976.

APPENDIX

Components of Eshelby's S_{ijkl} Tensor

For a fiber-like spheroidal inclusion, the components of Eshelby's tensor S_{ijkl} are given by

$$S_{1111} = \frac{1}{2(1-\nu_0)}\left\{1 - 2\nu_0 + \frac{3\alpha^2-1}{\alpha^2-1} - \left[1 - 2\nu_0 + \frac{3\alpha^2}{\alpha^2-1}\right]g\right\}$$

$$S_{2222} = S_{3333} = \frac{3}{8(1-\nu_0)}\frac{\alpha^2}{\alpha^2-1} + \frac{1}{4(1-\nu_0)}\left[1 - 2\nu_0 - \frac{9}{4(\alpha^2-1)}\right]g$$

$$S_{2233} = S_{3322} = \frac{1}{4(1-\nu_0)}\left\{\frac{\alpha^2}{2(\alpha^2-1)} - \left[1 - 2\nu_0 + \frac{3}{4(\alpha^2-1)}\right]g\right\}$$

$$S_{2211} = S_{3311} = -\frac{1}{2(1-\nu_0)}\frac{\alpha^2}{\alpha^2-1} + \frac{1}{4(1-\nu_0)}\left\{\frac{3\alpha^2}{\alpha^2-1} - (1-2\nu_0)\right\}g$$

$$S_{1122} = S_{1133} = -\frac{1}{2(1-\nu_0)}\left[1 - 2\nu_0 + \frac{1}{\alpha^2-1}\right] + \frac{1}{2(1-\nu_0)}\left[1 - 2\nu_0 + \frac{3}{2(\alpha^2-1)}\right]g$$

$$S_{2323} = S_{3232} = \frac{1}{4(1-\nu_0)}\left\{\frac{\alpha^2}{2(\alpha^2-1)} + \left[1 - 2\nu_0 - \frac{3}{4(\alpha^2-1)}\right]g\right\}$$

$$S_{1212} = S_{1313} = \frac{1}{4(1-\nu_0)}\left\{1 - 2\nu_0 - \frac{\alpha^2+1}{\alpha^2-1} - \frac{1}{2}\left[1 - 2\nu_0 - \frac{3(\alpha^2+1)}{\alpha^2-1}\right]g\right\}$$

where ν_0 is Poisson's ratio of the matrix, α is the aspect ratio of the inclusion ($=\ell/d$), and g is given by

$$g = \frac{\alpha}{(\alpha^2-1)^{3/2}}\{\alpha(\alpha^2-1)^{1/2} - \cosh^{-1}\alpha\}.$$

For a spherical inclusion,

$$S_{1111} = S_{2222} = S_{3333} = \frac{7-5\nu_0}{15(1-\nu_0)}$$

$$S_{1122} = S_{2233} = S_{3311} = \frac{5\nu_0-1}{15(1-\nu_0)}$$

$$S_{1212} = S_{2323} = S_{3131} = \frac{4-5\nu_0}{15(1-\nu_0)}.$$

For a disc-shaped spheroidal inclusion, S_{ijkl} is given by expressions similar to the case of a fiber-like inclusion, with g replaced by g', where

$$g' = \frac{\alpha}{(1-\alpha^2)^{3/2}}\{\cos^{-1}\alpha - \alpha(1-\alpha^2)^{1/2}\}$$

and α, the aspect ratio of the inclusion, is given as t/a, where a and t are the major and minor axes of an ellipsoidal penny-shaped inclusion with its minor axis directed along x_1.

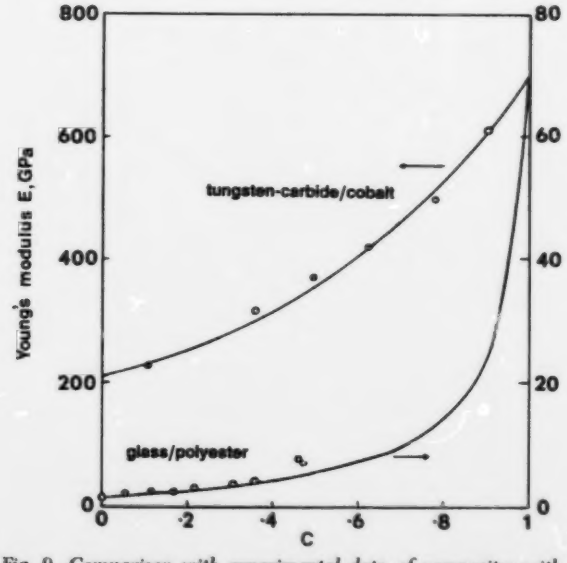

Fig. 9. Comparison with experimental data of composites with spherical inclusions.

REFERENCES

1. J. K. Lees, *Polym. Eng. Sci.*, **8**, 186 (1968).
2. H. D. Conway and C. I. Chang, *Fibre Sci. Technol.*, **5**, 249 (1971).
3. J. C. Halpin and S. W. Tsai, *AFML TR 67-423* (1967).
4. H. Fukuda and K. Kawata, *Fibre Sci. Technol.*, **7**, 207 (1974).
5. H. L. Cox, *Brit. J. Appl. Phys.*, **3**, 72 (1952).
6. J. Cook, *Brit. J. Appl. Phys. (J. Phys. D), Ser. 2*, **1**, 799 (1968).
7. Z. Hashin and B. W. Rosen, *J. Appl. Mech.*, **31**, 223 (1964).
8. R. Hill, *J. Mech. Phys. Solids*, **12**, 199 (1964).
9. Z. Hashin, *J. Mech. Phys. Solids*, **13**, 119 (1965).
10. R. Hill, *J. Mech. Phys. Solids*, **13**, 189 (1965).
11. N. Laws and R. McLaughlin, *J. Mech. Phys. Solids*, **27**, 1 (1979).
12. T.-W. Chou, S. Nomura, and M. Taya, *J. Compos. Mater.*, **14**, 178 (1980).

13. W. B. Russel, *J. Appl. Math. Phys.*, **24**, 581 (1973).
14. J. D. Eshelby, *Proc. Roy. Soc. Lond.*, **A241**, 376 (1957).
15. T. Mori and K. Tanaka, *Acta Metall.*, **21**, 571 (1973).
16. M. Taya and T.-W. Chou, *Int. J. Solids Structr.*, **17**, 553 (1981).
17. M. Taya and T. Mura, *J. Appl. Mech.*, **48**, 361 (1981).
18. G. J. Weng, *Int. J. Eng. Sci.*, volume 22, in press (1984).
19. T. W. Chou, S. Nomura, and M. Taya, in "Modern Developments in Composite Materials and Structures," J. R. Vinson, Ed., ASME, 149 (1979).
20. C. Nishimatsu and J. Gurland, *Trans. ASM*, **52**, 469 (1960).
21. T. G. Richard, *J. Compos. Mater.*, **9**, 108 (1975).

XIII. DISCUSSION G. J. WENG

Q. Samak: For the ranges of length of short fibers, which ones are of industrial interest? Is there any reason to think that this method is superior to what we can get from the current methods? Which method are you proposing to use for averaging the partial alignment of filler particles during an industrial process? How is this going to be different from, let us say, Halpin-Tsai or other currently used calculation schemes?

G. J. Weng: To my knowledge, this method is the first quantitative one developed without any adjustable parameters or complicated iterations. The equations are simple and exact and their predictions cover the whole range of concentration. This does not mean that we should preempt the previously developed theories. As for the comparison with the Halpin-Tsai equation, we note that it is an empirical one. The differences at various aspect ratios are shown in *Fig. 8*.

As far as the averaging is concerned, Mr. Tandon just finished his thesis in which he also calculated the influence of the aspect ratio on the Young's modulus of the randomly oriented chopped fiber composites. The averaging technique he used was the standard one, developed in 1972 by Christensen and Waals. As long as we can accurately determine the properties of unidirectionally aligned composites, the calculation of partially aligned or randomly oriented composites is a straight-forward matter.

L. A. Utracki: I am very grateful to you for presenting this excellent paper during our symposium. As you said, this is the first exact theory of the elastic properties of composites containing anisometric particles. Knowing Lanné's constants for filler and matrix bodies, one can explicitly calculate all the elastic parameters for any filler concentration. Not only that, if these constants are available, one can treat them as empirical constants in Young's moduli and from the value of these equation parameters, one can compute the remaining elastic parameters. This is the advantage of a good, exact theoretical treatment. Congratulations.

I would like to raise three points. First, it seems that you are treating the composite as a mixture of two bodies; inclusions and matrix are considered as homogeneous non-interacting entities. The effect of the interphase is not taken into account. The second point: from the graph of E_{11} *vs.* c, one finds that E_{11} for flakes is lower than that for spherical inclusions. Certainly, you are not suggesting that Young's modulus for a composite filled with glass flakes (or mica) will be less than that for a system containing glass spheres. Finally, the third: did you try to compare some elastic parameters with others, i.e., bulk modulus from Young's?

G. J. Weng: Thank you. Regarding your first point, this is a good question. No, we did not consider the effect of the interphase. The reason is that it is very difficult to determine the interface stress. The stress at the interface is not uniform; this presents a formidable mathematical difficulty. However, if the interphase is considered to be infinitesimally thin, the problem is to some extent tractable, but still difficult. This is what we are considering now, assuming the interphase to have different elastic properties but zero thickness. But we still do not have any results yet.

Regarding the second problem, I might have given you the wrong impression that mica is not as effective as glass spheres. This was not my intention. My conclusion was that if the mica flakes are aligned perpendicular to the tensile stress then E_{11} for mica composite is lower than that for a system filled with spheres. However, the Young's modulus for randomly oriented mica composite will be not only higher than that of the one containing the spheres but also higher than one of materials reinforced with continuous fibers. This is the remarkable part of the mica reinforcing ability.

I hope that we will be able to find more experimental data to evaluate our equations as you suggested. Existing data on the effect of aspect ratio appear to be rather incomplete. I hope that perhaps someone in the audience will do a systematic experiment (which by itself will be an important contribution to the literature) and allow us to check our theory. However, for spherical inclusions the agreement with experiments, as shown in *Fig. 9*, is very good.

L. A. Utracki: In the absence of these data, you could consider the continuous fiber composites as a limiting case. There is plenty of information regarding all the elastic parameters for these systems. So, at least you could check the correlations at the limit.

G. J. Weng: This has been done and the results have been found to be satisfactory.

Damping of Composite Materials

S. V. HOA *and* P. OUELLETTE

Concordia University
Montreal, Quebec, Canada H3G 1M8

A rule of mixture for the prediction of the loss factor of hybrid laminates of graphite/epoxy and kevlar/epoxy composite materials is developed. The theoretical values agree reasonably with the experimental values for ten samples. An optimal laminate having the modulus of aluminium and twice the loss factor of graphite/epoxy laminates is achieved.

INTRODUCTION

Due to their light weight and high strength, fiber reinforced composite materials have been used more and more for making aircraft and aerospace structures. Since these structures are subjected to vibrations, it is desirable to reduce the vibration amplitudes to prolong the component service life. One way to do this is to increase the damping capacity of the material.

In the past two decades, many researchers have examined the damping characteristics of fiber reinforced composite materials. Schultz and Tsai (1) examined the dynamic moduli and damping ratios of fiber reinforced composites at different frequencies. Adams and Bacon (2, 3) investigated the effect of fiber orientation and laminate geometry on the moduli and damping capacity of composites in flexure and torsion. McLean and Read (4) showed that discontinuous fiber composites have larger damping capacity than continuous fiber composites. Gibson and Plunkett (5) performed analytical and experimental study on the internal damping and elastic stiffness of E glass fiber reinforced epoxy beams under flexural vibration. Nelson and Hancock (6) indicated that interfacial slipping can increase the damping capacity of composites. Dupont company (7) also carried out a study on the damping capacity of graphite/epoxy, Kevlar epoxy, and hybrids made of these materials and claimed that Kevlar fiber composites give better damping capacity than graphite or glass fiber composites. Gibson, Chaturvedi, and Sun (8) recently studied the effects of fiber aspect ratio, fiber spacing, and the viscoelastic properties of constituent materials on the damping and stiffness of aligned discontinous fiber reinforced polyester matrix composites. Recently, Morrison (9) proposed a method to compute the material damping of an arbitrary laminate based on the elastic lamina properties.

In the lamination of many composite layers to make a laminate, it is possible to combine laminae of different materials to make a hybrid laminate such as was done in *Ref. 7*. In order to tailor the properties of a hybrid laminate to design specifications, it is necessary to develop and prove predictive rules for property calculation. This paper proposes and proves rule of mixture for the calculation of the loss factor of hybrid laminates.

ANALYSIS

Consider the cross section of a beam made up of many layers of graphite/epoxy and Kevlar/epoxy laminae as shown in *Fig. 1*. Let U be the strain energy in bending of the beam; the energy dissipated per cycle D of vibration is

$$D_h = 2\pi\eta_h U_h \tag{1}$$

where the subscript h = hybrid

η = loss factor

The energies dissipated by the sum of the Kevlar layers and the sum of the graphite layers are respectively

$$D_K = 2\pi\eta_k U_k \tag{2}$$

$$D_g = 2\pi\eta_g U_g \tag{3}$$

where the subscripts k and g stand for Kevlar and graphite respectively.

Since
$$D_h = D_k + D_g \tag{4}$$

$$2\pi\eta_h U_h = 2\pi\eta_k U_k + 2\pi\eta_g U_g \tag{5}$$

Since, in general, the strain energy of a beam in bending is

$$U = \frac{1}{2} EI \int_0^l y''^2 dx \tag{6}$$

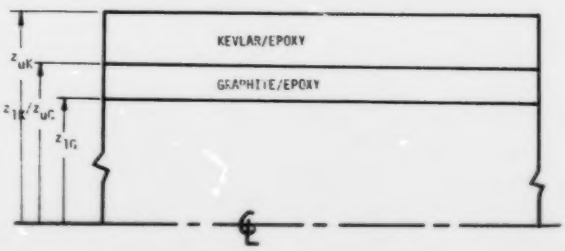

Fig. 1. Hybrid laminate arrangement.

where E = Young's modulus
I = Second moment of area
y = lateral deflection
x = longitudinal position along the beam

Substitution of *Eq 6* into *Eq 5* yields

$$\eta_h = \frac{\sum \eta_k E_k I_k}{E_h I_h} + \frac{\sum \eta_g E_g I_g}{E_h I_h} \tag{7}$$

Equation 7 is the rule of mixture giving the loss factor of the hybrid beam in terms of the loss factor of the individual Kevlar and graphite layers. The summation sign applies to all the Kevlar and graphite layers respectively.

The flexural modulus of the hybrid beam can be obtained by

$$E_h = \frac{12}{t^3 d_{11}} \tag{8}$$

where
t = thickness of the hybrid beam
d_{11} = component of the compliance matrix $[d]$ obtained from the laminae properties and arrangements as shown in the book by Tsai and Hahn (10).

Let b be the width of the beam, the various moments of area are

$$I_h = \frac{bt^3}{12} \tag{9}$$

$$I_k = \sum_k 2b \int_{z_l}^{z_u} z^2 dz = \sum_k \frac{2b}{3} (z_u^3 - z_l^3)_k \tag{10}$$

$$I_g = \sum_g 2b \int_{z_l}^{z_u} z^2 dz = \sum_g \frac{2b}{3} (z_u^3 - z_l^3)_g \tag{11}$$

Where z_l and z_u represent the lower and upper coordinates of the layers of either the Kevlar or the graphite layer, as shown in *Fig. 1*.

Substituting *Eqs 8–11* into *Eq 7* yields

$$\eta_h = d_{11} \left[\sum_k \eta_k E_k \frac{2}{3} (z_u^3 - z_l^3)_k + \sum_g \eta_g E_g \frac{2}{3} (z_u^3 - z_l^3)_g \right] \tag{12}$$

Assuming that both the loss factor η and the modulus E do not vary with the z coordinates of the layer, *Eq 12* can be written as

$$\eta_h = \frac{2}{3} d_{11} \left[\eta_k E_k \sum_k (z_u^3 - z_l^3)_k + \eta_g E_g \sum_g (z_u^3 - z_l^3)_g \right] \tag{13}$$

Equation 13 gives the rule of mixture prediction for the damping coefficient of a hybrid laminate based on the modulus and damping coefficient of the individual layers.

EXPERIMENTS

Since unidirectional graphite/epoxy and Kevlar 49 fabric/epoxy composites are commonly used in making spacecraft structures, these two kinds of composites are tested in this preliminary investigation. The graphite/epoxy was T300/5208 and the Kevlar/epoxy was Kevlar 49 type 281 (plain weave fabric) and Narmco 5208 epoxy. The thickness of the cured graphite/epoxy lamina is taken to be 0.127 mm and that of each layer of the Kevlar/epoxy fabric is taken to be 0.203 mm. Whenever there is discrepancy between the measured total thickness and the anticipated total thickness, the thicknesses of the individual laminae are corrected accordingly for the theoretical model in *Eq 8* and *13*. All laminates were made at the Composite Materials lab at Concordia University.

The properties of the individual graphite/epoxy and Kevlar/epoxy layers are shown in *Table 1*. Most of the elastic properties were obtained from *Ref 11* except E_L which was determined experimentally.

Different combinations of graphite/epoxy and Kevlar/epoxy laminates were tested with. Apart from proving the rule of mixture (*Eq 13*), an optimal laminate having the stiffness of aluminum and twice the damping coefficient of the regular graphite/epoxy laminate was sought. These laminates are shown in *Table 2*. Strain gages were bonded onto

Table 1. Engineering Constants for Kevlar/Epoxy and Graphite/Epoxy Laminae

	Graphite/Epoxy (Unidirectional tape)	Kevlar 49/Epoxy (Fabric)
E_L (GPa)	124 (Experimental)	39.1 (Experimental)
E_T (GPa)	10.3 [11]	39.1 (Experimental)
G_{LT} (GPa)	6.5 [11]	2.1 [11]
ν_{LT}	0.25 [11]	0.10 [11]

Table 2. Specimen Description

Specimen #	Material	Lay Up	Nom. Length (mm)	Width (mm)	Thickness (mm)
3	Kevlar fabric/epoxy	$[(\text{Kev. } 0°\text{–}90°)_8]_T$	200	34.1	1.0
4	Kevlar fabric/epoxy	$[(\text{Kev. } 45°)_8]_T$	200	35.2	1.0
5	Graphite tape/epoxy	$[(\text{Gr. } 0°)_8]_T$	200	35.1	1.1
6	Kev. fabric/Gr. tape	$[(\text{Gr. } 0°)_2/(\text{Kev. } 45°)_2/(\text{Gr. } 0°/_2]_T$	200	34.90	1.16
9	Kev. fabric/Gr. tape	$[(\text{Gr. } 0°)_2/\text{Kev. } 0°\text{–}90°)_2/(\text{Gr. } 0°)_2]_T$	200	35.00	1.10
10	Kev. fabric/Gr. tape	$[(\text{Kev. } 0°\text{–}90°)_2/(\text{Gr. } 0°)_2/(\text{Kev. } 0°\text{–}90°)_2]_T$	200	35.14	1.23
11	Kev. fabric/Gr. tape	$[(\text{Kev. } 0°\text{–}90°)_1/(\text{Gr. } 0°)_1/(\text{Kev. } 0°\text{–}90°)_1/(\text{Gr. } 0°)_1/(\text{Kev. } 0°\text{–}90°)_1]_T$	200	32.90	0.81
12	Kev. fabric/Gr. tape	$[(\text{Kev. } 0°\text{–}90°)_2/(\text{Gr. } 0°)_2/(\text{Kev. } 0°\text{–}90°)_1]_S$	200	35.04	1.73
13	Kev. fabric/Gr. tape	$[(\text{Kev. } 0°\text{–}90°)_2/(\text{Gr. } 0°)_2/(\text{Kev. } 0°\text{–}90°)_1]_S$	200	35.20	2.14

these laminates. The laminates were held in a rigid clamp as shown in *Fig. 2*. A loading mechanism was used to give the end of the cantilever beam a step excitation input as shown in *Fig. 3*. The whole assembly could be placed inside a vacuum chamber as shown in *Fig. 4*.

The cantilever beams were excited both in air and in vacuum. The decrease in amplitude of vibration from the step excitation gave a measure of the damping capacity via the log decrement method. The damping capacities at different starting strains are given in *Table 3*. It can be seen that there is a large difference in the loss factor in air and in vacuum. Also, the initial strain has a larger influence

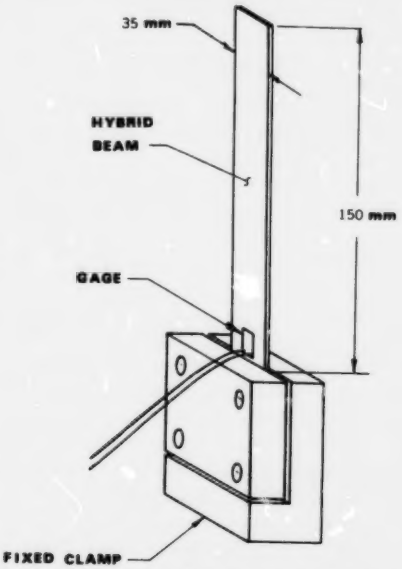

Fig. 2. Specimen clamping arrangement.

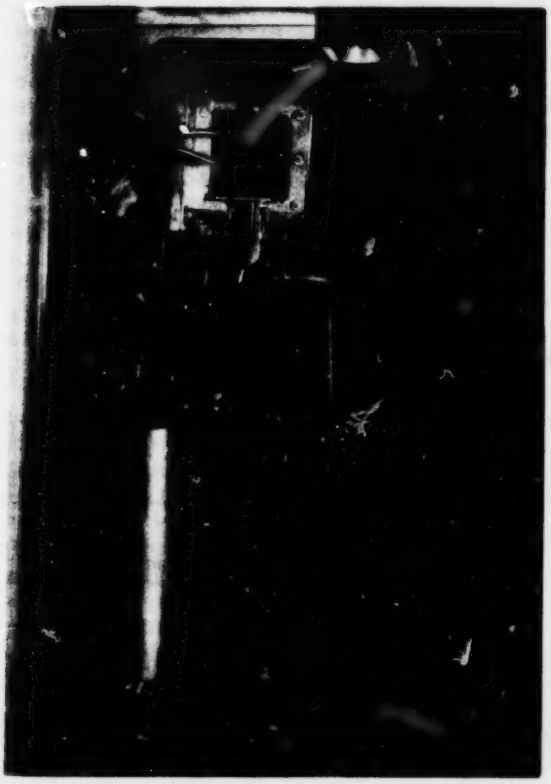

Fig. 3. Step excitation loading device.

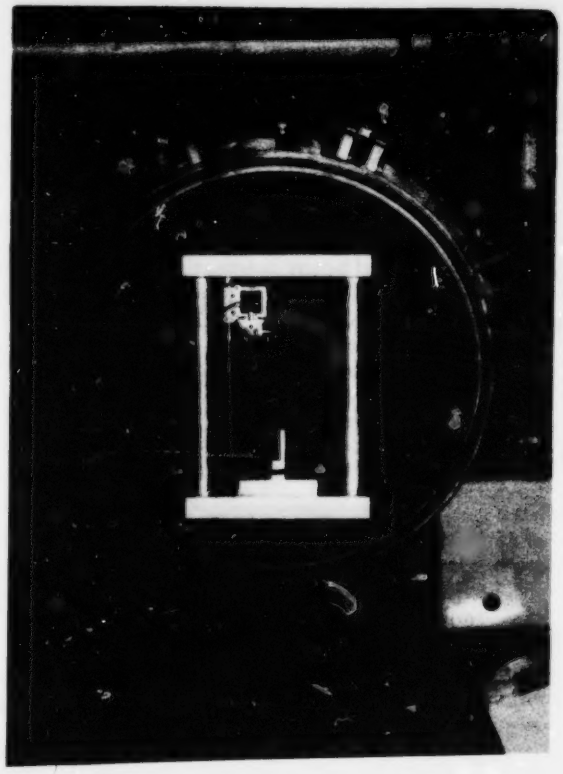

Fig. 4. Load assembly and vacuum chamber.

Table 3. Experimental Damping Results

Specimen #	Initial Strain ($\mu\epsilon$)	Log Decrement d	Loss Factor $\eta = d/\pi$	m^* (cycles)	Fr_1 (Hz)**
3A***	300	0.0607	0.0193	21	33.9
3V	300	0.0422	0.0134	21	34.0
4A	300	0.1158	0.0369	11	17.1
4V	300	0.0618	0.0197	11	17.1
5A	300	0.0312	0.0099	37	62.3
5V	300	0.0133	0.0042	37	63.0
6A	300	0.0266	0.0082	40	66.7
6V	300	0.0128	0.0041	41	67.8
6A	600	0.0370	0.0118	39	67.8
6V	600	0.0157	0.0050	38	67.8
6A	900	0.0445	0.0142	39	67.8
6V	900	0.0166	0.0053	40	67.8
9A	300	0.0311	0.0099	39	65.6
9V	300	0.0133	0.0042	39	65.6
10V	300	0.0435	0.0138	30	50.6
11V	300	0.0374	0.0119	23	34.1
12V	300	0.0276	0.0088	47	83.3
13V	300	0.0303	0.0096	47	97.1

* m is the number of cycles over which the attenuation was measured.
** fr_1 is the 1st mode natural frequency.
*** A indicates value obtained in air.
V indicates value obtained in vacuum.

Table 4. Experimental and Predicted Results

Specimen #	Experimental[1] Modulus, E (GPa)	Predicted Modulus, E_T (GPa)	% Difference in Modulus[2]	Experimental Loss Factor η^*	Predicted Loss Factor η_T	% Difference in Loss Factor[3]
3	39.1	N/A	N/A	0.0134	N/A	N/A
4	**	N/A	N/A	0.0197	N/A	N/A
5	124.0	N/A	N/A	0.0042	N/A	N/A
6	110.0	106.4	−3.3	0.0041	0.0048	17.1
9	116.1	110.3	−5.0	0.0042	0.0047	11.9
10	36.1	41.9	16.1	0.0138	0.0125	−9.4
11	45.9	50.6	10.2	0.0119	0.0104	−12.6
12	70.0	68.3	−2.4	0.0088	0.0077	−12.6
13	61.4	68.4	11.4	0.0096	0.0077	−19.8

* The Values Apply to Loss Factors Determined in 'Vacuum'.
** Too low to measure accurately.
[1] ASTM D790
[2] $[(E_T-E)/E]100$
[3] $[(\eta_T-\eta)/\eta]100$
N/A Indicates Not Applicable

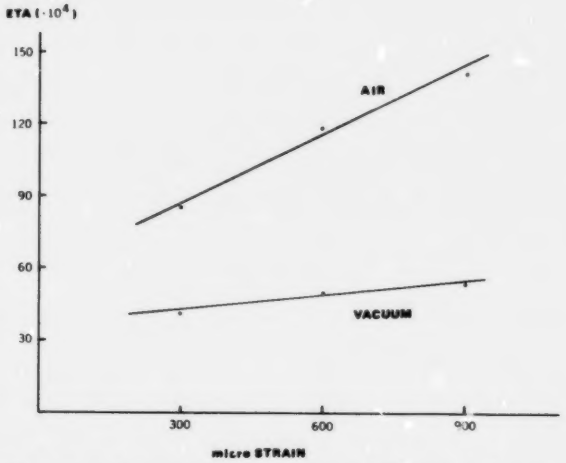

Fig. 5. Loss factor η in air and vacuum at different initial strains.

on the loss factor in air than in vacuum. The variation for the different initial strains imposed on Specimen 6 is shown in *Fig. 5*.

RESULT COMPARISON AND OPTIMUM LAMINATE

The flexural stiffnesses of the laminates were also measured using the ASTM D790 flexural bending standard. These experimental moduli are compared against the values calculated using *Eq 8*. The loss factors were calculated using *Eq 13*. These are compared with experimental values as shown in *Table 4*. In the calculation of the loss factors, experimental loss factors obtained from Specimens #3, 4, and 5 were used as a base in *Eq 13* to calculate loss factors for other specimens. The maximum difference in the moduli is 16.1 percent and that of the loss factor is 19.8 percent. The discrepancies can be due to the values used for the calculation of the moduli in *Table 1* where both the experimentally determined values and those obtained from the literature are used for the calculation. The errors in the moduli calculation are also responsible for the errors in the loss factor since the theoretical moduli are used in the loss factor calculation.

Table 4 shows that by changing from 0°/90° laminate to 45° laminate, the loss factor is increased (Specimen #3 & 4). Placing the Kevlar layers at the middle of the laminate does not modify the loss factor at all and it actually decreases the modulus of the laminate (Specimens #5, 6, and 9). Placing the Kevlar on the outside of the laminate and the graphite layers at the middle increases the loss factor but decreases the flexural moduli (Specimens #5, 10, and 11). The best laminate that meets the objective is Specimen #12 where the graphite layers and Kevlar layers were placed at appropriate positions to give a modulus of 70 GPa and a loss factor of 0.0088 which is more than twice the loss factor of graphite/epoxy alone (0.0042). Specimen #13, is a lot thicker than Specimen #12 but its loss factor is only slightly larger whereas its modulus is smaller. The above observation shows that thicker does not always mean stiffer or more damping capacity.

CONCLUSION

A rule of mixture for the prediction of the damping coefficient of a hybrid laminate based on the damping coefficient and elastic modulus of individual layers has been proposed. The results show reasonable agreement with experimental values. An optimal laminate having the same modulus as that of aluminum and twice the damping coefficient of regular graphite/epoxy laminates is also obtained.

REFERENCES

1. A. B. Schultz and S. W. Tsai, *J. Compos Mater.*, **2**, 368 (1968).
2. R. D. Adams and D. G. C. Bacon, *J. Compos. Mater.*, **7**, 53 (1973).
3. R. D. Adams and D. G. C. Bacon, *J. Compos. Mater.*, **7**, 402 (1973).
4. D. McLean and B. E. Read, *J. Mater. Sci.*, **10**, 481 (1975).
5. R. F. Gibson and R. Plunkett, *J. Compos. Mater.*, **10**, 325 (1976).
6. D. J. Nelson and J. W. Hancock, *J. Mater. Sci.*, **13**, 2429 (1978).
7. "Vibration Damping of Kevlar 49 Aramid, Graphite and Fiber Glass Fibers and of Composites Reinforced With These Fibers", Dupont Report #428, Nov. 1981.
8. R. F. Gibson, S. K. Chaturvedi, and C. T. Sun, *J. Mater. Sci.*, **17**, 3499 (1982).
9. W. D. Morrison, *Canadian Aeronautics and Space Journals*, **28**, 4 (1982).
10. S. W. Tsai and H. T. Hahn, "Introduction to Composite

Materials", Technomic (1980).
11. S. V. Kulkarni, B. W. Rosen, and H. C. Boehm, Proceedings of the 31st Ann. Techn. Conf., 1976, SPI, RP/C Institute, Paper #17A.

XIV. DISCUSSION: S. V. HOA

C. L. Beatty: Are you certain that these data were collected within the linear viscoelastic regime?
S. V. Hoa: I think so. Almost all tests were done using 300 micro-strains. This is not very much.
L. A. Utracki: What was the method of computation of the "predicted" values of the laminate modulus and the loss factor?
S. V. Hoa: The equations are given in the preprint. They are based on the additivity of the graphite and Kevlar layers' properties (see *Eqs 8* and *13*). Each fiber-epoxy layer is considered an entity. In the relation, the only important parameter is the distance, z, of the layer from the center of the laminate. The damping coefficients for Kevlar and graphite layers were experimentally determined. The derived equations allow us to calculate the properties of any laminate formed from combination of these two types of layers.
C. L. Beatty: In your equation, you have the sum of the two damping terms, for these two materials without any weighing coefficients in front of them. Did I miss something there?
S. V. Hoa: The loss equation comes from writing the loss energy equation for the laminate. I assumed that we can separate this into two terms: one which will represent the loss energy of all Kevlar layers and the other all the graphite layers. This assumption seems to work within 15 to 16 percent.
C. L. Beatty: If you have, for instance, one layer of Kevlar and two layers of graphite, how do you take into account their different mass?
S. V. Hoa: The weighing is done by the distance parameter, z, via the location of the layer in the laminate.
L. A. Utracki: The structure of the single layer specially prepared to measure its properties and that within the laminate, may be different; in a single ply usually one has an epoxy enriched layer whereas in a multiple system the concentration of fibers will be more uniform. Maybe you could get better agreement in your predictions using an iterative process to determine the single layer properties from a multiple laminate.

The Optimum Property Concept—Part II
The Relative Order in Failure Property Maxima With Increasing Filler Levels

F. K. LAUTENSCHLAEGER

Dunlop Research Centre
Sheridan Park Research Community
Mississauga, Ontario L5K 1Z8 Canada

Properties are identified which pass through a maximum when the filler loading in a polymer is increased; all are failure properties. Under standard test conditions of strain rate and temperature, the order of the failure property maxima with increasing filler loadings is identical in different polymers. The optimum level for maximum tear strength is higher than the optimum level for tensile strength. In general, the optimum level is even higher for abrasion resistance. The order in which these maxima develop is different when the degree of crosslinking is increased. The optimum level depends on characteristics of the polymer, e.g., the glass transition temperature. It can be shown that an increase in the pore volume of silica fillers, or an increase in the length of the crystalline segment in thermoplastic elastomers, leads to similar property trends as increased filler levels. Thus, the property trend which was established for increasing filler levels provides a scheme against which polymer or compound modifications can be assessed. The implications of the observed property trends on several generalizations in the literature are assessed.

INTRODUCTION

In a previous publication, a classification of elastomer properties was suggested (1). It was shown that a large number of properties, which are all failure properties, pass through a maximum when the temperature or other properties, which are defined as "Basic Properties of Materials", are varied. Typical "Basic Properties of Materials" are tensile modulus, hardness, and crosslink density. Factors which control the optimum "Basic Properties of Materials" value, at which "Maximum Properties" or "Properties which exhibit a Maximum" develop their highest value, were discussed. It was emphasized that this optimum value depends on the conditions under which the "Maximum Property" is measured. It was shown that the optimum values for different "Maximum Properties" do not generally coincide. Therefore, "Maximum Properties" pass through their maximum at different states of cure as the degree of crosslinking is increased. It was also suggested that a similar phenomenon can be expected if the "Basic Properties of Materials" are introduced not by crosslinking, but by increasing levels of fillers.

We have extended the studies in the literature, and have established the effects on the "Maximum Properties" when the "Basic Property of Materials" are introduced by

a) increasing filler loading
b) increasing the surface activity at a constant filler loading
c) increasing the crystalline segment in block copolymers.

The extension of our studies to thermoplastic elastomers is a logical consequence of the fact that the "hard segment" in these polymers responds similarly to a finely-divided filler (2).

EXPERIMENTAL

Several of the compounding studies included in this analysis have been reported before, except for their analysis in the trend in Maximum Properties. The description of the test instrumentation can be found in the original literature. In our new studies, Crescent Tear refers to ASTM, Die B, and Angle Tear to Die C. The Rotoflex instrument applied in our fatigue studies was described (24). Modulus 100 percent refers to tensile modulus at 100 percent strain.

Physical properties are reported in the units in which they were originally reported. Although abrasion data is reported as abrasion loss, the trends are discussed as abrasion resistance.

RESULTS

In *Table 1* are listed those Maximum Properties for which a maximum is observed with increasing filler loadings. It is evident from the relatively small number of these properties compared with the number of maximum properties identified (1), that the effect of filler loadings on property trends is less well established. The interest in the effect of filler variations has largely been restricted to mechanical properties. It is scientifically important and of practical relevance that failure properties exhibit a maximum over a temperature range, and in several instances, also over a range of filler loadings.

The trends in several maximum properties with increasing filler levels were studied in several polymers and for a variety of particulate additives. The examples chosen describe three or more properties. The polymers, fillers, and properties which have been selected are summarized in *Table 2*. When published data are included, the values are given in units in which these were originally reported. The available data is presented in *Figs. 1* to *15*.

The general trends observed for increasing filler levels can be schematically presented as shown in *Fig. 16*, and some generalizations can be established.

The trend in fatigue life depends on the type of test. Fatigue life may show a maximum at a lower

Table 1. Properties which Exhibit a Maximum with Increasing Filler Loading

Elongation at break (3)[a]	Abrasion resistance or wear resistance (9)
Tensile strength (4, 5)	Impact strength (9, 10)
Tear strength (4, 5)	Flexural strength (10)[b]
Cut growth resistance (6)	
Fatigue life (7)	
Flex fatigue (8)	

[a] Indicates reference numbers.
[b] Flexural strength has not been identified as Maximum Property over a range of temperature. It is included since the maximum with filler loading is technologically important.

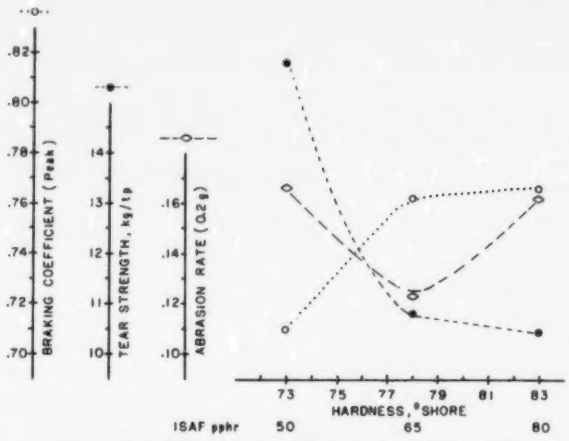

Fig. 1. The effect of carbon black levels (ISAF) in SBR.

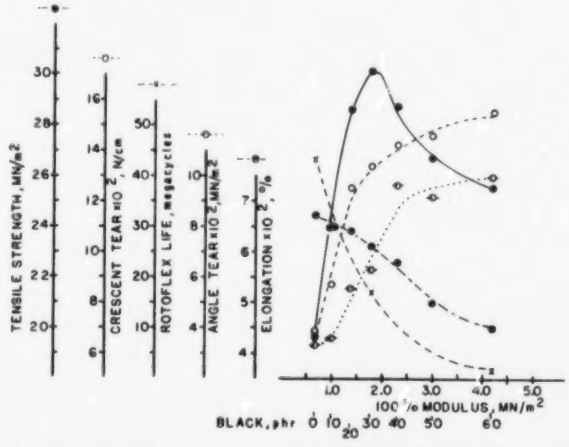
TENSILE STRENGTH, MN/m2
CRESCENT TEAR x10 2, N/cm
ROTOFLEX LIFE, megacycles
ANGLE TEAR x10 2, MN/m2
ELONGATION x10 2, %
100 % MODULUS, MN/m2
BLACK, phr 0 10 20 30 40 50 60

Fig. 2. The effect of carbon black levels (HAF) in NR. (Identical formulations as in Fig. 3, but vulcanization at 90 percent cure, according to Monsanto rheometer).

Table 2. A Summary of Polymers, Particulate Additives, and Maximum Properties

Polymer	Additive or Polymer Modification	Maximum Property	Reference
SBR	Carbon black (ISAF)	Tear strength, braking coefficient, abrasion rate.	*Fig. 1*[a]
NR	Carbon black (HAF)	Tensile strength, crescent and angle tear, rotoflex, elongation	*Fig. 2*[a]
NR	Carbon black (HAF)	Tensile strength, crescent and angle tear, rotoflex, elongation	*Fig. 3*[a]
NR	Aniline-formaldehyde resin	Resilience, tensile strength, flex cracking, tear strength, abrasion loss	*Fig. 4* (8)
SBR	Rice Hull Ash	Tensile strength, rebound, elongation, tear strength	*Fig. 5* (3)
NR	Carbon black (HAF)	Tensile strength, tear strength, elongation, abrasion loss	*Fig. 6* (11)
NR	Glass spheres	Elongation, tear resistance, tensile strength, abrasion	*Fig. 7* (12)
NR	Carbon black (HAF) and Lignin	Resilience, tensile strength, tear strength, elongation, abrasion loss	*Fig. 8* (13)
NR	Carbon black (HAF and MT)	Resilience, tensile strength, tear strength, elongation, abrasion loss	*Fig. 9* (12)
EPDM	Melamine-formaldehyde resin	Tensile strength, tear strength, elongation, rebound	*Fig. 10* (11)
NBR	Melamine-formaldehyde resin	Tensile strength, tear strength, elongation	*Fig. 11* (11)
NBR	Melamine-formaldehyde resin	Tensile strength,tear strength, elongation	*Fig. 12* (11)
Polyester[b]	Increasing hard polyester segment	Tensile strength, resilience, elongation	*Fig. 13* (14)
Polyurethane[c]	Increasing hard segment	Tear strength, elongation, tensile strength	*Fig. 14* (15)
NR	Carbon black oxidation	Tensile strength, wire adhesion, elongation	*Fig. 15* (16)

[a] Carried out at the author's laboratory. The carbon black was mixed into the rubber in a Banbury mixer.
[b] Based on polyalkylene ether terephthalate and tetramethylene terephthalate units in the polymer.
[c] Based on polycaprolactone diol and 4,4'-diphenylmethane diisocyanate.

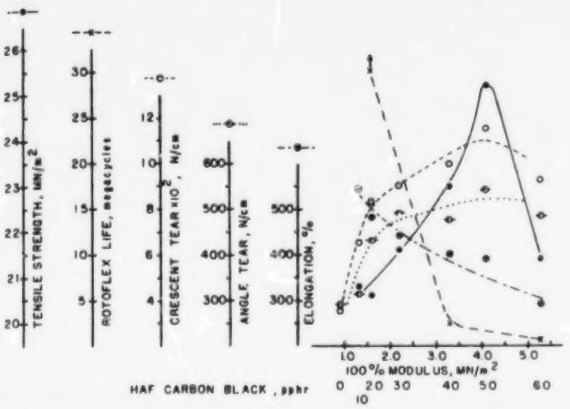

Fig. 3. The effect of carbon black levels (HAF) in NR. (Identical formulations as in Fig. 2, but vulcanization for 30 min. @ 150°C.)

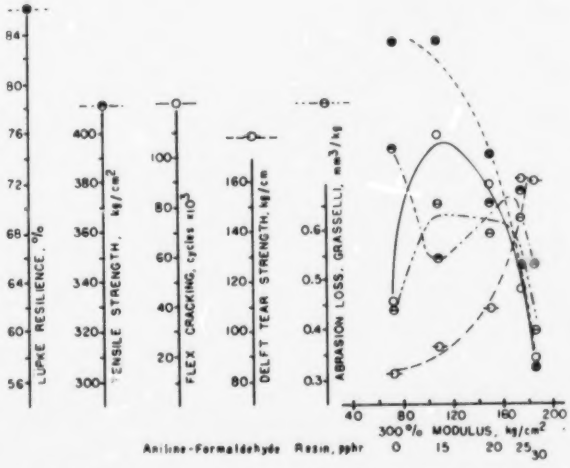

Fig. 4. The effect of aniline-formaldehyde resin in NR (8) (a) The tensile strength value for the gum vulcanizate requires confirmation.

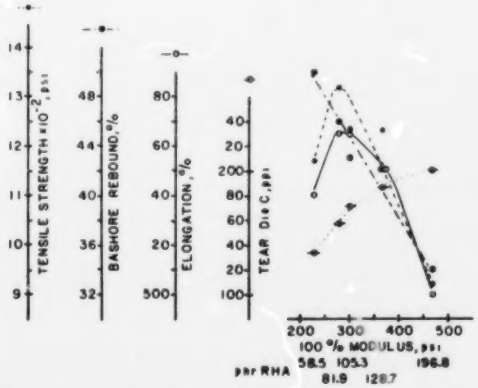

Fig. 5. The effect of Rice Hull Ash (RHA) in SBR (13).

filler level than elongation (17), but in other instances, fatigue may increase over the full range of filler loading (18).

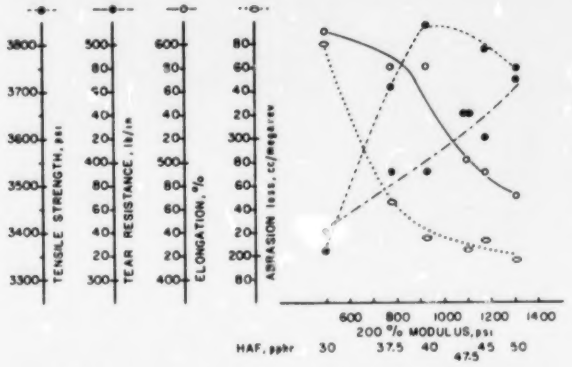

Fig. 6. The effect of carbon black (HAF) in NR (11).

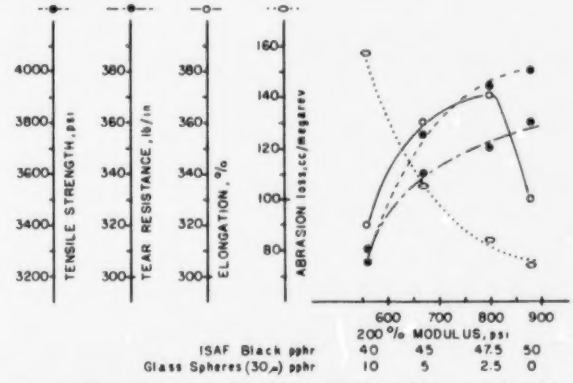

Fig. 7. The effect of carbon black (ISAF) substitution by glass spheres in SBR 1500 (12).

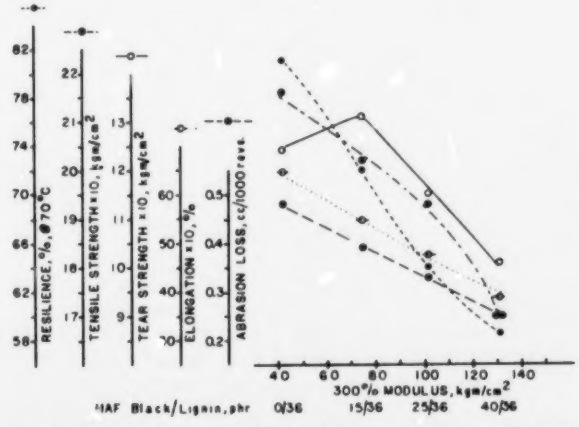

Fig. 8. The effect of carbon black (HAF) and Lignin in SBR 1500 (13).

Variation in the Composition of Filler Blends

A variation in the composition of a mixture of two different fillers leads to changes in basic properties of materials (BPM's) and the expected changes in the maximum properties (*Fig. 16*) as if the BPM is introduced by increased filler loadings. One example is a variation in the composition of a mixture of carbon blacks (19) (*Fig. 17*). Over the whole range of compositions there is essentially no change in hardness (69 to 68 Shore A) or tensile modulus

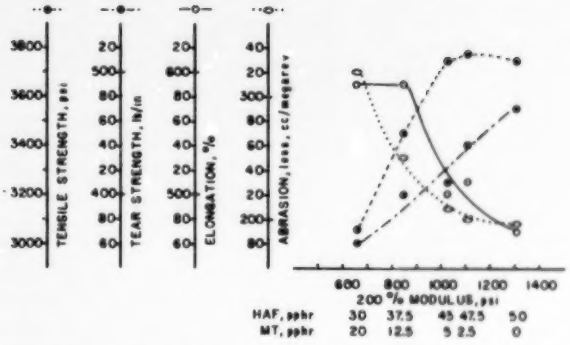
TENSILE STRENGTH, psi
TEAR STRENGTH, lb/in
ELONGATION, %
ABRASION, loss, cc/megarev
200 % MODULUS, psi
HAF, pphr 30 37.5 45 47.5 50
MT, pphr 20 12.5 5 2.5 0

Fig. 9. The effect of carbon black substitution (MT by HAF) in SBR 1500 (12).

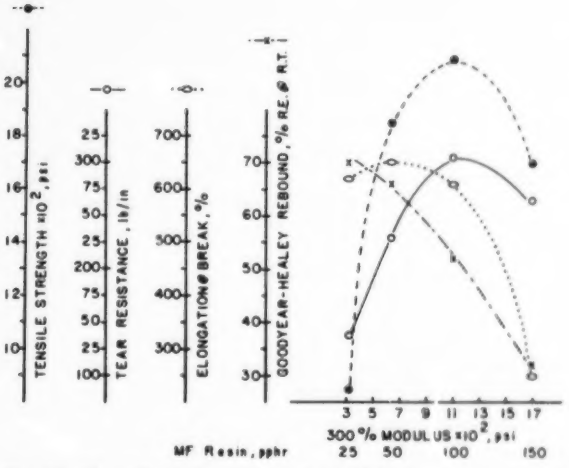
TENSILE STRENGTH ×10², psi
TEAR RESISTANCE, lb/in
ELONGATION @ BREAK, %
GOODYEAR-HEALEY REBOUND, % RE. @ R.T.
300 % MODULUS ×10², psi
MF Resin, pphr 25 50 100 150

Fig. 10. The effect of melamine-formaldehyde resin in EPDM (11).

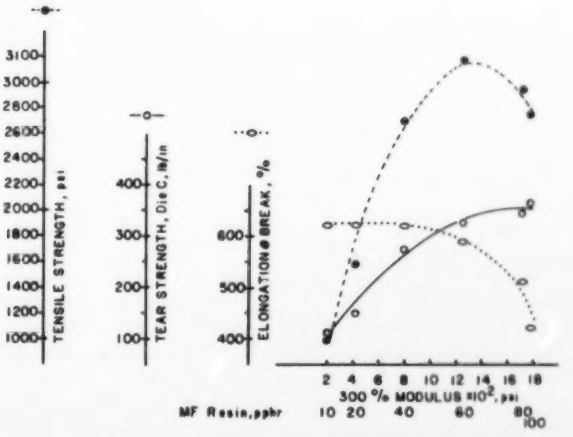

Fig. 11. The effect of melamine-formaldehyde resin in NBR (11). (Cure Time 30 min.)

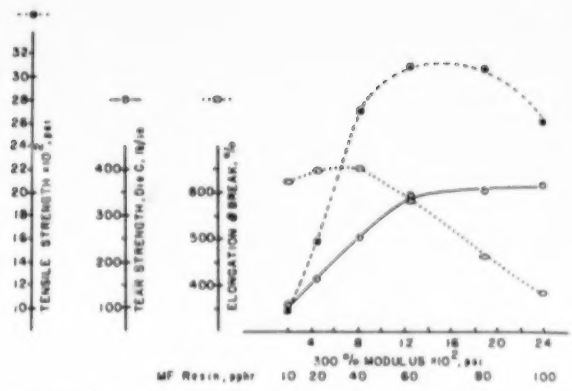

Fig. 12. The effect of melamine-formaldehyde resin in NBR (11). (Cure Time 40 min.)

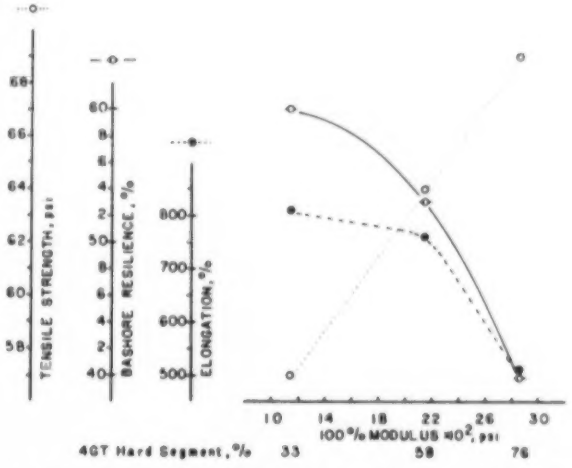

Fig. 13. The effect of increasing the crystalline segment (4GT) in a thermoplastic polyester (14).

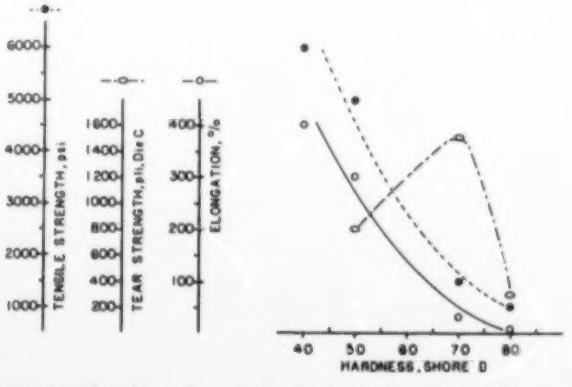

Fig. 14. The effect of increasing the hard segments in a thermoplastic polyurethane (15).

(216 to 221 kg/cm² at 300 percent strain). Nevertheless, there are significant differences in the surface parameters of the two carbon blacks (*Table 3*). Sterling So black is the coarser particle carbon black with the lowest surface area and largest diameter.

When the change in the carbon black composi-

tions is related to changes in PEM's (*Fig. 17*), the composition with the highest abrasion rating also shows the lowest resilience. This indicates that the overall trend schematically presented in *Fig. 16* can be observed even if the BPM variations in the vulcanizates are small or negligible. It also demonstrates that major differences in performance can

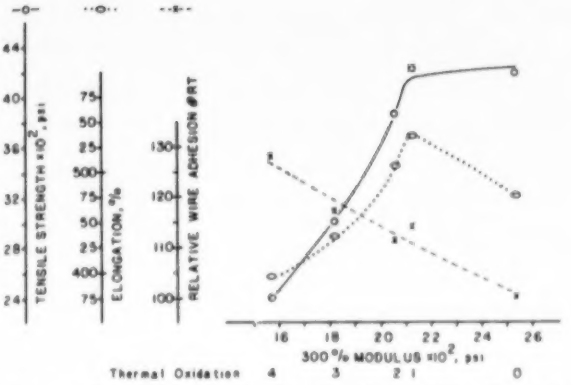

Fig. 15. The effect of carbon black oxidation (16). (Thermal oxidation 0 to 4 refers to nitrogen adsorption values of 79, 114, 142, 179, and 245 m^2/g respectively).

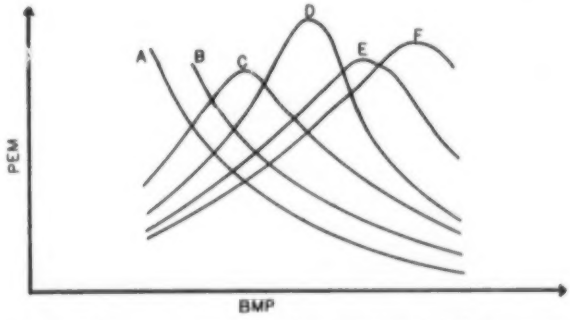

Fig. 16. Schematic presentation of property trends with increasing filler levels (A = resilience, B = adhesion, C = elongation at break, D = tensile strength, E = tear strength, F = abrasion resistance[a]. PEM = Property Exhibiting Maximum[1] BMP = Basic Property of Materials[1] a) The relative heights of the peaks are not meant to reflect actual differences between these properties.

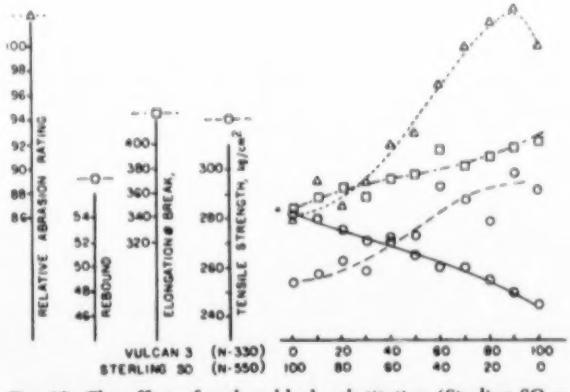

Fig. 17. The effect of carbon black substitution (Sterling SO = FEF by Vulcan 3 = HAF) (19). (Abrasion Rating = Graselli, DuPont Abrader.)

result at equal hardness or tensile modulus. The particle parameters are then better reflected in failure properties or maximum properties than in basic properties of materials or network properties. From this follows that a distinction between different fillers can best be made on the basis of PEM's. The concept of rating fillers on the basis of such

Table 3. Particle Parameters of Vulcan 3 (N-330), Sterling So (N-550) Carbon Blacks

	DBP Number (ml/100g)	Surface Area (Nitrogen) (m^2/g)	D_w[a] (Å)	D_a[b] (Å)	D_s[c] (Å)	S_{BM}[d] (m^2/g)
Vulcan 3	93	74	220	253	364	92
Sterling So	121	42	325	370	482	69

[a] Statistically most frequent diameter.
[b] Arithmetic average diameter.
[c] Surface average diameter.
[d] S_{BM}: $6 \times 10^3/d\,D_s$ (S_{BM} in m^2/g, D_s in Å), d = density.

maximum properties was discussed separately (20). The results in *Fig. 17* support the earlier observation that changes in maximum properties can be large even when changes in network properties are small, and also supports the concept that property improvements should be judged by comparisons at equal values of network properties.

Figure 17 reveals an exceptional trend. The trend in elongation at break over a range of filler levels is normally in the same direction as resilience, and opposite to abrasion resistance and tensile strength. This phenomenon deserves further analysis and exploration.

Variation in the Filler Activity, e.g. Surface Area

The general trend in properties shown in *Fig. 16* is not only observed if the basic property of materials is increased by increasing the level of a particulate additive, but also when the type of filler is varied. Two recent studies show this similarity.

Increasing the pore volume of silica causes an increase in tensile modulus (21), which leads to a decrease in resilience and an increase in tear strength over the whole range of increasing pore volume. Also observed is a maximum in elongation, and there is an indication of a maximum in tensile strength. It was also evident that the ultimate particle size is less critical than is pore volume, since silicas of different particle sizes but similar pore volume fall essentially on a single curve. Related to these results are studies on the effect of carbon black surface area on vulcanizate properties. An increase in the surface area of carbon black causes a decrease in resilience (17), accompanied by a decrease in cut growth and fatigue life; the data for tensile strength and tear strength indicate a maximum. A maximum in tensile strength and tear strength is also observed when the surface area of carbon black is increased at an equal filler level.

It is of interest that increasing thermal oxidation of carbon black leads to a reduction in the tensile modulus of a vulcanizate which is accompanied by a reduction in elongation and tensile strength, but by an increase in relative wire adhesion (16) (*Fig. 15*). The implications are that adhesion, as measured under the reported conditions, is highest at a low surface activity or BPM levels. The detrimental effect of carbon black on adhesion is also evident in experiments where the level of carbon black is increased (22).

Thermoplastic Elastomers

Opposite trends are observed for resilience when a basic property of materials is increased by higher curative levels or higher filler levels. The trend in resilience is therefore of diagnostic interest. For example, a loss in resilience is observed with an increasing length of the hard segment in a thermoplastic elastomer (*Fig. 13*). Therefore, the hard segment resembles the effect of a filler rather than that of a crosslink. This conclusion is supported by the high BPM_{opt} value for tear strength relative to tensile strength (*Fig. 14*) for a thermoplastic elastomer. It was observed that the maximum in tear strength is at a lower BPM value than the maximum in tensile strength when the degree of crosslinking is increased (20). This is in contrast to the trends observed for increasing filler levels (*Fig. 16*). The observed trends in thermoplastic elastomers support the suggestion that the spherical domains in styrene-diene-styrene block copolymers virtually constitute a finely divided filler, dispersed within an elastic medium (23).

The Displacement of Maxima by Compositional Changes in the Polymer Matrix

A maximum in a property at a given filler level represents an optimum in the sum of all molecular processes which contribute to the viscoelastic response. Therefore such a maximum will shift when either the test conditions, e.g., test temperature or frequency, or the polymer compositions are varied. For example, the tensile strength and flexural strength maxima will shift to a different asbestos level as the composition of the binder resin is changed. Evidently the optimum asbestos loading will depend on the physical characteristics of the polymer (24). In a similar way, the optimum loading of cellulose fiber/elastomer composites for tensile fatigue was shown to depend on the Young's modulus of the elastomer (25). This leads to a systematic displacement of the fatigue maxima in different polymers.

The maximum in a property will also shift if the type of particulate additive is changed. The optimum value in a basic property of materials will shift systematically as particle size or surface area are varied. This technologically important aspect was analyzed on several fillers and polymers (19).

Some Implications of the "Optimum Property Concept" on Property Trends

Reinterpretations of several property trends discussed in the literature have been proposed on the basis of the optimum property concept (1). Examples illustrating the effect of increasing filler levels provided in *Figs. 1* to *16* support previous conclusions based on the effect of increased degree of crosslinking. It is again evident that

a) the relationship between a failure property and a basic property of materials such as tensile modulus and hardness is not linear
b) the relationship between two maximum properties over a wide range of increasing filler levels can only be described by an envelope, although it may appear linear over a narrow range of filler levels.

The observed trends suggest that a reinterpretation of several technologically important observations can now be considered. For example, the observation of a maximum in elongation with increasing filler levels (*Figs. 5, 10,* and *12*), with increasing surface activity such as pore volume (21), or a variation in the filler composition (*Fig. 7*), indicates that a linear correlation between elongation and dibutyl phthalate adsorption of carbon blacks (23) can only be of limited validity.

Since there is a maximum in abrasion resistance with increasing carbon black loading, or increasing hardness, the cause of increased wear resistance is unlikely to be the higher hardness or greater resistance to deformation, as had been proposed (9).

A significant implication of the optimum property concept is that the optimum network property or basic property of materials and the magnitude of the maximum property cannot be calculated, since both values represent the balance of all molecular factors and polymer-filler interactions, as well as the magnitude and quality of all external forces, such as strain rate, test frequency, and test temperature.

A Summary of Observed Property Trends for Increasing Filler Levels

Some general trends for the effect of increasing filler levels on some failure properties and resilience can be established on the basis of the available data.

Resilience: The addition of fillers causes a decrease in resilience or rebound (*Figs. 4, 5, 8, 10,* and *13*).

Elongation at Break: Similar to resilience, elongation at break decreases in most instances with increased filler loading (*Figs. 2, 3, 6, 8, 11,* and *14*). However, it may also show a maximum, but always at a very low filler level (*Figs. 5, 7,* and *15*).

Fatigue or Flex Life: The varying trends in fatigue or flex life illustrate the effect of test conditions and of the type of polymer on these properties. Fatigue life may show a maximum at a lower filler level than elongation (17), and decrease over a range where tensile strength and tear strength increase. Rotoflex fatigue of NR vulcanizates (24) decreases with increasing filler levels (*Figs. 2* and *3*), similar to the trend observed with an increasing degree of crosslinking (20). Depending on the type of fatigue test, e.g., Tensile Fatigue, DeMattia or Rotoflex, increasing carbon black levels may either increase or decrease the life of a vulcanizate (18).

Tensile Strength and Tear Strength: The optimum filler level for tensile strength is generally lower than for tear strength (*Figures. 2, 5, 6, 11, 12,* and *14*), although both can coincide (*Figs. 3* and *10*). This is not restricted to hydrocarbon polymers. Tear strength also shows its maximum at a higher level than tensile strength in copolymers of vi-

nylidine fluoride/hexafluoropropylene and chlorotrifluoroethylene/vinylidine (26) if the specific surface area of the carbon black is increased, but the carbon black level is maintained. When two tear tests are compared, the trends can coincide (*Figs. 2* and *3*).

Tensile Strength and Abrasion Resistance: Traditionally, abrasion data are presented as abrasion loss rather than in terms of abrasion resistance, which is the inverse. Since abrasion resistance has been introduced as a failure property or maximum property (20), we prefer to discuss the results in terms of abrasion resistance rather than abrasion loss.

The optimum filler level for tensile strength is lower than for abrasion resistance (*Figs. 4, 6,* and *8*). This is in contrast to the position of the abrasion resistance maximum when the network property is increased by increasing the degree of crosslinking (20). It was shown before (27) that abrasion loss can increase when the degree of crosslinking is increased, whereas it is decreased with increasing carbon black levels. From this follows that hardness, per se, is not conducive to abrasion resistance. It is equally critical how the hardness is introduced into the vulcanizate.

Cut Growth: The trend in cut growth can follow the trend in fatigue, indicating that its highest value is at a very low filler loading (17).

Friction vs. Wear Resistance: The opposite trends in abrasion resistance and friction (e.g., braking force coefficient) is evident from *Fig. 2*. Since there can be a maximum in abrasion resistance at high filler levels, this inverse trend can only be relevant over a limited range of filler loadings. Therefore, there must be conditions where the opposite trend in wear resistance and friction does not prevail. Data on experimental carbon blacks in tire tread formulations support this conclusion (28). Adhesion decreases with increasing tensile modulus—in that case as a result of a modification of the carbon black surface (*Fig. 15*), but insufficient data is available to permit a generalization.

CONCLUSIONS

It was shown that elongation at break, tensile strength, tear strength, cut growth, fatigue life, flex fatigue, abrasion resistance, impact strength, and flexural strength can show a maximum with increasing filler loadings.

The order in which various failure properties or maximum properties—measured under standard conditions—pass through their maximum with increasing filler loading is different from the order observed with increasing degree of crosslinking.

The trends in the balance of properties in thermoplastic elastomers with increasing concentrations of the crystalline segment is similar to the trend established for increasing filler loadings.

Several opposing trends in failure properties reported in the literature can be rationalized on the basis of a shift of the maximum in these properties.

The relationship between filler loading and failure properties should not be assumed to be linear. Linearity is approached in the case of maximum properties which show their maximum either at a very low or a very high value in a basic property of materials.

An increase in the pore volume of silaceous fillers leads to similar trends in properties as the increase in filler level. In both variations, resilience decreases and tear strength increases. Filler particle size is less critical than pore volume.

APPENDIX

Maximum Properties	Basic Properties
Elongation at Break	Storage Modulus
Tensile Strength	Shear Modulus
Tear Strength	Hardness
Cut Growth	Tensile Stress (Modulus)
Resilience	Crosslink Density
Adhesion	
Tack	
tan δ or Hysteresis	
Friction	
Loss Modulus E"	
Flex/Fatigue	
Abrasion (wear) Resistance	
Impact Strength	
Sound Absorptions or Damping	

REFERENCES

1. F. K. Lautenschlaeger and M. Myhre, *J. Appl. Polym. Sci.*, **24**, 605 (1979).
2. M. Morton, *Elastoplastics*, **3**, 112 (1971).
3. H. E. Haxo, Jr., and P. K. Mehta, *Rubber Chem. Technol.*, **48**, 271 (1975).
4. H. Westlinning and H. Fleischhauer, in "Reinforcement of Elastomers", G. Kraus, Ed., p. 425, Interscience Publishers, New York, (1965).
5. M. Studebaker in "Reinforcement of Elastomers", G. Kraus, Ed., p. 319, Interscience Publishers, New York, (1965).
6. E. E. Auer, K. W. Doak, and I. J. Schaffner, *Rubber Chem. Technol.*, **31**, 185 (1958).
7. E. S. Dizon, Cities Service Co. priv. commun.
8. J. van Alphen, "Proceed. Third Rubb. Techn. Conf.", p. 670, W. Heffer & Sons Ltd., England, (1954).
9. R. F. Peterson, C. F. Eckert, and C. I. Carr, in "The Physics of Tire and Traction, Theory and Experiment", p. 233, D. F. Hays and A. L. Browne, Eds., Plenum Press, (1974).
10. J. W. Axelson, *Polym.-Plast. Technol. Eng.*, **4**, 93 (1975).
11. Cabot Corporation Technical Literature.
12. B. B. Boonstra and A. I. Medalia, *Rubber Chem. Technol.*, **36**, 115 (1963).
13. I. Sagajillo, "Proceed. Third Rubber Techn. Conf.", p. 610, W. Heffer & Sons Ltd., England, (1954).
14. G. K. Hoeschele, *Polym. Eng. Sci.*, **14**, 848 (1974).
15. C. G. Seefried, Jr., J. V. Koleske, and F. E. Critchfield, *J. Appl. Polym. Sci.*, **19**, 2503 (1975).
16. A. E. Hicks, V. E. Chirico, and J. D. Ulmer, presented at the 100th Meeting of the Rubber Division, American Chemical Society, Cleveland, Ohio, Oct. 12–15, 1971.
17. E. S. Dizon, A. E. Hicks, and V. E. Chirico, presented at the 107th Meeting of the Rubber Division of the American Chemical Society, Cleveland, Ohio, May 6–9, 1975.
18. F. K. Lautenschlaeger and F. Fechter, unpublished results.
19. J. B. Donnet, B. Bariou, J. Schultz, Y. Schwob, and J. Gosset, *J. IRI*, **6**, 119 (1972).
20. F. K. Lautenschlaeger, *J. Appl. Polym. Sci.*, in press.

21. K. E. Polmanteer and C. W. Lentz, presented at the 107th Meeting of the Rubber Division of the American Chemical Society, Cleveland, Ohio, May 6–9, 1975.
22. D. E. Erickson, *Rubber Chem. Technol.*, **47**, 213 (1974).
23. A. Voet, J. C. Morawski, and J. B. Donnet, *Rubber Chem. Technol.*, **50**, 342 (1977).
24. H. W. Grinter and J. R. Beatty, *Adhes. Age*, p. 32, (Sept. 1966).
25. P. Hamed and A. Y. Coran, presented at the 175th Meeting of the American Chemical Society, Anaheim, CA, March 12–17 (1978).
26. A. A. Dontsov, A. B. Ivanov, V. I. Treshchalov, and A. V. Chulyukina, *Kauchuk i Rezina*, No. 5, 17 (1976).
27. H. Westlinning, Koll. Z. Z. *für Polymere*, **211**, 76 (1966).
28. B. B. Boonstra, *Tire Sci. Technol.*, **2**, 312 (1974).

XI. DISCUSSION: F. K. LAUTENSCHLAEGER

L. A. Utracki: I have two questions: (1) What is the reason that in the optimization scheme you are using the modulus as the fundamental reference property, against which all others are plotted? and (2) How do the processing conditions affect the property "A" *vs.* modulus dependence? For example, is the tensile strength *vs.* modulus dependence uniquely defined for a given system or not? If the answer is no, as I suspect, then is it possible to generate a "master curve" by some particular shifting mechanism?

F. K. Lautenschlaeger: We could select any of the basic material's properties that have been suggested (tensile modulus, hardness, degree of cross-linking etc). (*Appl. Polym. Sci.*, **24**, 605 (1979)). We have selected tensile modulus since it is commonly measured property, and thus permits the analysis of a wide selection of published material. With regard to your second question, on the effect of processing conditions, we have not carried out systematic studies to determine the effect of dispersion or molecular weight changes during processing. However the shape of the peak for the maximum property must change, either in width of height, as these physical parameters are varied. Particle attrition, the wetting of fillers, and interfacial effects of coupling agents will also affect peak size and shape. Widening of peaks would broaden the performance over a wider range of test severities.

The Application of Endless-Fiber Reinforced Polymers

G. MENGES *and* J. MINTE

Institut für Kunststoffverarbeitung
Pontstrasse 49, D 5100
Aachen, West Germany

Both in aircraft and automobile construction, the transition from metals to fiber reinforced polymer resins is taking place with increasing regularity. Beginning with the wide selection of possible materials, definite examples of the mechanical properties of construction parts are discussed in this article. Different production possibilities based on fiber winding technology are shown. The application of robots in production is also considered.

INTRODUCTION

For plastics used in the manufacture of functional components subject to high loading, the physical properties required can be obtained only through modifying the base materials, in accordance with the particular application. Fiber composites are formed by embedding a fibrous reinforcement component in a homogeneous material (the matrix) and are distinguished by their anisotropic properties. They allow the engineer to create a specially tailored component material that provides considerable freedom in shaping yet ensures a minimum weight factor. In developing the component, attention must be paid at all stages to: the required properties of the end component, the physical properties, and the production engineering capacities. The set of requirements of any given component will be a function of mechanical, thermal and chemical load, and will also depend on any special marginal conditions such as given load inputs. The selection of a material and questions relating to production will be examined in greater detail in the sections below.

MATERIAL SELECTION AND PHYSICAL PROPERTIES

The complexity of fiber composite materials becomes immediately apparent when selecting the right material for a particular component. The final properties of the component are a function of fiber type, matrix material, fiber/resin interface, and manufacturing conditions. Polymers are generally reinforced with glass fibers (GRP). Plastics reinforced with aramid fibers (ARP) and carbon fibers (CRP) yield properties which are of technical interest.

Figure 1 (1) shows strength in terms of weight (so-called "tenacity") over Young's modulus in terms of weight for different materials. Titanium, aluminum, and steel fall into the lower left-hand portion of the diagram, indicating relatively poor "tenacity" due to their high specific weight. GRP fares much better in terms of specific strength. The

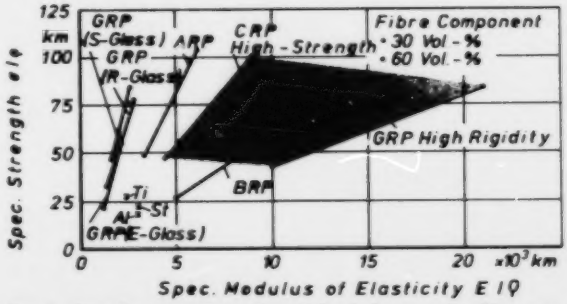

Fig. 1. Specific strengths and moduli of elasticity for fiber reinforced materials (1).

metals show improvement relative to rising fiber content, but as far as stiffness goes this is not true for GRP. A further improvement in specific strength and also in terms of Young's modulus can be achieved with aramid fiber reinforced plastic (ARP). High strength grades of carbon fiber reinforced plastics (CRP) give values similar to ARP and if the carbon fibers are modified they then extend to cover a wide range, up to very high specific stiffness. This entails a loss of strength, however. Boron fiber reinforced materials (BRP) are considerably inferior to the different types of CRP. Besides their very good weight-specific properties compared with metals, fiber composites are also notable for their better fatigue strength.

Figure 2 shows a series of load cycle curves from the literature (2, 3) for different materials. An aluminum alloy curve is included in the diagram for purposes of comparison. GRP with *E*-glass fiber reinforcement gives fatigue behavior virtually identical to that of the aluminum alloy. Only when *S*-glass is used are distinct improvements achieved at a low number of load cycles. ARP and BRP show a good level of fatigue strength and are only surpassed by CRP. Boron fibers in an aluminum matrix do not attain this level. Recent findings show the static and dynamic strength of CRP to be identical in the direction of the fiber.

A further factor in the application of fiber com-

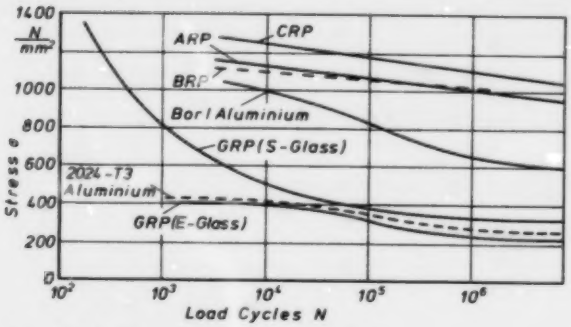

Fig. 2. Fatigue strength of fiber composites. $\vartheta = 23°C$; $R = 0.1 = \sigma_u/\sigma_o$

posites is the coefficient of thermal expansion. This characterizes dimensional stability under thermal loading. The coefficients of thermal expansion of metals are considerably greater than those of the different fibers in common use (4).

Apart from other advantages, fiber composites are distinguished from metals by their relatively good resistance to corrosion. This is ultimately reflected in maintenance and servicing costs (5).

SAMPLE APPLICATIONS

Aircraft Construction

The weight factor in air and space travel has made this the lead industry for application of fiber composites. The plastic parts that have replaced metal on the B-767 are well known. A considerable proportion of the secondary structure, including rudder, flaps, and cladding is made up of composite materials. GRP is only used to a very limited extent as a constructional material, presently for applications such as the radome.

Figure 3 shows development trends in the commercial airline industry which is still very conservative in its use of fiber composites compared with military aircraft construction. The percentage by weight of fiber composites is still relatively low at 3 percent, although some development is in evidence since the 747 jumbo jet of the 1960's. The amount of fiber composites has thus risen from 1 to 3 percent, with GRP being used less than in the past. The increase in composites has been achieved at the expense of aluminum; this becomes particularly evident in calculations for the future. In the 1990's, composites will account for 65 percent of structural weight, while aluminum will have declined to 11 percent. Weight savings achieved by substituting fiber composites for metal components are currently in the order of 15 to 30 percent.

If CRP is to be used for functional components that are subject to high loading, then it is necessary to know the deterioration limits and have a means of calculating these in advance. For CRP laminates that are reinforced in the longitudinal direction (0°), the transverse direction (90°), and diagonally to the direction of load (±45°), it is possible to predict initial Young's moduli with the aid of the continuum theory (6). *Figure 4* shows that experimental measurements confirm theoretical calcula-

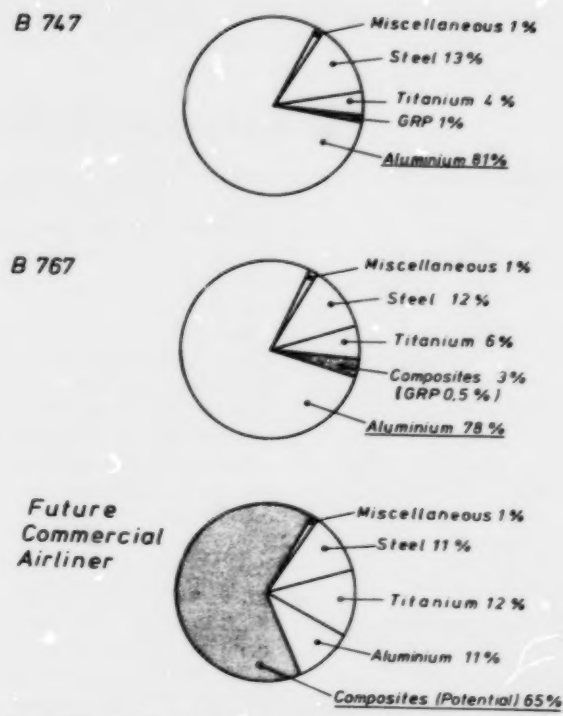

Fig. 3. Percentage of different materials in the structural weight of commercial airliners.

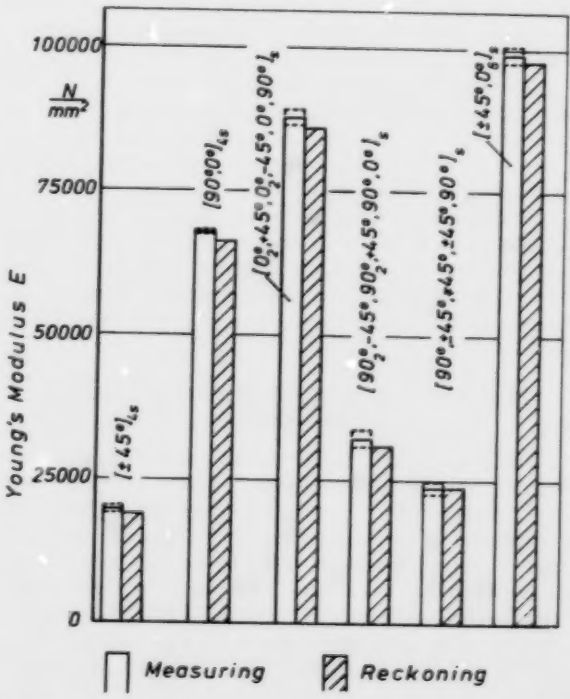

Fig. 4. Comparison between experimental and theoretical Young's modulus of different laminates.

tions, at all times slightly exceeding the latter. *Figure 5* permits a rapid estimate of the Young's moduli as a function of ply distribution.

The percentage of 0 and ±45° components that

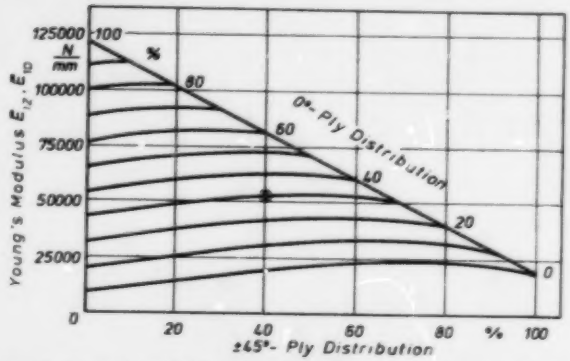

Fig. 5. Young's modulus of 0°, ±45°, 90° -laminate group (CRP).

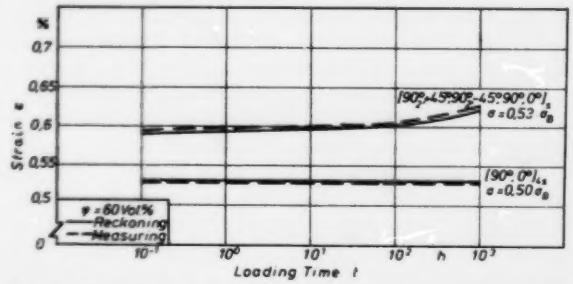

Fig. 6. Comparison between creep behavior of different CRP laminates.

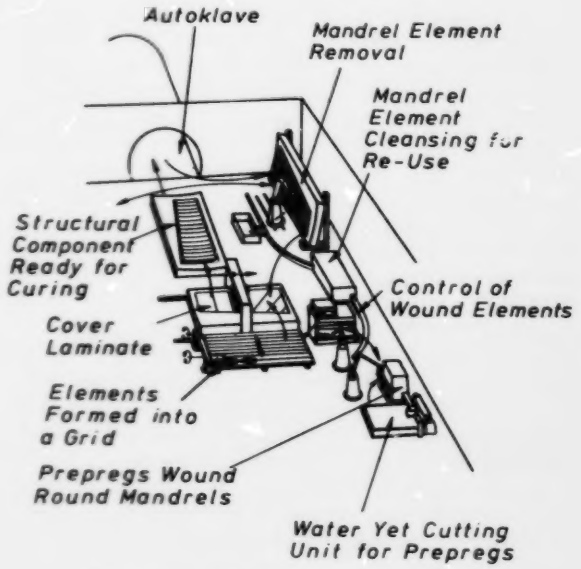

Fig. 7. Automatic prepreg processing, Ref. 7.

can be read off for the overall laminate here have to be made up to 100 percent; the difference is the percentage of 90° layers. A CRP laminate with a 40 percent ± 45° ply component and a 30 percent 0° ply component (giving a 30 percent 90° component) thus has a composite Young's modulus of $E = 5200\ N/mm^2$. The coefficient of thermal expansion can be expressed in a similar manner (6).

The time dependence of the physical properties can likewise be calculated. An example is given in *Fig. 6*. The high proportion of longitudinal reinforcement in the laminate in the lower curves produces constant expansion over time. This can be calculated in advance in the same way as the increase in expansion over time in the other laminate in this *figure*. Cracking marks the limit on application of the continuum theory for the individual layers. It is thus necessary to know at which level of expansion damage first occurs.

A clear-cut distinction can be drawn between micro-damage, interfiber fracture, and fiber failure by applying sound emission analysis in conjunction with various signal processing methods. The microcracking limits for individual carbon fiber reinforced layers, which are at right angles to the direction of flow and subject to shear stress, come out higher than for GRP at strains: $\epsilon = 0.2$ percent (expansion transverse to the fiber direction) and $\gamma = 0.7$ percent (shear deformation). This is due to the anisotropic properties of the carbon fiber which possesses considerably less stiffness at right angles to the fiber axis compared with the isotropic glass fiber, and hence places a comparatively lighter load on the resin in microscopic terms. As well, glass fiber has a higher shear modulus than carbon fiber. Initial fiber fractures must be expected at a deformation of above $\epsilon = 1.0$ percent (6).

Production processes for CRP components currently still involve a relatively large number of manual steps. Comprehensive processing centers which also perform supplementary processing and machining operations are currently under development at various locations (7). An example of these is shown in *Fig. 7*. The components, produced from prepregs, are cured in an autoclave where they are put through an elaborate pressure and temperature cycle. Thermoplastic matrix materials which are currently coming into use could effectively reduce production times in this field as well as open up new applications for the process.

Automobile Construction

The substitution of plastics for metals is well underway for outer shells and bumpers. Visitors to the "K '83" Plastics Trade Fair in Düsseldorf were thus able to see the Pontiac Fiero which has bodywork constructed of SMC planking over a steel frame. The Citroen BX with an engine bonnet and rear flap in fiber-reinforced plastic was also on show.

The substitution of plastics for parts subject to rapid translational or rotary movement is of greater interest, from the technical point of view, due to the weight reduction factor that is achieved. This will be illustrated with the examples of a cardan shaft and connecting rod.

Cardan Shaft

The cardan shaft is a critical component in terms of rigidity. Apart from the torsional strength, the stiffness in torsion and longitudinal stiffness under flexure are decisive for component dimensioning (8). Vibration-free transmission of torque must be

guaranteed. *Figure 8* gives a comparison of different materials. The graph shows the span that can be bridged with a single-piece shaft, i.e., without any intermediate bearing, as a function of shaft diameter. The *figure* shows the capacities and the limits of the different materials. The length of the cardan shaft in passenger vehicles varies from 1.2 to 1.8 m. Shaft diameter is limited by the space available. Assuming a mean shaft diameter of 70 mm, it is seen that only steel, aluminum, and GRP will permit shaft driving lines to be made up with single-piece shafts. Most makes of cars require two-piece shafts. With high-modulus carbon fiber, however, the whole range can be achieved with a single-piece shaft. The middle range is of particular interest from the technical and economic angles. Taking a shaft length of 1.5 m, for instance, it would be possible to use not only pure CRP but also ARP or CRP/GRP hybrids as well.

Considerable scope also exists when it comes to selecting fiber configuration and optimizing the structure. If the component were wound in the direction of the shaft axis, designated by 0° here, this would certainly give an even greater transmittable length but would also entail a considerable loss of stiffness in torsion, making this version technically impractical. Cardan shafts of this type have already been tried out in test vehicles and racing cars. The shafts are produced by filament winding, a process that is already computer controlled but which is still beset by the problem of low output. This can be remedied by:

- a high winding speed
- winding a large number of filaments in parallel
- winding several mandrels in parallel (9).

Connecting rod

A reduction in oscillating weight can also be achieved directly inside the engine through the use of carbon fiber reinforced plastics. Components that come to mind here are pistons and connecting rods (10). Both these parts have already been produced at the IKV. The basic structure of a connecting rod features a small bearing, large bearing, and pressure hull (*Fig. 9*). With the carbon fibers, the bearings are braced against each other via the pressure hull (*Fig. 10*). To produce a winding pattern of this type, it is necessary to have a high degree of

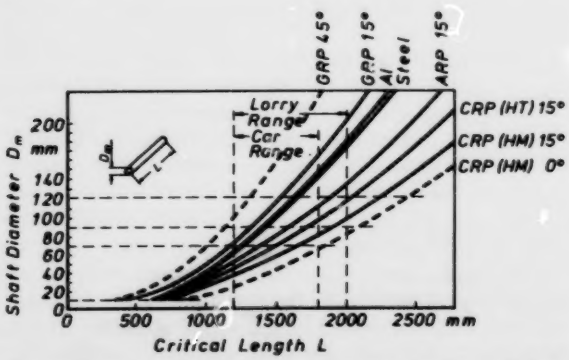

Fig. 8. Bridgeable length of a cardan shaft for 7200 rpm Ref. 8.

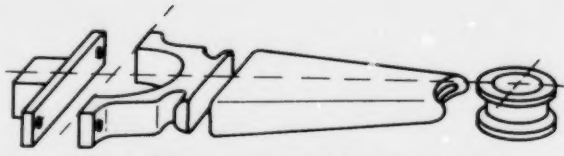

Fig. 9. Laboratory wound body for connecting rods.

Fig. 10. Sample winding pattern for connecting rods.

mobility in the filament eye which deposits the roving. In laboratory operation, the filament is laid in a defined pattern by a freely programmable robot (*Fig. 11*).

Testpieces of this type are currently at the trial stage and have already withstood more than 10^7 load alternations at room temperature (50 Hz; tension: 14 kN; pressure 35 kN). Media influence and high temperatures must be taken into consideration separately; these are the prime factors which influence selection of the matrix system. Several matrix systems were therefore investigated to see how their properties alter in hot motor oil (11). Pure resin testpieces were stored at 130°C in fresh oil, changed every 100 hours and at 180°C in used oil. These two test conditions were selected so that information could be obtained firstly on resistance to the additives in fresh oil, and secondly on the oxidative productions of combustion in the used oil.

In some cases, a considerable weight loss occurred (7 percent over 100 h, see *Fig. 12*). DSC analysis pointed to secondary cross-linking of systems that had not completely cured after 1000 h storage at 180°C (*Fig. 13*). Despite this, a certain increase in the Young's modulus was observed in this system (12). The tests are being continued.

Once again, there is the problem of having to

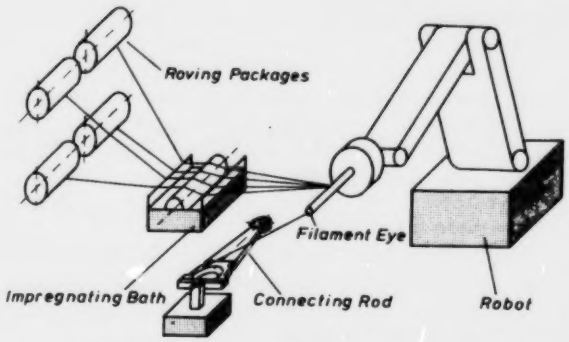

Fig. 11. Laboratory winding of connecting rods.

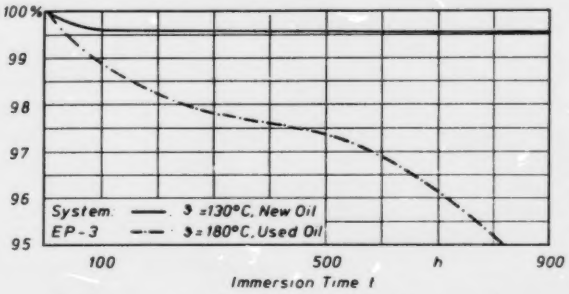

Fig. 12. Loss in weight after immersion in motor oil.

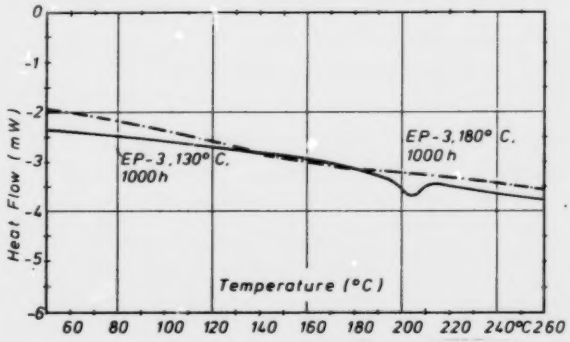

Fig. 13. Results of DSC analysis.

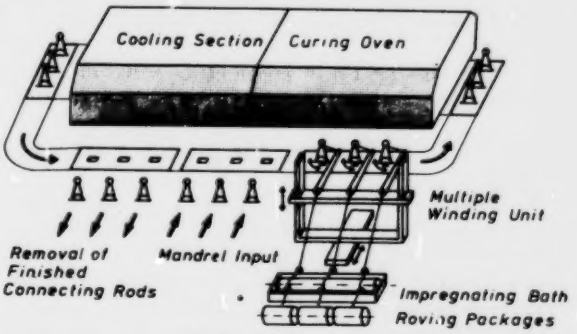

Fig. 14. Series production of fiber-reinforced connecting rods.

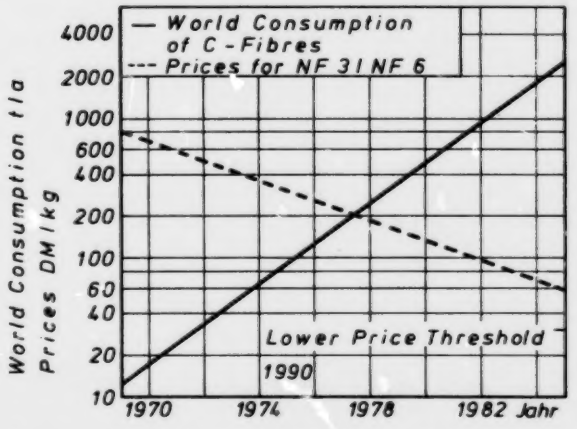

Fig. 15. Volume and price developments in C-fibers on a PAN basis (12).

produce a large number of components in the short period of time. It may be assumed that filament eye mobility will be reduced in series production as compared with laboratory production. This would then make it feasible to employ a multiple winding unit with corresponding downstream facilities (*Fig. 14*) (9).

PROSPECTS

Although the cost of carbon fibers will sink as world consumption increases (see *Figs. 12* and *15*), it is forecast that the price of CRP laminates will remain constant at some DM 200/kg until approximately 1990 (4, 13). Despite the high price, the application of fiber reinforced plastics will not be confined solely to the aviation and the automobile industries. As the production process for this type of component becomes increasingly automated and further insight is gained into material (physical) behavior, the trend will doubtless be towards substitution throughout mechanical engineering in general. Carbon and aramid reinforced plastics will be used to an ever increasing extent for rapidly moving components such as found on textile and printing machines.

REFERENCES

1. G. Niederstadt, "Kriterien und Beispiel für die Wahl von Verbundwerkstoffen mit Fasern hoher spezifischer Eigenschaften, Kohlenstoffund aramidfaserverstärkte Kunststoffe", BDI-Verlag, (1977).
2. C. Norman, "Kevlar aramid fibers, Developments in Reinforced Plastic and Friction Materials, Advances in Structural Composite Technology for Commercial Transportation Industry", Southfield, Michigan 1978.
3. S. Wood, *Mod. Plast. Int.*, 11, 46 (1981).
4. U. Bieling, "Einsatz von Faserverbundwerkstoffen im Leichtbau", Doctoral lecture, IKV, Aachen, June 16, 1983.
5. M. Kurzmeier and J. Zöhren, *Kunststoffe*, 72, 362 (1982).
6. U. Bieling, Dissertation, Aachen University, 1983.
7. D. Brownbill, *Mod. Plast. Int.*, 12, 30 (1982).
8. C. Rüegg, Ciba Geigy Company Documentation, Bale, Publ. No. 24876/d, July 1981.
9. W. Ermert, Doctoral Lecture, IKV, Aachen, August 1983.
10. E. A. Hille, Dissertation, Aachen University, 1981.
11. W. Müller, Experimental thesis (No. S 8344), IKV, 1983.
12. P. G. Rose, "Hochfeste C-Fasern auf PAN-Basis, Einsatzformen und Eigenschaften im CFK-Verbund", VDI-Verlag, (1981).
13. H. Prem, *Kunststoffe*, 72, 622 (1982).

XII. DISCUSSION: J. MINTE

S. V. Hoa: Making these connecting rods, did you use glass or graphite fibers? Did you use a resin bath?

J. Minte: Carbon fiber was used in a wet-winding method.

L. A. Utracki: You showed an amazing agreement between the experimental and calculated Young's moduli for a series of laminates. Could you tell us which method of calculation you used to achieve these predictions?

J. Minte: This is a well-known method in Germany, based on the classical lamination theory by Puck. It is a 3-dimensional tensor calculation of mechanical strength based on the law of Hooke which considers the properties up to the limit when they become heterogeneous. It is rather a sophisticated and complicated method for anisotropic materials, but it gives good results. We are using it to precalculate our GRP-prototypes, e.g., the GRP tanks for the chemical industry. Presently, we are trying to adapt this theory to carbon fiber reinforced plastics. My aim was to show you that this is possible.

Q. Samak: Did you subject the GRP parts, such as these connecting rods, to dynamic loading tes
What kind of results have you gotten?

J. Minte: We are starting these tests. In general,
the fiber direction the static and dynamic streng
are the same. It is seldom that all the fibers
aligned in the loading direction. Therefore, we ha
to test how the dynamic and static strength
related to the fibers which are not aligned. This
what we are doing right now.

C. L. Beatty: I have an impression that there i
large oversupply of carbon fiber on the market ri
now. Is this true, and if so, will this have a depre
ing effect on price of these fibers?

J. Minte: I am only an engineer, not an economi
but I think that you are right. There is an oversup
in the world. However, at the same time, as mo
and more applications of these fibers are disco
ered, the possibilities of applications are increasi
I feel that the oversupply will soon disappear. Co
cerning the price, producing methods are relative
expensive and unless new ones are developed, t
price will be high for quite a while. However, t
manufacturers are working on new, more econon
methods of carbon-fiber production that will bri
the price down.

Subject Index

A

Adhesive joints, molecular and microstructure of coupling agents, 101
Alkaline, solution environment, stress-rupture lifetime of poly(ethylene terephthalate)/glass composite, 208
Alkyl ether elastomer, perfluorinated, modification of epoxy-reinforced glass-cloth composites, 198
Aspect ratio of inclusions, effect on elastic properties of unidirectionally aligned composites, 327

B

Bismaleimide, processing and flammability parameters, for composites, 143
Bulk modulus, melt polymer composites, statistical versus macro-mechanics, 3

C

Celion 6000 graphite/PMR 15, polymide composites, tensile properties and fracture, 179
Coatings, molecular and microstructure of coupling agents, 101
Composite materials, damping of, 334
Composites, molecular and microstructure of coupling agents, 101
Condensation, hydrolysis and, silates in aqueous solution, 242
Coupling agents
mica-reinforced polypropylene, 250
molecular and microstructure of, their functions in composites, coatings and adhesive joints, 101
monolayers, surface of mica, 11
phenomena, technique for study, 258
Creep behavior, polyurethane foam, particulate reinforcement effects, 155

D

Damping, composite materials, 334
Deformation design, short-fiber reinforced thermoplastics, 72

E

Electric breakdown, poly(ethylene terephthalate)/glass composite, 215
Electrostatic phenomena, molecular motion and, glass/polymer composites, 224
Endless-fiber reinforced polymers, application of, 347
Epoxies
amine-cured, dynamic mechanical experiments, probing process-structure-property relations in, 124
reinforced glass-cloth components, perfluorinated alkyl ether elastomer, 198
Extrusion, particle flow, sintering process and, 52

F

Fabrication, control of fiber orientation during, mechanical property enhancement in short-fiber composites, 60
Fatigue crack propagation, composites, spherical fillers, 231
Fiber
continuous rearrangement, during molding of fiber composites, 191
orientation during fabrication, short-fiber composites, 60
Fiber composites, molding, continuous fiber rearrangements during, 191
Fiberglass stack, free-standing, design concepts, 186
Fillers
increasing levels, optimum property concept, 339
interaction with matrix polymers, via transition maps, 319

G

Glass-cloth composites, epoxy-reinforced, perfluorinated alkyl ether elastomer, 198
Glass-epoxy composite laminates, thermal and mechanical properties, 173
Glass fibers, rheological behavior of propylene melts, rotating parallel plates, 29
Glass/polymer composites, electrostatic phenomena, molecular motion and, 224
Graphite/polymide composites, unidirectional, off-axis tensile properties and fracture, 179

H

Hydrolysis, condensation and, silates in aqueous solution, 242

I

Internal reflection spectroscopy, coupling agent phenomena, 258
Isotactic poly(propylene oxide), crystallization, effect of silica on, 307

J

Jute, reinforced, polyester structures, 141

L

Laminate, glass-epoxy composite, thermal and mechanical properties of, 173

M

Matrix polymers, interaction of fillers, via transition maps, 319
Melt polymer composites, bulk modulus and thermal expansivity, statistical versus macro-mechanics, 3
Mica
mechanical degradation, during processing with polypropylene, 264
polyethylene, extensional flow of, 44
polyethylene melts, rheology of, 36
polypropylene, processing aids and coupling agents in, 250
polypropylene system, dynamic and steady state flow of, 277
surface, formation of coupling agent monolayers, 11
Mica-polypropylene composites, extruded, factors affecting surface texture, 299
Molecular motion, electrostatic phenomena and, glass/polymer composites, 224

O

Optimum property concept, relative order in failure property maxima, with increasing filler levels, 339

P

Particle flow, sintering process and, extrusion, 52
Particulate fillers, silane coupling agent structures on, studies of simulation, pH effect, 18
pH effect, silane coupling agent structures, particulate fillers, 18
Polyester structures, jute reinforced, 141
Polyethylene, mica-filled, extensional flow of, 44
Polyethylene films, paper-like filled, 81
Polyethylene melts, mica-reinforced, rheology, 36
Poly(ethylene terephthalate)/glass composite
electric breakdown, 215
under alkaline solution environment, stress-rupture lifetime, 208
Polymers, endless-fiber reinforced, application of, 347
Polypropylene
elastomer-modified, talc-filled, 202
mica processing with, mechanical degradation, 264
mica-reinforced, processing aids and coupling agents in, 250
Polypropylene melts
rheological behavior of, glass fiber effects, 29
short glass fiber reinforced, elongation behavior, 289
Polypropylene/mica systems, dynamic and steady state flow of, 277
Polyurethane foam, creep behavior, particulate reinforcement effects, 155
Process-structure-property relations, amine-cured epoxies, 124
Propropylene composites, mechanical properties and morphology, 202

R

Reaction injection molded systems, stress relaxation properties, 151

Resin matrices, thermally stable, processing and flammability parameters, for composites, 143
Rheology, mica-reinforced polyethylene melts, 36

S

Sheet molding compound technology, recent developments, 88
Short-fiber composites, mechanical property enhancement, control of fiber orientation during fabrication, 60
Short glass fiber, reinforced polypropylene melts, elongation behavior, 289
Silane coupling agent, studies of simulation, particulate fillers, pH effect, 18
Silates, aqueous solution, hydrolysis and condensation of, 242
Silica, crystallization of isotactic poly(propylene oxide), 307
Sintering process, particle flow and, extrusion, 52
Solid composite polymers, characterization, dynamic mechanical method, 312
Spherical fillers, composites with, fatigue crack propagation, 231
Stress relaxation properties, reaction injection molded systems, 151
Syntactic foam, three-phase, 159

T

Thermal expansivity, melt polymer composites, statistical versus macro-mechanics, 3
Thermoplastics
short-fiber reinforced, deformation design, 72
versus thermosetting composites, 169
Thermosetting composites, versus thermoplastics, 169
Transition maps, matrix polymers, interaction of fillers with, 319

U

Unidirectionally aligned composites, elastic properties of, aspect ratio of inclusions and, 327

Author Index

Alperstein, D., 155

Bagley, E. B., 52
Baker, T. E., 186
Bata, G. L., 1
Beatty, C. L., 319
Blanchard, L. P., 11, 242
Brown, G. R., 307

Chen, T. S., 198
Chu, H. S., 124
Chun, I., 250

Fanta, G. F., 52
Favis, B. D., 11, 264, 277, 299
Fesko, D. G., 88
Fisa, B., 36, 264, 277, 299

Gadkaree, K. P., 231
Garton, A., 258
Gearing, J. W. E., 312
Goettler, L. A., 60

Harbourne, D. A., 81
Harper, J., 179
Hoa, S. V., 334
Hoh, K.-P., 18
Hsiue, E. S., 191
Hurwitz, F. I., 179

Ishida, H., 18, 101

Jain, R. K., 3
Jain, S. C., 3

Kamal, M. R., 29, 289
Kays, A. O., 169
Kenig, S., 155, 159
Kennedy, M. A., 307
Kourtides, D. A., 143

Lara, J., 44
Lautenschlaeger, F. K., 339
Léonard, J., 11, 242
Lhymn, C., 208, 215
Lotfali, A. R., 141

McCammond, D., 72
Menges, G., 347
Miller, J. D., 18
Minte, J., 347
Mirzadeh, H., 141
Mutel, A. T., 29, 289
Muzzy, J. D., 169

Narkis, M., 155, 159
Newman, S., 88
North, P. A., 72

Pham, M., 186
Plecnik, J. M., 186
Prud'Homme, R. E., 11, 242
Puterman, M., 159

Quellette, P., 334

Raghava, R. S., 173
Robertson, R. E., 191
Rosser, R. W., 198

Salee, G., 231
Sanschagrin, B., 264, 299
Savard, S., 242
Schultz, J. M., 208, 215
Seferis, J. C., 124
Semsarzadeh, M. A., 141
Siegmann, A., 155
Simha, R., 3
Stamhuis, J. E., 202
Stone, M. R., 312
St-Pierre, L. E., 307
Stupp, S. I., 224
Swanson, C. L., 52

Tandon, G. P., 327
Taylor, M., 198
Turner, R. B., 151

Utracki, L. A., 2, 36, 44, 241, 277, 289

Weldert, S. C., 224
Weng, G. J., 327
Whitman, W. E., 186
Whittenberger, J. D., 179
Woodhams, R. T., 250

Yeh, G. S. Y., 191

Zboril, V. G., 81

U.S. Postal Service

STATEMENT OF OWNERSHIP, MANAGEMENT AND CIRCULATION

Required by 39 U.S.C. 3685)

1A. TITLE OF PUBLICATION	1B. PUBLICATION NO.	2. DATE OF FILING
Polymer Composites		9/24/84
3. FREQUENCY OF ISSUE	**3A. NO. OF ISSUES PUBLISHED ANNUALLY**	**3B. ANNUAL SUBSCRIPTION PRICE**
Quarterly	4	$24.00 Member $60.00 Non-Member

4. COMPLETE MAILING ADDRESS OF KNOWN OFFICE OF PUBLICATION *(Street, City, County, State and ZIP Code) (Not printers)*

14 Fairfield Drive, Brookfield Center, CT 06805

5. COMPLETE MAILING ADDRESS OF THE HEADQUARTERS OF GENERAL BUSINESS OFFICES OF THE PUBLISHER *(Not printer)*

14 Fairfield Drive, Brookfield Center, CT 06805

6. FULL NAMES AND COMPLETE MAILING ADDRESS OF PUBLISHER, EDITOR, AND MANAGING EDITOR *(This item MUST NOT be blank)*

PUBLISHER *(Name and Complete Mailing Address)*

Robert D. Forger 14 Fairfield Drive, Brookfield Center, CT 06805

EDITOR *(Name and Complete Mailing Address)*

Dr. Roger S. Porter 14 Fairfield Drive, Brookfield Center, CT 06805

MANAGING EDITOR *(Name and Complete Mailing Address)*

7. OWNER *(If owned by a corporation, its name and address must be stated and also immediately thereunder the names and addresses of stockholders owning or holding 1 percent or more of total amount of stock. If not owned by a corporation, the names and addresses of the individual owners must be given. If owned by a partnership or other unincorporated firm, its name and address, as well as that of each individual must be given. If the publication is published by a nonprofit organization, its name and address must be stated.) (Item must be completed.)*

FULL NAME	COMPLETE MAILING ADDRESS
Society of Plastics Engineers, Inc.	14 Fairfield Drive Brookfield Center, CT 06805

8. KNOWN BONDHOLDERS, MORTGAGEES, AND OTHER SECURITY HOLDERS OWNING OR HOLDING 1 PERCENT OR MORE OF TOTAL AMOUNT OF BONDS, MORTGAGES OR OTHER SECURITIES *(If there are none, so state)*

FULL NAME	COMPLETE MAILING ADDRESS
None	

9. FOR COMPLETION BY NONPROFIT ORGANIZATIONS AUTHORIZED TO MAIL AT SPECIAL RATES *(Section 423.12 DMM only)*
The purpose, function, and nonprofit status of this organization and the exempt status for Federal income tax purposes *(Check one)*

(1) [x] HAS NOT CHANGED DURING PRECEDING 12 MONTHS

(2) [ ] HAS CHANGED DURING PRECEDING 12 MONTHS

(If changed, publisher must submit explanation of change with this statement.)

10. EXTENT AND NATURE OF CIRCULATION	AVERAGE NO. COPIES EACH ISSUE DURING PRECEDING 12 MONTHS	ACTUAL NO. COPIES OF SINGLE ISSUE PUBLISHED NEAREST TO FILING DATE
A. TOTAL NO. COPIES *(Net Press Run)*	800	800
B. PAID CIRCULATION 1. Sales through dealers and carriers, street vendors and counter sales	---	---
2. Mail Subscription	448	459
C. TOTAL PAID CIRCULATION *(Sum of 10B1 and 10B2)*	448	459
D. FREE DISTRIBUTION BY MAIL, CARRIER OR OTHER MEANS SAMPLES, COMPLIMENTARY, AND OTHER FREE COPIES	---	---
E. TOTAL DISTRIBUTION *(Sum of C and D)*	448	459
F. COPIES NOT DISTRIBUTED 1. Office use, left over, unaccounted, spoiled after printing	352	341
2. Return from News Agents	---	---
G. TOTAL *(Sum of E, F1 and 2—should equal net press run shown in A)*	800	800

11. I certify that the statements made by me above are correct and complete

SIGNATURE AND TITLE OF EDITOR, PUBLISHER, BUSINESS MANAGER, OR OWNER

Circulation Manager

PS Form 3526
July 1982

(See instruction on reverse)

SI METRIC UNITS

The following list shows the names, symbols, and equivalence of the more common quantities allowed in the SI metric system. The prefixes and symbols for the more common multiple units are also shown. Neither list is complete. Full details are given by F. S. Conant, Polym. Eng. Sci., 17, 222 (1977). A table of the more frequently needed conversion factors required to use the SI system is also shown. This journal prefers that SI metric units be employed in manuscripts submitted for publication.

Units and Symbols

Quantity	Name	Symbol	Equivalent to:
Length	metre	m	—
Time	second	s	—
	minute	min	—
	hour	h	—
Mass	kilogram	kg	—
Electric current	ampere	A	—
Plane angle	radian	rad	—
Capacity	litre	L	$10^{-3}m^3$
Frequency	hertz	Hz	s^{-1}
Force	newton	N	$m \cdot kg \cdot s^{-2}$
Pressure, Stress	pascal	Pa	$N \cdot m^{-2}$
Energy, Work, Heat	joule	J	$N \cdot m$
Power	watt	W	$J \cdot s^{-1}$
Viscosity, dynamic	pascal second	Pa · s	$N \cdot s \cdot m^{-2}$

(The following units should *not* be used: micron, angstrom, dyne, erg, calorie, poise, or stoke.)

Multiple Units

Prefix	Symbol	Equivalent to:
giga	G	10^9
mega	M	10^6
kilo	k	10^3
deci	d	10^{-1}
centi	c	10^{-2}
milli	m	10^{-3}
micro	μ	10^{-6}
nano	n	10^{-9}

Conversion Factors

Force: $1N = 10^5$ dynes $= 1.02 \times 10^{-1}$ kgf $= 2.248 \times 10^{-1}$ lbf.
Pressure, Stress: $1 Pa = 10$ dyne $cm^{-2} = 7.5 \times 10^{-3}$ mm Hg $= 10^{-5}$ bar $= 1.02 \times 10^{-5}$ kg cm^{-2} $= 1.45 \times 10^{-4}$ psi.
Energy: $1 J = 2.387 \times 10^{-1}$ cal.
Viscosity: 1 Pa · s = 10 poise.

INFORMATION FOR AUTHORS

Submission of original and review articles is encouraged. There is no limit on length. Three copies of the manuscript should be submitted, which should be typed, one side only, double space, with at least a 1-inch margin. Submission will be taken to imply that the paper has not been previously published, that it is not being considered elsewhere for publication, and that if accepted it will not be published elsewhere in the same form, in any language, without the consent of the editor or publisher. Authors must agree to transfer copyright to the publisher when an article is accepted for publication. Unless notified to the contrary by the authors, the publisher assumes that the act of submitting the article signifies the author's agreement to such copyright transfer to the publisher. The journal carries a voluntary page charge. Each manuscript should include:

A separate title page, headed by a concise, meaningful title (avoid abbreviations) for the paper. This page should provide:

- The name and affiliations of each contributing author at the time the paper was prepared.
- Indicate by asterisk any changes of address for each author since article preparation.
- Acknowledgment of any prior oral presentation and original source of the material.

A separate abstract page, consisting of a single paragraph of 100–200 words to include the title and the names and addresses of the authors. Define any abbreviations for substances or methods (such as ABS, SAXS, etc.).

A list of references, on a separate page at the end of the text, numbered in order of text citation. The references are to be abbreviated in the form used in Chemical Abstracts using the names of all authors preceded by initials; see Bibliographic Guide for Editors and Authors, American Chemical Society, Washington, D.C.

- Within the text, the reference citations are typed in parentheses in line with the main copy (no superscripts or subscripts), thus:

  According to Young, et al. (1) . . .

- In the list of references the general style is as follows:

For periodicals:

1. S. S. Young, J. L. White, E. S. Clark and Y. Oyanogi, Polym. Eng. Sci., 20, 798 (1980).

The journal name and volume are to be underlined and the year is placed in parentheses. The issue number is given only when needed for identification. The article name is eliminated unless the reference is unclear without it.

For books: The title to be spelled out in full.

5. H.-G. Elias, "Macromolecules," Ch. 1, Vol. 2, Plenum Press, New York (1977). (Include the state when the city is not identifiable.)

A list of nomenclature, identifying symbols and abbreviations, commonly desirable at the end of the text. Footnotes are to be avoided.

Equations, numbered and typed in the appropriate place in the text. Where symbols cannot be typed, write them neatly in ink.

Tables, each typed on a separate page, with a heading, and numbered with arabic numerals that correspond to the order in which they are cited in the text. The tables should be inserted in the manuscript after the references and before the figures.

Figures, assembled at the end of the manuscript and preceded by a typed list of captions that explain them. Please also supply a set of original figures or sharp glossy photos thereof, on 8½ × 11 paper or attached to sheets of this size, one sheet for each figure. Each should be identified on the front edge or on the back (photographs) with the name of the first author and the figure number (e.g., Smith, Fig. 1). Originals are to be prepared with high contrast India ink and to bear uniformly stencilled notations. Line drawings and photos should be of a quality suitable for good photographic reproduction and retained legibility upon size reduction to one quarter. Manuscript transmittal letter should indicate if the figures need be returned.

Send manuscripts to:
Roger S. Porter, Editor
POLYMER COMPOSITES
% Polymer Science & Engineering
University of Massachusetts
Amherst, Massachusetts 01003

For information concerning publication dates, page charges and reprint orders contact:
Editorial Department
Society of Plastics Engineers
14 Fairfield Drive
Brookfield Center, Connecticut 06805

Continued From Front Cover

347 G. MENGES and J. MINTE/The Application of Endless-Fiber Reinforced Polymers

353 Subject and Title Index

354 Author Index

SOCIETY OF PLASTICS ENGINEERS, INC., 14 Fairfield Drive, Brookfield Center, Conn. 06805